Improved Modelling of Sub-Grid Pipework within a CFD Flow Simulation

Alice Catherine Ely

A dissertation presented in part fulfilment of the degree of MSc in Computational Fluid Dynamics, University of Leeds

Centre for Computational Fluid Dynamics

September 2004

Supervisors

Mobius Dynamics – Dr Robert Cairns

University of Leeds, School of Mathematics – Professor D.B. Ingham

Abstract

Offshore platforms and onshore process plants frequently include large amounts of small-bore pipework. Due to the size of such facilities, when conducting CFD-predictions of flow around them, it is not practical to include each length of pipework explicitly within the computational mesh, since this would lead to a prohibitive number of computational cells. For this reason sub-grid pipework must be represented as a resistance to the flow, applied as a source term in the Navier-Stokes equations.

A popular method for representing sub-grid pipework that is currently in use involves grouping clusters of pipework of similar diameter into volumes, usually in the form of orthogonal rectangular volumes. A pipe diameter and pipe spacing are assigned to each of the volumes that are representative of the pipe cluster within. This method, descibed as the Volume of Uniform Resistance (VUR) method, has limitations in terms of accuracy, reliability and human interpretation.

This thesis describes a new automated method (the Approximation of Cylindrical Elements or ACE method) for representing sub-grid pipework. Validation of the ACE method was performed for selected benchmark pipe configurations by comparing CFD-predictions with the ACE method to CFD-predictions with the pipework represented explicitly within the computational mesh. A comparison of the ACE method with the current, popular method is also given. The ACE method provides a more realistic representation of sub-grid pipework that is independent of human interpretation.

Acknowledgements

Firstly, I would like to acknowledge Mobius Dynamics for proposing this project and allowing me to undertake the work with them.

I would like to thank Steve Howell, of Mobius Dynamics, for his continuing advice and support throughout this work and all the time he has spent on this, and also Professor D.B. Ingham for his advice on the thesis.

Thanks also go to everyone at Mobius Dynamics for all their help and interest in the work, and to Pete for his support through the time spent working on the project.

Contents

Nomenclature

$\underline{a}$, $\underline{b}$	Vectors
A_i	Projected Area in Coordinate Direction i (m^2)
C_d	Drag Coefficient
$C_{d\,b}$	Drag Coefficient taking into account Blockage ratio
d_C , d_i	Determinants of 3 x 3 matrices, $i = 0, \cdots, 2$
D_C , D_i	Determinants of 4 x 4 matrices, $i = 0, \cdots, 3$
D	Diameter (m)
$\underline{e}$	Coordinates of the End of a Pipe
E_i	Edge of a Triangle, $i = 0, \cdots, 2$
f''	Frictional Resistance
F_i	Face of a Tetrahedron, $i = 0, \cdots, 3$
g_c	Conversion Factor
$G_{\max}$	Maximum x-Velocity multiplied by fluid density (Pa s m^{-1})
$\underline{\hat{i}}$, $\underline{\hat{j}}$, $\underline{\hat{k}}$	Unit Direction Vectors in the x-, y- and z- direction, respectively
k	Turbulence Energy (m^2 s^{-2})
L_i	Length in Coordinate Direction i (m)
$L_{P\,i}$	Projected Length in Coordinate Direction i (m)
L	Length Scale
M_i	Node of a Face, $i = 0, \cdots, 2$
n	A Function of X_L
$\underline{n}$	Normal Vector
n_i	Node of a Triangle, $i = 0, \cdots, 2$
N_i	Node of a Tetrahedron, $i = 0, \cdots, 3$
N	Number of Rows of Pipes
P_t , p_t	Test Points
P	Pressure (Pa)

$\underline{r}_0$, $\underline{r}$	Position Vectors
Re	Reynolds Number
$\underline{s}$	Coordinates of the Start of a Pipe
$S_{C\,i}$	Coefficient of Source Term of Momentum Equation (m^2)
S_i	Source Term of Momentum Equation (Pa m^{-1})
t	Parametric Distance
U_i	Velocity Component (m s^{-1})
U	Velocity Magnitude (m s^{-1})
$\underline{v}$	Direction Vector
V	Cell Volume (m^3)
x, y, z	Cartesian Coordinates
x_i, y_i, z_i	Cartesian Coordinates
X_L	Longitudinal Pitch Divided by Diameter
X_T	Transverse Pitch Divided by Diameter
ΔP	Pressure Difference
ε	Turbulence Dissipation Rate ($m^2\,s^{-3}$)
μ	Dynamic Viscosity/Dynamic Laminar Viscosity (Pa s)
ρ	Density (kg m^{-3})
ν	Kinematic Viscosity ($m^2\,s^{-1}$)
ACE	Approximation of Cylindrical Elements
CFD	Computational Fluid Dynamics
QUICK	Quadratic Upstream Interpolation for Convective Kinematics
SIMPLE	Semi-Implicit Method for Pressure-Linked Equations
UDF	User-Defined Function
UDM	User-Defined Memory
VUR	Volume of Uniform Resistance

1.0 Introduction

1.1 Overview

Offshore platforms and onshore process plants frequently include large amounts of small-bore pipework. Due to the size of such facilities, when conducting CFD-predictions of flow around them, it is not practical to include each length of pipework explicitly within the computational mesh, since this would lead to a prohibitive number of computational cells. For this reason sub-grid pipework must be represented as a resistance to the flow, applied as a source term in the Navier-Stokes equations.

In this thesis a new method of representing sub-grid pipework is developed and discussed.

An example of an offshore platform (with a large amount of small-bore pipework is shown in Figure (1.1.1).

Figure 1.1.1 – Petrobras XXIII (ex. Vinni) Semi-Submersible Offshore Platform

1.2 A Method that is Currently Popular for Modelling Sub-grid Pipework

A popular method that is often used to model the effect of a complex network of sub-grid pipework on the flow, is to group clusters of pipework with similar diameters into volumes, usually in the form of orthogonal rectangular volumes, and to assign a pipe diameter and pipe spacing to each of the volumes that is representative of the pipe cluster within.

Using this information, a resistance to the flow is then applied as a source term in the Navier-Stokes equations, throughout each of the volumes according to the empirical Formula provided by McAdams (1954), which describes the pressure drop, ΔP, across a uniform piperack. The pressure drop is given by,

$$\Delta P = 4f'' N G_{\max}^2 / 2 g_c \rho \qquad \text{(Eq. 1.2.1)}$$

Where N is the number of rows of pipes, ρ is the fluid density, G_{max} is the maximum x-velocity multiplied by the fluid density and g_c is the conversion factor which is equal to 1.0.

For turbulent air flow across a rack of staggered tubes of diameter, D, with a range of transverse and longitudinal spacings, the frictional resistance (f'') depends on the arrangement of the pipes and on a Reynolds number.

$$4f'' = \left(0.176 + \frac{0.32 X_L}{(X_T - 1)^n}\right) \mathrm{Re}^{-0.15} \qquad \text{(Eq. 1.2.2)}$$

Where,

$$\mathrm{Re} = (\mathrm{D}\mathrm{G}_{\max} / \mu) \qquad \text{(Eq. 1.2.3)}$$

Here, μ is the laminar fluid viscosity, X_L is the longitudinal pitch divided by D and X_T is the transverse pitch divided by D. The pitch is the distance between tube centres and n is given by,

$$\mathrm{n} = 0.43 + 1.13 / \mathrm{X}_{\mathrm{L}} \qquad \text{(Eq. 1.2.4)}$$

This method, henceforth described as the Volume of Uniform Resistance (VUR) method, has several limitations. With this method, the spatial variation of pipe spacing within any given volume, and the direction and diameter of individual pipes are not represented.

Rarely, on an offshore platform or onshore power plant is pipework uniformly distributed. Generally, the pipework is a complex arrangement with varying pipe diameters, spacing and direction. Identifying clusters of pipework of similar diameter therefore, is a non-trivial process that cannot be easily automated. Instead, the resistive volumes must be defined manually, which can be a time-consuming task, and one that is inexact in the sense that the volumes identified are open to human interpretation and may differ upon the analyst who creates them. Figures (1.2.1) and (1.2.2) show how a volume around two irregularly spaced pipes, with different diameters could be drawn.

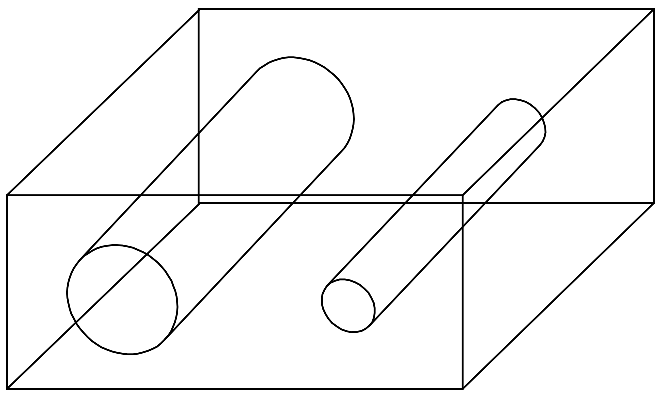

Figure 1.2.1 – Volume Surrounding Two Irregularly Spaced Pipes with Different Diameters – Option 1

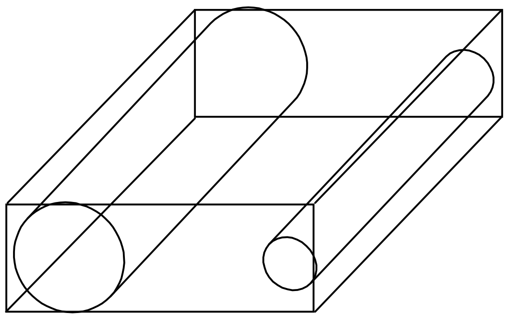

Figure 1.2.2 – Volume Surrounding Two Irregularly Spaced Pipes with Different Diameters – Option 2

1.3 Aims of this Work

The aim of this work was to develop a new, generic method to model the effects of cylindrical sub-grid pipework on flows for CFD applications.

Given a pipework database containing the diameter and the coordinates of the end points of individual linear pipe segments, the new method should automate the process of specifying resistive source terms for the discretised Navier-Stokes equations, within the CFD-solver. The new method should track individual lengths of pipe form the ends points given in the database and allocate a resistance to the flow only in those computational cells through which the pipe passes, in order to provide a more realistic representation of the sub-grid pipework, than was possible with the VUR method.

The new method, henceforth described as the Approximation of Cylindrical Elements (ACE) method, should be validated by comparison with experimental benchmark data or CFD-predictions for the flow through some defined pipework represented explicitly within the computational mesh.

1.4 Outline of Thesis

Following this introduction, a literature review of previous, related work is given in §2.0, followed by a description of the computational method used by the ACE method in §3.0. §4.0 is a discussion of the source terms that have been added to the Navier-Stokes equations for the ACE method and §5.0 is a description of the methods used to validate the ACE method. The results of the validation study are presented and discussed in §6.0 and conclusions drawn from the development of the ACE method and validation study are presented in §7.0, along with an example of the ACE method being used to represent pipework on an offshore platform and suggestions for further work.

2.0 Literature Review

2.1 Introduction

Previous work looking at flow across cylinder arrays or tube bundles has been carried out both experimentally and numerically with the CFD approach, and provide predictions of velocities and lift and drag forces. Although there were limitations with much of the experimental work, with regard to the apparatus that was used to collect data and the way in which the data was measured, this work provides useful benchmark data for comparison with numerical simulations. The numerical work that was reviewed shows how modelling the flow across cylinder arrays has been conducted in the past. In some cases the numerical CFD-predictions were compared with experimental benchmark data. In the past, others have used experimental work to validate CFD simulations where cylinders have been represented explicitly within the mesh, and in many cases the results have been successful. Other previous work gives information on sub-grid models that have been used to represent obstacles that are too small to be included explicitly in a computational mesh; the size of objects that should be represented as sub-grid models and the source terms that should be used if this is the case.

2.2 Experimental Work

The flow of water through a number of tube bundle configurations was investigated experimentally by Balabani (1996). The tube bundles were mounded within a square tunnel, the cross-section of which measured 72 mm wide by 72 mm tall. All of the tubes had a diameter of 0.1 m and in every case the velocity of the water passed across them was 0.93 m/s. Three different tube bundles were considered; a staggered array with a cross-stream spacing of 16 mm, a staggered array with a cross-stream spacing of 21 mm and an inline array with a cross-stream spacing of 21 mm. The streamwise tube spacing was 36 mm. For each tube bundle array the streamwise and cross-stream mean velocities and the corresponding root mean square (rms) velocities were recorded at a number of measurement locations throughout each of the tube bundle configurations using the Laser Doppler Anemometer (LDA) technique. Pressure measurements were not provided.

A similar experimental study was carried out and reported by Simonin and Barcouda (1988). They considered the flow of water across a tube bank with an average velocity of 1.06 m/s. Their tube bank was an arrangement of seven horizontal, staggered rows of rods each with a diameter of 21.7 mm. The streamwise and cross-stream components of velocity and corresponding rms velocities were recorded using the LDA technique. The flow was considered to be periodic for this arrangement of pipes, so measurements were confined to one small area of the test section. The spacing between the rods is very small here in comparison to the configurations used by Balabani (1996).

Experimental work was also carried out by Lam and Fang (1995), Lam *et al.* (2003) and Avisar *et al.* (2001). Lam and Fang (1995) used a wind tunnel to investigate the flow past four cylinders in a square configuration. They presented measurements of the pressure distribution, obtained by using a differential pressure transducer. Lam *et al.* (1995) used a water tunnel to investigate the flow around four cylinders, also in a square configuration. They presented sequential photographs for the purpose of flow visualization, obtained by using Laser-Induced Fluorescence Visualization and Particle Image Velocimetry. Avisar *et al.* (2001) towed an array of cylinders through a tank filled with tap water. Measurements of the velocity field were obtained using Acoustic Doppler Velocimetry.

2.3 Numerical Simulations

Peric (1985) performed a numerical investigation of laminar and turbulent flow across tube bundles. A series of CFD-analyses were preformed using different grids and differencing schemes, and the predictions were compared with experimental results. The numerical results were reported to be 'favourable' for most of the laminar cases, but 'significant disagreements' were observed between the numerical predictions and the experimental data when the flow was turbulent.

A more recent numerical analysis was presented by Watterson *et al.* (1999). They performed turbulent CFD-calculations for incompressible flow through a staggered array of cylinders using an unstructured mesh and a low-Reynolds number k-ε model of turbulence. They compared their predictions to the experimental data of Simonin and Barcouda (1988) and concluded that "the results of the computations were surprisingly good" and that "the agreement between the predictions and the experiments was encouraging".

In contrast, Rollet-Miet *et al.* (1999) suggested that Large-Eddy simulation (LES) should be used to model turbulent flow in tube bundles, as opposed to Reynolds Averaged Navier-Stokes methods, such as the k-ε model. They also claim that 'LES yields results in good agreement with the experimental data of Simonin and Barcouda (1988)'.

2.4 Sub-grid Models and Source Terms

In the numerical simulations carried out by Peric (1985), Watterson *et al.* (1999) and Rollet-Miet *et al.* (1999) cylinders, or tube bundles have been represented explicitly within a mesh. However, for practical applications it is often prohibitive to represent pipes in this way due to the number of cells that would be required for the CFD-mesh. For example, the size of the computational domain that is required to model the flow for a typical offshore safety study can be several hundred metres in the streamwise direction. It is therefore, not practical to represent small-bore pipework explicitly within the mesh. The number of cells that can be modelled depends on the amount of computational time available, and the distribution of cells is affected by the geometry that is being meshed around, as well as areas of varying importance, in terms of the safety analysis, on the platform. Therefore other methods of representing small-bore pipework have been developed.

A porous media method to represent cylinder arrays and other objects, similar to the VUR method, has been used by Lea *et al.* (1993) and Martin *et al.* (1998). Lea *et al.* (1993) compared results obtained using this porous media approach to those obtained by resolving obstacles in a flow. The results suggested that the porous approach was better in some regions of the flow than others, but generally the results of resolving obstacles were slightly better than those obtained using the porous media approach.

Lea *et al.* (1993) also highlighted the importance of deciding which geometrical features should be modelled explicitly within a mesh. In making this decision, the location of the objects within the flow should be considered as well as their size. This was supported by the FLACS-95 User Guide, the AutoReaGas Theory Manual, Gilham *et al.* (1999) and Ivings *et al.* (2004).

Ivings *et al.* (2004) stated that small objects need to be modelled at a sub-grid level, and a porous media sub-model was suggested. A rule of thumb was put forward, suggesting that objects with a diameter of less than 1/100th of the cube root of the volume of the domain should not be resolved by the mesh unless they are located in a region of the geometry where they will have an important effect on the flow. Objects smaller than this can be represented by a sub-grid model, or if they are unlikely to have a significant effect on the flow, then they may be completely excluded from the model.

Ivings *et al.* (2004) also suggested that due to the usual high porosity of pipework, source terms should be introduced into the momentum equations to represent the resistance to the flow in the region. The AutoReaGas Theory Manual suggested that the source term for drag in the momentum equations should be expressed as a pressure drop per unit length, given by,

$$\Delta P = C_d D \rho U^2 \qquad \text{(Eq. 2.4.1)}$$

where C_d is the drag coefficient, D is the diameter of the pipe and U is the velocity of the flow.

It was shown by Lea *et al.* (1993) that using the porous media approach to represent pipework is not always as accurate as is desired. This approach has deficiencies in that the diameter of individual pipes, the spacing between individual pipes and the direction of pipes are not represented. If pipework is represented by a method similar to the ACE method, developed in this thesis, then source terms can be allocated on a cell-by-cell basis, and information about individual pipes can be included. Gilham *et al.* (1999) suggested a source term to represent the drag caused by pipes in each cell, and this is given by,

$$S_i = -\frac{\frac{1}{2} C_d \rho U_i |U_i| A_i}{V} \qquad \text{(Eq. 2.4.2)}$$

C_d is the drag coefficient and is taken to be 1.2 for cylinders with a circular cross-section and 2.0 for cylinders with a square cross-section. U_i is the velocity of the flow in direction i, $|U_i|$ is the magnitude of the velocity of the flow in direction i and A_i is the projected area of the cylinder in the direction of i. V is the volume of the cell containing the pipe.

Ivings *et al.* (2004) and Gilham *et al.* (1999) suggested that the level of congestion due to the pipework should be taken into account when calculating the source term to represent drag. They suggested that if there are a large number of small pipes in a region, they may have more effect than if there are a small number of large pipes in the region. In highly congested regions, Gilham *et al.* (1999) suggested that the drag coefficient should be taken to be a function of the blockage ratio, which is the fraction of the cross-sectional area that is closed to the flow. This function is given by,

$$C_{db} = C_d b/(1-b)^2 \qquad \text{(Eq. 2.4.3)}$$

if $b \leq 0.6$, or

$$C_{db} = C_d b^2/(1-b)^2 \qquad \text{(Eq. 2.4.4)}$$

if $b > 0.6$. C_{db} is drag coefficient taking into account blockage ratio, C_d is drag coefficient and b is blockage ratio.

The AutoReaGas Theory Manual suggested that source terms for drag and turbulence kinetic energy should also be added. However, Ivings *et al.* (2004) reported that although it is possible to derive source terms for the turbulence equations, they are less important than those for the drag terms in the momentum equations.

In many situations, pipes are not at ambient temperature. Gilham *et al.* (1999) reported that due to the large combined surface area of the pipes, they will be a significant source of heat in the region. Therefore, enthalpy source terms should also be implemented, and heat transfer rates can be estimated from empirical formulae. The importance of heat transfer from pipes is also recognised by Ivings *et al.* (2004), who reported that the pipework can have a 'significant effect on the overall heat balance and air movement' within a region. Yao *et al.* (1989), Aiba *et al.* (1980) and Wang *et al.* (1996) are examples from a wide range of research into the effect of heat transfer in flow across cylinder arrays, emphasizing the importance of taking heat transfer into account if the pipes are at a sufficiently high temperature. They also identify the interaction that the heat transfer has with other aspects of the flow such as Reynolds number and the length of the vortex formation region behind the cylinders.

3.0 The ACE Method

3.1 Introduction

The User-Defined function (UDF) facility, which is available in the CFD-solver, was used to write the ACE method. A number of memory locations are available in the CFD-solver for storing information from UDFs. This is known as the cell User-Defined Memory (UDM). Three memory locations are used by the ACE method, to store information in the x-, y- and z-directions. The code for the UDF is given in Appendix 2.

The UDF begins by reading in the information stored in the pipework database, which is described in §3.3.1. The cell UDM is initialised so that a value of zero is stored for every cell in the domain. The UDF then loops through each of the pipes. The centre line of each pipe is tracked through the cells of the CFD-mesh from one end, henceforth described as the start of the pipe, to the other end, henceforth described as the end of the pipe. Firstly, the cells are identified that contain the coordinates of the start and end of the pipe that is being tracked. The method for identifying cells is described in §3.3.2 and the more specific method for identifying the cells that contain the start and end of pipes is described in §3.3.3. The cell containing the start of the pipe is selected and is set to be the “test cell”. Providing the pipe does not start and end in the same cell, the face of the “test cell” that the pipe passes through is found by using the method described in §3.3.4. The cell that shares a face with the identified face of the “test cell” is the cell that the pipe passes through next. This is found by using either of the methods described in §3.3.5. The cell that is identified is set to be the “test cell”. This procedure continues until the “test cell” is the cell that contains the end of the pipe.

If at any time during a CFD-simulation the mesh is refined, hanging nodes are created on quadrilateral faces on the border of the refined region. This causes a problem with the method used to find the cell that the pipe passes through next, when a pipe passes into the region. In this situation, the UDF resorts to an alternative method to find the cell the pipe passes through next, and this is described in §3.3.6.

Other problems with the UDF may occur for several reasons. In some situations, error messages are output to the screen. The pipe that caused the problem is no longer tracked and the UDF starts tracking the next pipe. In other situations, additional functions have been included in the UDF to overcome the problem, which allow the tracking of the pipe to be continued. These are described in §3.3.7.

Source terms for the momentum equations are calculated on a cell-by-cell basis and depend on the length and diameter of pipe within the cell. The source terms are calculated during a CFD-simulation, but it is necessary to store information as the UDF identifies the cells that pipes pass through. Therefore, the UDF calculates coefficients for the source terms, $S_{C\,i}$, and stores them in the three locations of the cell UDM. This is described in §3.3.8.

The ACE method for representing sub-grid pipework a generic method. The CFD-solver used to develop the method was Fluent (Version 6.1).

Figure 3.1.1 shows a flow diagram of the UDF.

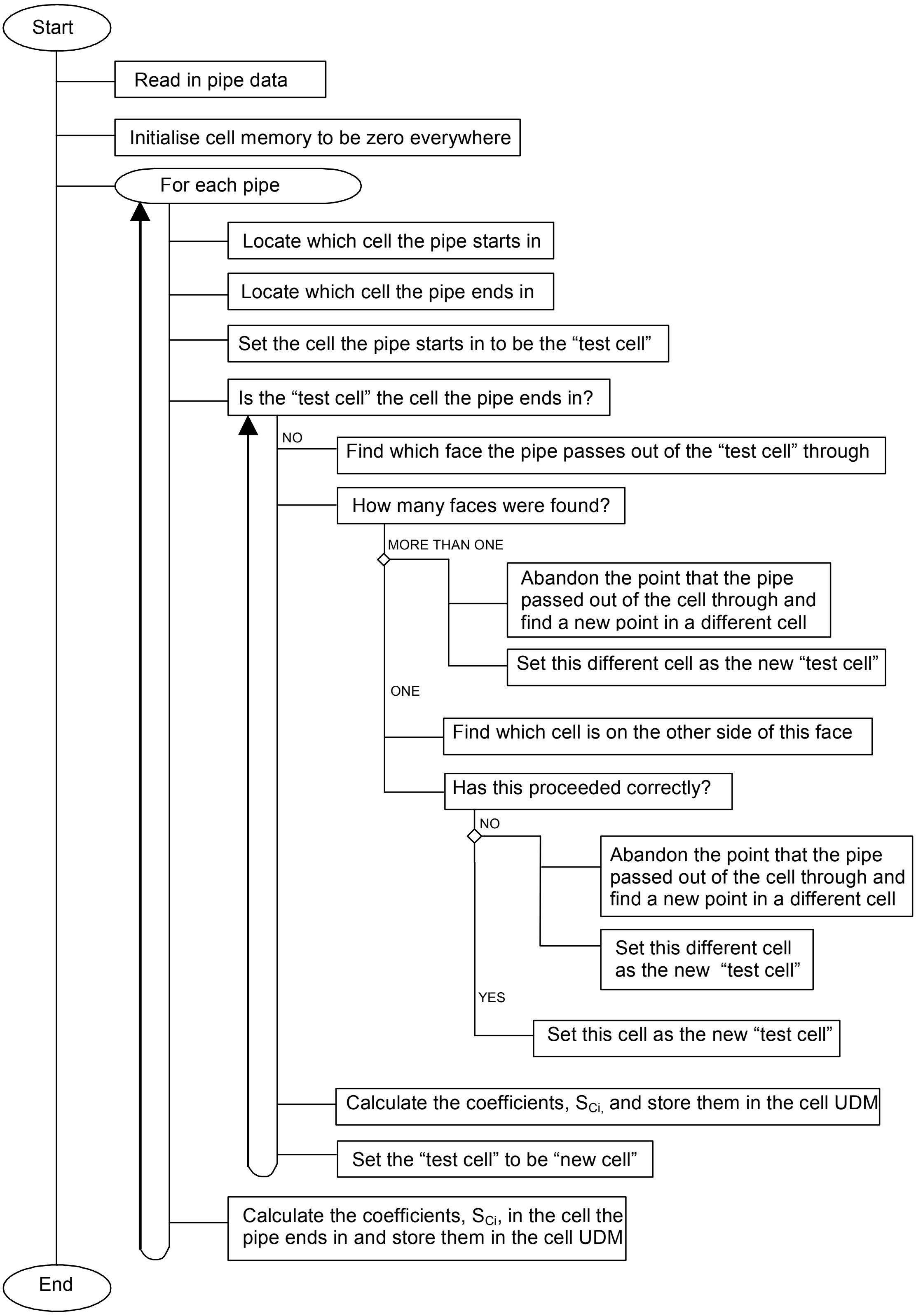

Figure 3.1.1 – Flow Diagram of the UDF used in the ACE Method

3.2 Method

3.2.1 The Pipework Database

Information regarding pipework is stored in a pipework database. The number of pipes is given on the first line followed by a list of pipes. Information for one pipe is stored on each row and there are seven columns of data. The first column contains the x-coordinate of the start of the pipe; the second column contains the x-coordinate of the end of the pipe; the third column contains the y-coordinate of the start of the pipe; the fourth column contains the y-coordinate of the end of the pipe; the fifth column contains the z-coordinate of the start of the pipe; the sixth column contains the z-coordinate of the end of the pipe and the seventh column contains the diameter of the pipe in metres. An example of a pipework database is shown below in Figure 3.2.1.

```
12
-19.6   -2.31   -14.0   -15.6   -10.1   -10.1   0.22
-5.6    7.291   3.012   -9.7    4.1     -4.1    0.0805
4.524   25.514  4.505   25.542  4.50    25.51   0.37
32.7    39.8    39.61   33.7    22.1    25.5    0.5
10.1    20.101  15.3    15.355  15.31   15.312  0.2816
10.01   30.51   30.0    5.0     20.0    30.5    0.40
20.0    10.3    30.0    7.01    10.012  20.263  0.264
2.512   39.255  2.5     39.2    29.3    29.3    0.19
-10.0   6.2     -2.54   1.712   3.9     1.5     0.06
4.610   4.34    3.7116  3.7     -17.2   8.23    0.382
22.5    16.21   -13.4   -19.28  -5.242  27.91   0.35
-17.8   -9.51   21.4    35.8    2.801   16.3    0.4
```

Figure 3.2.1 – An Example of a Pipework Database

3.2.2 Identifying Cells that Contain Specific Points

In the CFD-solver, each cell is identified by the cell thread that it lays on and by a cell number on that thread. Each cell thread includes all the cells lying within one region of the domain.

The UDF loops over all the cell threads in the domain, and all the cells on each thread. On each cell, the UDF recognises the shape of the cell and can then find out if a given point lies within the cell. Cells can be tetrahedrons, pyramids, triangular prisms or hexahedrons. An algorithm is used to determine if a point lies within a tetrahedron and this is described in §3.3.2. For cells that are not tetrahedrons, a short UDF was written to determine the local numbering of nodes on the cells. The code for this UDF is given in

Appendix 3. It was found that the CFD-solver uses the same numbering system for all cells of each shape. For example, on a pyramid, the nodes on the square are always numbers 0 – 3, labelled in the clockwise direction, and the node where the four triangles meet is always number 4, as shown in Figure 3.2.3. Therefore, using appropriate nodes, pyramids are divided into two tetrahedrons, triangular prisms are divided into three tetrahedrons, and hexahedrons are divided into five tetrahedrons (Electromagnetic Compatibility Laboratory, University of Missouri-Rolla, 1998). The algorithm to determine if a point lies within a tetrahedron (Herron, 1994) is then used in each of the tetrahedrons making up a cell. If the point is found within one of the tetrahedrons, then it is within the cell. The different shaped cells are shown in Figures 3.2.2, 3.2.3, 3.2.4 and 3.2.5, along with their tetrahedral composition and local node numbers.

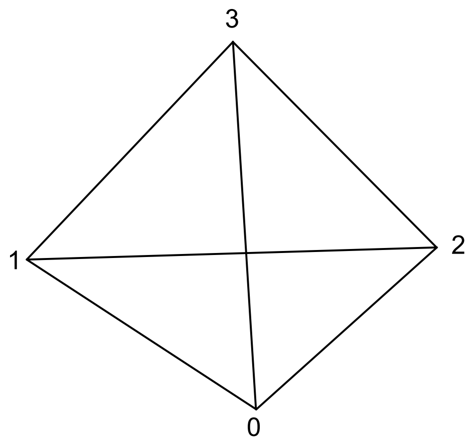

Figure 3.2.2 – A Tetrahedral Cell

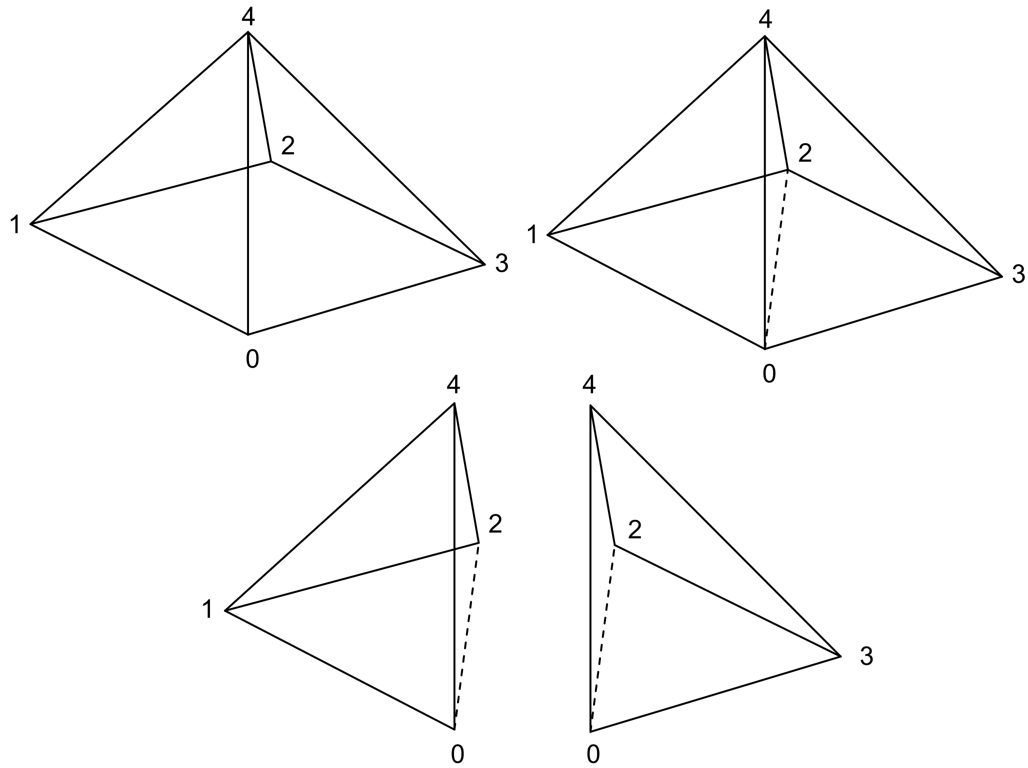

Figure 3.2.3 – A Pyramid-Shaped Cell and its Tetrahedral Components

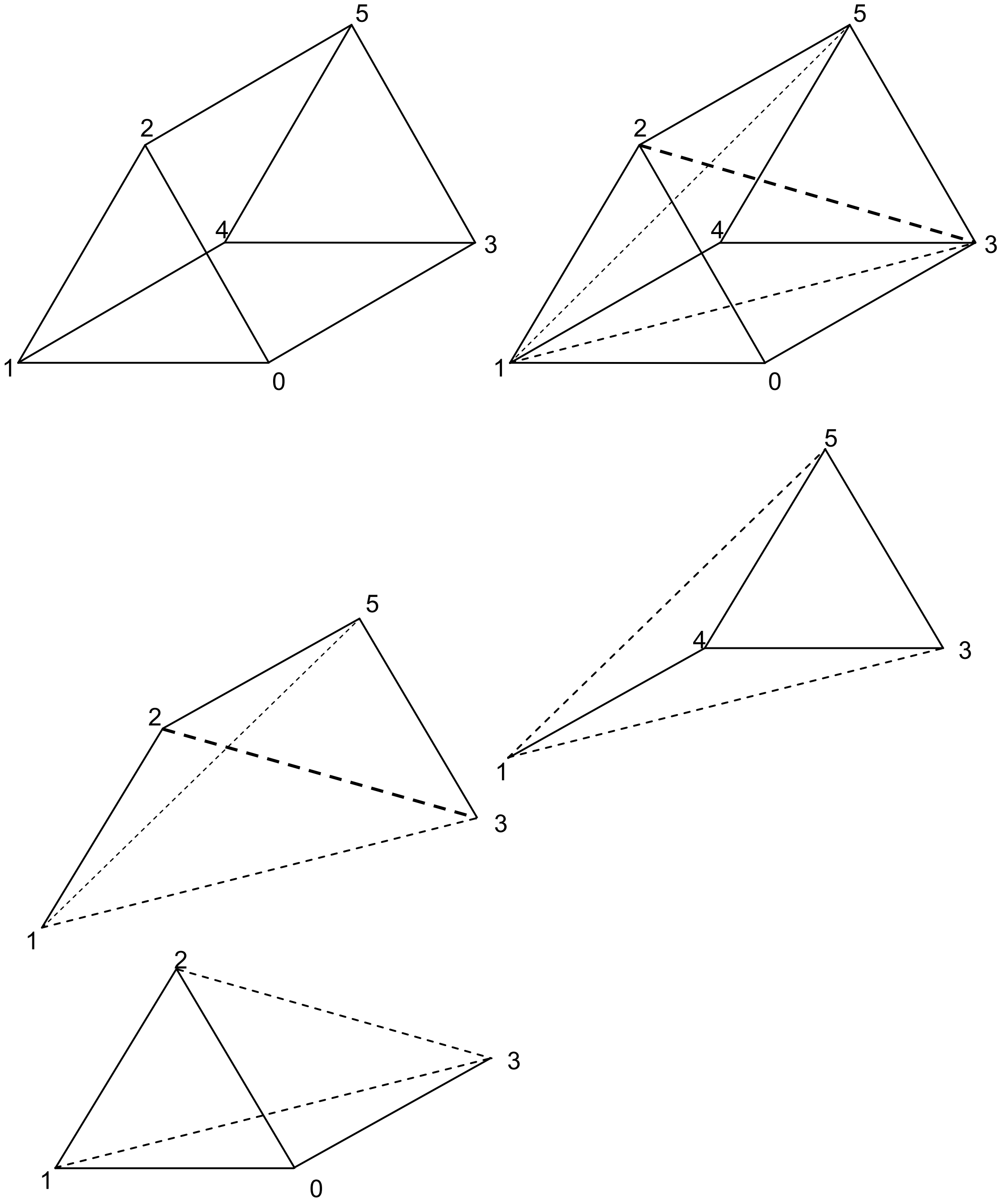

Figure 3.2.4 – A Triangular Prism-Shaped Cell and its Tetrahedral Components

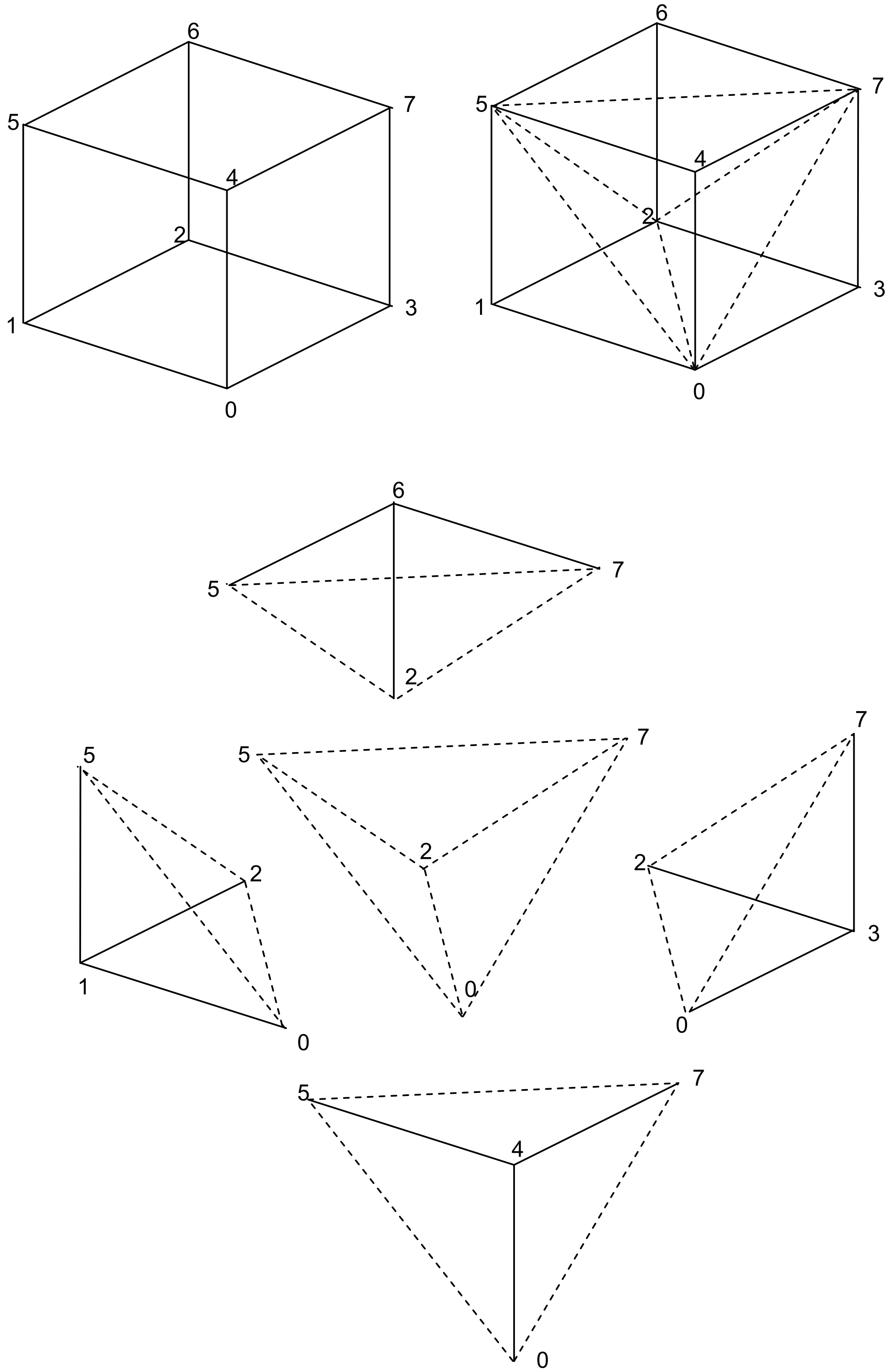

Figure 3.2.5 – A Hexahedral Cell and its Tetrahedral Components

3.2.2.1 Algorithm to determine if a point lies within a tetrahedron

The coordinates of the nodes, N_i, of the tetrahedron are given by,

$$N_0 = (x_0,\ y_0,\ z_0) \quad \text{(Eq. 3.2.1)}$$

$$N_1 = (x_1,\ y_1,\ z_1) \quad \text{(Eq. 3.2.2)}$$

$$N_2 = (x_2,\ y_2,\ z_2) \quad \text{(Eq. 3.2.3)}$$

$$N_3 = (x_3,\ y_3,\ z_3) \quad \text{(Eq. 3.2.3)}$$

The point that is being tested is given by,

$$P_t = (x,\ y,\ z) \quad \text{(Eq. 3.2.4)}$$

The determinants of the five matrices, D_C, and D_i, $i = 0, 1, 2, 3$, are then calculated. These are given by,

$$D_C = \begin{vmatrix} x_0 & y_0 & z_0 & 1 \\ x_1 & y_1 & z_1 & 1 \\ x_2 & y_2 & z_2 & 1 \\ x_3 & y_3 & z_3 & 1 \end{vmatrix} \quad \text{(Eq. 3.2.5)}$$

$$D_0 = \begin{vmatrix} x & y & z & 1 \\ x_1 & y_1 & z_1 & 1 \\ x_2 & y_2 & z_2 & 1 \\ x_3 & y_3 & z_3 & 1 \end{vmatrix} \quad \text{(Eq. 3.2.6)}$$

$$D_1 = \begin{vmatrix} x_0 & y_0 & z_0 & 1 \\ x & y & z & 1 \\ x_2 & y_2 & z_2 & 1 \\ x_3 & y_3 & z_3 & 1 \end{vmatrix} \quad \text{(Eq. 3.2.7)}$$

$$D_2 = \begin{vmatrix} x_0 & y_0 & z_0 & 1 \\ x_1 & y_1 & z_1 & 1 \\ x & y & z & 1 \\ x_3 & y_3 & z_3 & 1 \end{vmatrix} \quad \text{(Eq. 3.2.8)}$$

$$D_3 = \begin{vmatrix} x_0 & y_0 & z_0 & 1 \\ x_1 & y_1 & z_1 & 1 \\ x_2 & y_2 & z_2 & 1 \\ x & y & z & 1 \end{vmatrix} \qquad \text{(Eq. 3.2.9)}$$

For example, the determinant of D_C is given by (Schmitt, 2004),

$$\begin{aligned} D_C = {} & x_1y_2z_3 - x_1y_2z_4 + x_1y_4z_2 - x_1y_3z_2 + x_1y_3z_4 - x_1y_4z_3 - \\ & x_2y_1z_3 + x_2y_1z_4 - x_4y_1z_2 + x_3y_1z_2 - x_3y_1z_4 + x_4y_1z_3 + \\ & x_2y_3z_1 - x_2y_4z_1 + x_4y_2z_1 - x_3y_2z_1 + x_3y_4z_1 - x_4y_3z_1 - \\ & x_2y_3z_4 + x_2y_4z_3 - x_4y_2z_3 + x_3y_2z_4 - x_3y_4z_2 + x_4y_3z_2 \end{aligned}$$

(Eq. 3.2.10)

and the determinants of D_i, $i = 0, 1, 2, 3$, are calculated in the same way.

The point, P_t, is in the tetrahedron if all five determinants have the same sign. The faces of the tetrahedron, F_i, where $i = 0, 1, 2, 3$, are formed by the nodes other than N_i. If the sign of D_i is the same as the sign of D_C, then P_t is inside face F_i. If the sign of D_i is different to the sign of D_C, then P_t is outside face F_i. If $D_i = 0$ then P_t lies on face F_i. Therefore, if P_t lies inside all four faces, then P_t is inside the tetrahedron.

For the purposes of the ACE method, a point is considered to be in a tetrahedron if it is found to be inside it, or on a face. If a point is on a face, edge or node of a cell, then the UDF will find the point to be in more than one cell.

3.2.3 Identifying the Cells that Contain the Start and End of the Pipe

The method described in §3.2.2 is used to find the cells that contain the end point of pipes. However, if it is found that either end of a pipe lies on a face, edge or node of a cell, then the end will be found in more than one cell. Although this is an unlikely situation, it can occur, particularly with regular, hexahedral meshes. As the method for tracking pipes tracks them through one cell at a time, this situation raises several problems. If the start of a pipe is in more than one cell, how should the cell be found that the pipe goes through next? It would not pass out of a face of all the cells that it starts in, and to search through all the faces on every cell that it is in would be inefficient. Also, how should the source terms be allocated? If, for example, the pipe goes along the edges of four cells or faces of two cells, then should the source terms be split evenly between all those cells?

To simplify this problem, the whole pipe is moved a small amount, so that both ends are fully within one cell each. The reason for moving both ends of the pipe, even though only one end may be on a face, edge or node of a cell, is to keep the pipe the same length. Every time the start and end of a pipe are moved, the UDF searches for the cells that contain the start and end of the pipe by the method described in §3.2.2. The more times this search is done, the longer the UDF takes to run

A length scale is calculated, L, which is 100th of the cube root of the cell. This is based on being 100th of the side length, if the cell is a cube. Before the pipe is tracked, parameters, of value 1 or -1, are set in each direction, according to the direction of the pipe. If the start of the pipe, has an x-coordinate of lower numerical value than the end of the pipe, then the parameter in the x-direction is set to be 1. If the start of the pipe has an x-coordinate of higher numerical value than the end of the pipe, then the parameter in the x-direction is set to be -1. The same conditions are used to set the parameters in the y- and z-directions.

If either of the ends of the pipe lies on a face, edge or node, then the ends are moved by the set parameter multiplied by L in each of the x-, y- and z-directions. The parameter is there to help the tracking of the pipe progress in the correct direction. The importance of this is described in §3.2.5.2. L is small enough that it will not have a large effect on the accuracy of the UDF, but is enough to simplify the problem.

3.2.4 Identifying Faces that Contain Specific Points

In the CFD-solver, each face is identified by the face thread that it lays on and by a face number on that thread. Each face is also given a local face number, between 0 and 5, of the cell that it is on. Specific faces are located by looping over all the faces on a cell. On each face the UDF recognises the shape of the face, and can then find out whether a pipe travels through the face. All of the different shaped cells used by the CFD-solver are composed of combinations of triangular and quadrilateral faces. It is necessary to identify which face or faces the pipes pass out of each cell through.

In order to do this, two algorithms are used. The first algorithm finds the intersection point of a line with a plane (Department of Mathematics, Oregon State University, 1996 and Olive, 2003). This is used to find the intersection point of the line of the centre of a pipe, with the plane that a face of a cell lies in. Once this is found, it is necessary to determine whether this point of intersection lies within the boundaries of the face. To do this, the algorithm for determining if a point lies within a tetrahedron is extended, to form an algorithm to determine if a point lies within a triangle (Herron, 1994).

A short UDF was written to determine the local numbering of nodes on the faces. The code for this is given in Appendix 3. It was found that the CFD-solver always numbers the nodes in the anticlockwise direction, on both triangular and quadrilateral faces. The quadrilateral faces are divided into two triangles using appropriate nodes. The algorithm to determine if a point lies within a triangle is used in each triangle making up a cell face. If the pipe is found to pass through a triangle, then it passes through that face. Triangular and quadrilateral faces are shown in Figures 3.2.6 and 3.2.7, along with their local node numbers, and the triangular composition of a quadrilateral face.

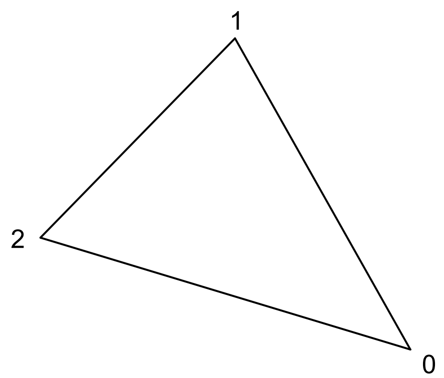

Figure 3.2.6 – A Triangular Face

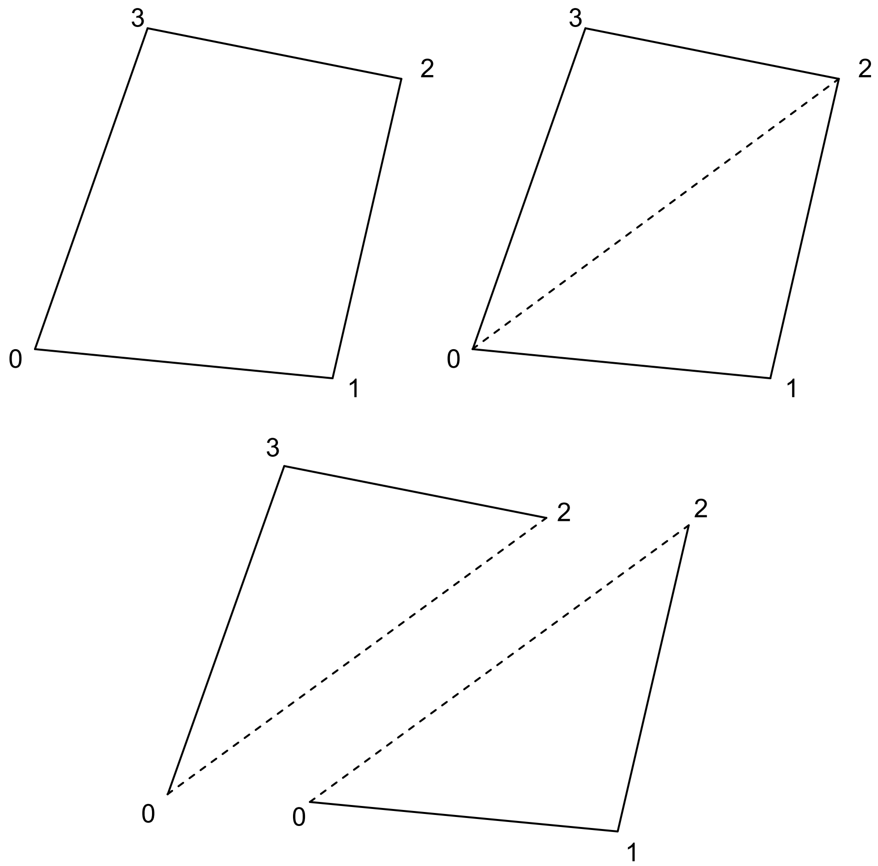

Figure 3.2.6 – A Quadrilateral Face and its Triangular Components

3.2.4.1 Algorithm to Determine if a Line Passes through a Plane

The equation of a plane is given by,

$$\underline{n} \cdot (\underline{r} - \underline{r}_0) = 0 \qquad \text{(Eq. 3.2.11)}$$

where $\underline{n}$ is a normal vector to the plane, $\underline{r}_0$ is the position vector of a point known to be in the plane and $\underline{r}$ is the position vector of any other point in the plane. The normal vector can be found by taking three points that are known to be on the plane. On a triangular face, the three nodes of the face can be used. On a quadrilateral face, any three of the four nodes on the face can be used. Take the coordinates of the three nodes, M_i to be,

$$M_0 = (x_0,\ y_0,\ z_0) \qquad \text{(Eq. 3.2.12)}$$

$$M_1 = (x_1,\ y_1,\ z_1) \qquad \text{(Eq. 3.2.13)}$$

$$M_2 = (x_2,\ y_2,\ z_2) \qquad \text{(Eq. 3.2.14)}$$

To calculate the normal vector, take the cross product of the vectors $\underline{a}$ and $\underline{b}$, where,

$$\underline{a} = (a_x,\ a_y,\ a_z) = M_1 - M_0 = (x_1 - x_0,\ y_1 - y_0,\ z_1 - z_0)$$

(Eq. 3.2.15)

$$\underline{b} = (b_x,\ b_y,\ b_z) = M_2 - M_1 = (x_2 - x_1,\ y_2 - y_1,\ z_2 - z_1)$$

(Eq. 3.2.16)

Then $\underline{n}$ is given by,

$$\underline{n} = \underline{a} \times \underline{b} = \begin{vmatrix} \underline{\hat{i}} & \underline{\hat{j}} & \underline{\hat{k}} \\ a_x & a_y & a_z \\ b_x & b_y & b_z \end{vmatrix} = (a_y b_z - a_z b_y)\underline{\hat{i}} + (a_z b_x - a_x b_z)\underline{\hat{j}} + (a_x b_y - a_y b_x)\underline{\hat{k}}$$

$$= n_i\,\underline{\hat{i}} + n_j\,\underline{\hat{j}} + n_k\,\underline{\hat{k}}$$

(Eq. 3.2.17)

Therefore the equation of the plane can be given by,

$$\underline{n} \cdot (\underline{r} - M_0) = n_i(x - x_0) + n_j(y - y_0) + n_k(z - z_0) = 0$$

(Eq. 3.2.18)

The general equation of a straight line is given by,

$$\underline{r} = \underline{r}_0 + t\,\underline{v} \qquad \text{(Eq. 3.2.19)}$$

where $\underline{r}$ is the position vector of any point along the line, $\underline{r}_0$ is the position vector of a point known to be on the line, $\underline{v}$ is a direction vector of the line, which is any non-zero vector parallel to the line, and t is the parametric distance along the line. The start and end points of the pipe both lie on the line. (Or if a point on the pipe has been moved, then the new point and the end point both lie on the line (§3.2.5.2)). If the coordinates of the start (or new point) of the pipe are given by,

$$\underline{s} = (s_x , s_y , s_z) \qquad \text{(Eq. 3.2.20)}$$

and the coordinates of the end of the pipe are given by,

$$\underline{e} = (e_x , e_y , e_z) \qquad \text{(Eq. 3.2.21)}$$

Then $\underline{v}$ can be taken to be the difference between the coordinates of the end of the pipe and the start (or new point) of the pipe.

$$\underline{v} = (v_x , v_y , v_z) = \underline{e} - \underline{s} = (e_x - s_x , e_y - s_y , e_z - s_z) \qquad \text{(Eq. 3.2.22)}$$

$\underline{r}_0$ can be taken to be the coordinates of the start (or new point) of the pipe, i.e.

$$\underline{r}_0 = \underline{s} = (s_x , s_y , s_z) \qquad \text{(Eq. 3.2.23)}$$

Therefore, the equation of the line of the centre of the pipe is given by,

$$\underline{r} = \underline{s} + t\,\underline{v} \qquad \text{(Eq. 3.2.24)}$$

or separated into each coordinate direction,

$$x = s_x + t v_x , \quad y = s_y + t v_y , \quad z = s_z + t v_z \qquad \text{(Eq. 3.2.25)}$$

In order to find the point, p_t, where the line of the centre of a pipe intersects the plane of a face of a cell, all these equations must be solved simultaneously. If the coordinates, x, y and z in (Eq. 3.2.25) are substituted into (Eq. 3.2.18) then this gives,

$$n_i(s_x + tv_x - x_0) + n_j(s_y + tv_y - y_0) + n_k(s_z + tv_z - z_0) = 0 \qquad \text{(Eq. 3.2.26)}$$

In (Eq. 3.2.26) everything other than t is known and so t is given by,

$$t = \frac{n_i(x_0 - s_x) + n_j(y_0 - s_y) + n_k(z_0 - s_z)}{n_i v_x + n_j v_y + n_k v_z} \qquad \text{(Eq. 3.2.27)}$$

Once t has been found, t is substituted back into (Eq. 3.2.24). Hence, the coordinates, x, y and z can be found, and this is the point, $p_t = (x, y, z)$, where the line intersects the plane.

3.2.4.2 Algorithm to determine if a point lies within a triangle

The coordinates of the nodes, n_i, of a triangle are given by,

$$n_0 = (x_0, y_0, z_0) \qquad \text{(Eq. 3.2.28)}$$

$$n_1 = (x_1, y_1, z_1) \qquad \text{(Eq. 3.2.29)}$$

$$n_2 = (x_2, y_2, z_2) \qquad \text{(Eq. 3.2.30)}$$

The point that is being tested is the point of intersection of the centre line of the pipe, with the plane of a face of a cell, $p_t = (x, y, z)$, as was obtained in §3.2.4.1. The determinants of the four matrices, d_C and d_i, $i = 0, 1, 2$, are then calculated. These are given by,

$$d_C = \begin{vmatrix} x_0 & y_0 & z_0 \\ x_1 & y_1 & z_1 \\ x_2 & y_2 & z_2 \end{vmatrix} \qquad \text{(Eq. 3.2.31)}$$

$$d_0 = \begin{vmatrix} x & y & z \\ x_1 & y_1 & z_1 \\ x_2 & y_2 & z_2 \end{vmatrix} \qquad \text{(Eq. 3.2.32)}$$

$$d_1 = \begin{vmatrix} x_0 & y_0 & z_0 \\ x & y & z \\ x_2 & y_2 & z_2 \end{vmatrix} \qquad \text{(Eq. 3.2.33)}$$

$$d_2 = \begin{vmatrix} x_0 & y_0 & z_0 \\ x_1 & y_1 & z_1 \\ x & y & z \end{vmatrix} \qquad \text{(Eq. 3.2.34)}$$

For example the determinant of d_C is given by (Schmitt, 2004),

$$d_C = x_1 y_2 z_3 - x_1 y_3 z_2 + x_3 y_1 z_2 - x_2 y_1 z_3 + x_2 y_3 z_1 - x_3 y_2 z_1 \qquad \text{(Eq. 3.2.35)}$$

and the determinants of d_i, $i = 0,1,2$, are calculated in the same way.

The point, p_t, is in the triangle if all four determinants have the same sign. The edges of the triangle, E_i, $i = 0,1,2$, are formed by the nodes other than n_i. If the sign of d_i is the same as the sign of d_C, then p_t is inside edge E_i. If the sign of d_i is different to the sign of d_C, then p_t is outside edge E_i. If $d_i = 0$ then p_t lies on edge E_i. Therefore, if p_t lies inside all four edges, then p_t is inside the triangle.

For the purposes of the ACE method, a point is considered to be in a triangle if it is found to be inside it, or on an edge or node. If a point is on an edge or a node of a face, then the UDF will find the point to be in more than one face.

3.2.5 Finding the Cells that the Pipes Pass Through

The UDF uses two methods to move between cells. If a pipe is found to travel out of a cell through just one face then Method 1, as described below in §3.2.5.1, is used. Method 1 is used for the vast majority of moves between cells. If a pipe is found to travel out of a cell through more than one face, which implies that it has gone through an edge or a node, then Method 2, as described below in §3.2.5., is used.

3.2.5.1 Method 1

A function in the UDF facility is used to obtain the cell and cell thread on either side of a face. One of these cells will be the cell that the pipe has come through already and the other will be the cell that the pipe passes through next. This cell is selected and becomes the new “test cell”.

3.2.5.2 Method 2

Since it has been found that the pipe passes through more than one face of a cell, it is not possible to use Method 1 to find out which cell the pipe goes into next. This situation raises several problems similar to the problems that occur if a pipe has either end on a face, edge or node, as is discussed in §3.3.3. If a point along the pipe is in more than one cell, how should the cell be found that the pipe passes through next? It would not pass out of a face of all the cells that the point is in, and to search through all the faces on every cell that it is in would not be efficient.

To simplify these problems, the point at which the pipe passed out of the cells through is abandoned and the UDF finds a new point a short distance away. The set parameters and length scale, L, that were defined in §3.3.3 are used in Method 2. The new point is found by moving the set parameter multiplied by L in each of the x-, y- and z-directions. Setting the parameter is important here, as it helps to ensure that the movement of the point is going to be into a cell closer to the cell the end of the pipe is in, rather than in another direction. Going into a cell in a different direction would not have a great affect on the overall modelling of a pipe, but progress in the correct direction is beneficial for accuracy.

If the new point that is found is in the cell that the pipe has just been found in, then a point the same distance in the opposite direction is chosen, to ensure that the new point is in a different cell. If after moving a point, it is still on an edge or a node of a cell, or has been moved into that position, then the point is moved by the same amount again, until it is in just one cell.

However, if three points along a pipe have had to be moved because the pipe passed through three nodes or edges, then it is possible that the pipe is travelling in a direction such that it will go through an edge or node of every cell it passes through. This is very unlikely with tetrahedral meshes, but is certainly possible for regular hexahedral meshes. Supposing a pipe is travelling in the direction x = y = z through the nodes of cells. If new points are always found by moving the same distance in the x-, y- and z-directions then, then the pipe will still travel through nodes of cells for its whole length. Therefore, different multiples of the set parameter and length scale, L, were chosen in each direction, to off-set the pipe slightly, so that it does not always pass through the nodes of cells, in this and similar situations. The different multiples that were chosen are one times the set parameter multiplied by L in the x-direction, twice the set parameter multiplied by L in the y-direction and three times the set parameter multiplied by L in the z-direction. Moving a point in this way means that the pipe is now travelling in a slightly different direction, and should prevent it from continuously passing through nodes or edges. The distances were chosen randomly, but with the intent of moving a different, but short, distance in each direction. The reason for this is that every time a pipe passes through an edge or a node of a cell, the UDF has to research through every cell in the domain to identify the cell containing the new point and this means that the UDF takes considerably longer to run. It is also better to minimise the number of times that points are moved and the amount they are moved by, as the more they are moved, the less accurate the line of the pipe is. Even if the direction of a pipe is changed slightly by using this method, the new line of the pipe will be between the new point that has been found, and the end point of the pipe, so movement between cells is still towards the end of the pipe.

Once a pipe has been moved in this way once, if further nodes or edges are encountered, the counter for the original method is reset to zero and that method is used again. Although the multiples in each direction are different, they are all still small enough not to have a significant effect on the accuracy of tracking the pipe, but will significantly reduce the time the UDF takes to run. It is very unusual for pipes to travel through a CFD-mesh in this way.

Once a new point is found that is in a different cell to the one that the pipe has just passed through, and wholly within one cell, the cell that the new point is found in becomes the new “test cell” and the UDF starts tracking the pipe again from there. Every time a point is moved, the method described in §3.2.2 is used to identify which cell contains the new point.

3.2.6 Refined regions of Mesh and Hanging Nodes

Method 1, as described in §3.2.5.1, relies each face of the cell the pipe has already been found in, also being a face belonging to one other cell. However, on the edge of a region where the mesh has been refined, hanging nodes are created. This means that one face of a cell on the outside of the refined region is shared with four faces of four cells, in the refined region. Therefore, the function used in Method 1 to find the next cell a pipe passes through breaks down.

The UDF identifies when the border of a region where the mesh has been refined, and uses Method 2, as described in §3.2.5.2, to move into the next cell the pipe passes through. This problem does not occur when the pipe passes out of a refined region, as there is only one face of a cell on the outside of the refined region that is shared, in part, by the face of the cell in the refined region.

If, whilst a CFD-simulation is running, the mesh is refined anywhere, then this UDF needs to be run again, so that the cells in the refined region, that contain the pipes, can be found.

3.2.7 Other Problems and Error Checking

3.2.7.1 Passing Through Axes and the Origin

Pipes passing through faces where the plane of the face is along an axis cause a problem. If all of the x-coordinates, or all of the y-coordinates, or all of the z-coordinates are zero, then the determinants, d_C and d_i will all be zero. Therefore, the test to see if all of d_i are of the same sign as d_C breaks down. To overcome this problem, the coordinates of all the nodes of the cell, the start and end of the pipe and the point of intersection with the plane of the face, are temporarily shifted by one unit whilst the determinants, d_C and d_i are recalculated. Once this recalculation is done, the point of intersection is kept as it was originally and the face that the pipe was found to pass through is correct, since all the coordinates were shifted.

If a node of a face that a pipe passes through is at the origin, then this will cause the determinant of d_C to be zero. Again, the coordinates of all the nodes of the cell, the start and end of the pipe and the point of intersection with the plane of the face, are temporarily shifted by one unit whilst the determinants, d_C and d_i are recalculated.

3.2.7.2 Accuracy

The condition to check whether a point lies within a triangle is described in §3.2.4.2. If a point lies on, or very close to, an edge or a node of a triangle then one or more of the determinants d_i should be equal to zero. However, due to computational inaccuracies, it is possible that the UDF could calculate d_i as being very close to zero, but not equal to zero in this situation. If a point is inside a of the triangle, then all the determinants, d_i, must be of the same sigh as d_C. If the UDF calculates a d_i that should be zero, to be very slightly greater than zero, when all the other determinants are less than zero, or vice versa, then the point will not be found on that face. If this happens on all the faces that the point is located on, then the pipe will not be found to pass through any of the faces of the cell it is in, other than the one is has already come through. To overcome this problem, instead of testing to see if all the determinants, d_i, are the same sign as d_C, the UDF tests to see if they are all either greater than –0.0001 or less than 0.0001. If this level of accuracy is still not enough to find one or more faces that a pipe passes through, then Method 2, as described in §3.2.5.2 is used to find the next cell the pipe passes through.

The same problem arises when checking whether a point lies within a tetrahedron, as is described in §3.2.2.1. To overcome this problem, the UDF tests to see if all the determinants, D_i, are either all greater than –0.0001 or less than 0.0001. If this level of accuracy is still not enough to find one or more cells that the pipe is in, then an error message will appear and the pipe that caused the problem will no longer be tracked.

3.2.7.3 Passing Through Solid Regions or Other Regions With No Mesh

If a pipe either starts or ends in a region that has not been meshed, then the pipe cannot be tracked, as its ends will not be found in any cells. The UDF always starts from one end of the pipe, and uses the other end to make sure the UDF stops tracking the pipe, so both ends of the pipes must be in cells for the UDF to work.

If a pipe passes through a region that has not been meshed, then it can no longer be tracked, as it would be very difficult to know which cell it passes through first after the unmeshed region, without making the UDF extremely time consuming to run. The first time a pipe passes through an unmeshed region, the UDF attempts to track the pipe from the end of the pipe to the start of the pipe. If a pipe only passes through one unmeshed region, the full length of pipe that is in the mesh can be tracked, but if a pipe passes through more than one unmeshed region, then the part or parts of the pipe between these regions will not be found.

Realistically, pipes cannot pass through solid regions, which would not usually be meshed in a CFD simulation, but due to the way in which geometries are often drawn, some pipes may appear to overlap solid regions.

3.2.7.4 Other Potential Problems that Output Error Messages

Throughout the UDF error checks are done to ensure that all the cells the pipes passes through are hexahedrons, triangular prisms, pyramids or tetrahedrons and that all the faces on the cells are either quadrilaterals or triangles. If one of these errors occurs then a message is output to the screen informing the analyst of which pipe has caused the error and the nature of the error. The pipe that caused the error will no longer be tracked and the UDF will move to the next pipe. In theory, none of these errors should occur.

3.2.8 Coefficients for the Source Terms

When CFD simulations are undertaken, source terms representing a resistance to pipework will be added to the momentum equations. The terms will be added on a cell-by-cell basis, and so information regarding the dimensions of the pipes in each cell needs to be stored as the cells are found that the pipes pass through.

The length of pipe in each cell, is found in each direction, and from this the projected length of pipe is calculated in each direction. For example, the length of pipe in the x-direction is calculated by finding the difference between the x-coordinate where the pipe leaves the cell and the x-coordinate where the pipe enters the cell. The lengths of pipe in the y- and z- directions are calculated in the same way. The projected length of pipe in each direction in the square-root of the sum of the lengths in the other two directions, squared. For example, the projected length of pipe in the x-direction is given by,

$$L_{Px} = \sqrt{L_y{}^2 + L_z{}^2} \qquad \text{(Eq. 3.2.36)}$$

L_y and L_z are the lengths of pipe in the y- and z-directions, respectively, and L_{Px} is the projected length of pipe in the x-direction. The projected lengths of pipe in the y- and z-directions are calculated in the same way.

The coefficients, S_{Cx}, S_{Cy} and S_{Cz}, for the source terms for the momentum equations, are given below.

$$S_{Cx} = \frac{\frac{1}{2} C_D L_{Px} D}{V} \qquad \text{(Eq. 3.2.37)}$$

$$S_{Cy} = \frac{\frac{1}{2} C_D L_{Py} D}{V} \qquad \text{(Eq. 3.2.38)}$$

$$S_{Cz} = \frac{\frac{1}{2} C_D L_{Pz} D}{V} \qquad \text{(Eq. 3.2.39)}$$

D is the diameter of the pipe, V is the volume of the cell, and C_D is the drag coefficient for the pipe. If more than one pipe passes through the same cell, the coefficients for the source terms in that cell are added together.

These coefficients are stored in separate memory locations, in the cell User-Defined Memory. Figure (3.2.8) shows an example of the coefficient, S_{Cy}, stored in cells of a regular hexahedral mesh, containing a region where the mesh has been refined, with sub-grid pipework passing through it, as shown in the pipework database in Figure (3.2.1). The colour of the cells is representative of the value of the coefficient, S_{Cy}, that is stored in the cell User-Defined Memory.

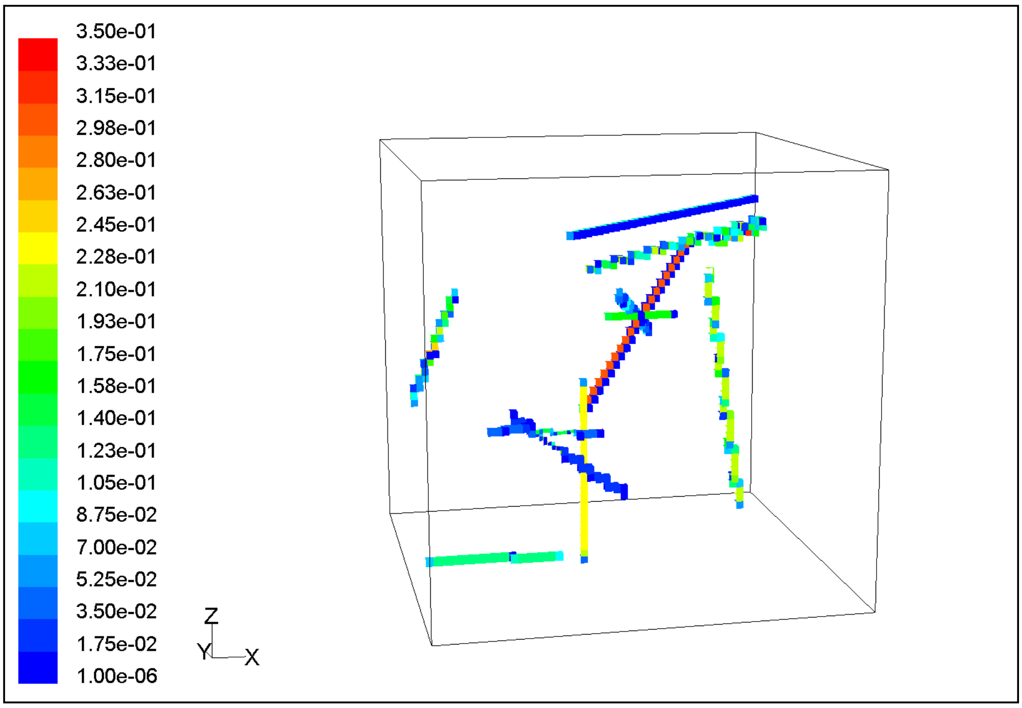

Figure 3.2.1 – The coefficient of the source term for the y-momentum equation, S_y.

Further information on the source terms and drag coefficient can be found in §4.0.

3.3 Discussion

The UDF has been tested on meshes with various shaped cells, refined areas and solid areas. Test pipes have been forced to start or end or both on faces, edges or nodes; pass through edges or node various amounts of times; pass through refined regions in various ways; start or end or both in refined regions; pass through solid areas; start or end or both in solid areas; start or end outside of the domain altogether; pass through the origin and pass through faces in the plane of an axis. The UDF includes checks to find all of these problems, and other potential problems including accuracy (§3.2.7.2) and irregularly shaped cells or faces (§3.2.7.4), and either has methods to overcome them, or prints error messages that stop individual pipes being tracked. If, out of several hundred pipes that are often found on offshore platforms and onshore power plants, a few are not tracked, then this is not usually a problem. It is more important that the UDF continues to run and tracks the majority of pipes.

The efficiency of the UDF, in terms of time, is also important. The function that is the most time consuming is searching through all the cells in the domain to find the cells containing specific points. This is done once, to find the start and end points of each pipe; again if either of these points is on a face, edge or node; again if any point along a pipe passes through an edge or node or enters a refined region of the mesh. The search for the end points of pipes must be done for each pipe, but it is unusual for pipes to start or end on faces edges or nodes, or pass through edges or nodes along the way. Every time a pipe does this, the run-time of the UDF is increased. Occurrences of these situations are most common with regular hexahedral meshes.

If there are any refined regions that introduce hanging nodes into the CFD-mesh, then it is likely that some pipes will pass into these regions, in which case the UDF searches through all the cells in the domain again. Unfortunately, a better test to see when this happens has not been found with the given functions available in the CFD-Solver. This means that the test which is used to find out if a pipe is on the edge of a region of refined cells, actually finds if the face the pipe is passing through is on a different face thread to the previous face that the pipe passes through. The CFD-solver labels different sections of a mesh with different face threads, and so the face thread will sometimes be different even if the pipe is not entering a refined region of the mesh. This means that searches for cells are often done unnecessarily, which considerably increase the run-time of the UDF. As hanging nodes can only occur in quadrilateral faces, this problem does not occur when moving between triangular faces. Ideally a better method should be used to find out if a pipe is passing into a refined region of mesh, but this is not possible at the moment.

If a region of a mesh is refined whilst a CFD simulation is running, then the cells in that area will change, which means that the UDF must be run again for all the pipes in the pipework database. This will add a considerable amount of time to a simulation.

Numerical accuracy has caused some problems with the UDF. The conditions described in §3.2.2.1 to find out whether a point is inside a tetrahedron, and §3.2.4.2 to find out whether a point is inside triangle, mean that small errors in calculations, which are inevitable with any computer program, cause problems with the UDF. This is, in part, overcome by the method described in §3.2.7.2, but ideally this method is not adequate.

If a point on a pipe is moved into another cell, for any reason, then the line of the pipe is changed. This means that different values of source terms could be allocated to cells. The coefficients could be different, if a different length of pipe is in a cell to what it should be, making the allocation of source terms incorrect, or the source terms could be distributed to the wrong cells. Also, the UDF tracks the centre line of each pipe, so if a pipe goes close to the faces of a cell, then it is likely to be in more than one cell at once. It has not been possible to track cells through more than one cell at once in this UDF, due to the complications of the problem. However, even if the UDF was to be extended to do this, more cells would need to be identified for the tracking of each pipe and this is likely to take considerably more time, restricting the efficiency of the UDF. Therefore, a balance must be met between accuracy and efficiency, which is the reason why sub-grid models are used for small objects, such as pipes, and that they are not modelled explicitly within a mesh, even though it is known that this provides more accurate results. Therefore, in this situation, it is reasonably accurate to assume pipes only pass through one cell at a time, and extending the UDF to track pipes passing through more than one cell at a time would not be practical.

4.0 Source Terms

4.1 Navier-Stokes Equations

The steady Navier-Stokes equations for conservation of momentum are given by (Acheson, 1990) (where there is no summation over i).

$$U_j \frac{\partial(\rho U_i)}{\partial x_j} = \frac{\partial P}{\partial x_i} + \mu \frac{\partial^2 U_i}{\partial x_j x_j} + S_i \qquad \text{(Eq. 4.1.1)}$$

U_i and U_j are components of the velocity of the fluid. ρ is the density of fluid in a cell, P is the pressure of fluid in a cell and μ is the dynamic viscosity of the fluid. S_i, where $i = x,\ y$ or z are additional source terms, which include any additional forces acting on the flow. In this work, the source terms were used to allocate a resistance to the flow within those cells through which a pipe segment passed.

4.2 The Source Terms That Have Been Used

Empirical formulae, given by Gilham *et al.* (1999), were used to calculate source terms for the x-, y- and z-momentum equations. The source terms represent the drag, or resistance to the flow due to the pipework, and are calculated in each cell, and on each iteration during a CFD-simulation. The coefficients of the source terms, S_{Cx} (Eq. 3.2.37), S_{Cy} (Eq. 3.2.38) and S_{Cz} (Eq. 3.2.39), are calculated when the cells that the pipes pass through are identified, and are used in the calculation of the source terms. Although the source terms are calculated in every cell, S_{Cx}, S_{Cy} and S_{Cz} are only calculated in cells that the pipes pass through. As they use the length of the pipe in that cell in the calculation, they would be zero in any cell not containing any pipe. If more than one pipe passes through the same cell, then the values of S_{Cx}, S_{Cy} and S_{Cz} that are calculated for each pipe are added together.

The source term for the x-momentum equation is given by,

$$S_x = -S_{Cx}\, \rho U_x \left|U_x\right| \qquad \text{(Eq. 4.2.1)}$$

The source term for the y-momentum equation is given by,

$$S_y = -S_{Cy}\, \rho U_y \left| U_y \right| \qquad \text{(Eq. 4.2.2)}$$

The source term for the z-momentum equation is given by,

$$S_z = -S_{Cz}\, \rho U_z \left| U_z \right| \qquad \text{(Eq. 4.2.3)}$$

ρ is the density of fluid in the cell, U_x, U_y and U_z are components of the velocity of the fluid in the cell in the x-, y- and z-direction respectively.

4.3 The Drag Coefficient

The drag coefficient is used in the calculations of the coefficients for the source terms. It depends on the shape of the object that the flow is passing around, and also on the Reynolds number of the flow, which is given by,

$$\mathrm{Re} = \frac{UD}{\nu} \qquad \text{(Eq. 4.3.1)}$$

where Re is Reynolds number, U is velocity magnitude, D, in this case, is the diameter of the pipes and ν is kinematic viscosity.

In the ACE method the drag coefficient is taken to be 1.2. A graph of drag coefficient for circular cylinders as a function of Reynolds number is shown in the below in Figure 4.2.1. The graph is taken from Schlichting (1987).

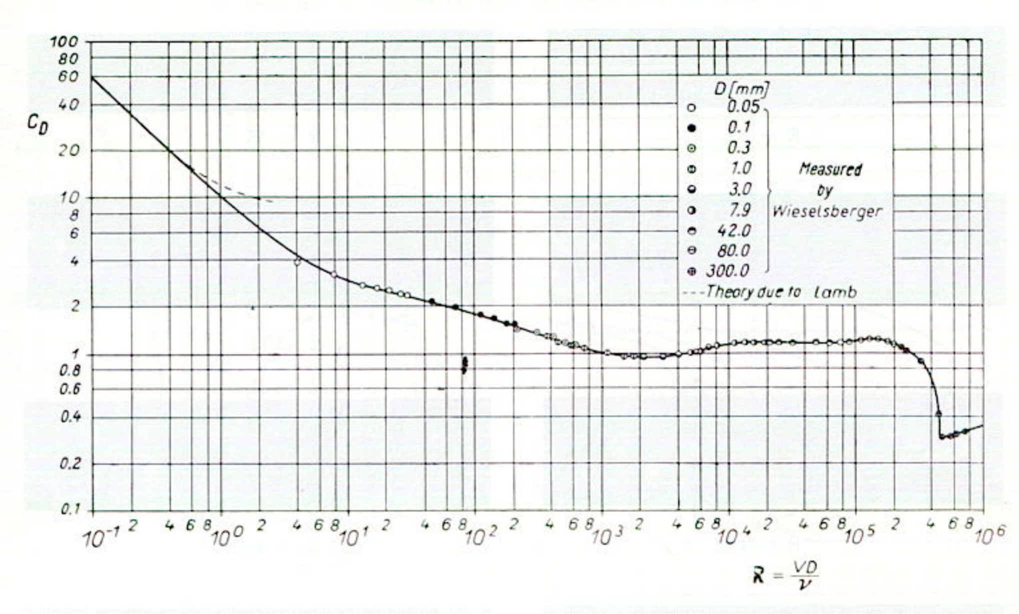

Figure 4.2.1 – Graph of Drag Coefficient for Circular Cylinders as a Function of Reynolds Number

The value of drag coefficient used in the ACE method assumes that the Reynolds number for the flow is somewhere between approximately 3×10^2 and 3×10^5 which is where the drag coefficient is close to 1.2. This covers a wide range of flows, as it covers three orders of magnitude of Reynolds numbers. Therefore, in terms of simplicity this provides a good estimation of the drag coefficient, as there is no need to calculate the Reynolds number. However, transition to turbulent flow occurs at Reynolds numbers of approximately 3×10^5 and for Reynolds numbers higher than this, the drag coefficient drops below 1.2. Choosing a drag coefficient of 1.2 assumes that the flow is laminar, and so for turbulent flows, the drag coefficient used in the ACE method is too high, and the resistance to the flow due to the pipes will be over-predicted. Reynolds numbers lower than 3×10^2 occur with slow flow; when the body the flow is going around is very small, or if the viscosity of the fluid is very high. In each of these cases the drag force from the body is not very large, and so the drag coefficient is not as important.

4.4 Discussion of Source Terms

The source terms that have been added to the momentum equations in the ACE method to represent resistance to the flow due to the pipes, is the standard calculation for drag caused by a cylinder, divided by the cell volume. It will be used for similar purposes to those investigated by Gilham *et al.* (1999), where it was implemented successfully, in the ACE method.

If more than one pipe passes through the same cell, then the contributions of source terms from each pipe are simply added together. However, it was suggested by Ivings *et al.* (2004) and Gilham *et al.* (1999), that the level of congestion caused by the pipes should be taken into account when calculating the source term to represent the drag. They proposed that a large number of small pipes in a region might cause more resistance to the flow than a small number of large pipes in the same region. Gilham *et al.* (1999) also suggested that in highly congested regions, the drag coefficient should be taken to be a function of the blockage ratio, which is the fraction of the cross-sectional area that is closed to the flow (Eq. 2.4.3 and Eq. 2.4.4). Given their suggestions, it is possible that adding a function depending on congestion should be added into the ACE method.

The AutoReaGas Theory Manual and Ivings *et al.* (2004) suggested that source terms could also be added to the k and ε equations to represent turbulence caused by the pipes. However, Ivings *et al.* (2004) suggested that turbulence source terms are not as important as those added to the momentum equations to represent drag. It is proposed that the ACE method will mainly be used in natural ventilation studies, where although turbulence is important, the turbulence generated by the pipework will, in general, not have a significant effect on the results, so source terms for turbulence have not been included in the method. However, if the ACE method was to be used in explosion studies or in natural ventilation studies where turbulence is important then adding suitable source terms to the k and ε equations should be considered. Gilham *et al.* (1999) and Ivings *et al.* (2004) suggested that source terms should also be added to represent heat transfer from the pipes. Under certain circumstances it would probably be beneficial to add these source terms. If the pipework is at a temperature considerably higher than ambient temperature, then the heat transfer to the surrounding fluid could be significant.

5.0 Methods of Validation

5.1 Introduction

The ACE method for modelling sub-grid pipework, has been validated by comparing the results of passing flow through a box containing pipework with those obtained when the pipework is modelled explicitly within the mesh. A considerably finer CFD-mesh was used when the pipes were represented explicitly within the mesh than when the ACE method was used. Results from the ACE method have also been compared to those obtained using the VUR method.

The model that has been set up is shown below in Figure 5.1.1.

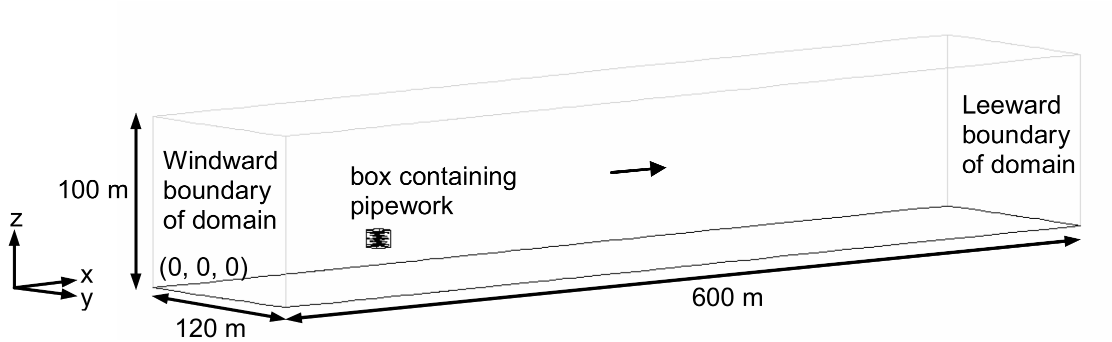

Figure 5.1.1 – Diagrammatic Representation of the Model used for Validation

The box containing pipework, henceforth described as ‘the box’, is 10 m by 10 m by 10 m. Its centre is located 120 m from the origin in the x-direction, 60 m from the origin in the y-direction and 25 m in the z-direction.

Arrangements of pipes go horizontally across the box, and flow, perpendicular to the pipes, is passed through the whole domain, from the windward boundary to the leeward boundary. Figure 5.1.2 shows a close-up view of the box containing the pipes.

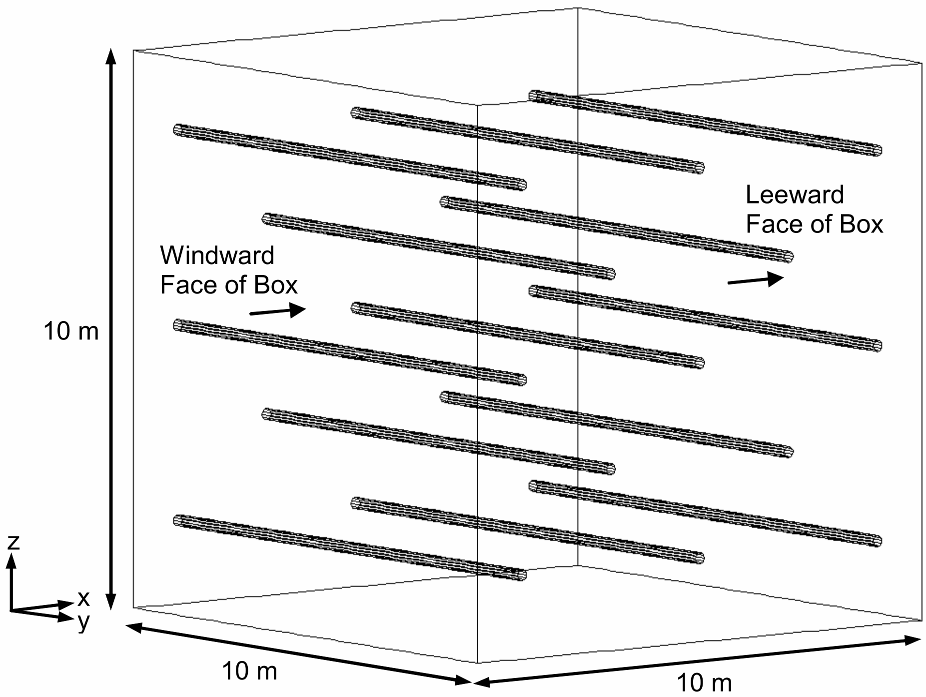

Figure 5.1.2 – Diagrammatic Representation of the Box Containing the Pipework

Two arrangements of pipes were used. The first is a staggered 5 x 5 array, shown in Figure 5.1.3, and the second is a staggered 3 x 5 array, shown in Figure 5.1.4.

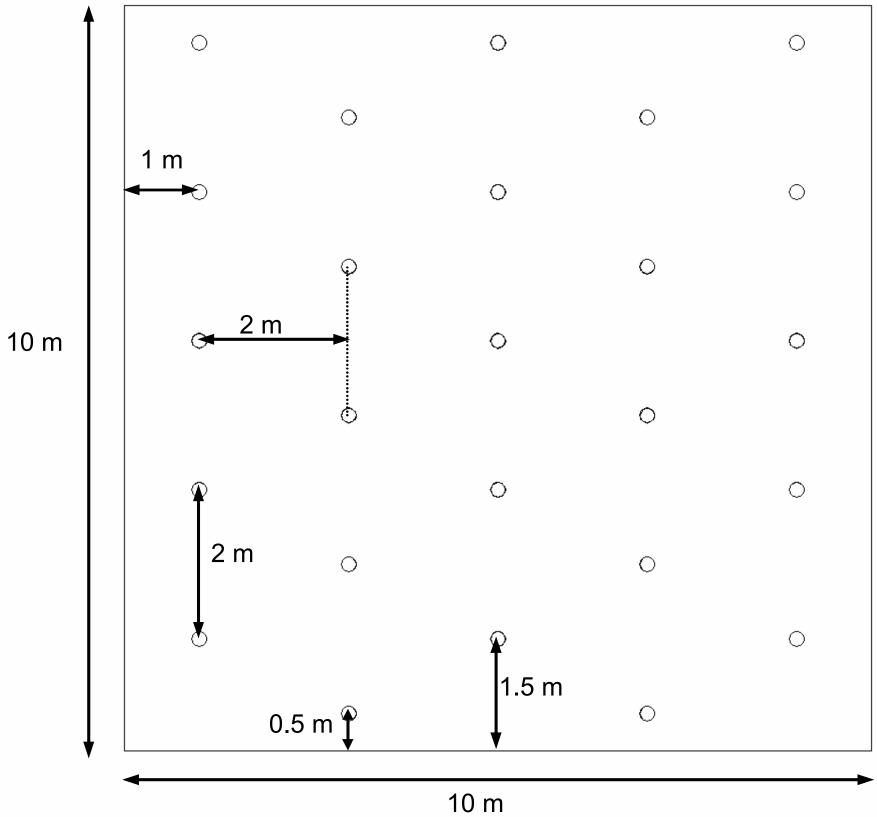

Figure 5.1.3 – Staggered 5 x 5 Array of Pipes

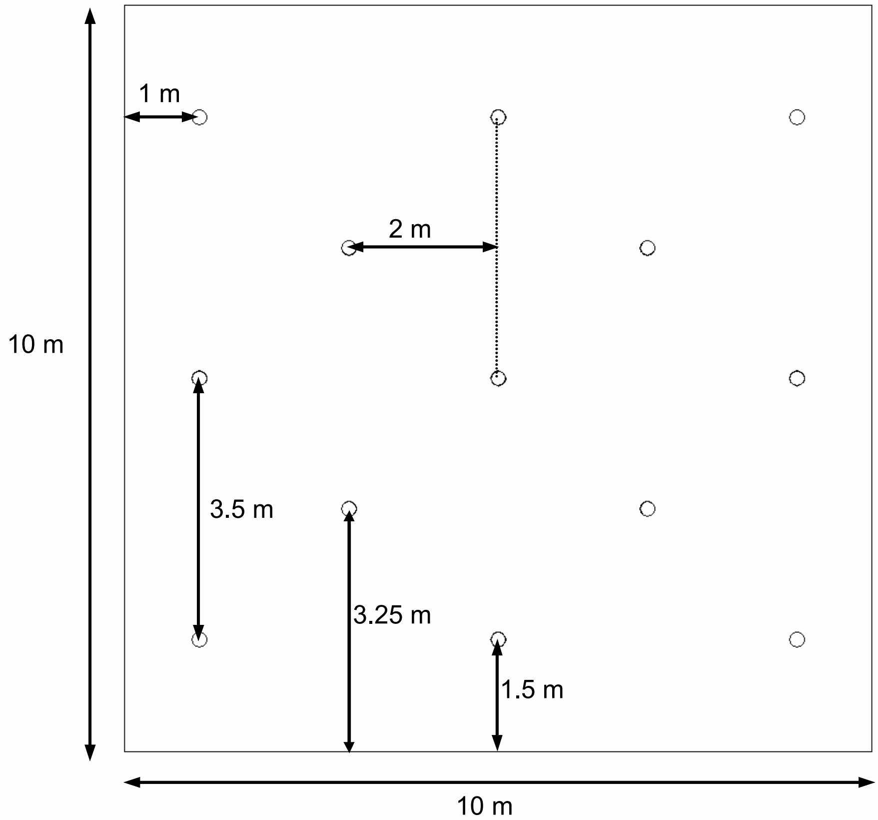

Figure 5.1.4 – Staggered 5 x 3 Array of Pipes

For each arrangement, three different diameters of pipe were investigated. These were 0.4 m, 0.2 m and 0.1 m. For the pipes with a diameter of 0.4 m, a case where the top and bottom walls of the box were removed was also investigated.

The total cell counts for the CFD-Meshes that were used for the cases with the VUR method and the ACE method, and for each configuration of pipes where the pipework was represented explicitly within the mesh are given in Figure 5.1.5.

Arrangement of Pipes	Diameter of Pipes	Total Cell Count
VUR Method and ACE Method	All diameters	171836
5 x 5	0.4 m	1548056
5 x 5	0.2 m	2547556
5 x 5	0.1 m	2706256
5 x 3	0.4 m	1425456
5 x 3	0.2 m	2012056
5 x 3	0.1 m	2010856

Figure 5.1.5 – Table Showing the Total Cell Counts in the CFD-Meshes

For each test case, predictions of the velocity and pressure fields in the box were obtained and the mass flow rate through the box was found.

5.2 The CFD Model

The wind speed was set at 10 m/s and the wind angle was set such that the flow was perpendicular to the length of the pipes. The top, back and front of the whole domain were represented as planes of symmetry and the bottom, which would be the sea on an offshore platform, was represented as a wall. The leeward boundary of the domain was set to be a pressure outlet, and the pressure on this boundary was set to be at atmospheric pressure. All measurements of pressure are relative to atmospheric pressure. The temperature of the air was assumed to be 10°C. The kinematic viscosity of air, ν, is approximately equal to 1.4×10^{-5} kg m^{-1} s^{-1} for this temperature of air (The Engineering Toolbox, (2004)). Therefore, the Reynolds number of the flow, based on the diameter of the pipework, ranges between approximately $\mathrm{Re} = 7.1 \times 10^{4}$ and $\mathrm{Re} = 2.8 \times 10^{5}$. This means that the flow is in the region where the drag coefficient can be approximated by a value of 1.2, as has been taken in the ACE method.

The windward boundary of the domain was set to be a velocity inlet and a model for the atmospheric boundary layer was applied. The incident wind flow through the windward face of the box containing the pipework was specified as a fully developed atmospheric boundary layer, reproducing the characteristics of the wind shear flow over the sea (Item No. 82026, ESDU International, London (1993); Item No. 85020, ESDU International, London (1993)). The variation in wind speed, turbulence kinetic energy and the rate of dissipation of turbulence kinetic energy with height above the water are imposed at the windward boundary of the computational domain and a corresponding sea surface roughness was applied to the base of the domain.

For all of the pipe configurations, a finite-volume discretisation of the Navier-Stokes, energy and turbulence equations were solved using the algebraic multigrid approach of Hutchinson and Raithby (1986). The SIMPLE algorithm of Patankar and Spalding (1972) was used to solve for pressure correction. The third-order accurate QUICK differencing scheme of Leonard (1979) was used to predict the convective terms in the discretised governing equations. The standard k-ε closure (Launder and Spalding, 1974) was used to model the effects of turbulence.

The CFD-Solver used for the validation of the ACE method was the commercial CFD software, Fluent (Version 6.1).

5.3 CFD-Meshes used with the Pipework Represented Explicitly Within the Mesh

Different meshes were used for every diameter of pipe and both arrangements of pipes. In the representations of pipes with diameters of 0.4 m and 0.2 m, the pipes are represented with dodecagon-shaped cross-sections and in the representations of pipes with diameters of 0.1 m, the pipes are represented with octagon-shaped cross-sections. The more sides the pipes are given in the representation, the more accurate they are, but representing the pipes with 0.1 m diameters with dodecagon-shaped cross-sections would increase the cell count over the whole domain beyond the number of cells that the computer can solve over in a reasonable amount of time. In every case, the side walls of the box have a triangular mesh around the ends of the pipes, which reaches a 0.2 m spacing at the edges of the box. The top, bottom, front and back of the box have a square mesh with a 0.2 m spacing. The box is meshed using the Cooper Scheme, using the sides of the box as sources. As an example, a close-up view of the mesh around a pipe with a diameter of 0.2 m is shown in Figure 5.3.1, below.

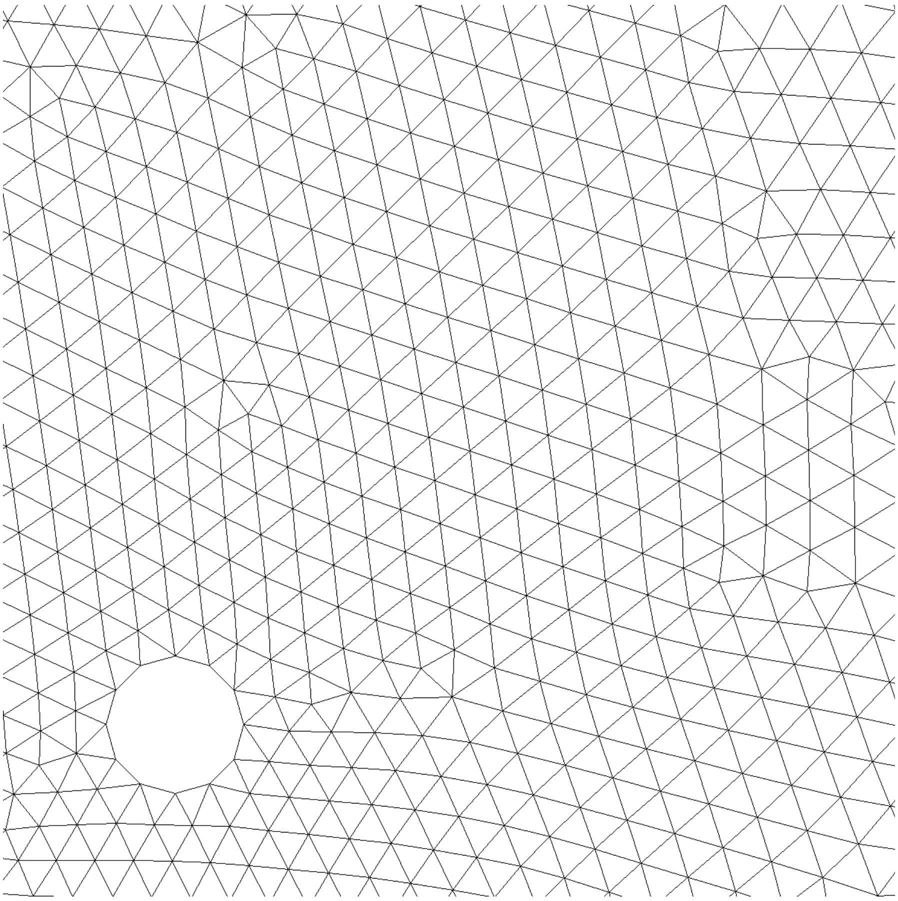

Figure 5.3.1 – Close-up View of the CFD-Mesh Around a Pipe Represented Explicitly the Mesh

For the region on the outside of the box, the sides of the box have a 0.2 m square mesh. The meshes for the box and the outside region do not match up on the sides of the box, but this does not matter as no fluid passes through the sides of the box in any of the cases. For the rest of the domain, in each case, a regular hexahedral mesh has been used, increasing in size away from the box. The meshes in the box are different for each case when the pipes are represented explicitly within the mesh, but the mesh in the rest of the domain is the same in each case. This is shown in Figure 5.3.2.

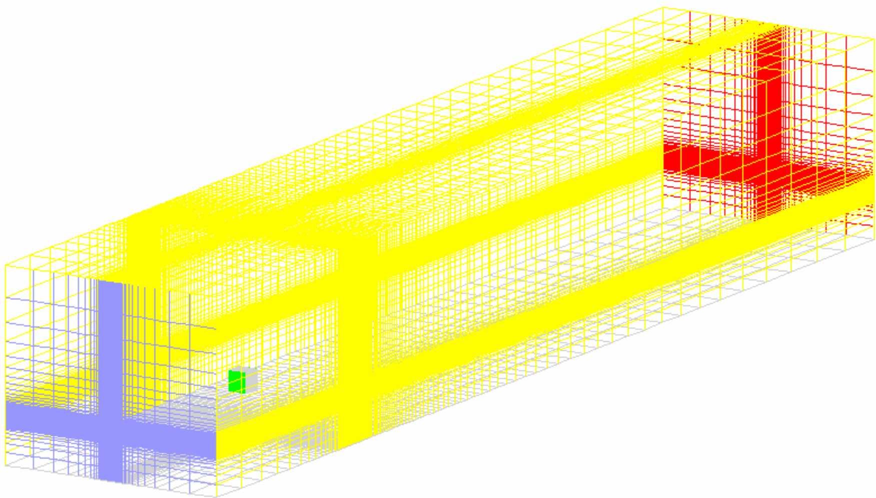

Figure 5.3.2 – CFD-Mesh over the Domain

The mesh is shown on a plane through y = 60 in Figure 5.3.3.

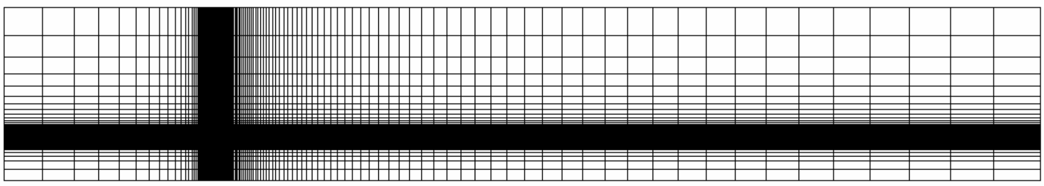

Figure 5.3.3 – CFD-Mesh on a Plane through the Domain

The meshes for the box, with the staggered arrangement of the 5 x 5 array of pipes and diameters of 0.4 m, 0.2 m and 0.1 m, are shown on a plane through y = 60, in Figures 5.3.4, 5.3.5 and 5.3.6, respectively.

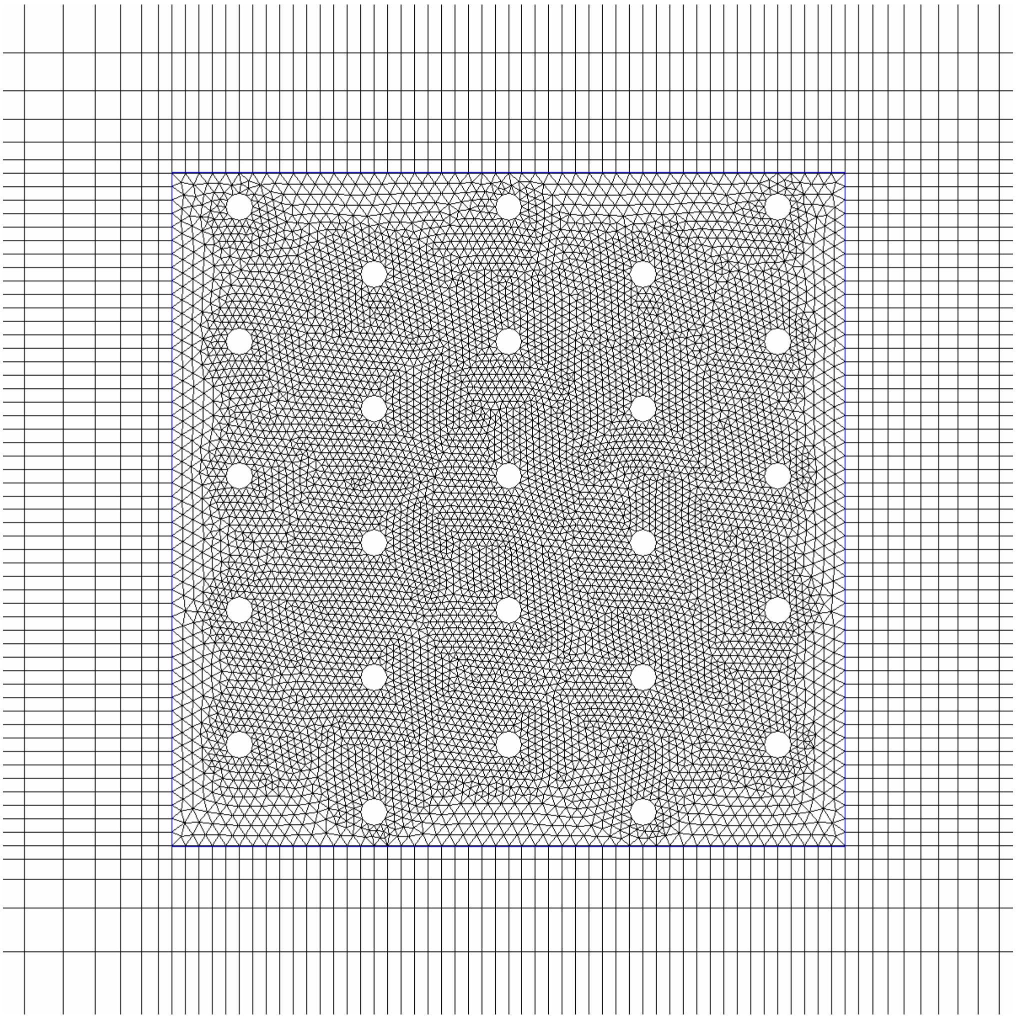

Figure 5.3.4 – CFD-Mesh on a Plane through the Box. 5 x 5 Array of Pipes, 0.4 m Diameter

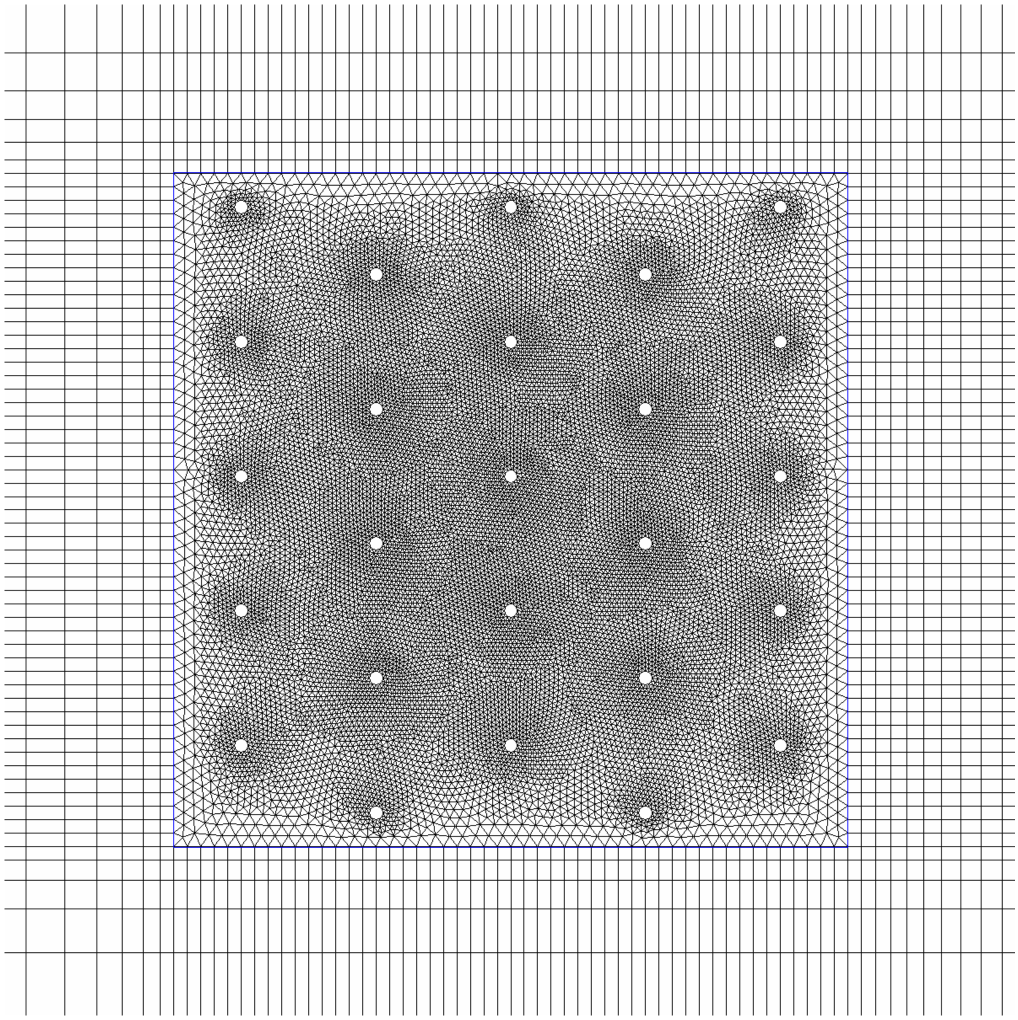

Figure 5.3.5 – CFD-Mesh on a Plane through the Box. 5 x 5 Array of Pipes, 0.2 m Diameter

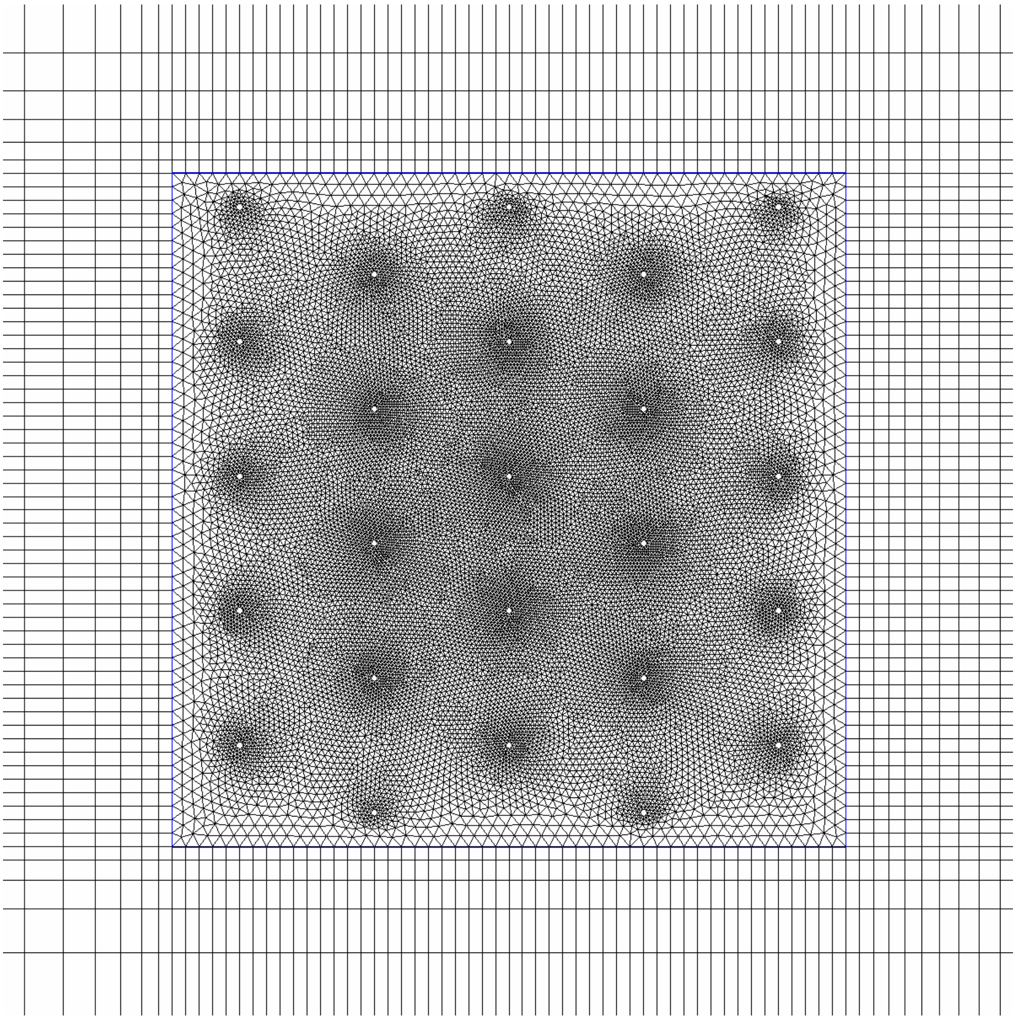

Figure 5.3.6 – CFD-Mesh on a Plane through the Box. 5 x 5 Array of Pipes, 0.1 m Diameter

The meshes for the box, with the staggered arrangement of the 5 x 3 array of pipes and diameters of 0.4 m, 0.2 m and 0.1 m, are shown on a plane through y = 60, in Figures 5.3.7, 5.3.8 and 5.3.9, respectively.

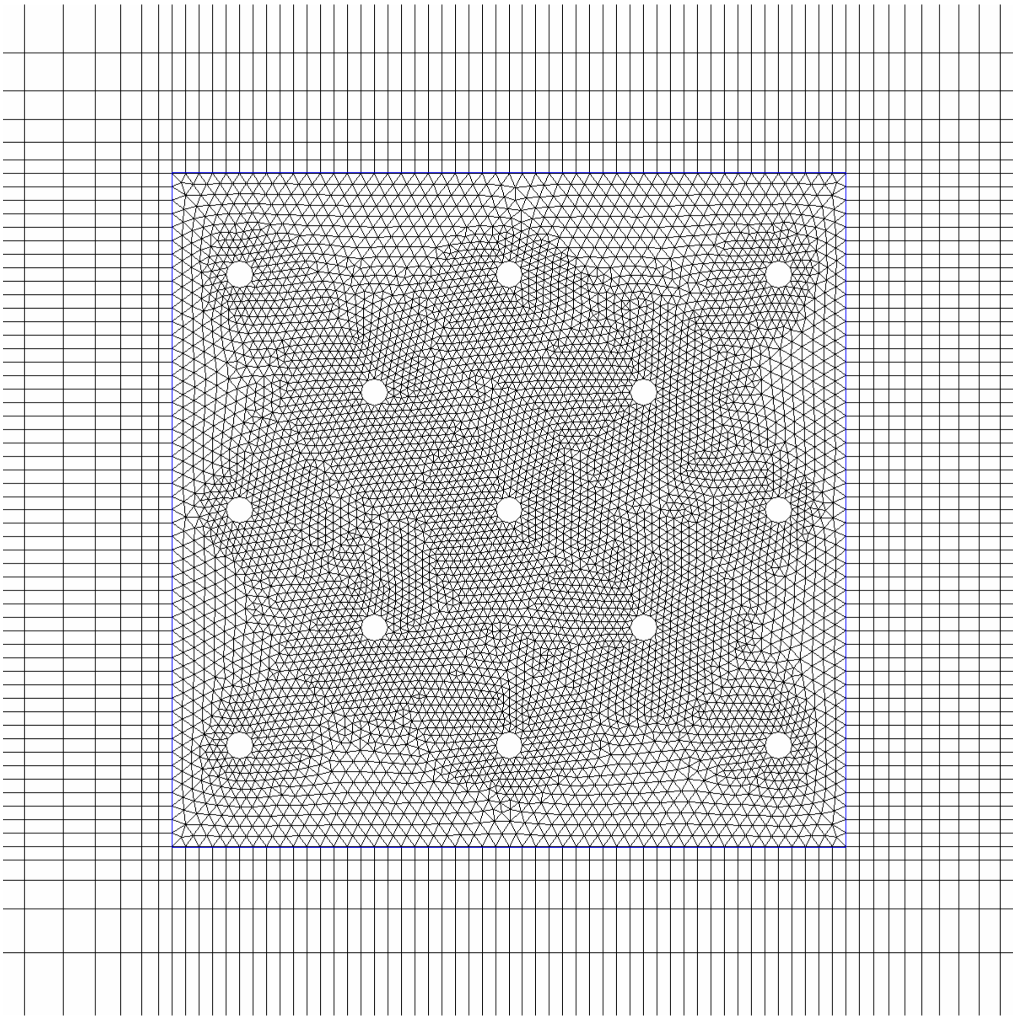

Figure 5.3.7 – CFD-Mesh on a Plane through the Box. 5 x 3 Array of Pipes, 0.4 m Diameter

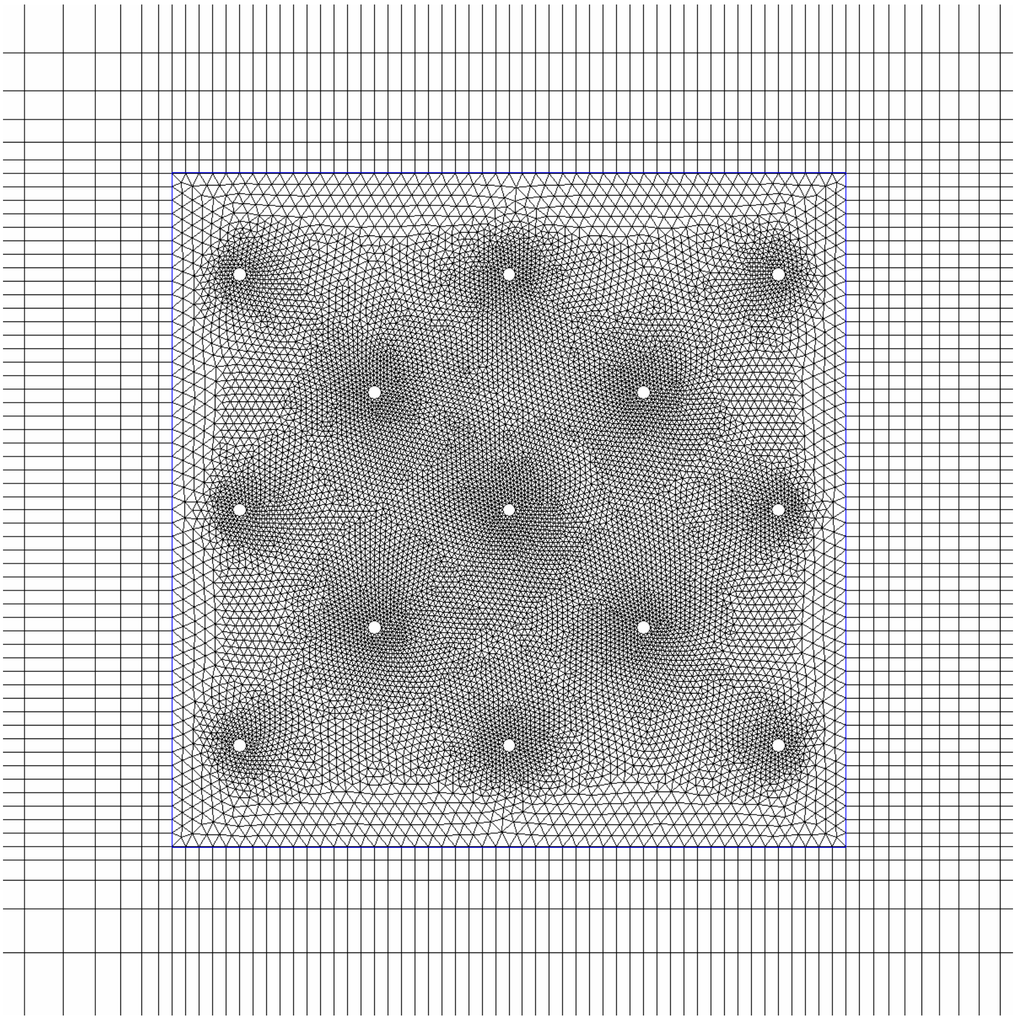

Figure 5.3.8 – CFD-Mesh on a Plane through the Box. 5 x 3 Array of Pipes, 0.2 m Diameter

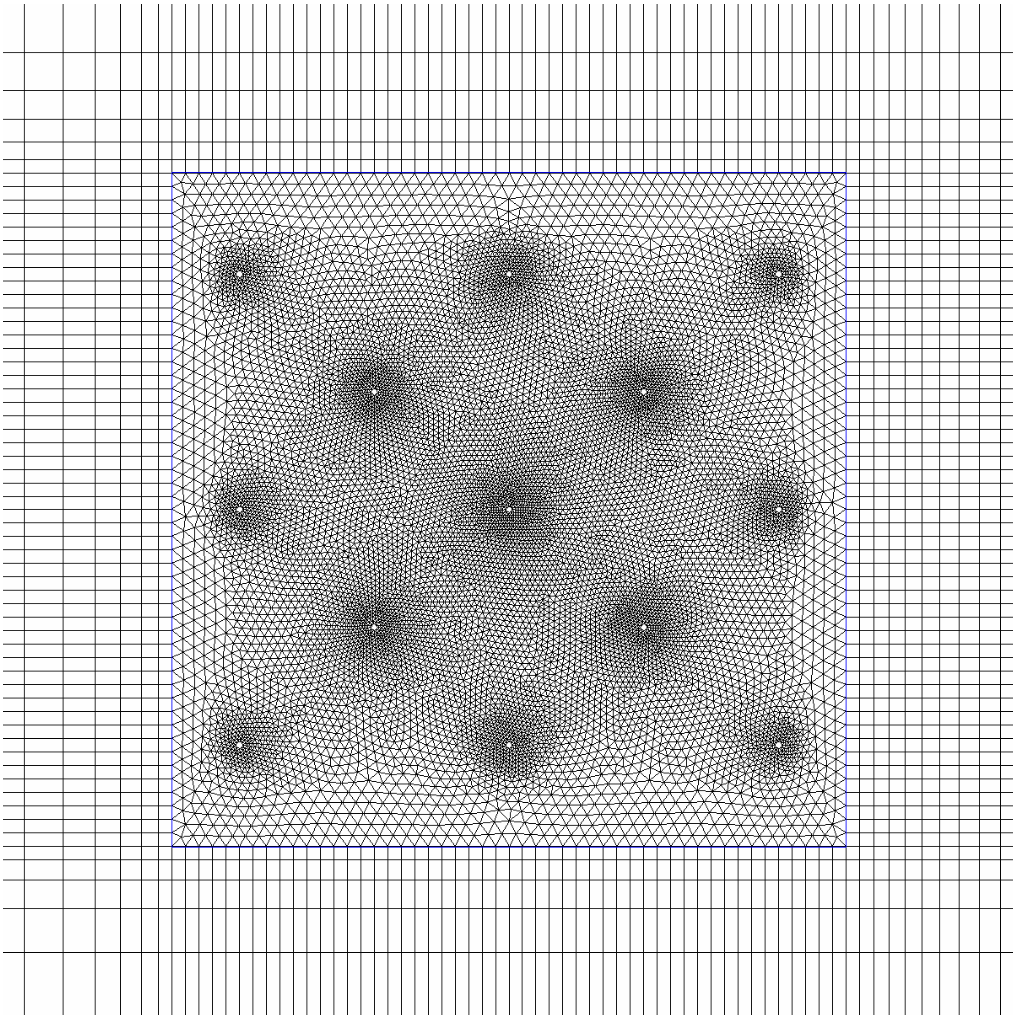

Figure 5.3.9 – CFD-Mesh on a Plane through the Box. 5 x 3 Array of Pipes, 0.1 m Diameter

5.4 CFD-Mesh used with the VUR Method and ACE Method

The same CFD-mesh was used in all cases with the VUR method and ACE method. A regular hexahedral mesh was used in the box, with a grid spacing of 1 m. In the rest of the domain, a regular hexahedral mesh was used, increasing in size away from the box by using the first length method. The mesh over the whole domain is shown in Figure 5.4.1.

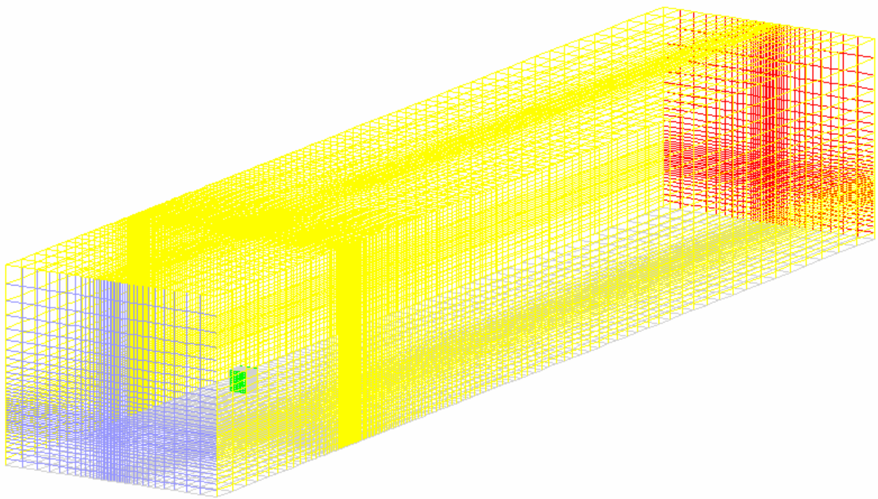

Figure 5.4.1 – CFD-Mesh over the Domain

The mesh is shown on a plane through y = 60 in Figure 5.4.2.

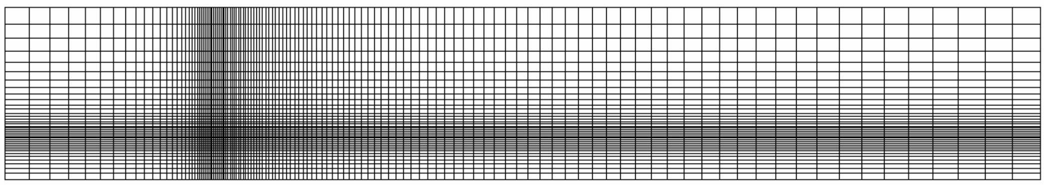

Figure 5.4.2 – CFD-Mesh on a Plane through the Domain

The mesh in the box is shown on a plane through y = 60, in Figure 5.4.3.

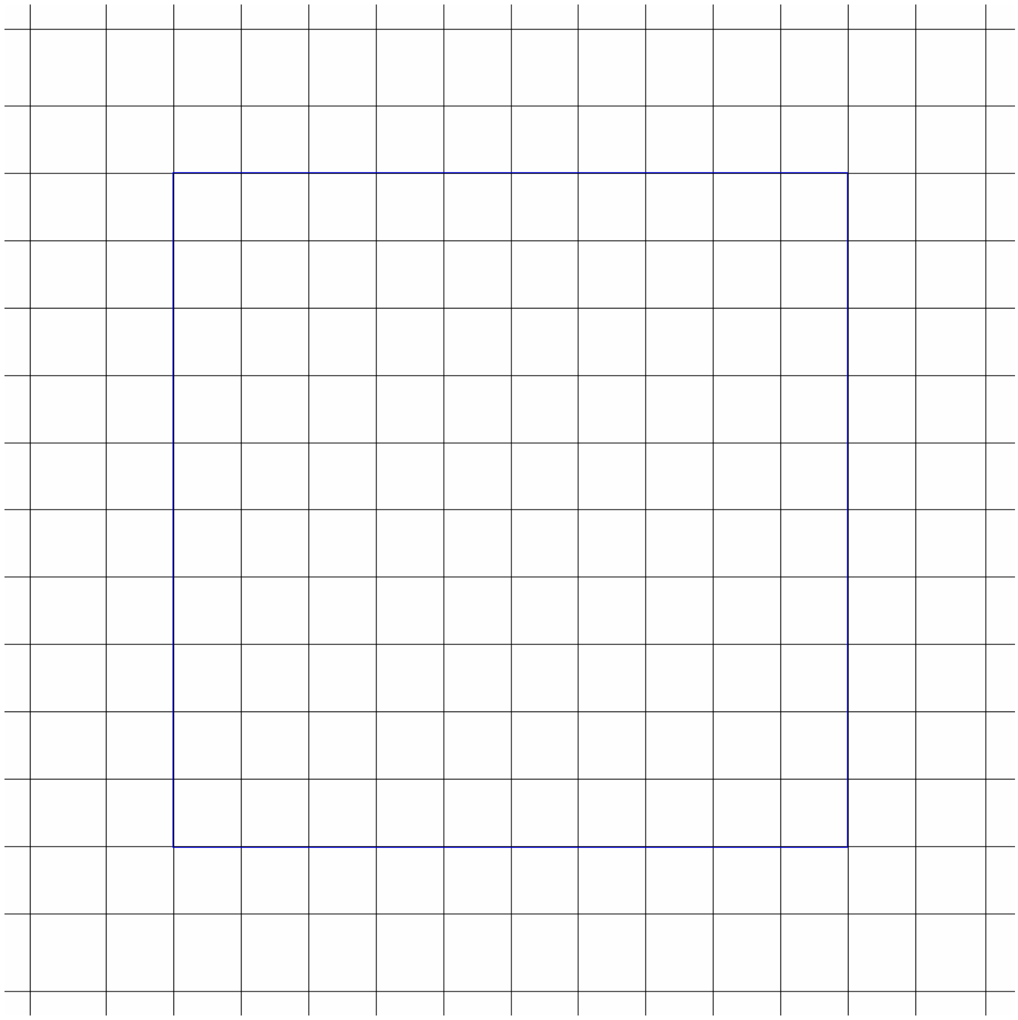

Figure 5.4.3 – CFD-Mesh on a Plane through the Box

6.0 Results

6.1 Introduction

For each of the arrangements of pipes, it was observed that their presence caused the mass flow rate through the box to decrease. All the arrangements caused a build up of pressure around the windward face of the box, and the pressure decreased as the flow went through the box. It was found that the degree of alteration to the flow depends on the number of pipes and their diameters.

When the pipes were represented explicitly in the computational mesh, a lot of detail in the flow is visible around each of the individual pipes. Localised peaks of pressure and velocity are visible close to each pipe, and slow flow was observed in the wakes behind each pipe.

When the VUR method was used to represent the pipes, there is no evidence of individual pipes, which is due to the constraints of the method. Only average values of velocity and pressure were visible across the box.

With the ACE method, some evidence of individual pipes is visible in many of the predicted pressure and velocity fields. Local regions of high pressure close to the locations of pipes are visible in the pressure fields and local acceleration and deceleration of the flow close to pipes is visible in the velocity fields.

Plots of the predicted velocity and pressure fields, along with the residual plots of the convergence history for each configuration of pipes are shown in Appendix 1. These are shown for the explicit representation of pipes, the VUR method with pipe spacings of 1 m and 2 m, and the ACE method. Plots of the predicted pressure field are also shown in §6.2 and §6.3, for easy comparison between the methods used to represent pipework. The mass flow rates through the box are shown in graphs for each diameter of pipe, in §6.2.5 and §6.3.5, along with tables for the cases where the top and bottom surfaces of the box were excluded.

6.2 Benchmark A – 5 x 5 Arrangement of Pipes

6.2.1 0.4 m Diameter Pipework

The pressure profiles predicted for flow through the box containing pipework in the 5 x 5 arrangement, with diameters of 0.4 m, are shown in Figure 6.2.1. Figure 6.2.1(a) shows the pressure profile when the explicit representation of pipes was used; Figures 6.2.1(b) and 6.2.1(c) show the pressure profiles when the VUR method was used, with pipe spacings of 1 m and 2 m, respectively; Figure 6.2.1(d) shows the pressure profile when the ACE method was used. The profiles were obtained using the QUICK differencing scheme.

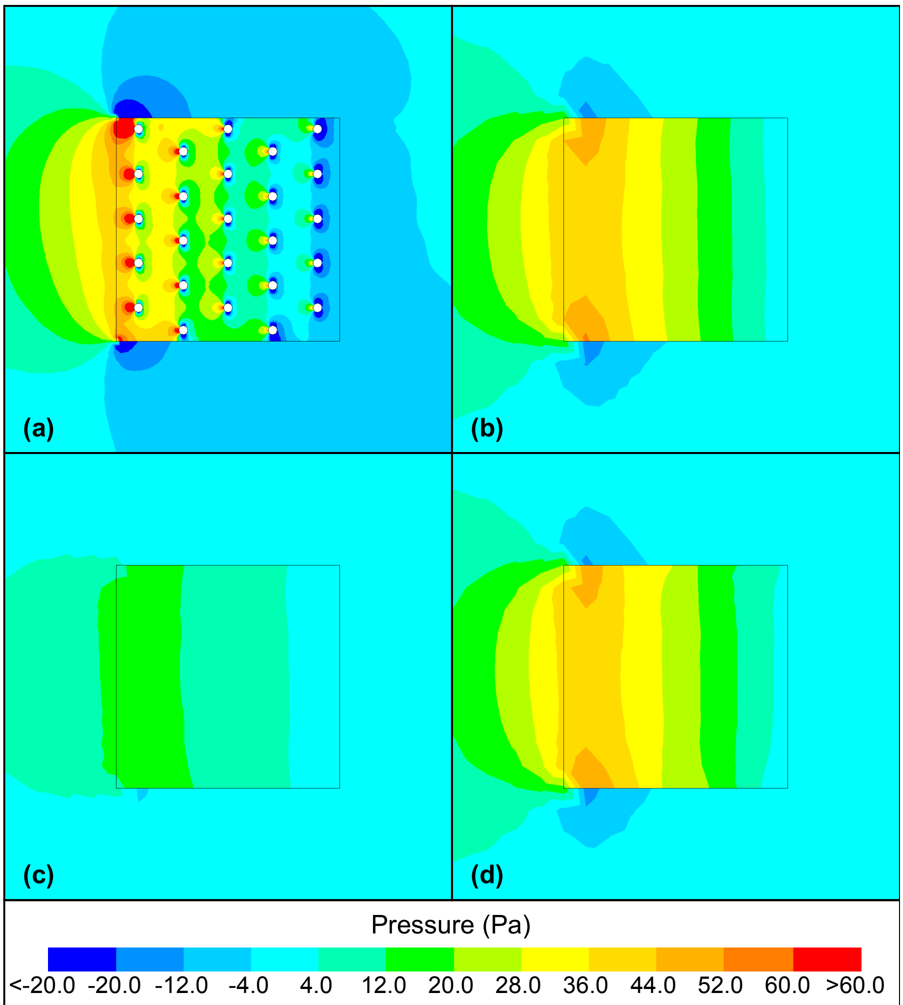

Figure 6.2.1 – Pressure Profiles obtained for the 5 x 5 Arrangement of Pipes with Diameters of 0.4.

(a) Explicit Representation (b) VUR Method, 1 m Pipe Spacing

(c) VUR Method, 2 m Pipe Spacing (d) ACE Method

The velocity profiles predicted for flow through the box containing pipework in the 5 x 5 arrangement, with diameters of 0.4 m, are shown in Figure 6.2.1V. Figure 6.2.1V(a) shows the pressure profile when the explicit representation of pipes was used; Figures 6.2.1V(b) and 6.2.1V(c) show the pressure profiles when the VUR method was used, with pipe spacings of 1 m and 2 m, respectively; Figure 6.2.1V(d) shows the pressure profile when the ACE method was used. The profiles were obtained using the QUICK differencing scheme.

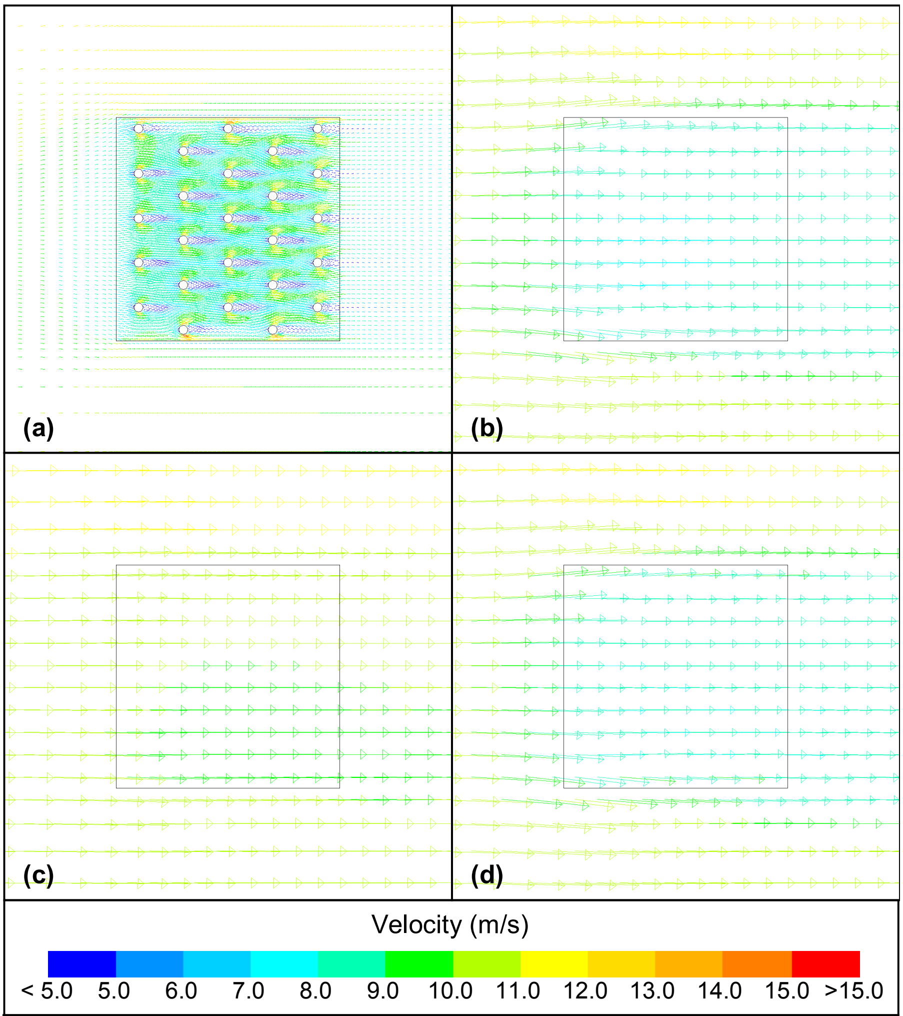

Figure 6.2.1V – Velocity Profiles obtained for the 5 x 5 Arrangement of Pipes with Diameters of 0.4 mm.

(a) Explicit Representation (b) VUR Method, 1 m Pipe Spacing

(c) VUR Method, 2 m Pipe Spacing (d) ACE Method

With the 5 x 5 arrangement modelled explicitly within the computational mesh, the CFD-prediction for the mass flow rate through the tube bundle was equal to 961.63 kg/s. The CFD-prediction for the pressure field for this case (Figure 6.2.1(a)) shows a localised peak of pressure at the leading edge of each of the individual pipes. For the pipes in the windward column, the localised peaks of pressure were approximately equal to 60 Pa. When averaged over the windward face, the predicted pressure was of the order of 40 Pa. Likewise, when averaged over the leeward face, the predicted pressure was roughly equal to -16 Pa. The predicted velocity vector plot for this case, (Figure 6.2.1V(a)), shows acceleration around the individual pipes. A local flow velocity of about 15 m/s was predicted as the flow accelerated around the windward column of pipes. In the wakes behind the windward pipes, the velocity was roughly equal to 5 m/s.

Using the VUR method to represent the pipework, for this pipe configuration, with a pipe spacing of 1 m, the CFD-prediction for the mass flow rate was equal to 1022.09 kg/s, which is considerably higher than that predicted with the explicit representation of pipes. The average pressure over the windward face (Figure 6.2.1(b)) was about 40 Pa, which is similar to the CFD-prediction with the explicit representation. The averaged pressure over the leeward face was roughly 0 Pa. This is not as low as the CFD-prediction using the explicit representation. No detail of flow around individual pipes is shown in the predicted velocity vector plot for this case, Figure 6.2.1V(b), or in the predicted pressure field.

Using the VUR method with a pipe spacing of 2 m, the CFD-prediction for the mass flow rate was equal to 1236.68 kg/s, which is significantly higher than that predicted with the explicit representation of pipes, and considerably worse than with a pipe spacing of 1 m. The average pressure over the windward face (Figure 6.2.1(c)) was between 12 and 20 Pa, which is a lot lower than the CFD-prediction using the explicit representation. The pressure averaged over the leeward face was approximately 0 Pa. This is not as low as the CFD-prediction using the explicit representation. No detail of flow around individual pipes is shown in the predicted velocity vector plot for this case, Figure 6.2.1V(c), or in the predicted pressure field.

The VUR-prediction with a pipe spacing of 1 m was better than the 2 m pipe spacing for this case, since the mass flow rate and pressure field predictions are closer to those predicted with the explicit representation of pipes.

When the ACE method was used to represent the pipes, the CFD-prediction of the mass flow rate was equal to 1068.76 kg/s. This is considerably higher than the prediction with the explicit representation of pipes, and is also higher than the prediction using the VUR method for a pipe spacing of 1 m. The CFD-predictions for the pressure field and velocity field, when using the ACE method, are presented in Figures 6.2.1(d) and 6.2.1V(b), respectively. The pressure averaged over the windward face was roughly 36 Pa, which is reasonably close to the prediction with the explicit representation. The pressure averaged over the leeward face was about 0 Pa, which is similar to the predictions using the VUR method, but not as low as the prediction with the explicit representation. Some evidence of individual pipes is visible in Figure 6.2.1(d), particularly close to the top and bottom of the box, in terms of higher pressures being visible close the pipes. No evidence of individual pipes is visible in the predicted velocity field. The predicted pressure and velocity fields with the ACE method and the VUR method, with a pipe spacing of 1 m, are very similar to each other.

For this particular case, the CFD-predictions using the VUR method with a pipe spacing of 1 m came closest to the CFD-predictions using the explicit representation of pipes, and the CFD-predictions using the ACE method were only slightly worse. However, the VUR method for both pipe spacings and the ACE method all considerably under-predicted the resistance to the flow due to the pipe-work. The VUR method with a pipe spacing of 2 m is not a suitable method here.

6.2.2 0.2 m Diameter Pipework

The pressure profiles predicted for flow through the box containing pipework in the 5 x 5 arrangement, with diameters of 0.2 m, are shown in Figure 6.2.2. Figure 6.2.2(a) shows the pressure profile when the explicit representation of pipes was used; Figures 6.2.2(b) and 6.2.2(c) show the pressure profiles when the VUR method was used, with pipe spacings of 1 m and 2 m, respectively; Figure 6.2.2(d) shows the pressure profile when the ACE method was used. The profiles were obtained using the QUICK differencing scheme.

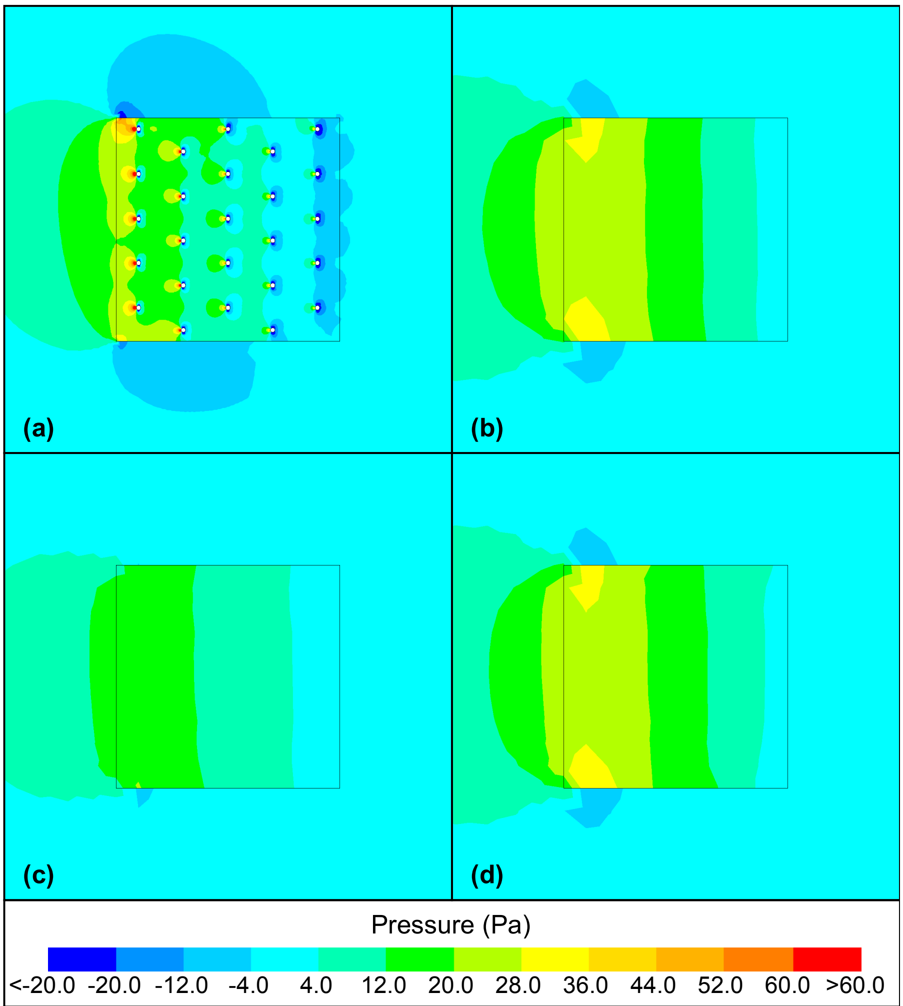

Figure 6.2.2 – Pressure Profiles obtained for the 5 x 5 Arrangement of Pipes with Diameters of 0.2 mm.

(a) Explicit Representation (b) VUR Method, 1 m Pipe Spacing

(c) VUR Method, 2 m Pipe Spacing (d) ACE Method

With the 5 x 5 arrangement of pipework, with diameters of 0.2 m, modelled explicitly within the computational mesh, the CFD-prediction for the mass flow rate through the tube bundle was equal to 1157.06 kg/s. The CFD-prediction for the pressure field for this case (Figure 6.2.2(a)) shows a localised peak of pressure at the leading edge of each of the individual pipes. When averaged over the windward face, the predicted pressure was around 24 Pa. Likewise, when averaged over the leeward face, the predicted pressure was roughly equal to -4 Pa. The predicted velocity vector plot for this case, (Appendix 1, Figure 1.2.1(a)), shows acceleration around the individual pipes and slow flow in the wakes behind them.

Using the VUR method to represent the pipework, for this pipe configuration, with a pipe spacing of 1 m, the CFD-prediction for the mass flow rate was equal to 1146.92 kg/s, which is only marginally lower than that predicted with the explicit representation of pipes. The average pressure over the windward face (Figure 6.2.2(b)) was about 24 Pa, which is comparable with the CFD-prediction with the explicit representation. The averaged pressure over the leeward face was roughly 0 Pa. This is not quite as low as the CFD-prediction using the explicit representation. No detail of flow around individual pipes is shown in the predicted velocity vector plot for this case, Appendix 1, Figure 1.10.1(a), or in the predicted pressure field.

Using the VUR method with a pipe spacing of 2 m, the CFD-prediction for the mass flow rate was equal to 1227.86 kg/s, which is considerably higher than that predicted with the explicit representation of pipes, and significantly worse than with a pipe spacing of 1 m. The average pressure over the windward face (Figure 6.2.2(c)) was between 12 and 20 Pa, which is slightly lower than the CFD-prediction using the explicit representation. The pressure averaged over the leeward face was about 0 Pa. This is not quite as low as the CFD-prediction using the explicit representation. No detail of flow around individual pipes is shown in the predicted velocity vector plot for this case, Appendix 1, Figure(1.10.2(a), or in the predicted pressure field.

The VUR-prediction with a pipe spacing of 1 m was better than the 2 m pipe spacing for this case, since the mass flow rate and pressure field predictions are closer to those predicted with the explicit representation of pipes.

When the ACE method was used to represent the pipes, the CFD-prediction of the mass flow rate was equal to 1169.42 kg/s. This is only marginally higher than the prediction with the explicit representation of pipes and the error is similar to that predicted using the

VUR method for a pipe spacing of 1 m. The CFD-prediction for the pressure field, when using the ACE method, is presented in Figure 6.2.2(d). The pressure averaged over the windward face was roughly 24 Pa, which is comparable with the predictions with the explicit representation and the VUR method with a pipe spacing of 1 m. The pressure averaged over the leeward face was about 0 Pa, which is similar to the predictions using the VUR method, but not quite as low as the prediction with the explicit representation. Some evidence of individual pipes is visible in Figure 6.2.2(d), particularly close to the top and bottom of the box, in terms of higher pressures being visible close to the pipes. The CFD-prediction for the velocity field, when using the ACE method, is presented in Appendix 1, Figure 1.2.2(a). No evidence of individual pipes is visible here. The predicted pressure and velocity fields with the ACE method and the VUR method, with a pipe spacing of 1 m, are very similar to each other.

For this particular case, the CFD-predictions using the ACE method and VUR method with a pipe spacing of 1 m are both close to the CFD-predictions using the explicit representation of pipes, providing reasonably accurate predictions of the resistance to the flow due to the pipework. The CFD-predictions from the VUR method with a pipe spacing of 2 m under-predicted the resistance to the flow due to the pipes, suggesting that this method was not suitable here.

6.2.3 0.1 m Diameter Pipework

The pressure profiles predicted for flow through the box containing pipework in the 5 x 5 arrangement, with diameters of 0.1 m, are shown in Figure 6.2.3. Figure 6.2.3(a) shows the pressure profile when the explicit representation of pipes was used; Figures 6.2.3(b) and 6.2.3(c) show the pressure profiles when the VUR method was used, with pipe spacings of 1 m and 2 m, respectively; Figure 6.2.3(d) shows the pressure profile when the ACE method was used. The profiles were obtained using the QUICK differencing scheme.

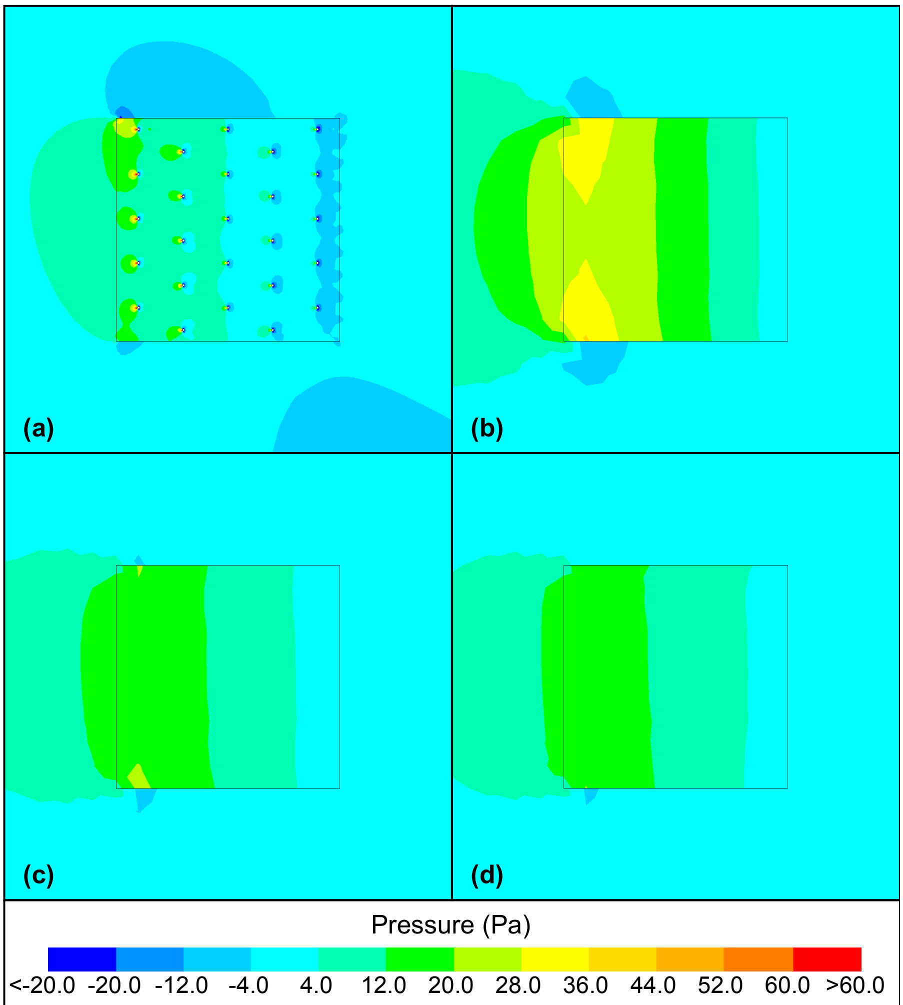

Figure 6.2.3 – Pressure Profiles obtained for the 5 x 5 Arrangement of Pipes with Diameters of 0.1 m.

(a) Explicit Representation (b) VUR Method, 1 m Pipe Spacing

(c) VUR Method, 2 m Pipe Spacing (d) ACE Method

With the 5 x 5 arrangement of pipework, with diameters of 0.1 m, modelled explicitly within the computational mesh, the CFD-prediction for the mass flow rate through the tube bundle was equal to 1232.33 kg/s. The CFD-prediction for the pressure field for this case (Figure 6.2.3(a)) shows a localised peak of pressure at the leading edge of each of the individual pipes. When averaged over the windward face, the predicted pressure was around 12 Pa. Likewise, when averaged over the leeward face, the predicted pressure was roughly equal to -4 Pa. The predicted velocity vector plot for this case, (Appendix 1, Figure 1.3.1(a), shows acceleration around the individual pipes and slow flow in the wakes behind them.

Using the VUR method to represent the pipework, for this pipe configuration, with a pipe spacing of 1 m, the CFD-prediction for the mass flow rate was equal to 1131.56 kg/s, which is significantly lower than that predicted with the explicit representation of pipes. The average pressure over the windward face (Figure 6.2.3(b)) was about 28 Pa, which is notably higher than the CFD-prediction with the explicit representation. The averaged pressure over the leeward face was roughly 0 Pa. This is not quite as low as the CFD-prediction using the explicit representation. No detail of flow around individual pipes is shown in the predicted velocity vector plot for this case, Appendix 1, Figure 1.11.1(a), or in the predicted pressure field.

Using the VUR method with a pipe spacing of 2 m, the CFD-prediction for the mass flow rate was equal to 1218.13 kg/s, which is only marginally lower than that predicted with the explicit representation of pipes, and considerably better than with a pipe spacing of 1 m. The average pressure over the windward face (Figure 6.2.3(c)) was between 12 and 20 Pa, which is slightly higher than the CFD-prediction using the explicit representation. The pressure averaged over the leeward face was about 0 Pa. This is not quite as low as the CFD-prediction using the explicit representation. No detail of flow around individual pipes is shown in the predicted velocity vector plot for this case, Appendix 1, Figure 1.11.2(a), or in the predicted pressure field.

The VUR-prediction with a pipe spacing of 2 m was better than the 1 m pipe spacing for this case, since the mass flow rate and pressure field predictions are closer to those predicted with the explicit representation of pipes.

When the ACE method was used to represent the pipes, the CFD-prediction of the mass flow rate was equal to 1237.95 kg/s. This is very close to the prediction with the explicit representation of pipes and better than both predictions with the VUR method. The CFD-prediction for the pressure field, when using the ACE method, is presented in Figure 6.2.3(d). The pressure averaged over the windward face was between 12 and 20 Pa, which is slightly higher than the predictions with the explicit representation but similar to the VUR-prediction with a pipe spacing of 2 m. The pressure averaged over the leeward face was about 0 Pa, which is similar to the predictions using the VUR method, but not quite as low as the prediction with the explicit representation. Slight evidence of individual pipes is visible in Figure 6.2.3(d) close to the top of the box, in terms of higher pressures being visible close to the pipes. The CFD-prediction for the velocity field, when using the ACE method, is presented in Appendix 1, Figure 1.3.2(a). Some evidence of individual pipes is also visible here, in terms of local acceleration close to the pipes.

For this particular case, the CFD-predictions using the ACE method are closest to the CFD-predictions using the explicit representation of pipes, and provide reasonably accurate predictions of the resistance to the flow due to the pipework. The CFD-predictions from the VUR method with a pipe spacing of 2 m are reasonably close to the CFD-predictions using the explicit representation, but not quite as accurate as the predictions with the ACE method. However, the VUR method with a pipe spacing of 1 m over-predicted the resistance to the flow due to the pipes, suggesting that this method was not suitable in this case.

6.2.4 0.4 m Diameter Pipework, Top and Bottom Surfaces of Box Excluded

The pressure profiles predicted for flow through the box with the top and bottom surfaces excluded and pipework in the 5 x 5 arrangement, with diameters of 0.4 m, are shown in Figure 6.2.4. Figure 6.2.4(a) shows the pressure profile when the explicit representation of pipes was used; Figures 6.2.4(b) and 6.2.4(c) show the pressure profiles when the VUR method was used, with pipe spacings of 1 m and 2 m, respectively; Figure 6.2.4(d) shows the pressure profile when the ACE method was used. The profiles were obtained using the QUICK differencing scheme.

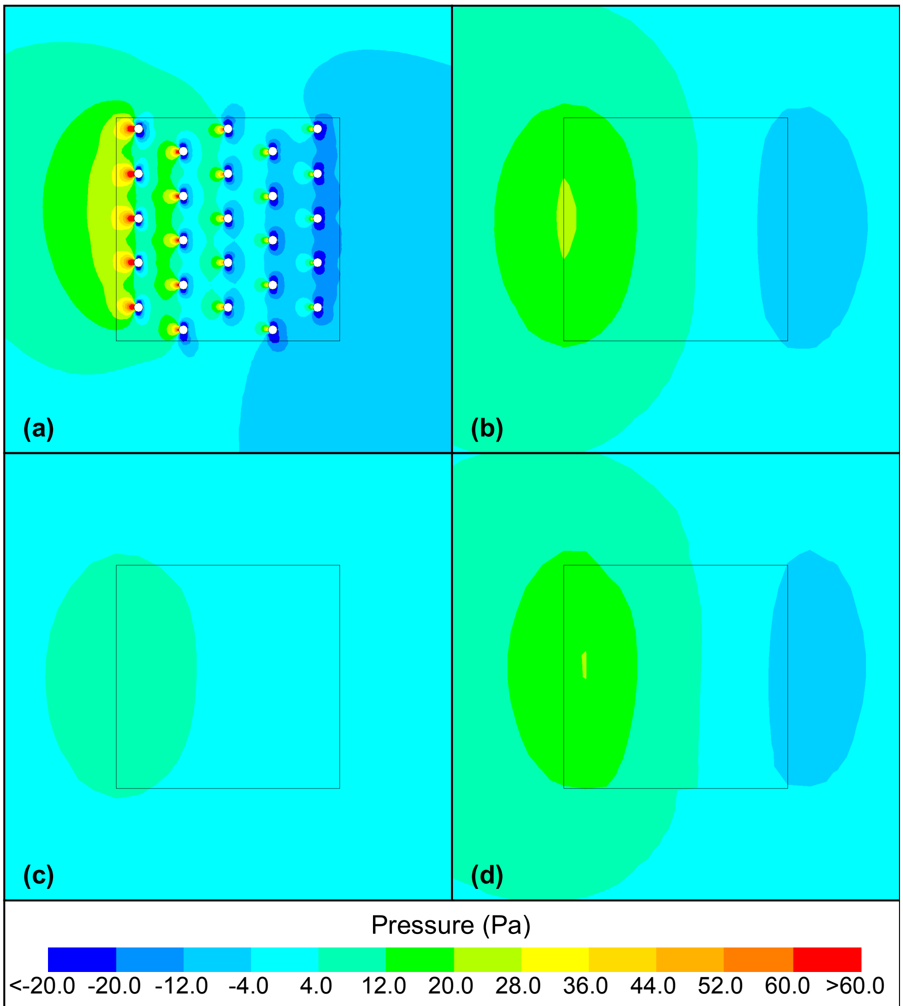

Figure 6.2.4 – Pressure Profiles obtained for the 5 x 5 Arrangement of Pipes with Diameters of 0.4 mm, with the Top and Bottom Surfaces of the Box Excluded.

(a) Explicit Representation
(b) VUR Method, 1 m Pipe Spacing
(c) VUR Method, 2 m Pipe Spacing
(d) ACE Method

With the 5 x 5 arrangement of pipework, with diameters of 0.4 m and the top and bottom surfaces of the box excluded, modelled explicitly within the computational mesh, the CFD-prediction for the mass flow rate through the tube bundle was equal to 966.65 kg/s. The CFD-prediction for the pressure field for this case (Figure 6.2.4(a)) shows a localised peak of pressure at the leading edge of each of the individual pipes. When averaged over the windward face, the predicted pressure was around 28 Pa. Likewise, when averaged over the leeward face, the predicted pressure was roughly equal to -12 Pa. The predicted velocity vector plot for this case, (Appendix 1, Figure 1.4.1(a), shows acceleration around the individual pipes and slow flow in the wakes behind them.

Using the VUR method to represent the pipework, for this pipe configuration, with a pipe spacing of 1 m, the CFD-prediction for the mass flow rate was equal to 1081.25 kg/s, which is considerably higher than that predicted with the explicit representation of pipes. The average pressure over the windward face (Figure 6.2.4(b)) was about 18 Pa, which is noticeably lower than the CFD-prediction with the explicit representation. The averaged pressure over the leeward face was about -8 Pa. This is not quite as low as the CFD-prediction using the explicit representation. No detail of flow around individual pipes is shown in the predicted velocity vector plot for this case, Appendix 1, Figure 1.12(a), or in the predicted pressure field.

Using the VUR method with a pipe spacing of 2 m, the CFD-prediction for the mass flow rate was equal to 1263.00 kg/s, which is significantly higher than that predicted with the explicit representation of pipes and with the VUR method with a pipe spacing of 1 m. The average pressure over the windward face (Figure 6.2.4(c)) was about 8 Pa, which is significantly lower than the CFD-prediction using the explicit representation. The pressure averaged over the leeward face was around 0 Pa. This is not as low as the CFD-prediction using the explicit representation. No detail of flow around individual pipes is shown in the predicted velocity vector plot for this case, Appendix 1, Figure 1.12.2(a), or in the predicted pressure field.

The VUR-prediction with a pipe spacing of 1 m was better than the 2 m pipe spacing for this case, but neither are close to the predictions of mass flow rate and pressure field with the explicit representation of pipes.

When the ACE method was used to represent the pipes, the CFD-prediction of the mass flow rate was equal to 1121.42 kg/s. This is considerably higher than the prediction with the explicit representation of pipes, and is also higher than the prediction using the VUR method for a pipe spacing of 1 m. The CFD-prediction for the pressure field, when using the ACE method, is presented in Figure (6.2.4(d)). The pressure averaged over the windward face was about 16 Pa, which is considerably lower than the predictions with the explicit representation but similar to the VUR-prediction with a pipe spacing of 1 m. The pressure averaged over the leeward face was about -8 Pa, which is similar to the prediction using the VUR method with a pipe spacing of 1 m, but not as low as the prediction with the explicit representation. The CFD-prediction for the velocity field, when using the ACE method, is presented in Appendix 1, Figure 1.4.2(a). No evidence of individual pipes is visible in either the predicted pressure field or velocity field.

For this particular case, the CFD-predictions using the VUR method with a pipe spacing of 1 m came closest to the CFD-predictions using the explicit representation of pipes, followed by the CFD-predictions using the ACE method. However, the VUR method for both pipe spacings and the ACE method all significantly under-predicted the resistance to the flow due to the pipework. The VUR method with a pipe spacing of 2 m is not a suitable method here.

6.2.5 Mass Flow Rates through the Box Containing Pipework

A graph showing mass flow rates obtained using the explicit representation of pipes, the VUR method with 1 m spacing and with 2 m spacing, and the ACE method past a plane half way between the windward and leeward planes, for pipework in the 5 x 5 arrangement, with diameters of 0.1 m, 0.2 m and 0.4 m, is shown in Figure 6.2.5(a). The results were obtained using the QUICK differencing scheme.

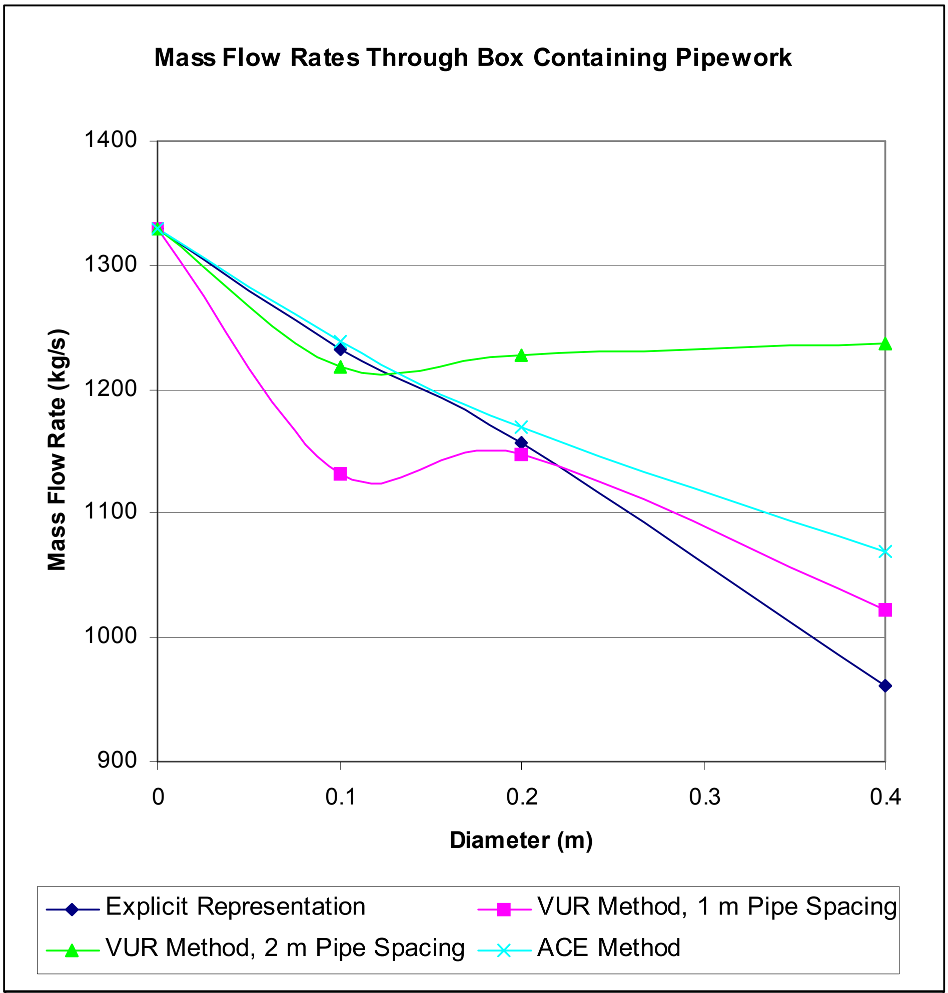

Figure 6.2.5(a) – Mass Flow Rates Obtained for the 5 x 5 Arrangement of Pipes, with Diameters of 0.1 m, 0.2 m and 0.4 m.

A table showing mass flow rates obtained using the explicit representation of pipes, the VUR method with 1 m spacing and with 2 m spacing, and the ACE method past a plane half way between the windward and leeward planes, for pipework in the 5 x 5 arrangement, with diameters 0.4 m and the top and bottom surfaces of the box excluded, is shown in Figure 6.2.5(b). The results were obtained using the QUICK differencing scheme.

Method Used to Represent the Pipes	Mass Flow Rate
No Pipes	1332.72
Explicit representation of pipes	966.65
VUR Method, 1 m Pipe Spacing	1081.25
VUR Method, 2 m Pipe Spacing	1263.00
ACE Method	1121.42

Figure 6.2.5(b) – Mass Flow Rates Obtained for the 5 x 5 Arrangement of Pipes, with Diameters of 0.4 m and the Top and Bottom Surfaces of the Box Excluded.

6.3 Benchmark B – 5 x 3 Arrangement of Pipes

6.3.1 0.4 m Diameter Pipework

The pressure profiles predicted for flow through the box containing pipework in the 5 x 3 arrangement, with diameters of 0.4 m, are shown in Figure 6.3.1. Figure 6.3.1(a) shows the pressure profile when the explicit representation of pipes was used; Figures 6.3.1(b) and 6.3.1(c) show the pressure profiles when the VUR method was used, with pipe spacings of 1 m and 2 m, respectively; Figure 6.3.1(d) shows the pressure profile when the ACE method was used. The profiles were obtained using the QUICK differencing scheme.

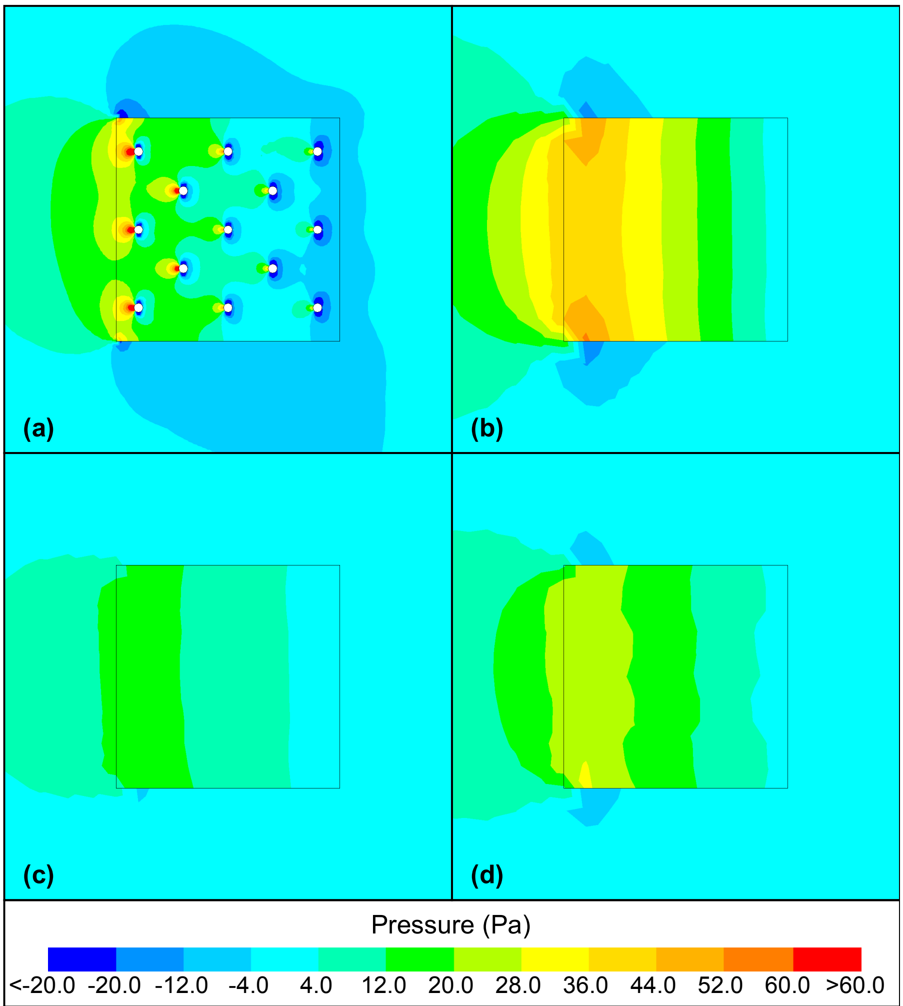

Figure 6.3.1 – Pressure Profiles Obtained for the 5 x 3 Arrangement of Pipes with Diameters of 0.4 m.

(a) Explicit Representation (b) VUR Method, 1 m Pipe Spacing

(c) VUR Method, 2 m Pipe Spacing (d) ACE Method

The velocity profiles predicted for flow through the box containing pipework in the 5 x 3 arrangement, with diameters of 0.4 m, are shown in Figure 6.3.1V. Figure 6.3.1V(a) shows the pressure profile when the explicit representation of pipes was used; Figures 6.3.1V(b) and 6.3.1V(c) show the pressure profiles when the VUR method was used, with pipe spacings of 1 m and 2 m, respectively; Figure 6.3.1V(d) shows the pressure profile when the ACE method was used. The profiles were obtained using the QUICK differencing scheme.

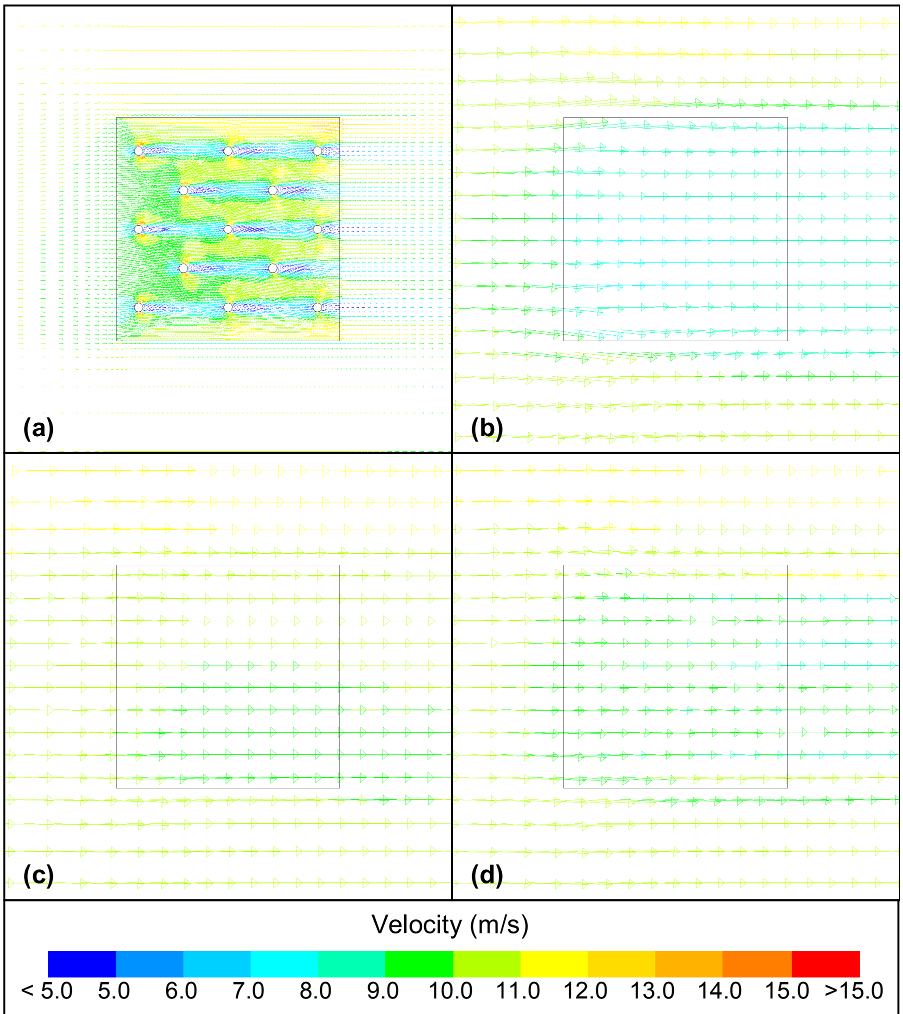

Figure 6.3.1V – Velocity Profiles Obtained for the 5 x 3 Arrangement of Pipes with Diameters of 0.4 m.

(a) Explicit Representation (b) VUR Method, 1 m Pipe Spacing

(c) VUR Method, 2 m Pipe Spacing (d) ACE Method

With the 5 x 3 arrangement modelled explicitly within the computational mesh, the CFD-prediction for the mass flow rate through the tube bundle was equal to 1132.32 kg/s. The CFD-prediction for the pressure field for this case (Figure 6.3.1(a)) shows a localised peak of pressure at the leading edge of each of the individual pipes. For the pipes in the windward column, the localised peaks of pressure were approximately equal to 60 Pa. When averaged over the windward face, the predicted pressure was of the order of 24 Pa. Likewise, when averaged over the leeward face, the predicted pressure was roughly equal to -8 Pa. The predicted velocity vector plot for this case, (Figure 6.3.1V(a)), shows acceleration around the individual pipes. A local flow velocity of about 15 m/s was predicted as the flow accelerated around the windward column of pipes. In the wakes behind the windward pipes, the velocity was roughly equal to 5 m/s.

Using the VUR method to represent the pipework, for this pipe configuration, with a pipe spacing of 1 m, the CFD-prediction for the mass flow rate was equal to 1022.09 kg/s, which is significantly lower than that predicted with the explicit representation of pipes. The average pressure over the windward face (Figure 6.3.1(b)) was about 40 Pa, which is considerably higher than the CFD-prediction with the explicit representation. The averaged pressure over the leeward face was roughly 0 Pa. This is not as low as the CFD-prediction using the explicit representation. No detail of flow around individual pipes is shown in the predicted velocity vector plot for this case, Figure 6.3.1V(b), or in the predicted pressure field.

Using the VUR method with a pipe spacing of 2 m, the CFD-prediction for the mass flow rate was equal to 1236.68 kg/s, which is significantly higher than that predicted with the explicit representation of pipes and the error is similar to that predicted with a pipe spacing of 1 m. The average pressure over the windward face (Figure 6.3.1(c)) was between 12 and 20 Pa, which is noticeably lower than the CFD-prediction using the explicit representation. The pressure averaged over the leeward face was approximately 0 Pa. This is not as low as the CFD-prediction using the explicit representation. No detail of flow around individual pipes is shown in the predicted velocity vector plot for this case, Figure 6.3.1V(c), or in the predicted pressure field.

Neither of the VUR-predictions with pipe spacings of 1 m and 2 m were very accurate for this case. The pipe spacing of 1 m over-predicted the resistance to the flow due to the pipes, and the pipes spacing of 2 m under-predicted the resistance to the flow due to the pipework.

When the ACE method was used to represent the pipes, the CFD-prediction of the mass flow rate was equal to 1177.82 kg/s. This is considerably higher than the prediction with the explicit representation of pipes, but more accurate than either of the predictions with the VUR method. The CFD-predictions for the pressure field and velocity field, when using the ACE method, are presented in Figures 6.3.1(d) and 6.3.1V(b), respectively. The pressure averaged over the windward face was between 20 and 28 Pa, which is reasonably close to the prediction with the explicit representation. The pressure averaged over the leeward face was about 0 Pa, which is similar to the predictions using the VUR method, but not as low as the prediction with the explicit representation. Some evidence of individual pipes is visible in Figure 6.3.1(d), in terms of higher pressures being visible close to the pipes. Some evidence of individual pipes is also visible in the predicted velocity field in terms of local acceleration close to the pipes.

For this particular case, the CFD-predictions using the ACE method came closest to the CFD-predictions using the explicit representation of pipes. The VUR method with a pipe spacing of 1 m significantly over-predicted the resistance to the flow due to the pipes and the VUR method with a pipe spacing of 2 m significantly under-predicted the resistance to the flow due to the pipes. Neither of the pipe spacings used with the VUR method are suitable here.

6.3.2 0.2 m Diameter Pipework

The pressure profiles predicted for flow through the box containing pipework in the 5 x 3 arrangement, with diameters of 0.2 m, are shown in Figure 6.3.2. Figure 6.3.2(a) shows the pressure profile when the explicit representation of pipes was used; Figures 6.3.2(b) and 6.3.2(c) show the pressure profiles when the VUR method was used, with pipe spacings of 1 m and 2 m, respectively; Figure 6.3.2(d) shows the pressure profile when the ACE method was used. The profiles were obtained using the QUICK differencing scheme.

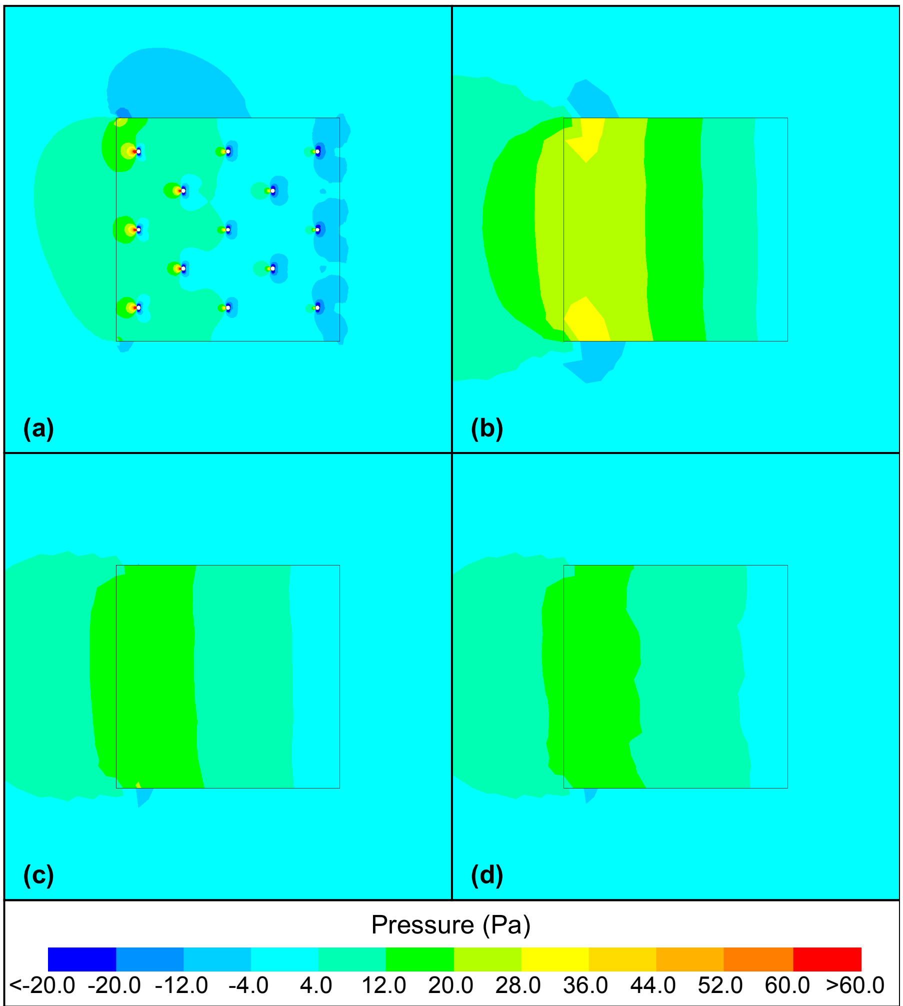

Figure 6.3.2 – Pressure Profiles Obtained for the 5 x 3 Arrangement of Pipes with Diameters of 0.2 m.

(a) Explicit Representation (b) VUR Method, 1 m Pipe Spacing

(c) VUR Method, 2 m Pipe Spacing (d) ACE Method

With the 5 x 3 arrangement of pipework, with diameters of 0.2 m, modelled explicitly within the computational mesh, the CFD-prediction for the mass flow rate through the tube bundle was equal to 1237.79 kg/s. The CFD-prediction for the pressure field for this case (Figure 6.3.2(a)) shows a localised peak of pressure at the leading edge of each of the individual pipes. When averaged over the windward face, the predicted pressure was around 10 Pa. Likewise, when averaged over the leeward face, the predicted pressure was roughly equal to -6 Pa. The predicted velocity vector plot for this case, (Appendix 1, Figure 1.6.1(a)), shows acceleration around the individual pipes and slow flow in the wakes behind them.

Using the VUR method to represent the pipework, for this pipe configuration, with a pipe spacing of 1 m, the CFD-prediction for the mass flow rate was equal to 1146.92 kg/s, which is significantly lower than that predicted with the explicit representation of pipes. The average pressure over the windward face (Figure 6.3.2(b)) was about 24 Pa, which is considerably higher than the CFD-prediction with the explicit representation. The averaged pressure over the leeward face was roughly 0 Pa. This is not as low as the CFD-prediction using the explicit representation. No detail of flow around individual pipes is shown in the predicted velocity vector plot for this case, Appendix 1, Figure 1.10.2(a), or in the predicted pressure field.

Using the VUR method with a pipe spacing of 2 m, the CFD-prediction for the mass flow rate was equal to 1227.86 kg/s, which is only marginally lower than that predicted with the explicit representation of pipes. The average pressure over the windward face (Figure 6.3.2(c)) was between 12 and 20 Pa, which is slightly higher than the CFD-prediction using the explicit representation. The pressure averaged over the leeward face was about 0 Pa. This is not as low as the CFD-prediction using the explicit representation. No detail of flow around individual pipes is shown in the predicted velocity vector plot for this case, Appendix 1, Figure 1.10.2(a), or in the predicted pressure field.

The VUR-prediction with a pipe spacing of 2 m was better than the 1 m pipe spacing for this case, since the mass flow rate and pressure field predictions are closer to those predicted with the explicit representation of pipes.

When the ACE method was used to represent the pipes, the CFD-prediction of the mass flow rate was equal to 1239.90 kg/s. This is very close to the prediction with the explicit representation of pipes and even closer than that predicted with the VUR method for a pipe spacing of 2 m. The CFD-prediction for the pressure field, when using the ACE method, is presented in Figure 6.3.2(d). The pressure averaged over the windward face was between 12 and 20 Pa, which is slightly higher than the CFD-prediction using the explicit representation, but similar to the prediction with the VUR method with a pipe spacing of 2 m. The pressure averaged over the leeward face was about 0 Pa, which is similar to the predictions using the VUR method, but not quite as low as the prediction with the explicit representation. Some evidence of individual pipes is visible in Figure 6.3.2(d), in terms of higher pressures being visible close to the pipes. The CFD-prediction for the velocity field, when using the ACE method, is presented in Appendix 1, Figure 1.6.2(a). Some evidence of individual pipes is also visible here, in terms of local acceleration close to the pipes. The predicted pressure and velocity fields with the ACE method and the VUR method with a pipe spacing of 2 m, are very similar to each other.

For this particular case, the CFD-predictions using the ACE method are closest to the CFD-predictions using the explicit representation of pipes, and provide reasonably accurate predictions of the resistance to the flow due to the pipework. The CFD-predictions from the VUR method with a pipe spacing of 2 m are reasonably close to the CFD-predictions using the explicit representation, but not quite as accurate as the predictions with the ACE method. However, the VUR method with a pipe spacing of 1 m over-predicted the resistance to the flow due to the pipes, suggesting that this method was not suitable here.

6.3.3 0.1 m Diameter Pipework

The pressure profiles predicted for flow through the box containing pipework in the 5 x 3 arrangement, with diameters of 0.1 m, are shown in Figure 6.3.3. Figure 6.3.3(a) shows the pressure profile when the explicit representation of pipes was used; Figures 6.3.3(b) and 6.3.3(c) show the pressure profiles when the VUR method was used, with pipe spacings of 1 m and 2 m, respectively; Figure 6.3.3(d) shows the pressure profile when the ACE method was used. The profiles were obtained using the QUICK differencing scheme.

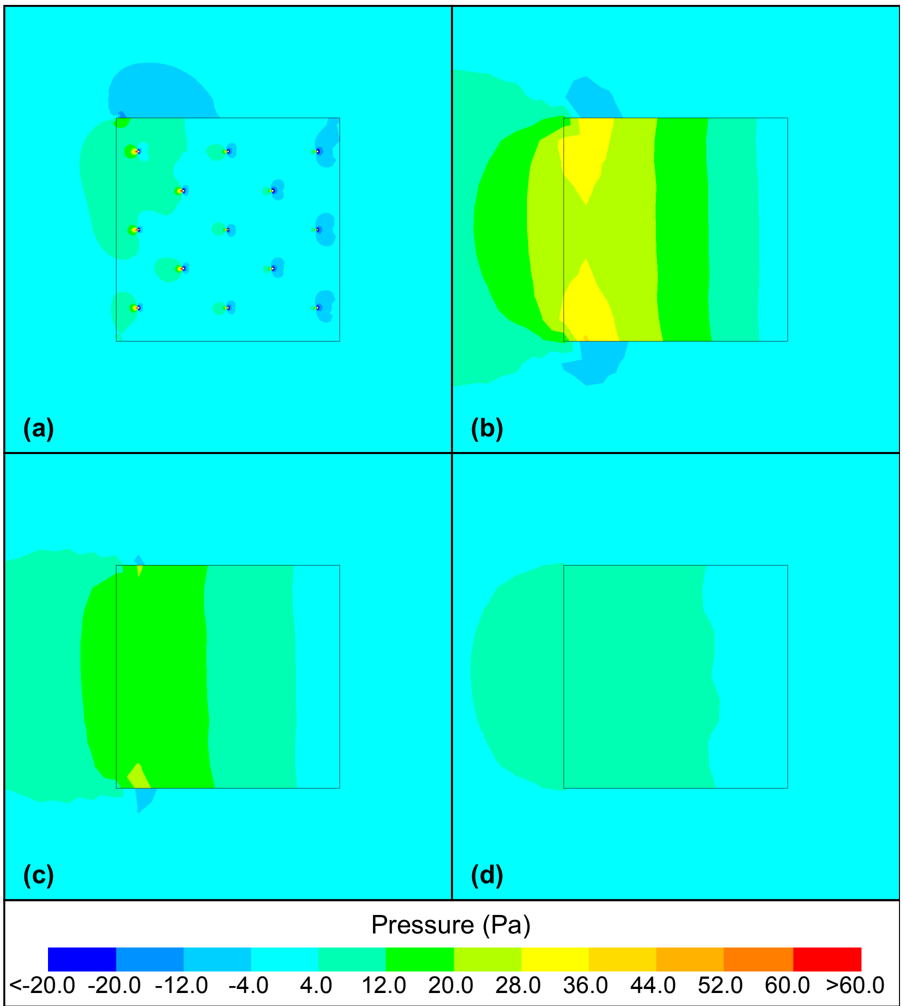

Figure 6.3.3 – Pressure Profiles Obtained for the 5 x 3 Arrangement of Pipes with Diameters of 0.1 m.

(a) Explicit Representation (b) VUR Method, 1 m Pipe Spacing

(c) VUR Method, 2 m Pipe Spacing (d) ACE Method

With the 5 x 3 arrangement of pipework, with diameters of 0.1 m, modelled explicitly within the computational mesh, the CFD-prediction for the mass flow rate through the tube bundle was equal to 1276.63 kg/s. The CFD-prediction for the pressure field for this case (Figure 6.3.3(a)) shows a localised peak of pressure at the leading edge of each of the individual pipes. When averaged over the windward face, the predicted pressure was around 6 Pa. Likewise, when averaged over the leeward face, the predicted pressure was roughly equal to -2 Pa. The predicted velocity vector plot for this case, (Appendix 1, Figure 1.7.1(a), shows acceleration around the individual pipes and slow flow in the wakes behind them.

Using the VUR method to represent the pipework, for this pipe configuration, with a pipe spacing of 1 m, the CFD-prediction for the mass flow rate was equal to 1131.56 kg/s, which is significantly lower than that predicted with the explicit representation of pipes. The average pressure over the windward face (Figure 6.3.3(b)) was about 28 Pa, which is significantly higher than the CFD-prediction with the explicit representation. The averaged pressure over the leeward face was roughly 0 Pa. This is not quite as low as the CFD-prediction using the explicit representation. No detail of flow around individual pipes is shown in the predicted velocity vector plot for this case, Appendix 1, Figure 1.11.1(a), or in the predicted pressure field.

Using the VUR method with a pipe spacing of 2 m, the CFD-prediction for the mass flow rate was equal to 1218.13 kg/s, which is considerably lower than that predicted with the explicit representation of pipes, but better than with a pipe spacing of 1 m. The average pressure over the windward face (Figure 6.3.3(c)) was between 12 and 20 Pa, which is considerably higher than the CFD-prediction using the explicit representation. The pressure averaged over the leeward face was about 0 Pa. This is not quite as low as the CFD-prediction using the explicit representation. No detail of flow around individual pipes is shown in the predicted velocity vector plot for this case, Appendix 1, Figure 1.11.2(a), or in the predicted pressure field.

The VUR-prediction with a pipe spacing of 2 m was better than the 1 m pipe spacing for this case, since the mass flow rate and pressure field predictions are closer to those predicted with the explicit representation of pipes.

When the ACE method was used to represent the pipes, the CFD-prediction of the mass flow rate was equal to 1280.19 kg/s. This is very close to the prediction with the explicit representation of pipes and notably better than both predictions with the VUR method.

The CFD-prediction for the pressure field, when using the ACE method, is presented in Figure 6.3.3(d). The pressure averaged over the windward face was about 8 Pa, which is close to the predictions with the explicit representation. The pressure averaged over the leeward face was about 0 Pa, which is similar to the predictions using the VUR method, but not quite as low as the prediction with the explicit representation. Evidence of individual pipes is visible in Figure 6.3.3(d), in terms of higher pressures being visible close to the pipes. The CFD-prediction for the velocity field, when using the ACE method, is presented in Appendix 1, Figure 1.7.2(a). Some evidence of individual pipes is also visible here, in terms of local deceleration between the pipes.

For this particular case, the CFD-predictions using the ACE method are easily the closest to the CFD-predictions using the explicit representation of pipes, and provide reasonably accurate predictions of the resistance to the flow due to the pipework. The CFD-predictions with the VUR method with both pipe spacings are significantly different from the predictions with the explicit representation. In both cases, the VUR over-predicted the resistance to the flow due to the pipes, suggesting that these methods were not suitable here.

6.3.4 0.4 m Diameter Pipework, Top and Bottom Surfaces of Box Excluded

The pressure profiles predicted for flow through the box with the top and bottom surfaces excluded and pipework in the 5 x 3 arrangement, with diameters of 0.4 m, are shown in Figure 6.3.4. Figure 6.3.4(a) shows the pressure profile when the explicit representation of pipes was used; Figures 6.3.4(b) and 6.3.4(c) show the pressure profiles when the VUR method was used, with pipe spacings of 1 m and 2 m, respectively; Figure 6.3.4(d) shows the pressure profile when the ACE method was used. The profiles were obtained using the QUICK differencing scheme.

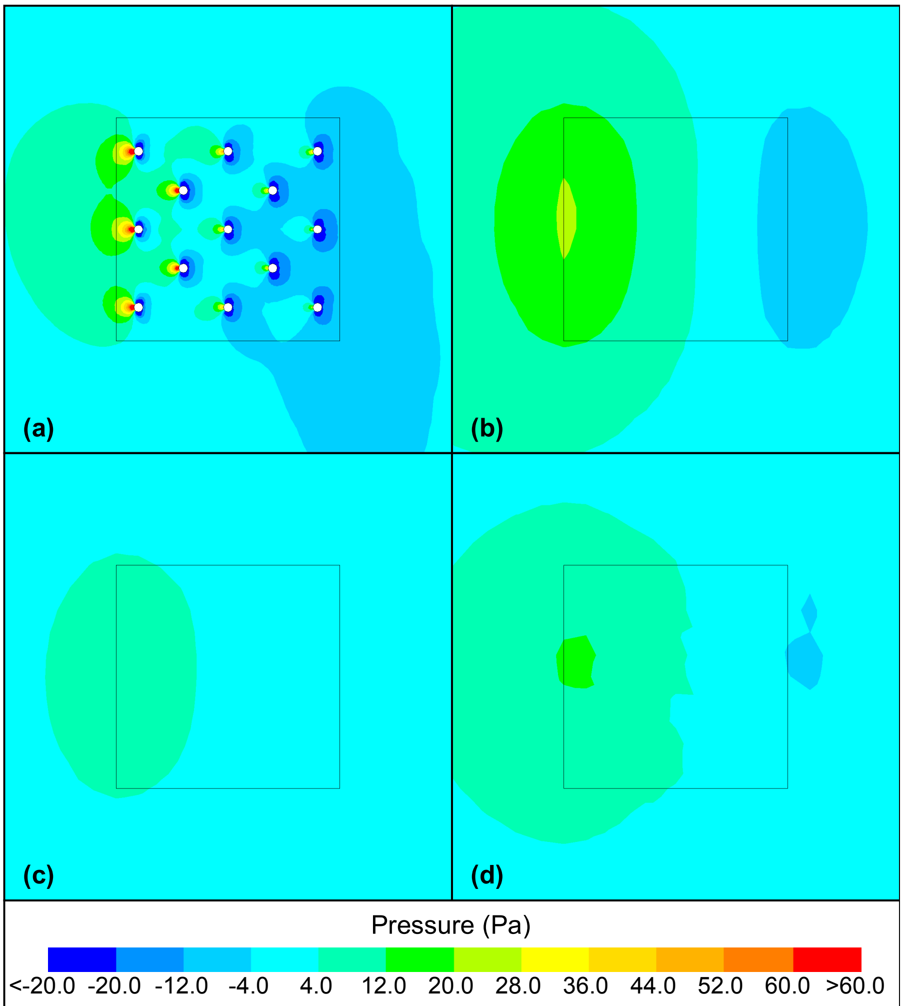

Figure 6.3.4 – Pressure Profiles Obtained for the 5 x 3 Arrangement of Pipes with Diameters of 0.4 m, with the top and bottom surfaces of the box excluded.

(a) Explicit Representation (b) VUR Method, 1 m Pipe Spacing

(c) VUR Method, 2 m Pipe Spacing (d) ACE Method

With the 5 x 3 arrangement of pipework, with diameters of 0.4 m and the top and bottom surfaces of the box excluded, modelled explicitly within the computational mesh, the CFD-prediction for the mass flow rate through the tube bundle was equal to 1128.52 kg/s. The CFD-prediction for the pressure field for this case (Figure 6.3.4(a)) shows a localised peak of pressure at the leading edge of each of the individual pipes. When averaged over the windward face, the predicted pressure was around 16 Pa. Likewise, when averaged over the leeward face, the predicted pressure was between –4 and -12 Pa. The predicted velocity vector plot for this case, (Appendix 1, Figure 1.8.1(a)), shows acceleration around the individual pipes and slow flow in the wakes behind them.

Using the VUR method to represent the pipework, for this pipe configuration, with a pipe spacing of 1 m, the CFD-prediction for the mass flow rate was equal to 1081.25 kg/s, which is considerably lower than that predicted with the explicit representation of pipes. The average pressure over the windward face (Figure 6.3.4(b)) was about 18 Pa, which is slightly higher than the CFD-prediction with the explicit representation. The averaged pressure over the leeward face was about -8 Pa. This is similar to the CFD-prediction using the explicit representation. No detail of flow around individual pipes is shown in the predicted velocity vector plot for this case, Appendix 1, Figure 1.12.1(a), or in the predicted pressure field.

Using the VUR method with a pipe spacing of 2 m, the CFD-prediction for the mass flow rate was equal to 1263.00 kg/s, which is significantly higher than that predicted with the explicit representation of pipes and is worse than the prediction with the VUR method with a pipe spacing of 1 m. The average pressure over the windward face (Figure 6.2.4(c)) was about 8 Pa, which is significantly lower than the CFD-prediction using the explicit representation. The pressure averaged over the leeward face was around 0 Pa. This is not as low as the CFD-prediction using the explicit representation. No detail of flow around individual pipes is shown in the predicted velocity vector plot for this case, Appendix 1, Figure 1.12.2(a), or in the predicted pressure field.

The VUR-prediction with a pipe spacing of 1 m was better than the 2 m pipe spacing for this case, but neither are particularly close to the predictions of mass flow rate and pressure field with the explicit representation of pipes.

When the ACE method was used to represent the pipes, the CFD-prediction of the mass flow rate was equal to 1210.31 kg/s. This is considerably higher than the prediction with the explicit representation of pipes, and in terms of error, is between the predictions with the VUR with a pipe spacing of 1 m, and the VUR with a pipe spacing of 2 m. The CFD-prediction for the pressure field, when using the ACE method, is presented in Figure 6.3.4(d). The pressure averaged over the windward face was about 10 Pa, which is considerably lower than the predictions with the explicit. The pressure averaged over the leeward face was about -2 Pa, which is not as low as the prediction with the explicit representation. Evidence of individual pipes is visible in Figure 6.3.4(d), in terms of higher pressures being visible close to the pipes. The CFD-prediction for the velocity field, when using the ACE method, is presented in Appendix 1, Figure 1.8.2(a). Evidence of individual pipes is also visible in the velocity field in terms of local acceleration close the pipes and deceleration between the locations of pipes.

For this particular case, the CFD-predictions using the VUR method with a pipe spacing of 1 m came closest to the CFD-predictions using the explicit representation of pipes, followed by the CFD-predictions using the ACE method. However, the VUR method with a pipe spacing of 2 m and the ACE method both significantly under-predicted the resistance to the flow due to the pipework and the VUR method with a pipe spacing of 1 m considerably over-predicted the resistance to the flow due to the pipework.

6.3.5 Mass Flow Rates through the Box Containing Pipework

A graph showing mass flow rates obtained using the explicit representation of pipes, the VUR method with 1 m spacing and with 2 m spacing, and the ACE method past a plane half way between the windward and leeward planes, for pipework in the 5 x 3 arrangement, with diameters of 0.1 m, 0.2 m and 0.4 m, is shown in Figure 6.3.5(a). The results were obtained using the QUICK differencing scheme.

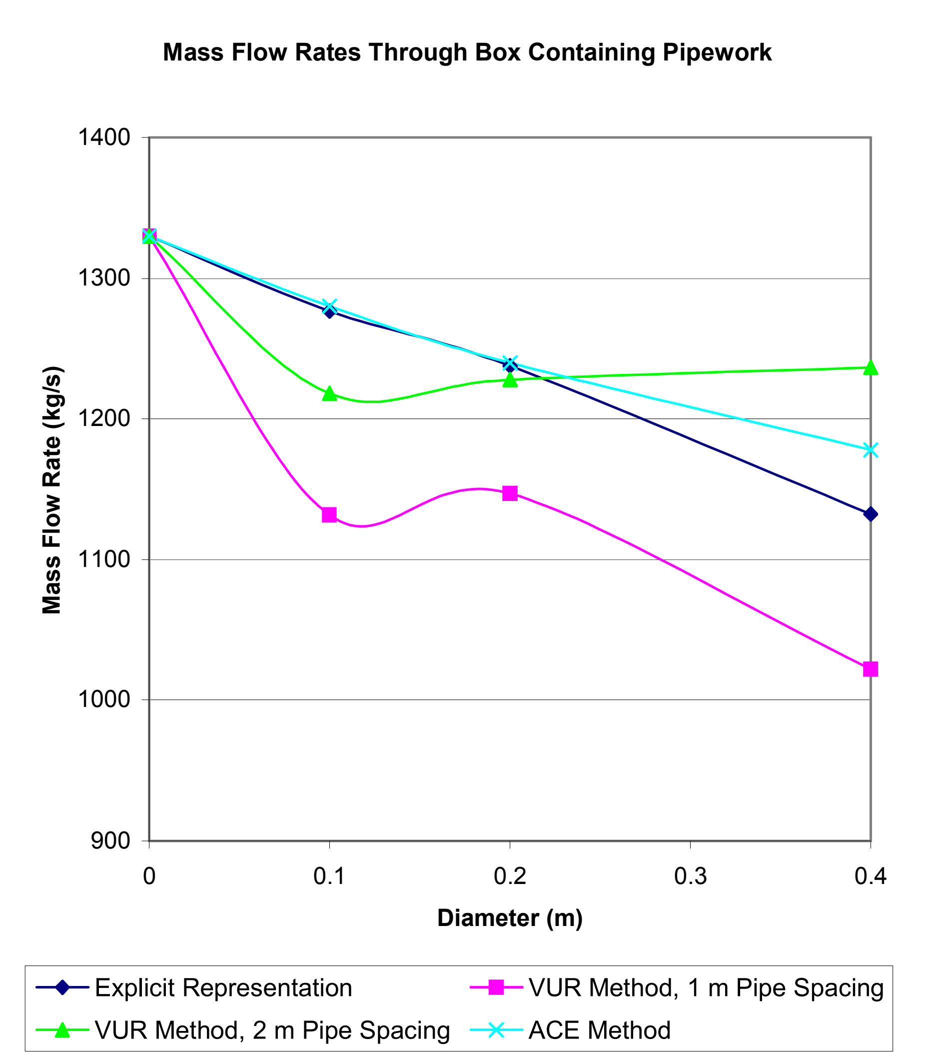

Figure 6.3.5(a) – Mass Flow Rates Obtained for the 5 x 3 Arrangement of Pipes with Diameters of 0.1 m, 0.2 m and 0.4 m.

A table showing mass flow rates obtained using the explicit representation of pipes, the VUR method with 1 m spacing and with 2 m spacing, and the ACE method past a plane half way between the windward and leeward planes, for pipework in the 5 x 3 arrangement, with diameters 0.4 m and the top and bottom surfaces of the box excluded, is shown in Figure 6.3.5(b). The results were obtained using the QUICK differencing scheme.

Method Used to Represent the Pipes	Mass Flow Rate
No Pipes	1332.72
Explicit representation of pipes	1128.52
VUR Method, 1 m Pipe Spacing	1081.25
VUR Method, 2 m Pipe Spacing	1263.00
ACE Method	1210.31

Figure 6.3.5(b) – Mass Flow Rates Obtained for the 5 x 3 Arrangement of Pipes, with Diameters of 0.4 m and the Top and Bottom Surfaces of the Box Excluded.

6.4 Discussion of Results

It was observed that when the pipework was represented explicitly within the CFD-mesh, there was a decrease in the mass flow rate across the box, as the diameter of the pipes was increased (Figures 6.2.5(a) and 6.3.5(a)). This is reflected in the predicted pressure fields, where the build up of pressure around the windward face increased as the diameter of the pipes increased. This is in contrast to the predictions with the VUR method, where this trend is not apparent.

Using the VUR method, the pipework is all represented by a series of volumes, the size of which must be selected at the discretion of the analyst. The distances between the pipes in both the 5 x 5 arrangement of pipes, (Figure 4.1.3), and the 5 x 3 arrangement of pipes, (Figure 4.1.4), mean that it is feasible for an analyst to choose a pipe spacing of 2 m to represent the pipes. However, as the results with the explicit representation of pipes show, there are considerable differences between the flow through each of the arrangements. It was observed that for the 5 x 5 representation of pipes the 2 m spacing predicted better results than the 1 m spacing for pipes with diameter of 0.1 m, whereas the 1 m spacing predicted better results than the 2 m spacing for pipes with diameters of 0.2 m and 0.4 m. This suggests that the spacing chosen for the VUR method is dependent on the diameter of the pipes, as well as the distance between each of the pipes, making it difficult for the analyst to select the correct representative diameter and spacing of the pipes in a volume.

The VUR-predictions do not show any evidence of individual pipes. This is because the method does not allow evidence of individual pipes, as all the pipework in one region is represented by one volume with one diameter and one pipe spacing chosen to represent all the pipes in the volume. The same source terms are allocated to every cell in that region, meaning that the detail of flow around pipes is completely lost by using this method.

Overall, the predictions by the VUR method suggest that it is open to considerable interpretation and depends heavily on the pipe diameter and spacing chosen by the analyst. Therefore, this method is unreliable in consistently predicting accurate results for flow across bundles of pipes.

The trends shown in the mass flow rate across the box and in the pressure fields that were observed when the pipes were represented explicitly within the CFD-mesh were also observed with the ACE method (Figures 6.2.5(a) and 6.3.5(a)). The predictions when the pipework was represented both explicitly within the CFD-mesh and by the ACE method also show that for the 5 x 5 arrangement of pipework the resistance to the flow was higher than with the 5 x 3 arrangement of pipes.

For both arrangements of pipes, the ACE method predicted remarkably accurate results for pipes with diameters of 0.1 m and 0.2 m. However, for the pipes with diameters of 0.4 m, both including and excluding the top and bottom surfaces of the box, the predictions were not as close to the predictions with the explicit representation of pipes. For these cases, the ACE method under-predicts the resistance to the flow due to the pipework. A possible explanation for this is that the relationship between the area of blockage to the flow due to the pipes and the resistance to the flow caused by the pipes is not linear. The prediction by the ACE method for pipes with a diameter of 0.2 m is more accurate with the 5 x 3 arrangement of pipes than with the 5 x 5 arrangement, where the resistance is very slightly under-predicted. This supports the idea that the relationship is non linear. This idea is also mentioned by Gilham *et al.* (1999) where it is suggested that the level of congestion should be taken into account when calculating the source term to represent the resistance to the flow due to the pipes, and the drag coefficient should by given by (Eq. 2.4.2) or (Eq. 2.4.3).

Many of the predictions for the pressure and velocity field obtained with the ACE method show some evidence of individual pipes. This is because source terms are allocated to individual cells that are known to contain part of a pipe. Although, the amount of detail in the flow that is evident with the ACE method is far from the amount of detail visible when the pipes are represented explicitly in the mesh, it is an improvement on the VUR method, where no detail is represented.

Generally the ACE method for representing pipework predicted results closer to those predicted with the explicit representation of pipes than the VUR method. In a few cases, the VUR method predicted more accurate results than the ACE method, but the VUR method did not perform consistently with each arrangement of pipework, or for the various diameters. The ACE method was observed to be more accurate in representing pipework with small diameters.

The worst prediction by the ACE method for the cases used in this thesis is approximately 16% in error, whereas errors of up to 30% occurred with the VUR method. In general, the ACE method provides more accurate results than the VUR method, and is not open to any user discretion. Even though the ACE method is not as accurate for large diameters as small diameters, the trend of increasing resistance to the flow with larger diameters of pipes is clear, implying that this method is reliable.

7.0 Conclusions and Further Work

7.1 Conclusions Derived from this Work

The VUR method for representing sub-grid pipework in a computational mesh has been improved upon by the ACE method, developed in this thesis. The ACE method automatically reads in information from a given pipework database, and allocates source terms on a cell-by-cell basis to represent the resistance to the pipes. Pipes are tracked through the computational mesh from one end to the other. Inaccuracies with the ACE method occur when pipes have either end on a face, edge or node of a cell; pass through an edge or node of a cell; enter of region of mesh that has been refined or pass through an unmeshed region. These are described in §3.2.3 and §3.2.5 - §3.2.7.

With the VUR method, an analyst chooses the size of the volume that contains the pipework in a region of the geometry. One representative diameter and one representative spacing for the pipes must be chosen to represent all the pipes in the volume, which is open to user discretion, and is a limitation of the technique. In contrast, the ACE method only uses the information stored in the pipework database, and so is not open to user discretion.

Using the VUR method can be time consuming as it is necessary to identify the volumes containing the pipework. With the ACE method, however, the process of allocating the resistance of the pipework within the flow domain is automated, saving time.

With the ACE method, source terms to represent the resistance to the flow due to the pipes are added to the momentum equations (Eq. 4.2.1, Eq. 4.2.2, Eq. 4.2.3) in cells that the pipes pass through. They depend on the length and diameter of pipe in each cell. With the VUR method, the same source terms are allocated to all the cells in the volume containing the pipework. Therefore, the spatial variation of resistance to the flow due to pipework, which is allocated with the ACE method, is more accurate than that allocated with the VUR method.

The results from the validation of the ACE method show that the method is good for all the pipe configurations considered, particularly for those with small pipe diameters. The deviation for pipes with large diameters may be because the relationship between the area of blockage to the flow due to the pipes and the resistance to the flow caused by the pipes is not linear. This idea is mentioned by Ivings *et al.* (2004) and Gilham *et al.*

(1999), where it is suggested that the level of congestion should be taken into account when calculating the source term to represent the resistance to the flow due to the pipes.

The ACE method is more reliable than the VUR method. More resistance to the flow is always predicted for more pipes or pipes with larger diameters. This is not the case with the VUR method, which does not show this clear trend. The pipe spacing allocated to the VUR method is dependent on the diameter of pipes in the region as well as the distance between the pipes, increasing the unreliability of this method.

Some evidence of flow around individual pipes is shown with the ACE method, whereas this is not possible with the VUR method.

7.2 Example of Pipework on an Offshore Platform Represented by the ACE Method

The ACE method was used to represent small-bore pipework on an offshore platform. Figures 7.2.1 and 7.2.2 show two different views of the pipework, both with and without the main structures of the platform. The pipework is shown in the form of isosurfaces of the values of the source term coefficients, S_{Cx}, S_{Cy} and S_{Cz}, that are stored in the cell User-Defined Memory.

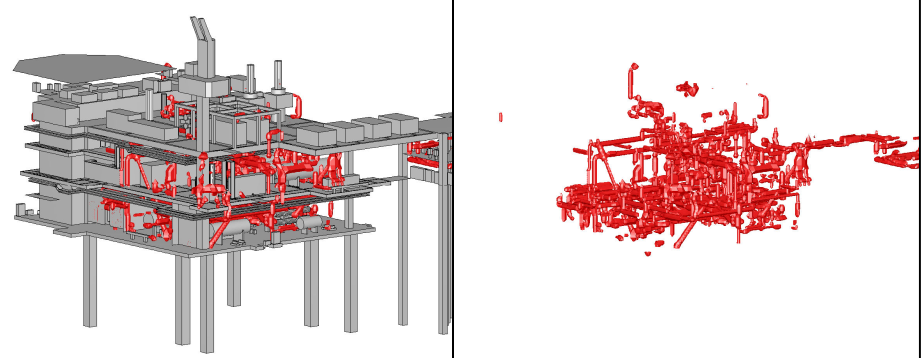

(a) (b)

Figure 7.2.1 – Pipework on an Offshore Platform Represented by the ACE Method.
(a) With the Platform (b) Without the Platform

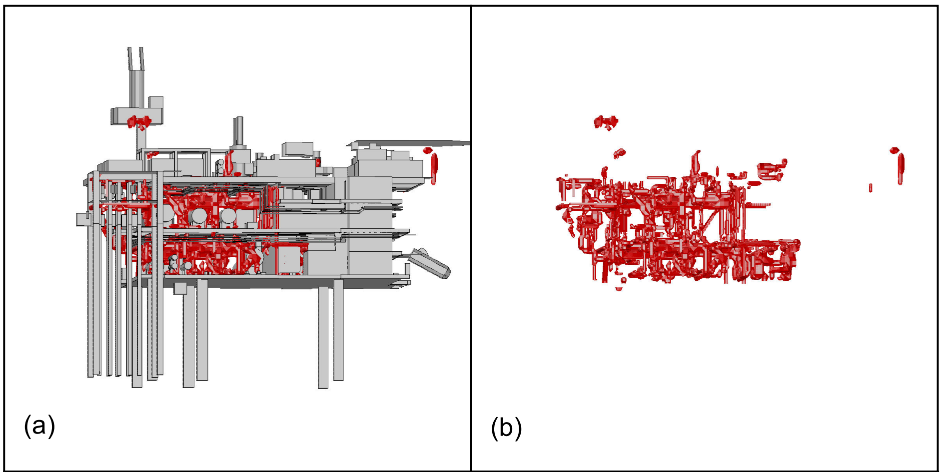

Figure 7.2.2 – Pipework on an Offshore Platform Represented by the ACE Method.
(a) With the Platform (b) Without the Platform

7.3 Suggestions for Further Work

Through developing the ACE method and looking at related work that has been done in the past, several improvements and possible further developments have become apparent and these are listed below:

- The ACE method tracks the centre lines of pipes through the cells in the computational mesh. Often the physical size of the pipes will mean that they overlap into adjacent cells. An extension of the work in this thesis could be to identify all the cells that each pipe passes through, and allocate appropriate source terms to all these cells. However, efficiency of the method is a key factor in an extension of this nature, and the balance between accuracy and efficiency must be considered.
- Another related extension would be to allow the method to track pipes that have an end on a face, edge or node of a cell, or pass through an edge or node of a cell, without altering the line of the pipe, as is done with the present ACE method.
- Further work should be done to improve the tracking of pipes through refined regions of a mesh containing hanging nodes. At present the condition to find these regions, and the method to overcome the problem (§3.2.6) significantly

increases the time taken to track pipes through meshes with cells with quadrilateral faces, even when the pipes do not pass through the refined region. This may be a problem with a large pipework database where the total time taken to interpret the pipework database may become an important factor.

- Source terms could be added to represent turbulence and heat transfer. This is suggested in a number of journal articles and books including Gilham *et al.* (1999) and Ivings *et al.* (2004). More information on this is given in §4.3.
- The ACE method could be extended to represent non-cylindrical elements, described by a different drag coefficient to cylinders. This could very easily be implemented into the ACE method and would allow the method to be used for a greater range of objects. Validation should be done on cases with square pipes.
- The source terms applied to the momentum equations to represent resistance to the flow could be developed, making them more accurate, but also more complex. The Reynolds number for the flow could be calculated in each cell, on each iteration, and this could be used to calculate the drag coefficient according to the graph shown in Figure 4.2.1. This would allow greater accuracy especially for turbulent flows where the drag coefficient drops well below 1.2, which is the value that is always used for drag coefficient in the present ACE method. Gilham *et al.* (1999) and Ivings *et al.* (2004) both suggest that the level of congestion should be taken into account when calculating the source term to represent the resistance to the flow due to the pipework. The validation of the ACE method discussed in §6.4 supports this suggestion. A function to represent the congestion could be calculated and implemented in the ACE method. More information on this area of improvement is given in §4.3.

8.0 References

ACHESON, D.J. 1990 Elementary Fluid Dynamics, *Clarendon Press.*

AIBA, S., OTA, T. & TSUCHIDA, H. 1980 Heat Transfer of Tubes Closely Spaced in an In-Line Bank. *International Journal of Heat and Mass Transfer* **Volume 23, Issue 3,** 311-319.

AUTOREAGAS THEORY MANUAL, Version 3.0.01, 3.8-3.9

AVISAR, B., SHEMER, L. & KRIBUS, A. 2001 Measurements of Velocity Fields in Finite Cylinder Arrays With and Without Tip Clearance. *Experimental Thermal and Fluid Science* **24,** 157-167.

BALABANI, S. 1996 An Experimental Investigation of the Crossflow Over Tube Bundles. *pHd Thesis, King's College London, University of London.*

CONLEY CORPORATION 2004 Offshore Photo Gallery.
http://www.conleyfrp.com/gallery/vinni.jpg, 08/09/2004.

DEPARTMENT OF MATHEMATICS, OREGON STATE UNIVERISTY 1996 Equations of Lines and Planes.
http://oregonstate.edu/dept/math/CalculusQuestStudyGuides/vcalc/lineplane/lineplane.html, 29/06/2004.

ELECTROMAGNETIC COMPATIBILITY LABORATORY, UNIVERSITY OF MISSOURI-ROLLA 1998 The EMAP4 Vector FEM Modeling Code, IV: Mesh Generation. http://www.emclab.umr.edu/emap4/Meshing, 02/07/2004.

ESDU INTERNATIONAL, London 1993 Strong Winds in the Atmospheric Boundary Layer. Part I: Mean Hourly Wind Speeds (+Amendments A to D). **Item No. 82026.**

ESDU INTERNATIONAL, London 1993 Characteristics of Atmospheric Turbulence Near the Ground. Part II: Single Point Data for Strong Winds (Neutral Atmosphere) (+Amendments A to F). **Item No. 85020.**

FLACS-95 USER'S GUIDE, Revision No.: 1.0, 15.

GILHAM, S., COWAN, I.R. & KAUFMAN, E.S. 1999 Improving Gas Turbine Power Plant Safety: The Application of Computational Fluid Dynamics to Gas Leaks. *Proceedings of the Institution of Mechanical Engineers* **Volume 213, Part A,** 475-489.

HERRON, G. 1994 Point Within a Tetrahedron. http://sworks.com/hollasch/cgindex/geometry/ptintet.html, 29/06/2004.

HUTCHINSON, B.R. & RAITHBY, G.D. 1986 A Multigrid Method Based on the Additive Correction Strategy. *Numerical Heat Transfer* **9,** 511-537.

IVINGS, M.J., LEA, C.J & LEDIN, H.S. 2004 Outstanding Safety Questions Concerning the Analysis of Ventilation and Gas Dispersion in Gas Turbine Enclosures: Best Practice Guidelines for CFD. *Health & Safety Laboratory, Buxton, UK* 6, 10-11, 15-16, 21.

LAM, K. & FANG, X. 1995 The Effect of Interface of Four Equispaced Cylinders in Cross Flow On Pressure and Force Coefficients. *Journal of Fluids and Structures* **9,** 195-214.

LAM, K., LI, J.Y., CHAN, K.T. & SO, R.M.C. 2003 Flow Pattern and Velocity Field Distribution of Cross-Flow Around Four Cylinders in a Square Configuration at a Low Reynolds Number. *Journal of Fluids and Structures* **17,** 665-679.

LAUNDER, B.E. & SPALDING, D.B. 1974 The numerical computation of turbulent flows. *Comp. Meth. App. Mech. Eng.* ***3*****,** 269-289.

LEA, C., PRITCHARD, D., IVINGS, M., LEDIN, S. & SAUNDERS, J. 2003 Outstanding Safety Questions Concerning the Use of Gas Turbines for Power Generation: Best Practice Guidelines for CFD. *Health & Safety Laboratory, Buxton, UK*

LEONARD, B.P. 1979 A stable and Accurate Convective Modelling Procedure Based on Quadratic Upstream Interpolation. *Computer Methods in Applied Mechanics and Engineering* **19,** 59-98.

MARTIN, A.R., SALTIEL, C. & SHYY, W. 1998 Frictional Losses and Convective Heat Transfer in Sparse, Periodic Cylinder Arrays in Cross Flow. *International Journal of Heat and Mass Transfer* **Volume 41, Issue 15,** 2283-2397.

MCADAMS, W.H. 1954 Heat Transmission. 3rd Edition. *McGraw Hill.*

OLIVE, J. 2003 Finding Where a Line Intersects a Plane. http://www.netcomuk.co.uk/~jenolive/vect18c.html, 29/06/2004.

PATANKAR, S.V. & SPALDING, D.B. 1972 A Calculation Procedure for Heat, Mass and Momentum Transfer in Three-Dimensional Parabolic Flows. *International Journal of Heat and Mass Transfer* **15,** 1787-1806.

PERIC, M. 1985 A Finite Volume Method for the Prediction of Three-Dimensional Fluid Flow in Complex Ducts. *Ph. D. Thesis, London Univeristy, UK* 208-226.

ROLLET-MIET, P., LAURENCE, D. & FERZIGER, J. 1999 LES and RANS of Turbulent Flow in Tube Bundles. *International Journal of Heat and Fluid Flow* **20,** 241-254.

SCHLICHTING 1987 Boundary-Layer Theory. 7th Edition. *McGraw Hill,* 16-17.

SCHMITT, S.R. 2004 Evaluation of Determinants using Minors and Cofactors. http://home.att.net/~srschmitt/det_minors.html, 29/06/2004.

SIMONIN, O. & BARCOUDA, M. 1986 Measuremens of a Fully Developed Turbulent Flow Across a Tube Bundle. *3rd International Conference on the Applications of Laser Anemometry with Fluid Mechanics.*

THE ENGINEERING TOOLBOX 2004 Air - Absolute and Kinematic Viscosity. http://www.engineeringtoolbox.com/24_601.html, 08/09/2004.

WANG, M. & GEORGIADIS, J.G. 1996 Conjugate Forced Convection in Crossflow Over a Cylinder Array with Volumetric Heating. *International Journal of Heat and Mass Transfer* **Volume 39, Issue 7,** 1351-1361.

WATTERSON, J.K., DAWES, W.N, SAVILL, A.M. & WHITE, A.J. 1999 Predicting Turbulent Flow in a Staggered Tube Bundle. *International Journal of Heat and Fluid Flow* **Volume 20, Issue 6,** 581-591

YAO, M., NAKATANI, M. & SUZUKI, K. 1989 Flow Visualization and Heat Transfer Experiments in a Duct with a Staggered Array of Cylinders. *Experimental Thermal and Fluid Science* **Volume 2, Issue 2,** 193-200.

Appendix 1 – Verification cases

Table of Contents

Figure Number	Representation of Pipes	Arrangement of Pipes/Pipe Spacing	Diameter of Pipes
1.1.1	Explicit	5 x 5	0.4 m
1.1.2	ACE Method	5 x 5	0.4 m
1.2.1	Explicit	5 x 5	0.2 m
1.2.2	ACE Method	5 x 5	0.2 m
1.3.1	Explicit	5 x 5	0.1 m
1.3.2	ACE Method	5 x 5	0.1 m
1.4.1	Explicit	5 x 5	0.4 m – Top and Bottom Surfaces of Box Excluded
1.4.2	ACE Method	5 x 5	0.4 m – Top and Bottom Surfaces of Box Excluded
1.5.1	Explicit	5 x 3	0.4 m
1.5.2	ACE Method	5 x 3	0.4 m
1.6.1	Explicit	5 x 3	0.2 m
1.6.2	ACE Method	5 x 3	0.2 m
1.7.1	Explicit	5 x 3	0.1 m
1.7.2	ACE Method	5 x 3	0.1 m
1.8.1	Explicit	5 x 3	0.4 m – Top and Bottom Surfaces of Box Excluded
1.8.2	ACE Method	5 x 3	0.4 m – Top and Bottom Surfaces of Box Excluded
1.9.1	VUR Method	1 m	0.4 m
1.9.2	VUR Method	2 m	0.4 m
1.10.1	VUR Method	1 m	0.2 m
1.10.2	VUR Method	2 m	0.2 m
1.11.1	VUR Method	1 m	0.1 m
1.11.2	VUR Method	2 m	0.1 m
1.12.1	VUR Method	1 m	0.4 m – Top and Bottom Surfaces of Box Excluded
1.12.2	VUR Method	2 m	0.4 m – Top and Bottom Surfaces of Box Excluded
1.13.1	No Pipes	No Pipes	No Pipes
1.13.2	No Pipes	No Pipes	No Pipes – Top and Bottom Surfaces of Box Excluded

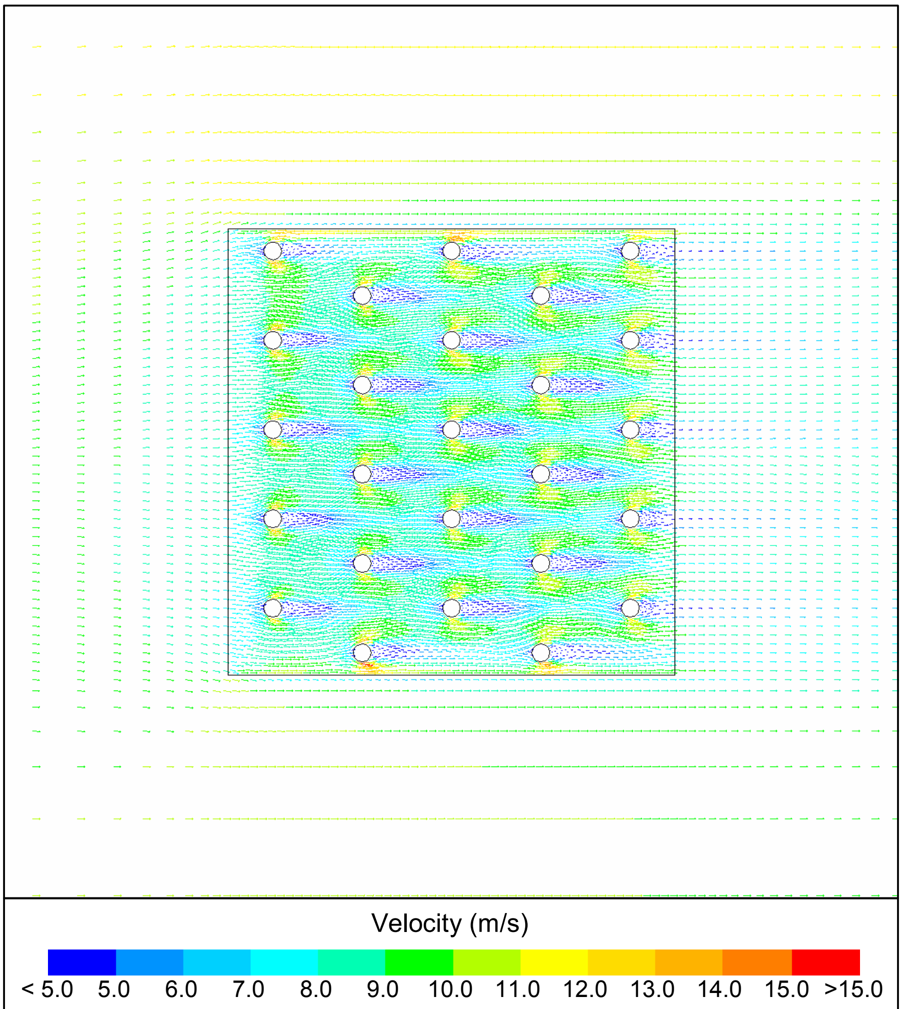

Figure 1.1.1(a) – Velocity Profile obtained for the 5 x 5 Arrangement of Pipes with a Diameter of 0.4 m. Pipes Represented Explicitly within the CFD Mesh

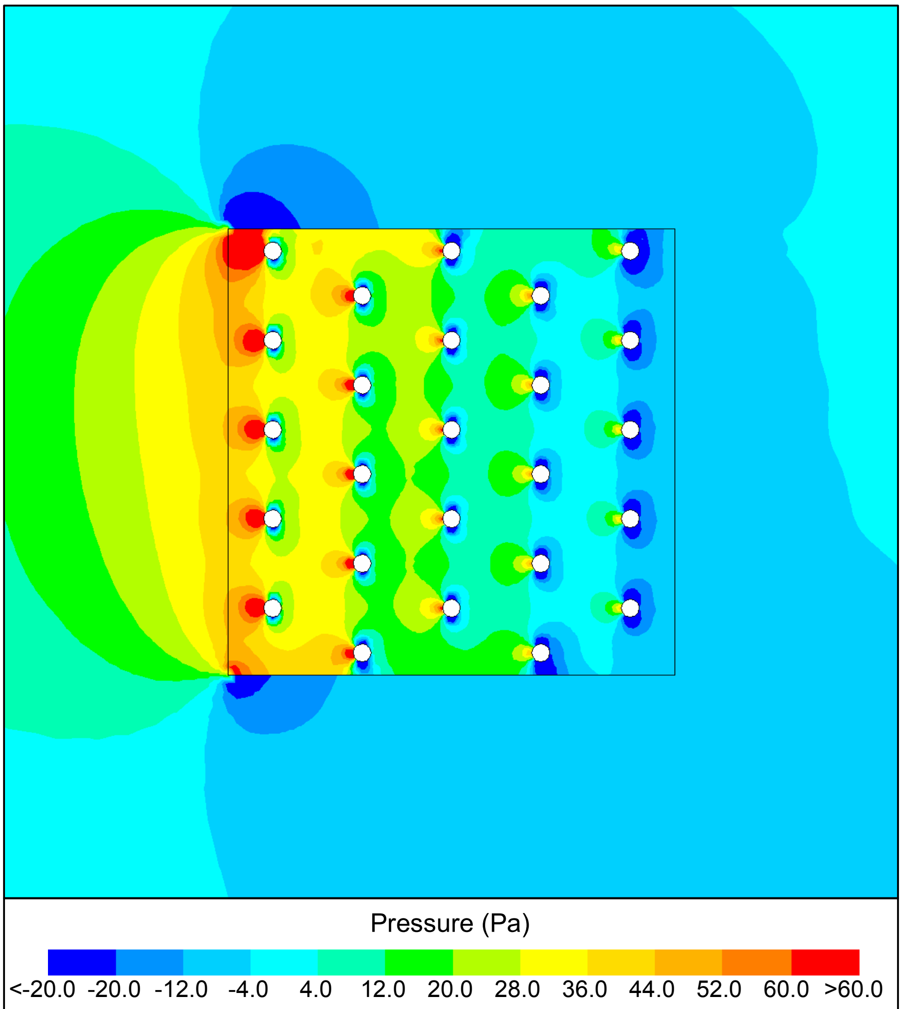

Figure 1.1.1(b) – Pressure Profile obtained for the 5 x 5 Arrangement of Pipes with a Diameter of 0.4 m. Pipes Represented Explicitly within the CFD Mesh

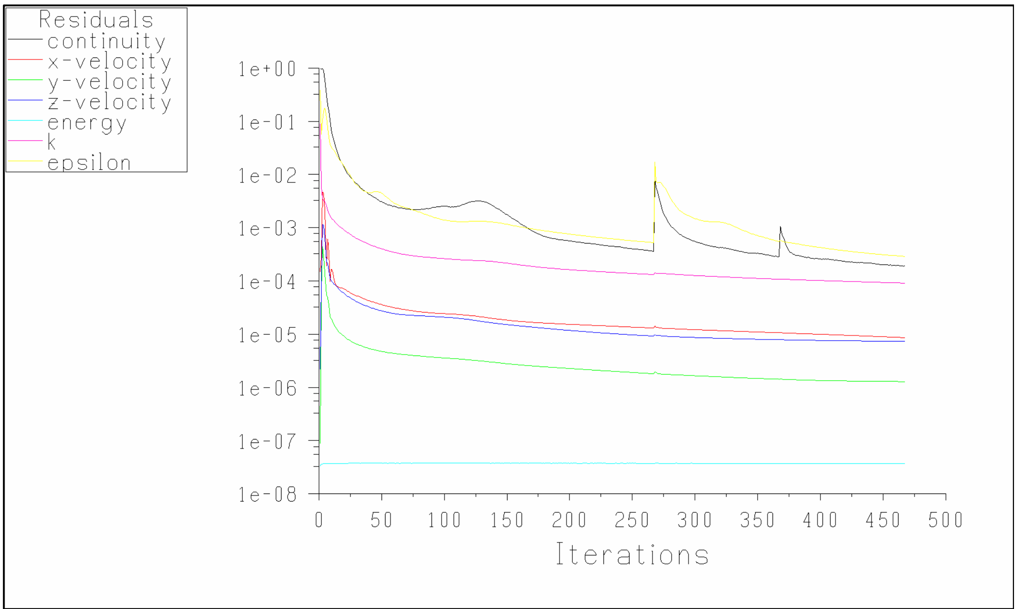

Figure 1.1.1(c) – Residual Plot Showing the Convergence History for the CFD-Predictions obtained for the 5 x 5 Arrangement of Pipes with a Diameter of 0.4 m. Pipes Represented Explicitly within the CFD Mesh

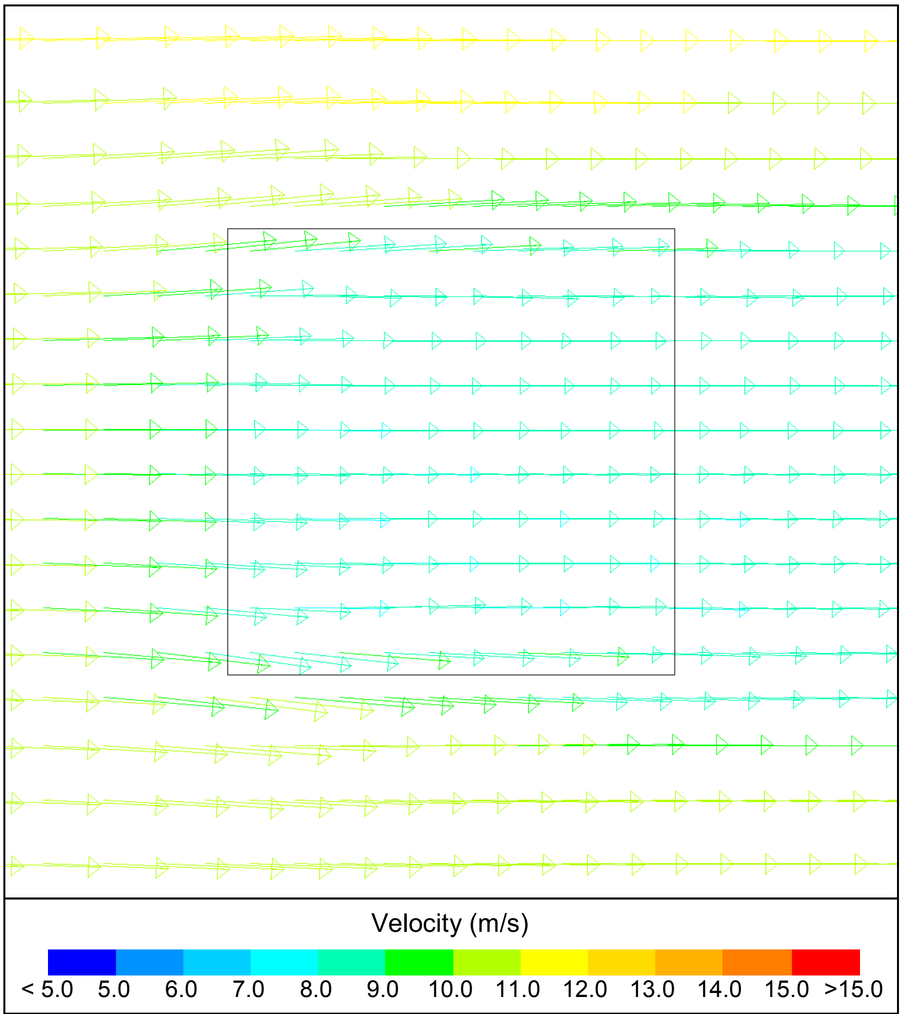

Figure 1.1.2(a) – Velocity Profile obtained for the 5 x 5 Arrangement of Pipes with a Diameter of 0.4 mm. Pipes Represented using the ACE Method

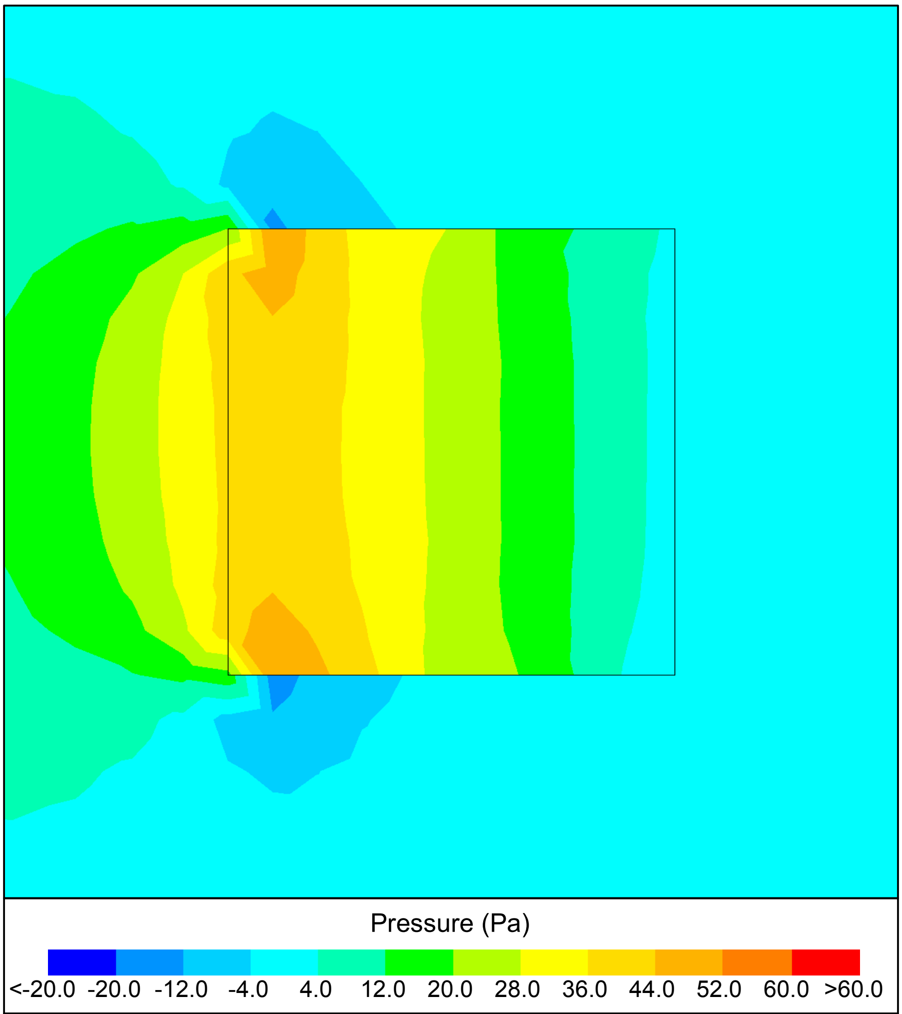

Figure 1.1.2(b) – Pressure Profile obtained for the 5 x 5 Arrangement of Pipes with a Diameter of 0.4 m. Pipes Represented using the ACE Method

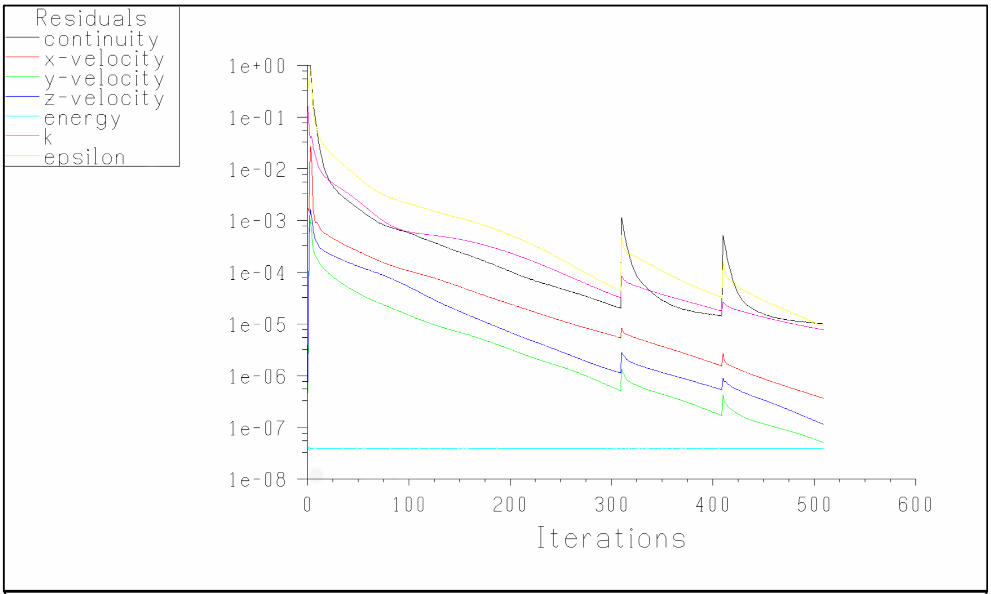

Figure 1.1.2(c) – Residual Plot Showing the Convergence History for the CFD-Predictions obtained for the 5 x 5 Arrangement of Pipes with a Diameter of 0.4 m. Pipes Represented using the ACE Method

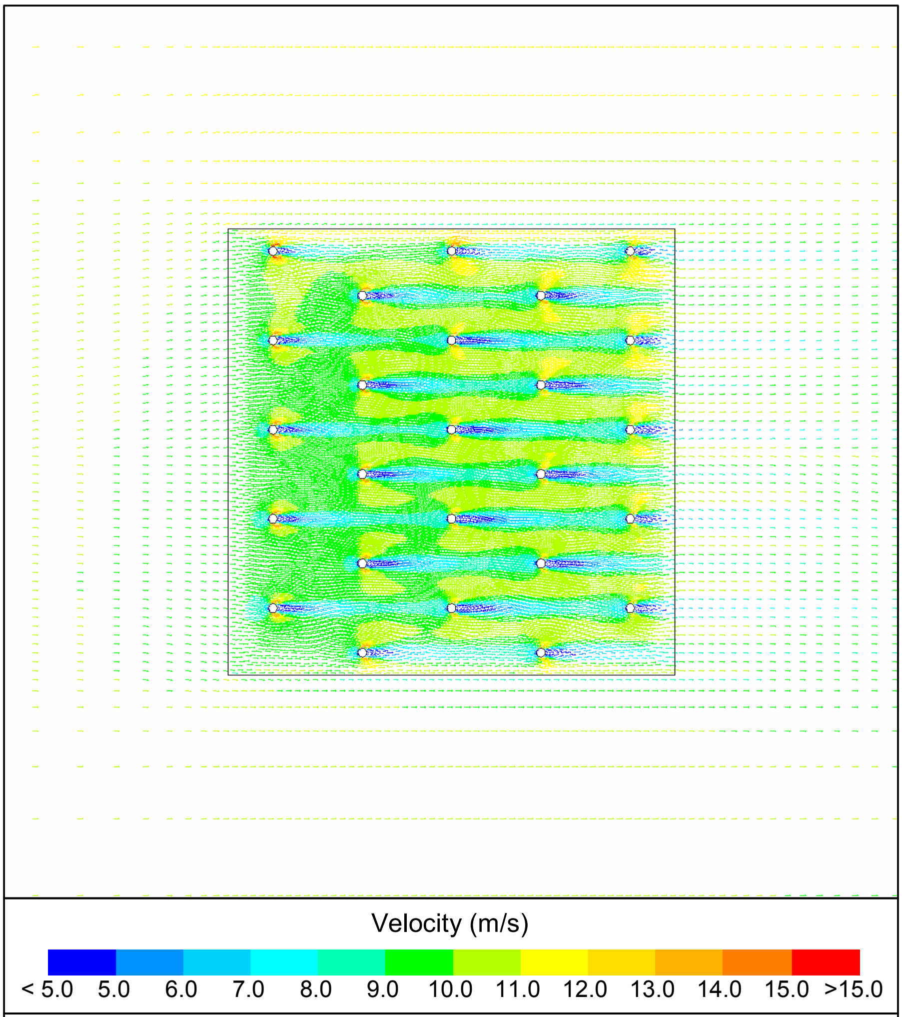

Figure 1.2.1(a) – Velocity Profile obtained for the 5 x 5 Arrangement of Pipes with a Diameter of 0.2 m. Pipes Represented Explicitly within the CFD Mesh

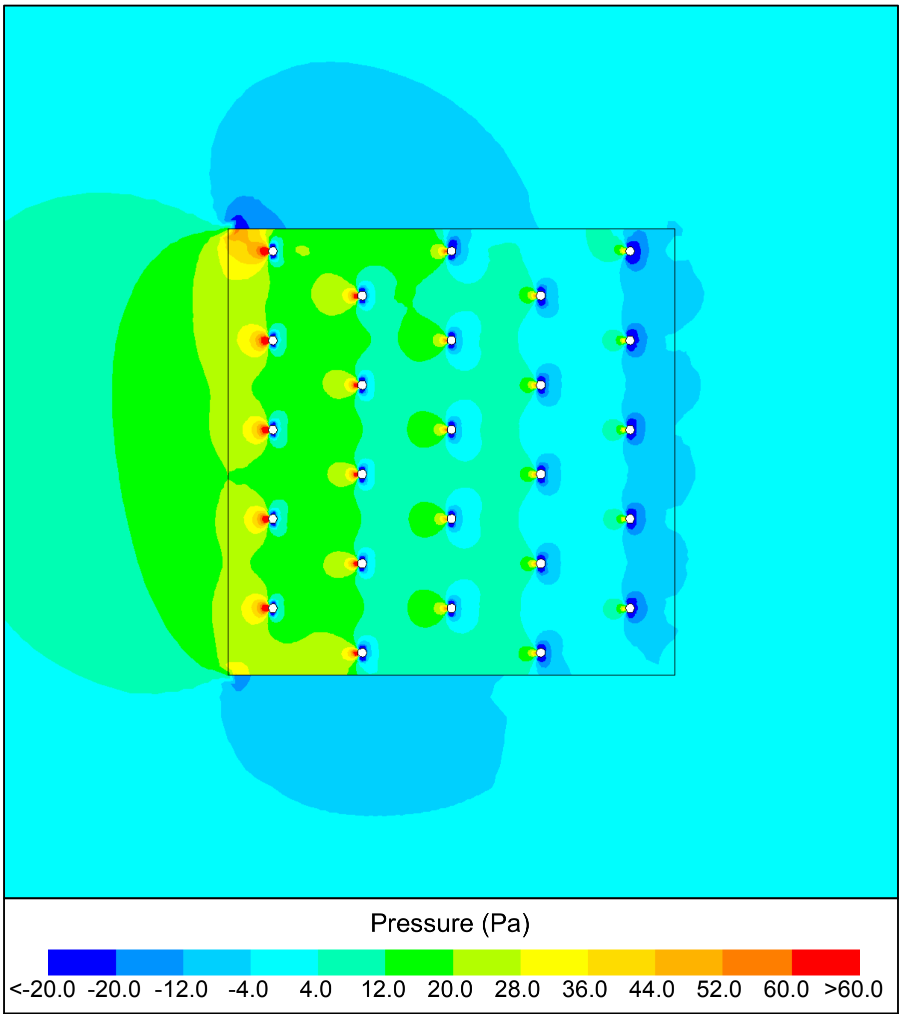

Figure 1.2.1(b) – Pressure Profile obtained for the 5 x 5 Arrangement of Pipes with a Diameter of 0.2 m. Pipes Represented Explicitly within the CFD Mesh

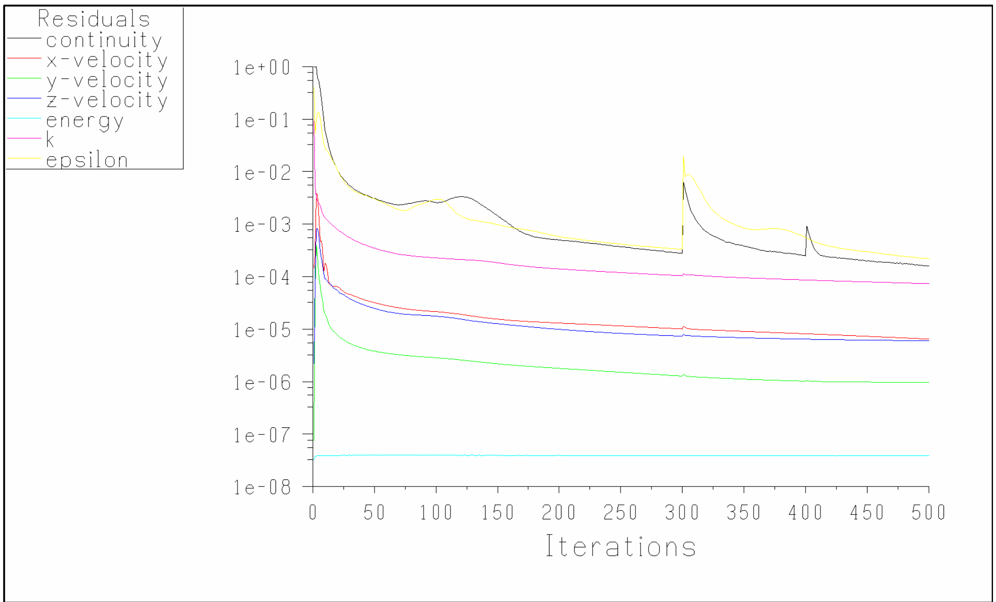

Figure 1.2.1(c) – Residual Plot Showing the Convergence History for the CFD-Predictions obtained for the 5 x 5 Arrangement of Pipes with a Diameter of 0.2 m. Pipes Represented Explicitly within the CFD Mesh

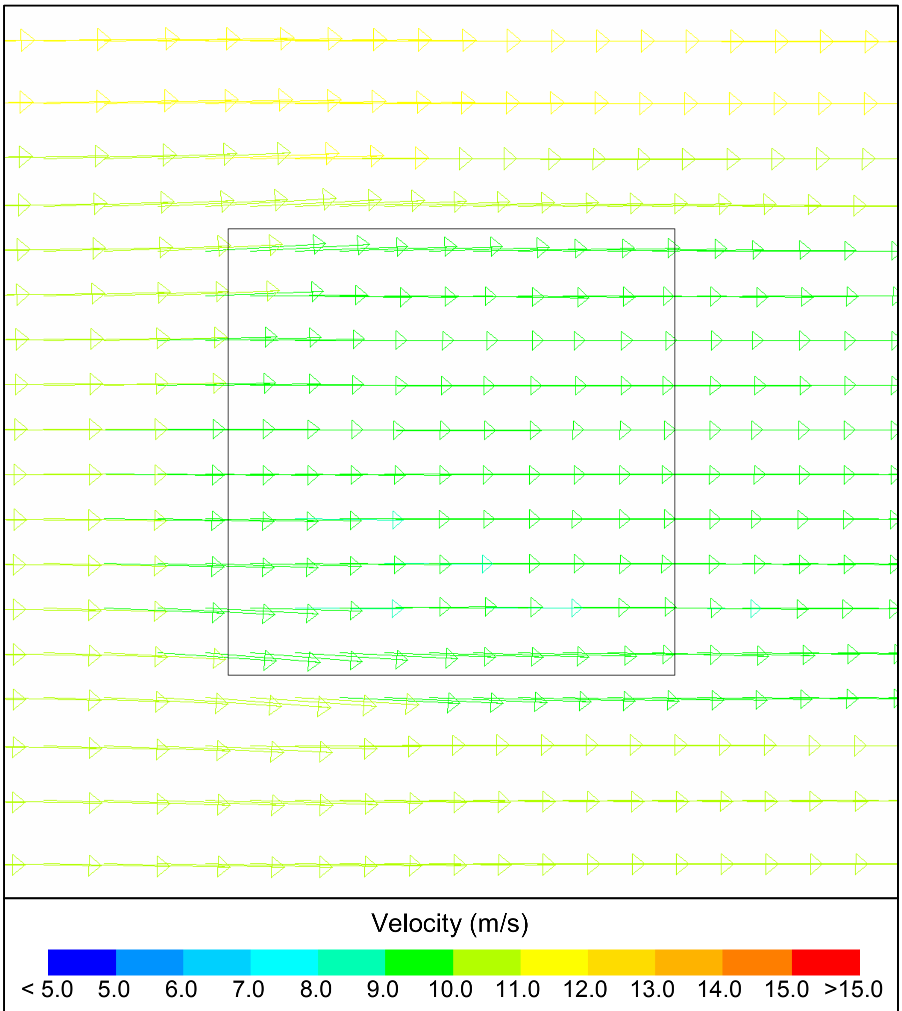

Figure 1.2.2(a) – Velocity Profile obtained for the 5 x 5 Arrangement of Pipes with a Diameter of 0.2 m. Pipes Represented using the ACE Method

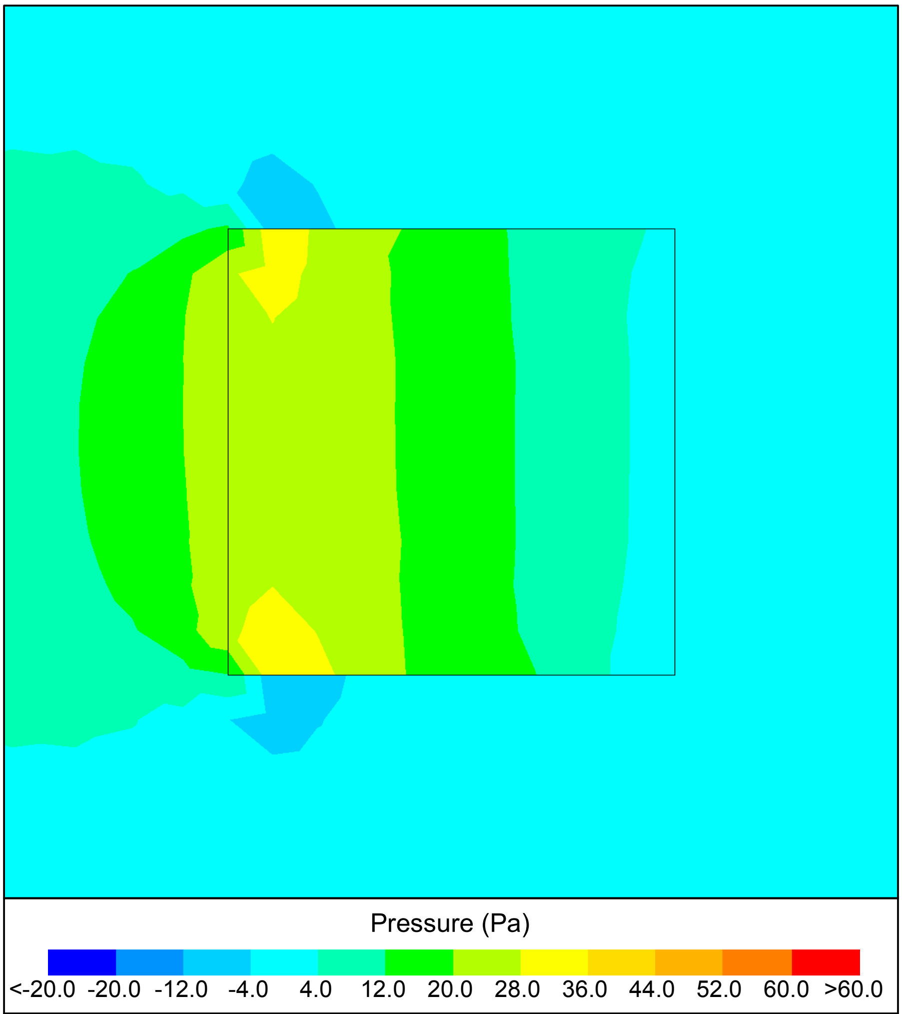

Figure 1.2.2(b) – Pressure Profile obtained for the 5 x 5 Arrangement of Pipes with a Diameter of 0.2 m. Pipes Represented using the ACE Method

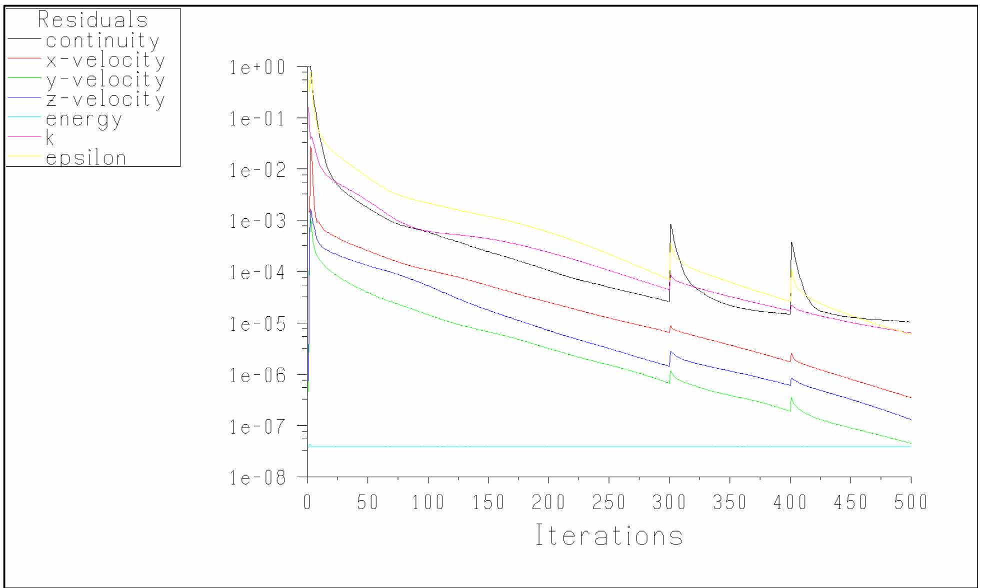

Figure 1.2.2(c) – Residual Plot Showing the Convergence History for the CFD-Predictions obtained for the 5 x 5 Arrangement of Pipes with a Diameter of 0.2 m. Pipes Represented using the ACE Method

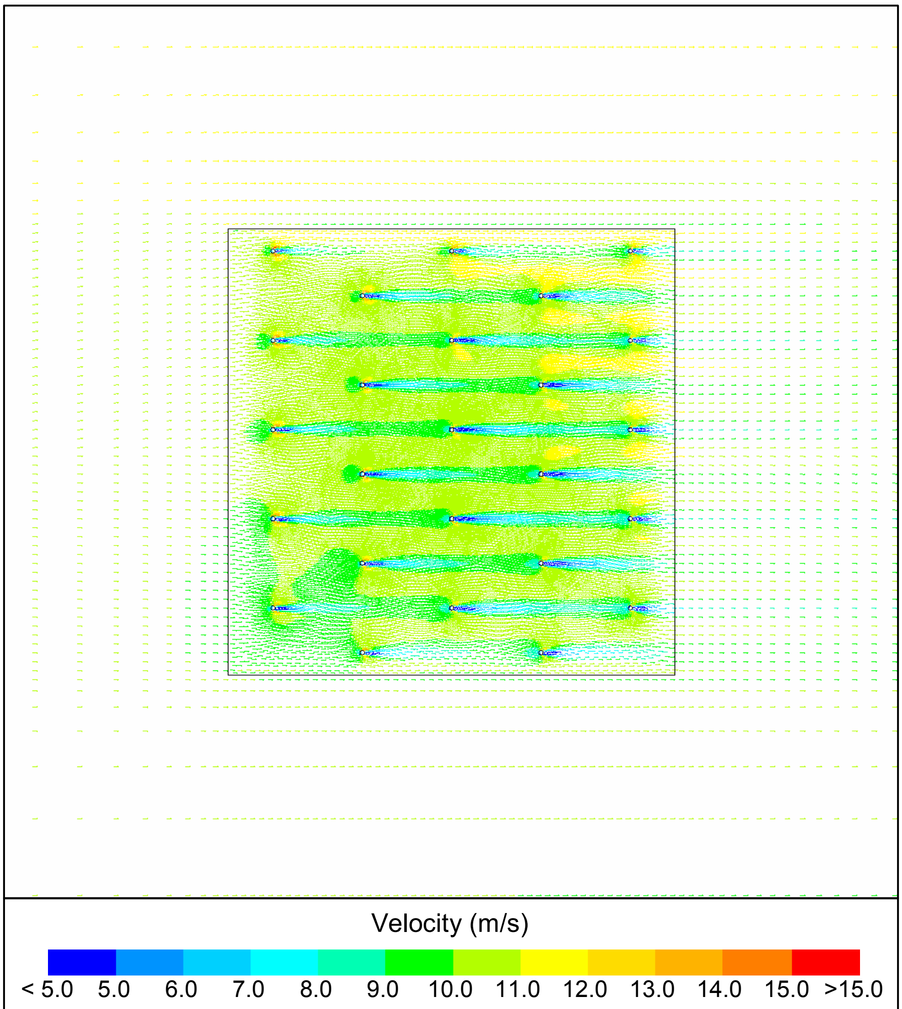

Figure 1.3.1(a) – Velocity Profile obtained for the 5 x 5 Arrangement of Pipes with a Diameter of 0.1 m. Pipes Represented Explicitly within the CFD Mesh

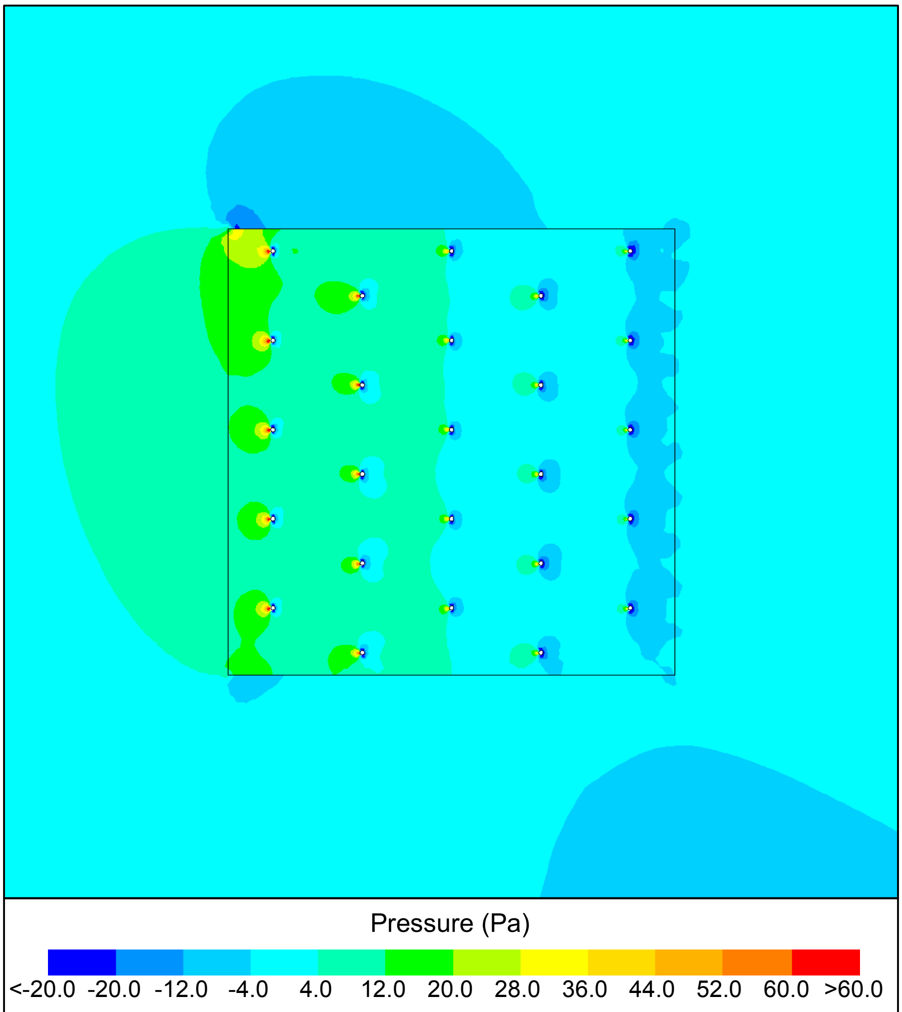

Figure 1.3.1(b) – Pressure Profile obtained for the 5 x 5 Arrangement of Pipes with a Diameter of 0.1 m. Pipes Represented Explicitly within the CFD Mesh

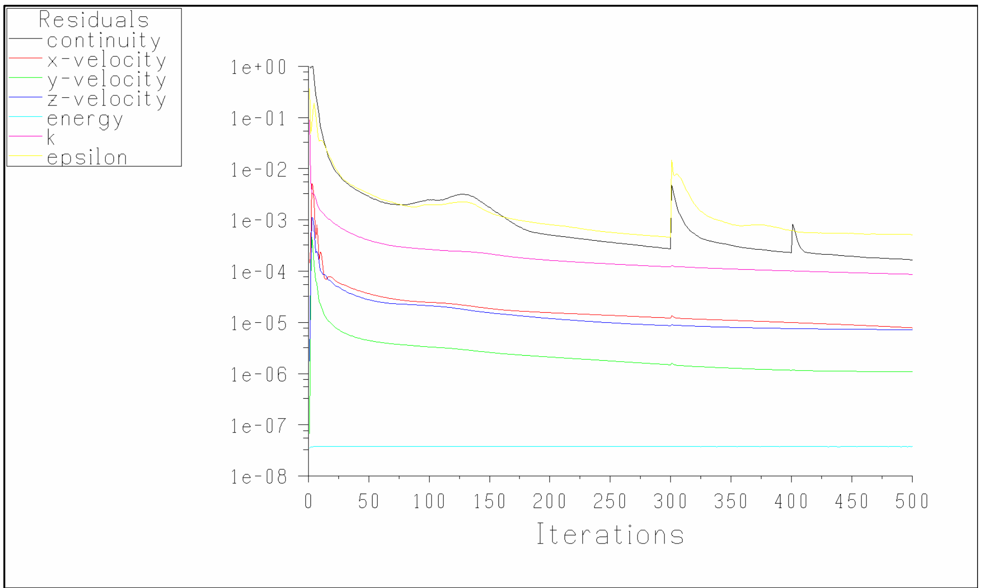

Figure 1.3.1(c) – Residual Plot Showing the Convergence History for the CFD-Predictions obtained for the 5 x 5 Arrangement of Pipes with a Diameter of 0.1 m. Pipes Represented Explicitly within the CFD Mesh

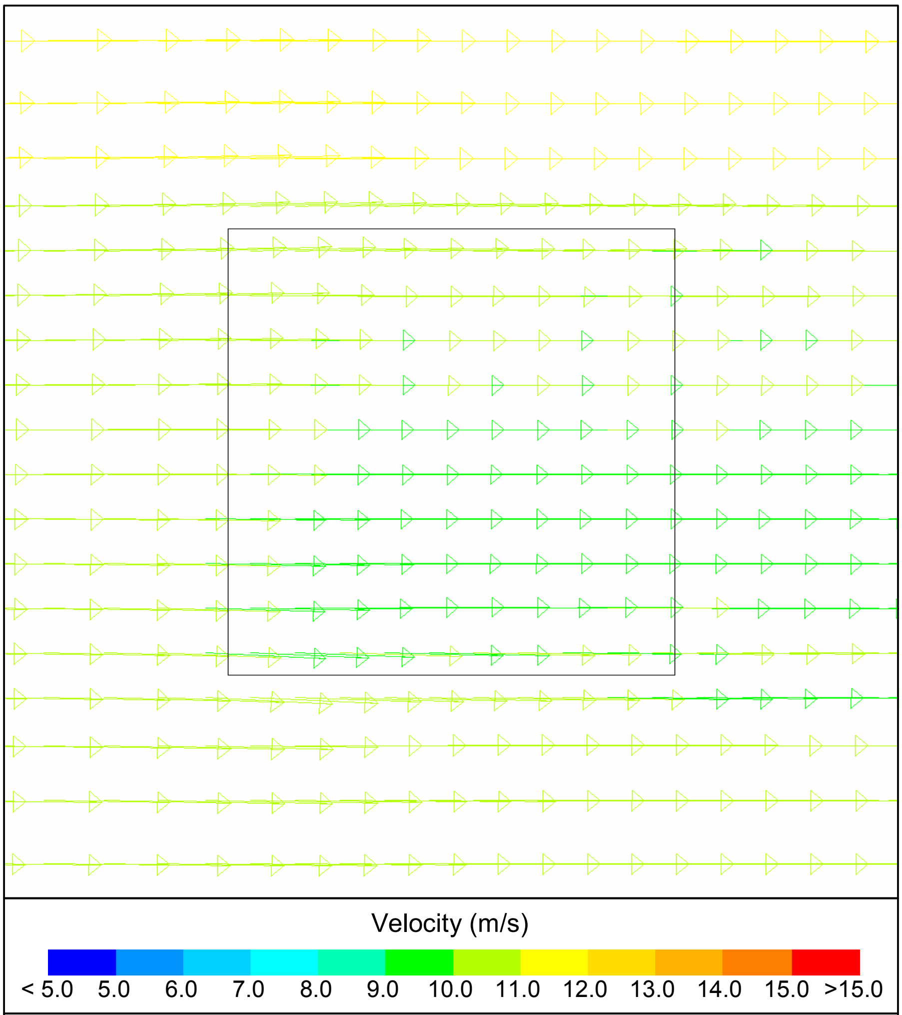

Figure 1.3.2(a) – Velocity Profile obtained for the 5 x 5 Arrangement of Pipes with a Diameter of 0.1 m. Pipes Represented using the ACE Method

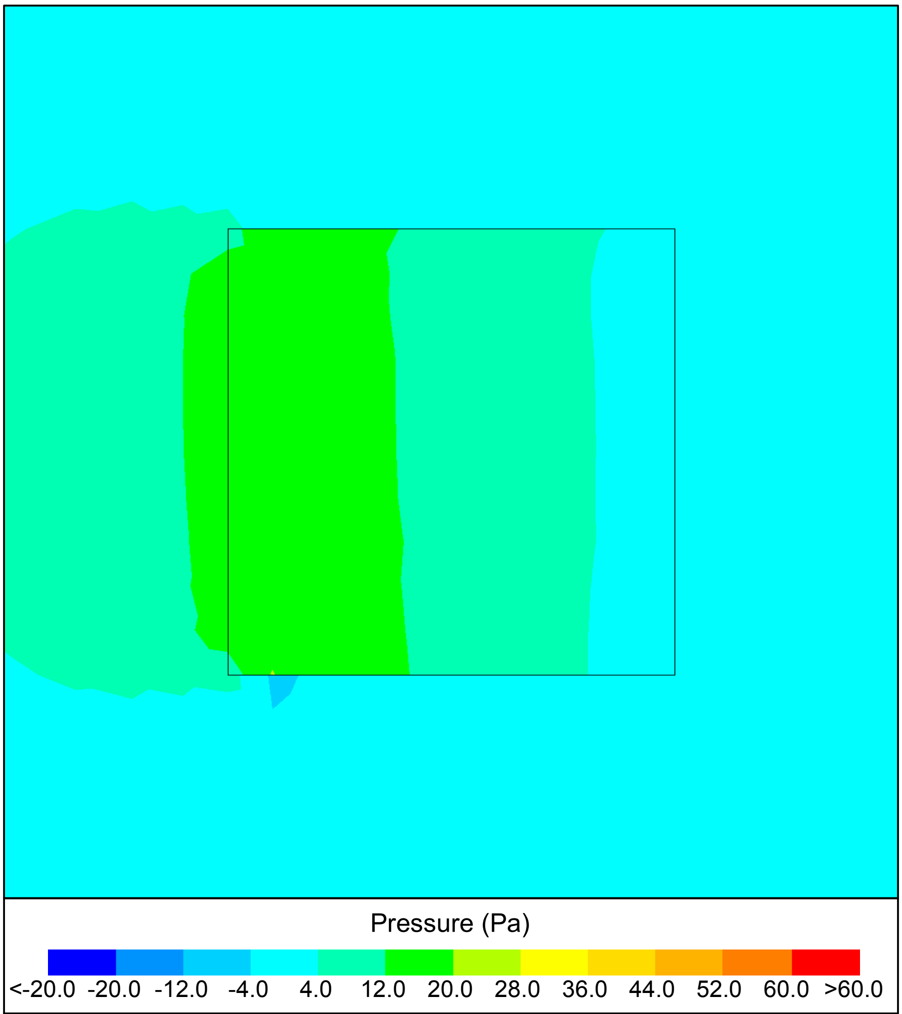

Figure 1.3.2(b) – Pressure Profile obtained for the 5 x 5 Arrangement of Pipes with a Diameter of 0.1 m. Pipes Represented using the ACE Method

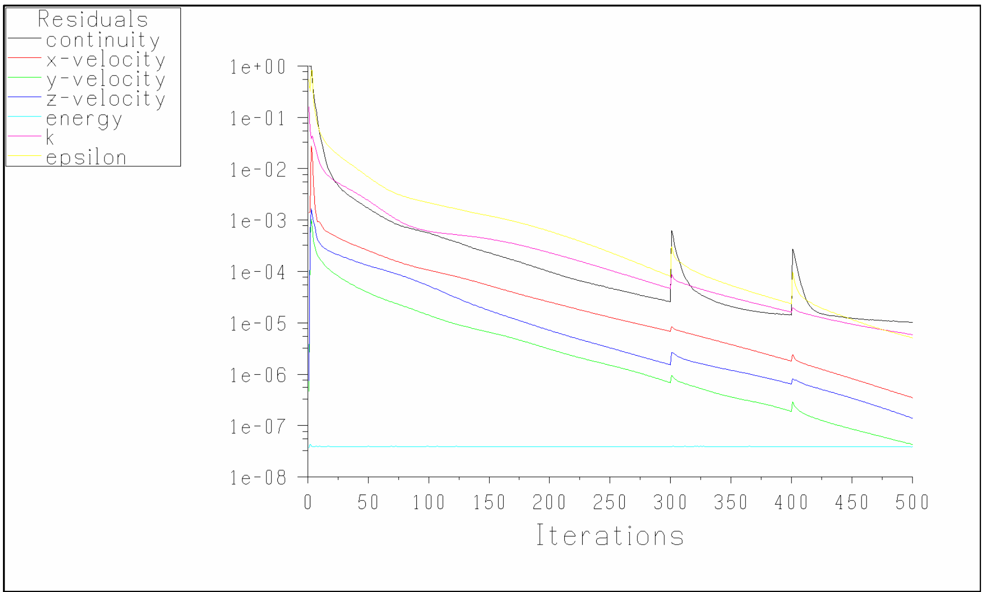

Figure 1.3.2(c) – Residual Plot Showing the Convergence History for the CFD-Predictions obtained for the 5 x 5 Arrangement of Pipes with a Diameter of 0.1 m. Pipes Represented using the ACE Method

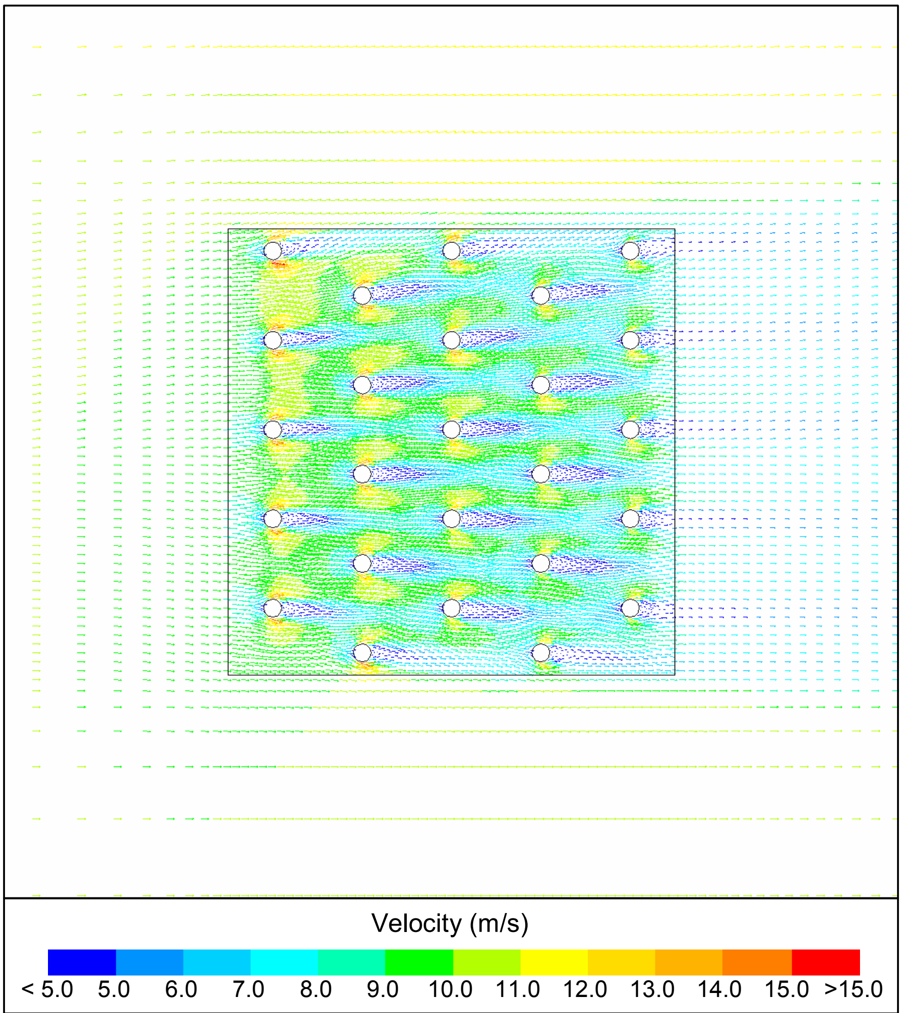

Figure 1.4.1(a) – Velocity Profile obtained for the 5 x 5 Arrangement of Pipes with a Diameter of 0.4 m and the Top and Bottom Surfaces of the Box Excluded. Pipes Represented Explicitly within the CFD Mesh

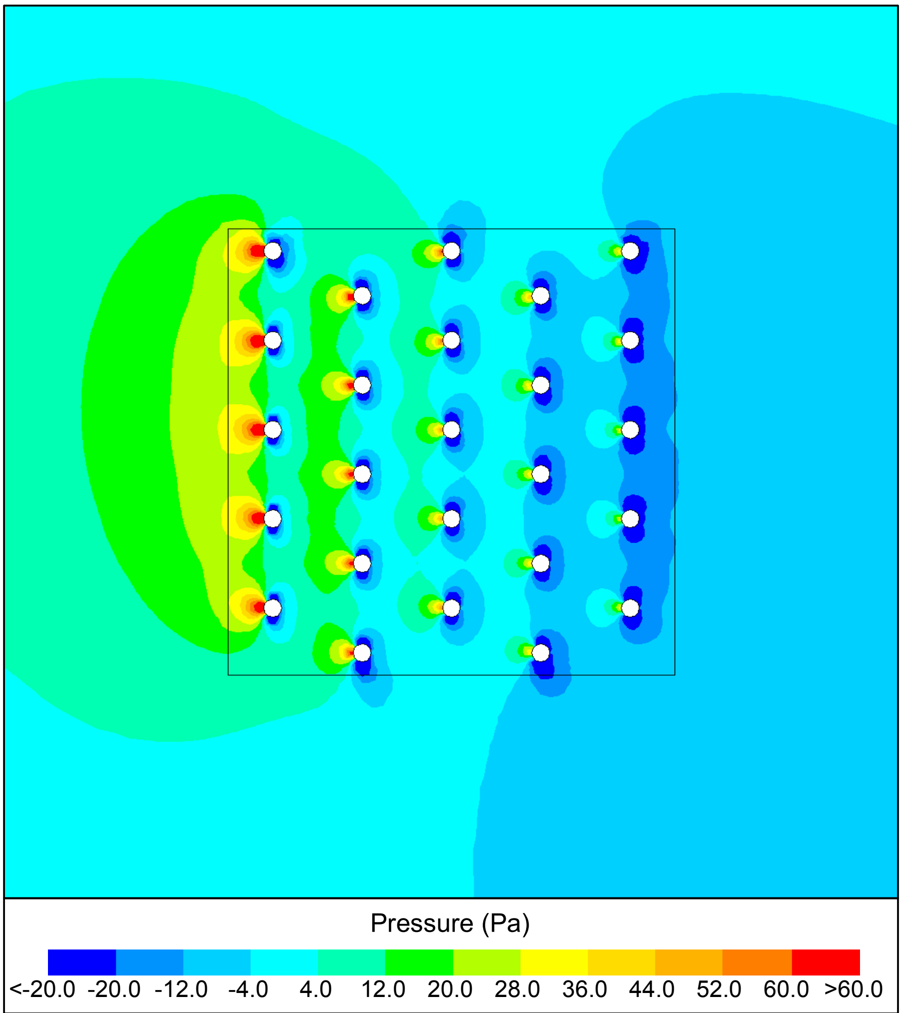

Figure 1.4.1(b) – Pressure Profile obtained for the 5 x 5 Arrangement of Pipes with a Diameter of 0.4 m and the Top and Bottom Surfaces of the Box Excluded. Pipes Represented Explicitly within the CFD Mesh

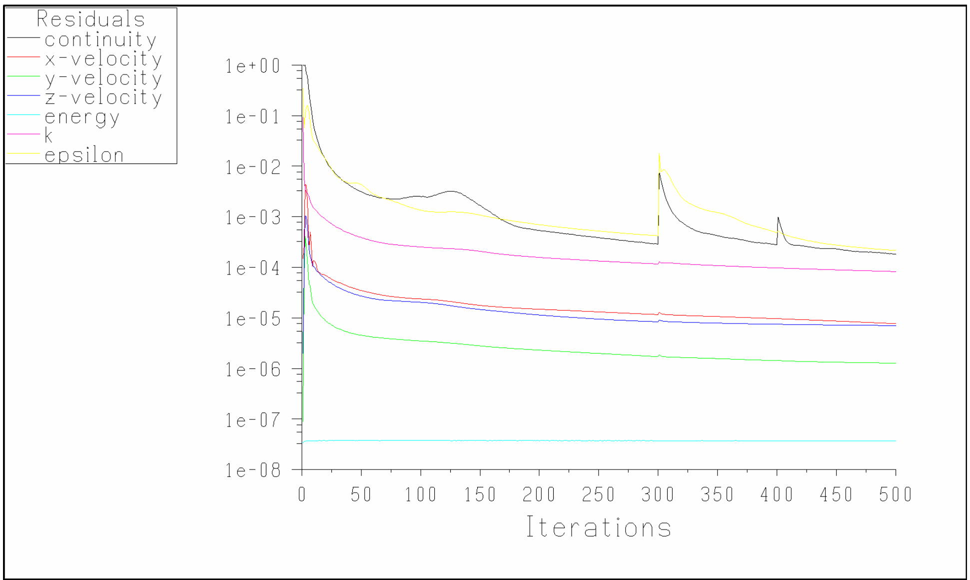

Figure 1.4.1(c) – Residual Plot Showing the Convergence History for the CFD-Predictions obtained for the 5 x 5 Arrangement of Pipes with a Diameter of 0.4 m and the Top and Bottom Surfaces of the Box Excluded. Pipes Represented Explicitly within the CFD Mesh

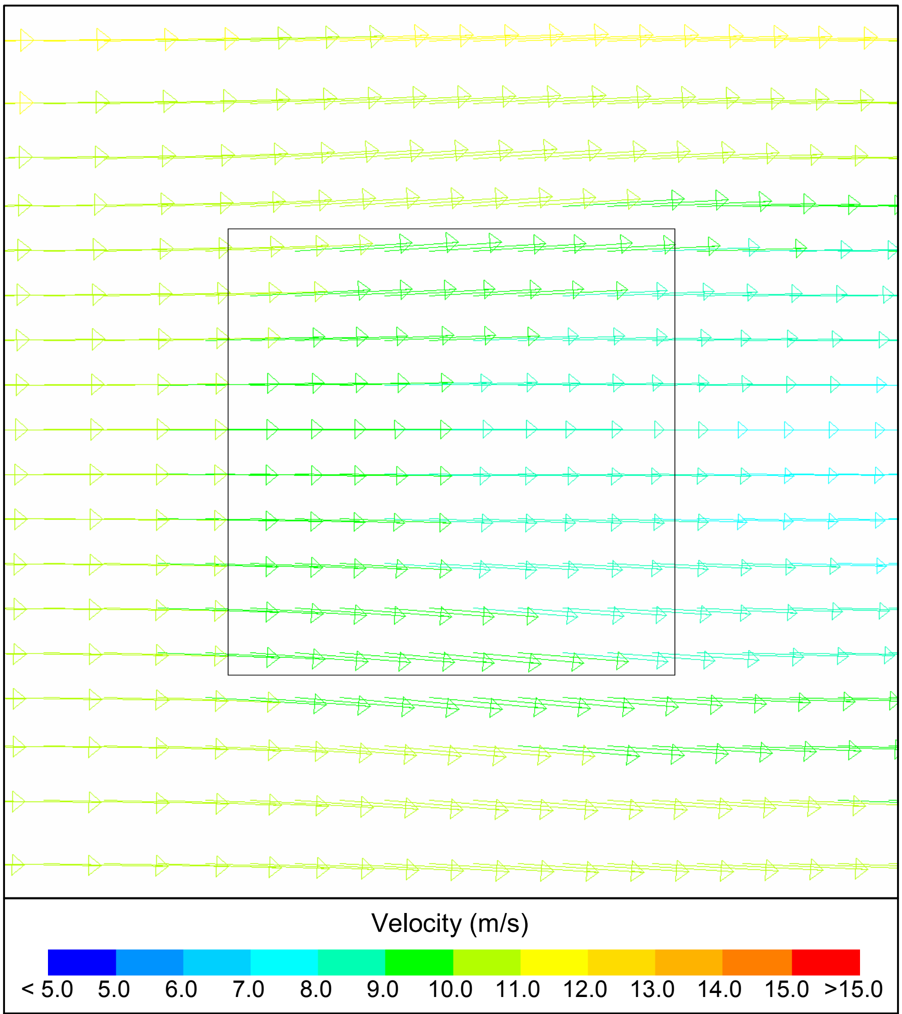

Figure 1.4.2(a) – Velocity Profile obtained for the 5 x 5 Arrangement of Pipes with a Diameter of 0.4 m and the Top and Bottom Surfaces of the Box Excluded. Pipes Represented using the ACE Method

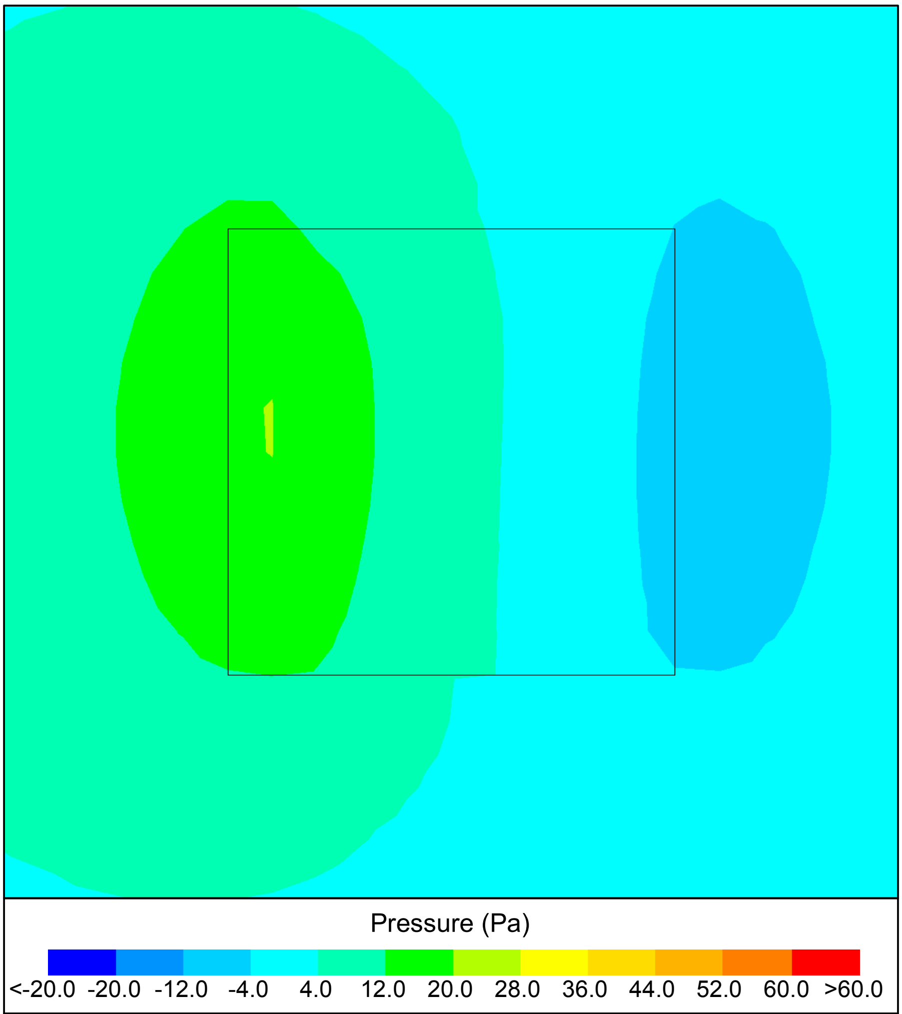

Figure 1.4.2(b) – Pressure Profile obtained for the 5 x 5 Arrangement of Pipes with a Diameter of 0.4 m and the Top and Bottom Surfaces of the Box Excluded. Pipes Represented using the ACE Method

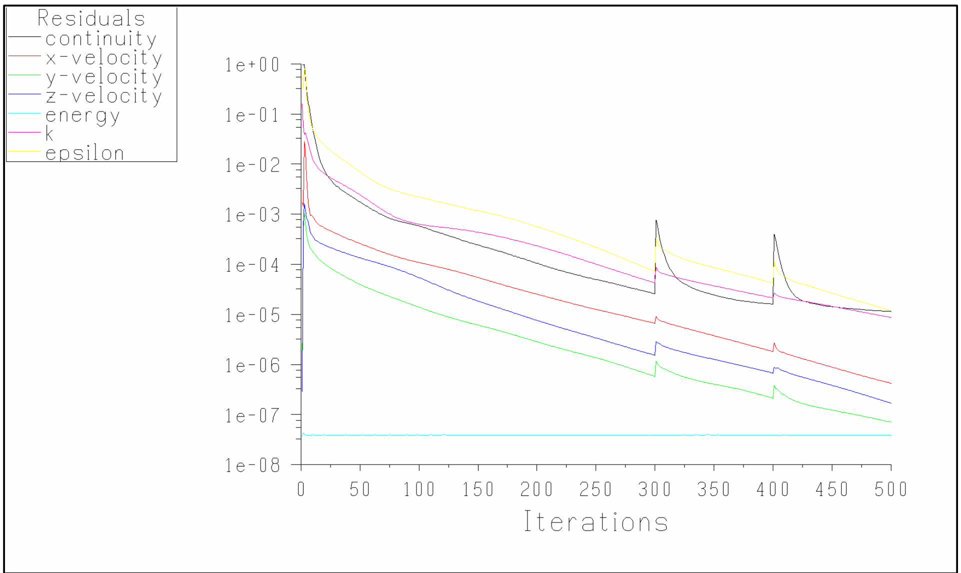

Figure 1.4.2(c) – Residual Plot Showing the Convergence History for the CFD-Predictions obtained for the 5 x 5 Arrangement of Pipes with a Diameter of 0.4 m and the Top and Bottom Surfaces of the Box Excluded. Pipes Represented using the ACE Method

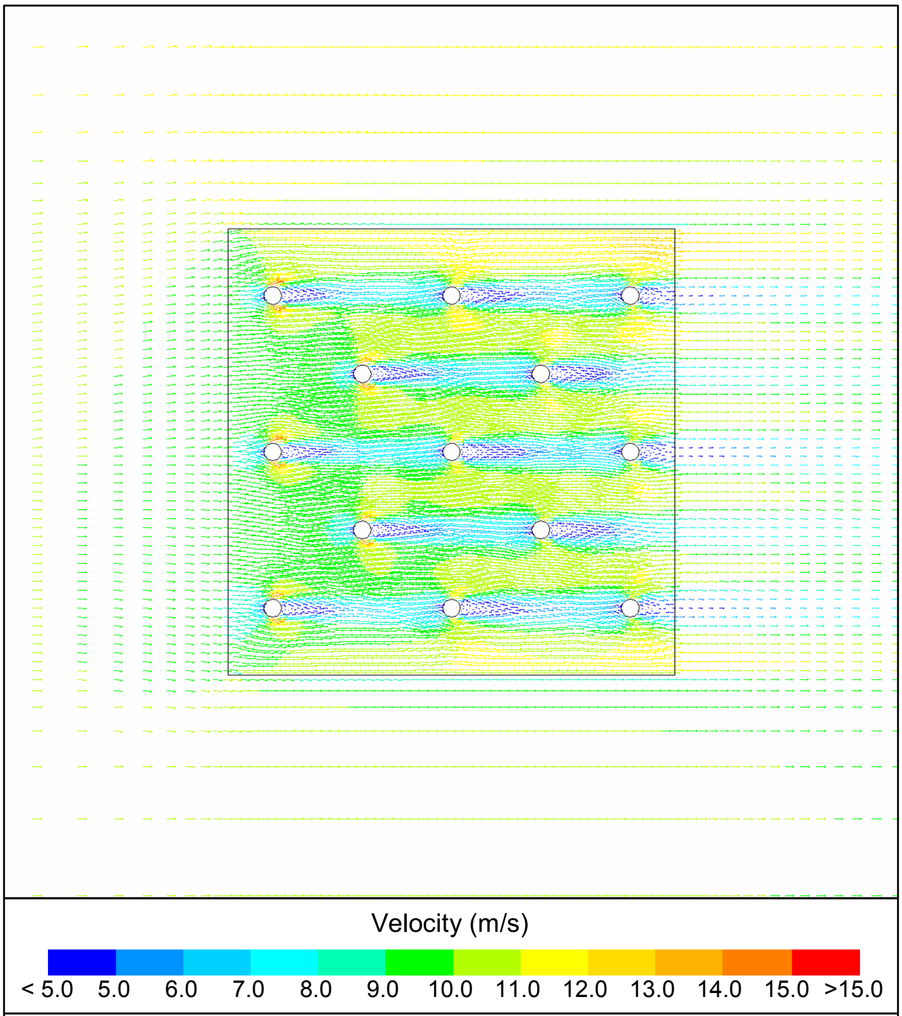

Figure 1.5.1(a) – Velocity Profile obtained for the 5 x 3 Arrangement of Pipes with a Diameter of 0.4 m. Pipes Represented Explicitly within the CFD Mesh

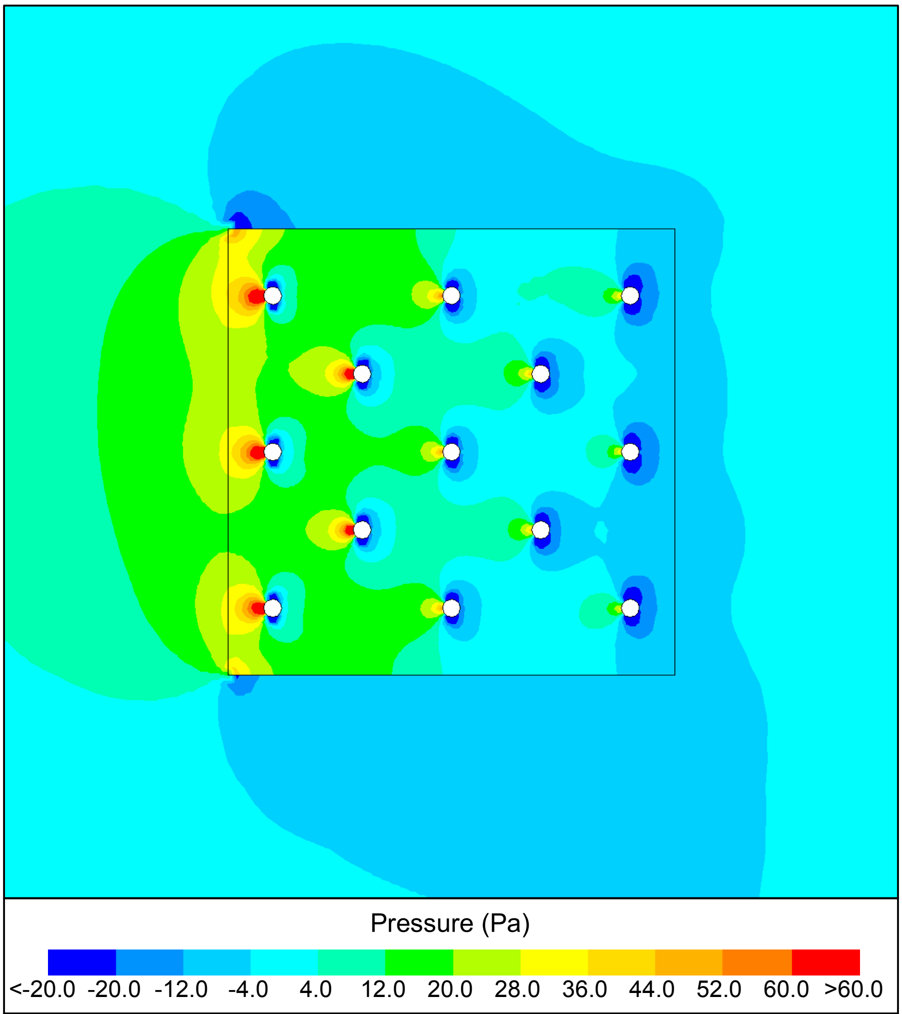

Figure 1.5.1(b) – Pressure Profile obtained for the 5 x 3 Arrangement of Pipes with a Diameter of 0.4 m. Pipes Represented Explicitly within the CFD Mesh

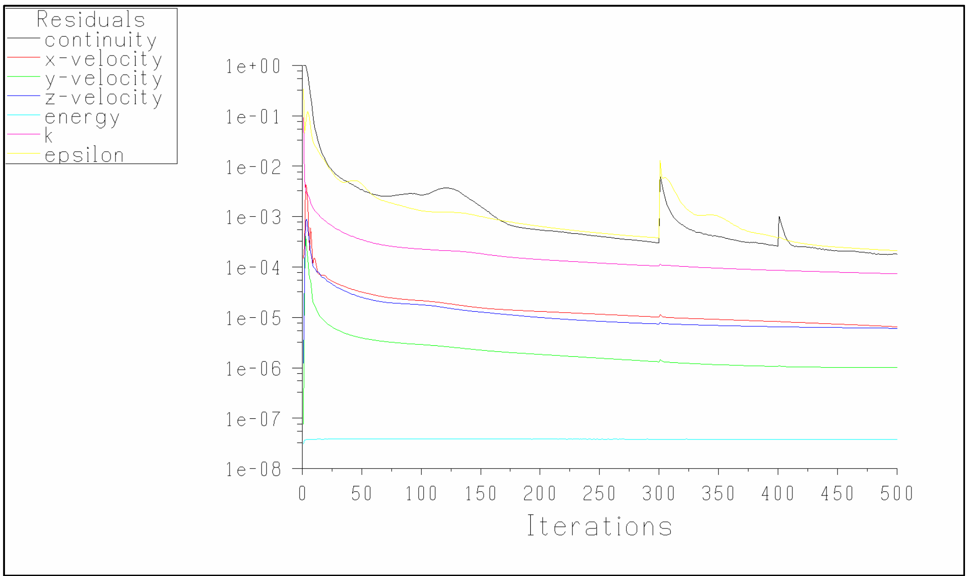

Figure 1.5.1(c) – Residual Plot Showing the Convergence History for the CFD-Predictions obtained for the 5 x 3 Arrangement of Pipes with a Diameter of 0.4 m. Pipes Represented Explicitly within the CFD Mesh

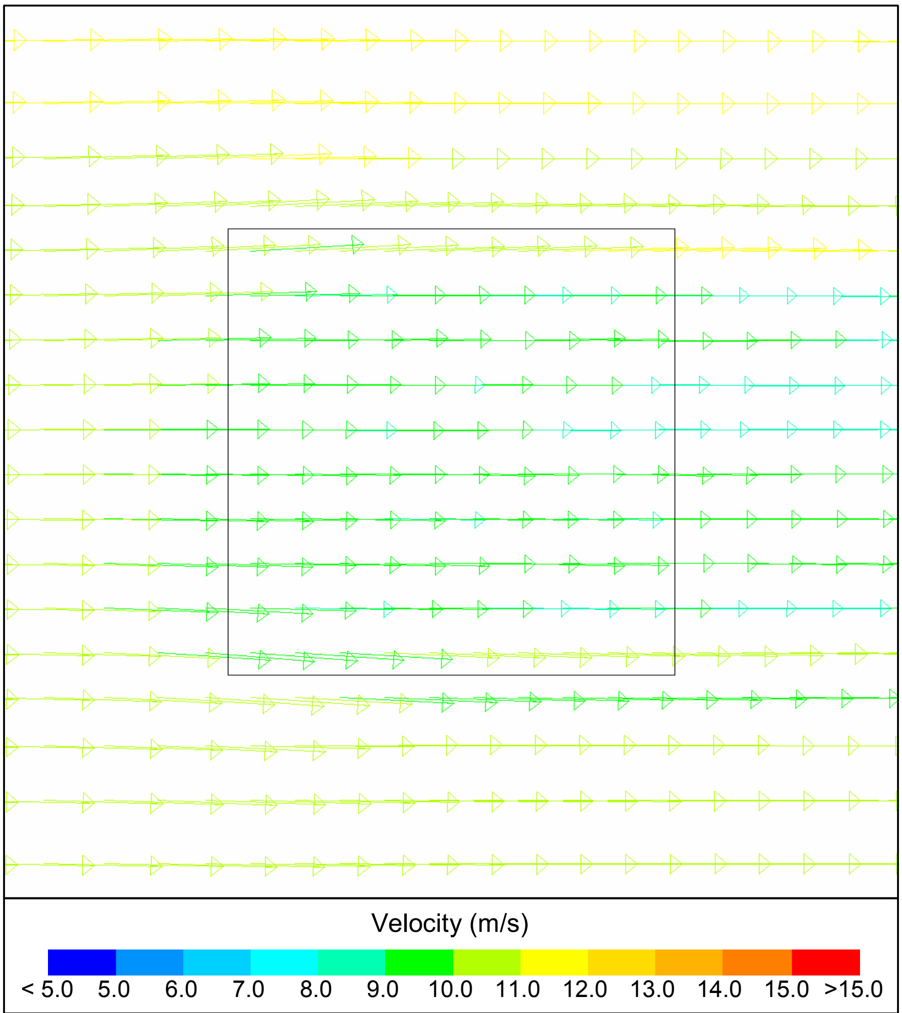

Figure 1.5.2(a) – Velocity Profile obtained for the 5 x 3 Arrangement of Pipes with a Diameter of 0.4 m. Pipes Represented using the ACE Method

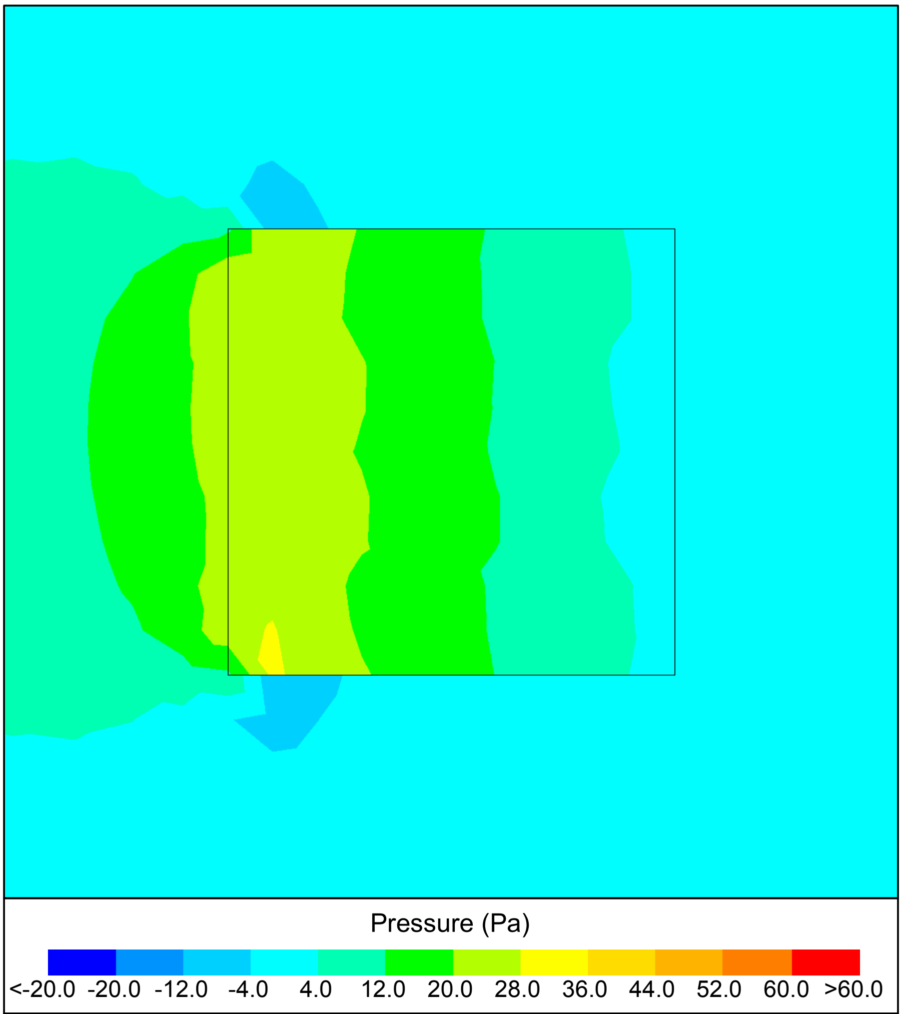

Figure 1.5.2(b) – Pressure Profile obtained for the 5 x 3 Arrangement of Pipes with a Diameter of 0.4 m. Pipes Represented using the ACE Method

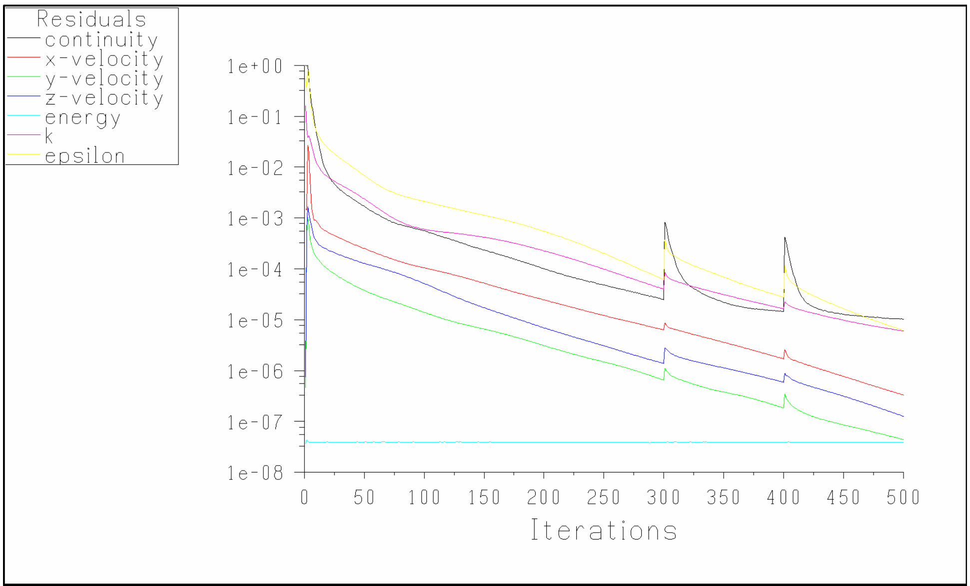

Figure 1.5.2(c) – Residual Plot Showing the Convergence History for the CFD-Predictions obtained for the 5 x 3 Arrangement of Pipes with a Diameter of 0.4 m. Pipes Represented using the ACE Method

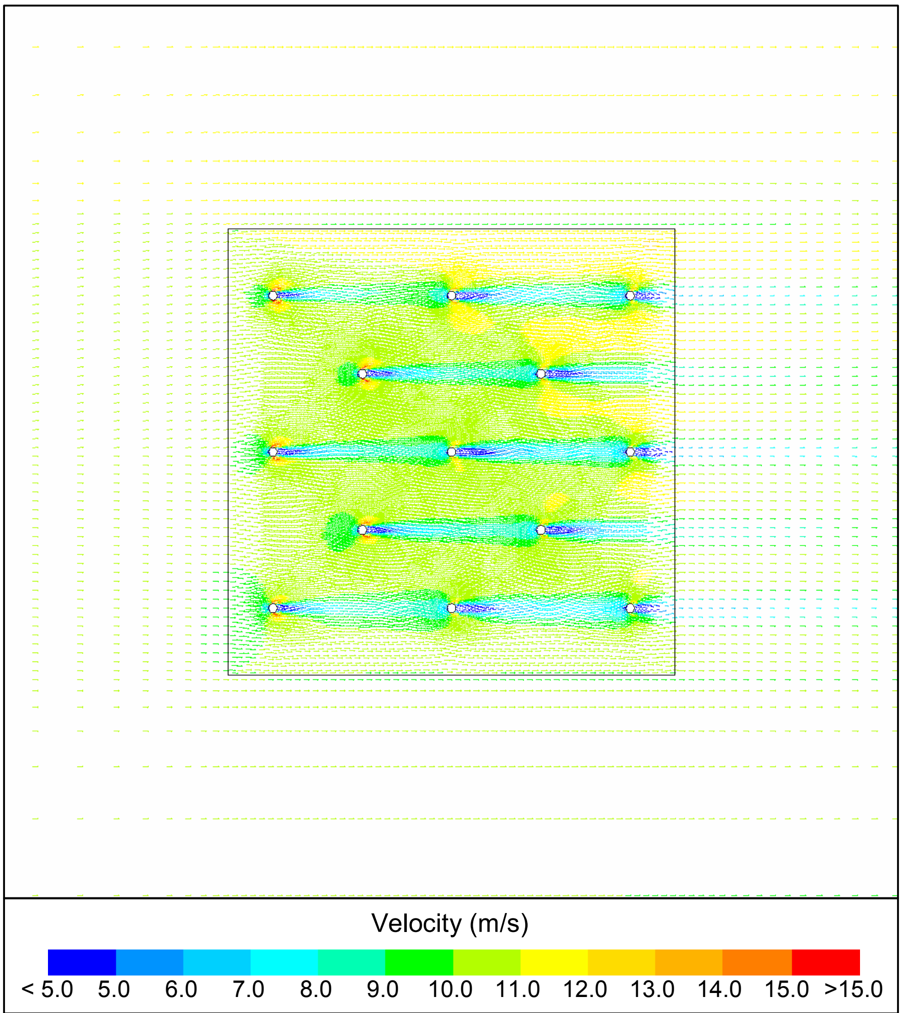

Figure 1.6.1(a) – Velocity Profile obtained for the 5 x 3 Arrangement of Pipes with a Diameter of 0.2 m. Pipes Represented Explicitly within the CFD Mesh

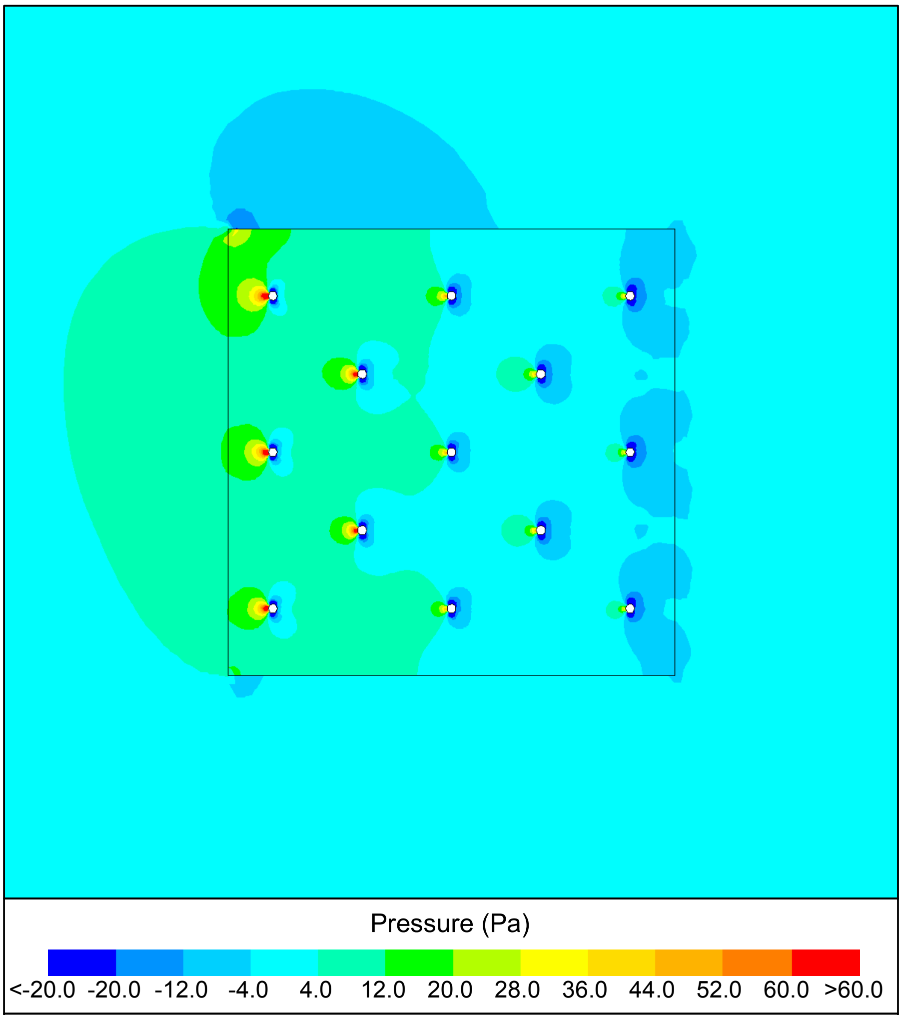

Figure 1.6.1(b) – Pressure Profile obtained for the 5 x 3 Arrangement of Pipes with a Diameter of 0.2 m. Pipes Represented Explicitly within the CFD Mesh

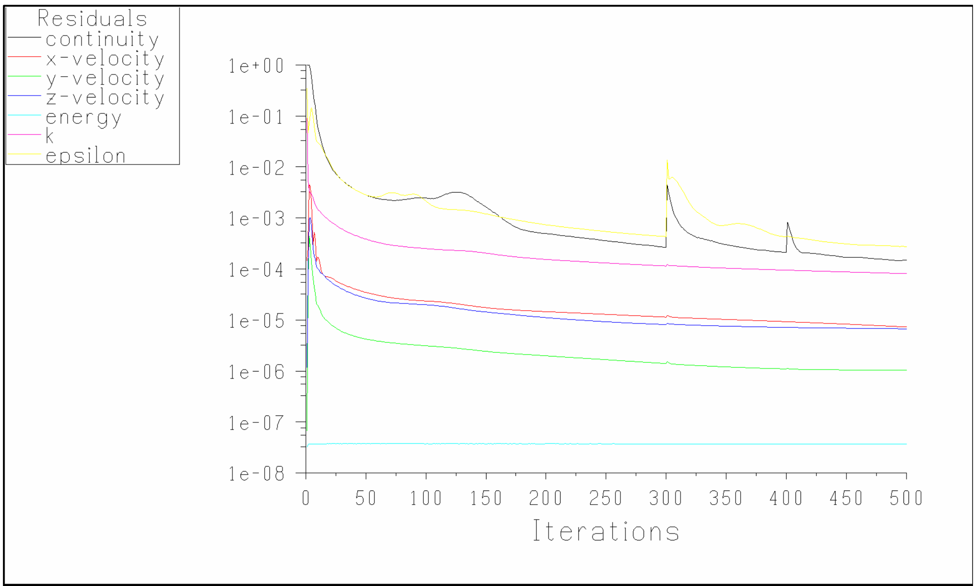

Figure 1.6.1(c) – Residual Plot Showing the Convergence History for the CFD-Predictions obtained for the 5 x 3 Arrangement of Pipes with a Diameter of 0.2 m. Pipes Represented Explicitly within the CFD Mesh

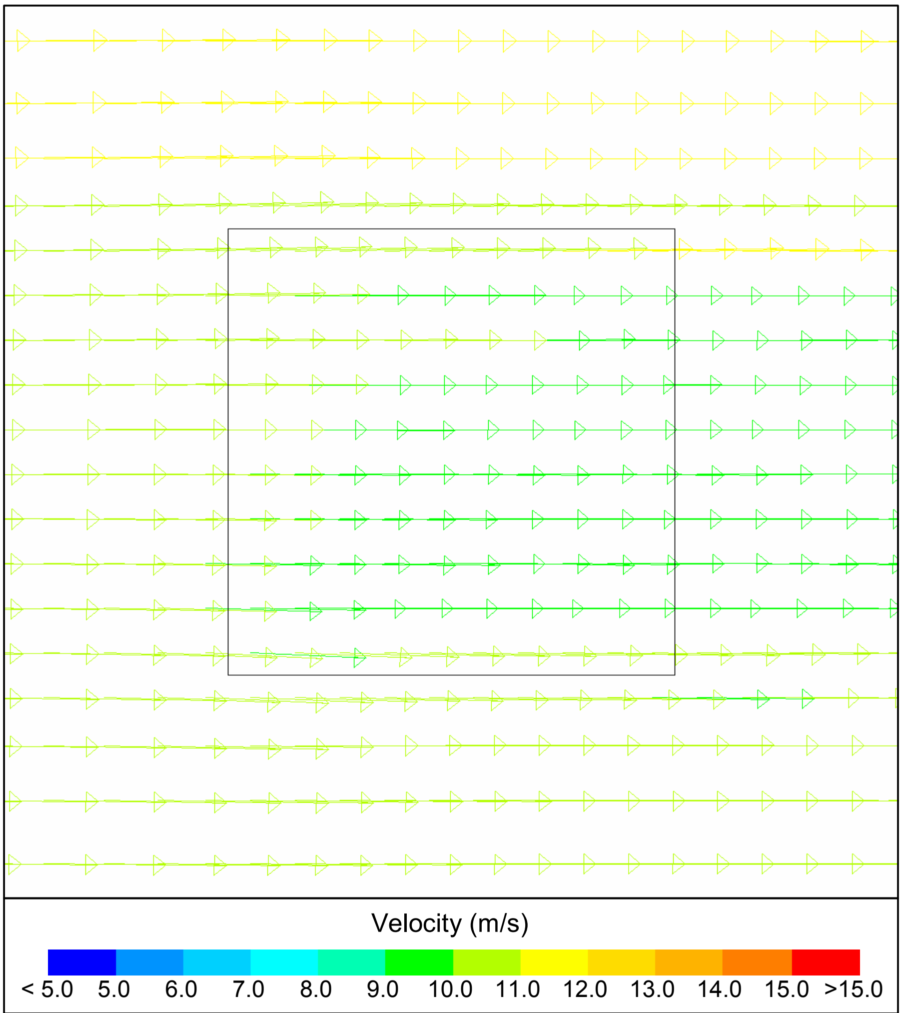

Figure 1.6.2(a) – Velocity Profile obtained for the 5 x 3 Arrangement of Pipes with a Diameter of 0.2 m. Pipes Represented using the ACE Method

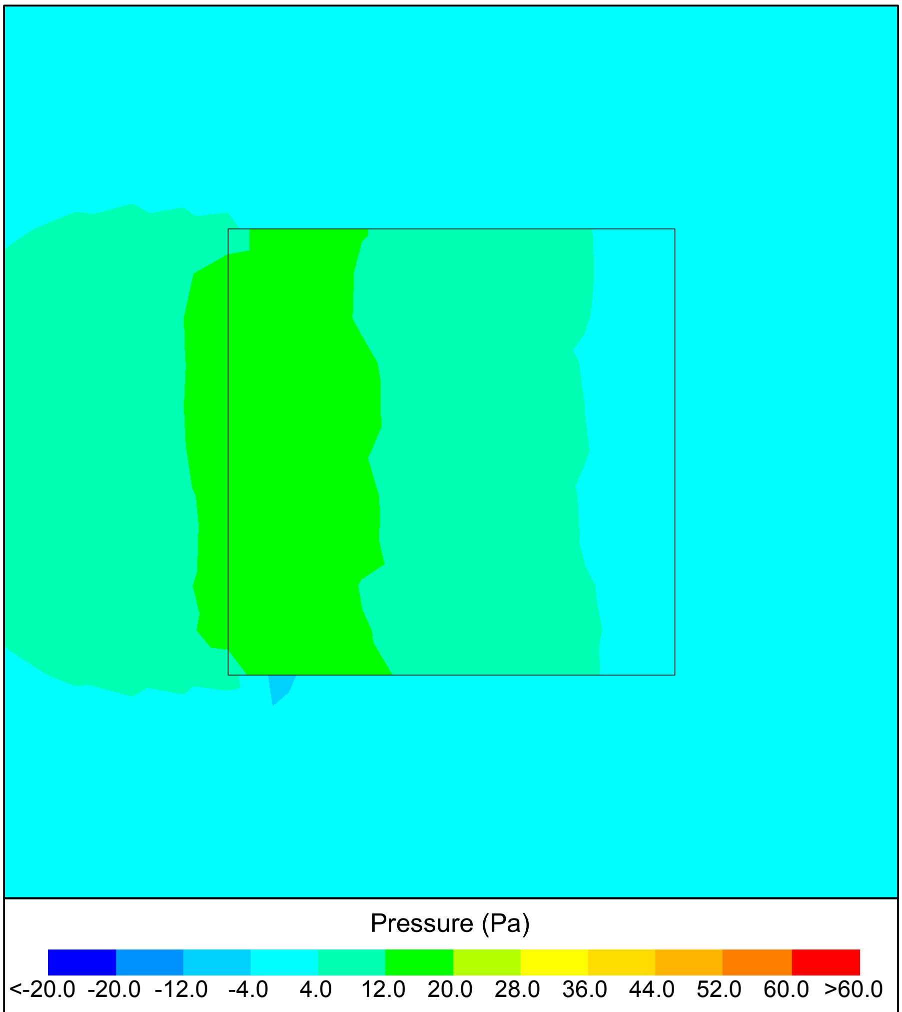

Figure 1.6.2(b) – Pressure Profile obtained for the 5 x 3 Arrangement of Pipes with a Diameter of 0.2 m. Pipes Represented using the ACE Method

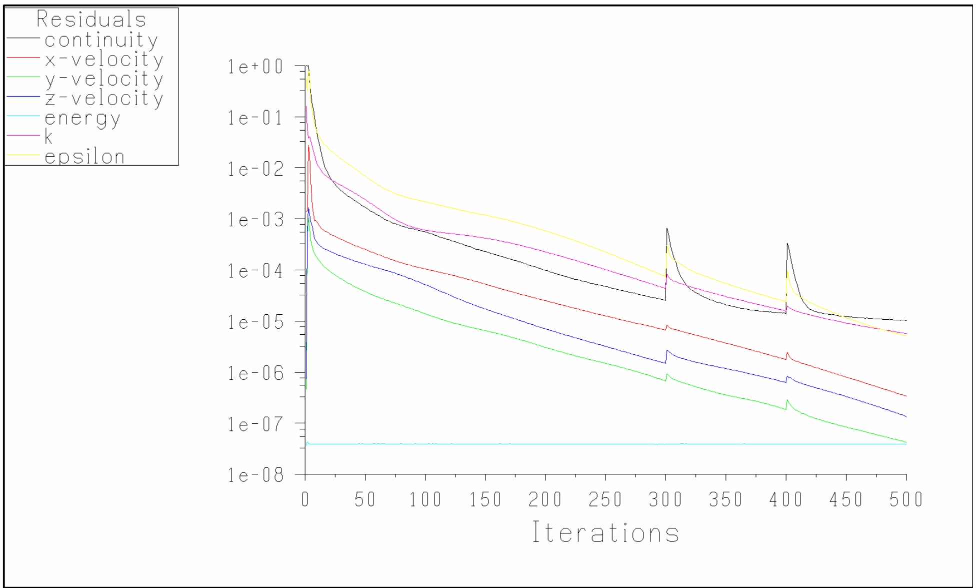

Figure 1.6.2(c) – Residual Plot Showing the Convergence History for the CFD-Predictions obtained for the 5 x 3 Arrangement of Pipes with a Diameter of 0.2 m. Pipes Represented using the ACE Method

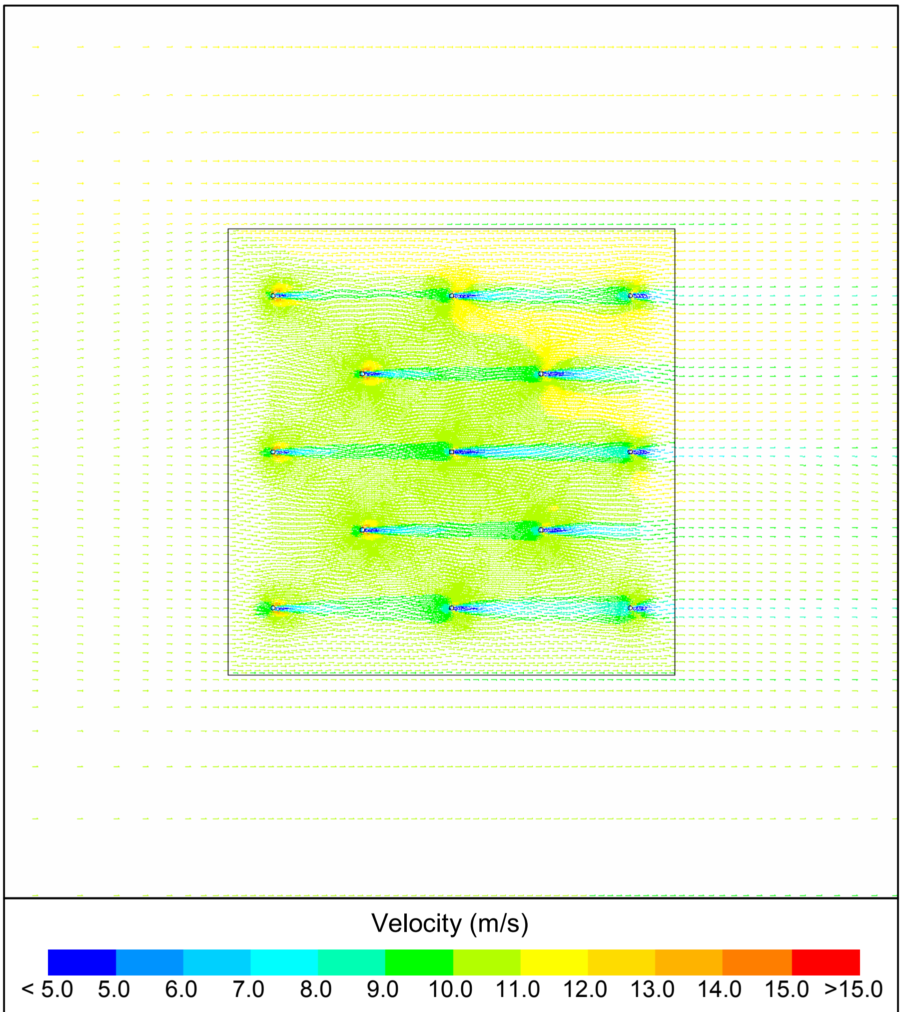

Figure 1.7.1(a) – Velocity Profile obtained for the 5 x 3 Arrangement of Pipes with a Diameter of 0.1 m. Pipes Represented Explicitly within the CFD Mesh

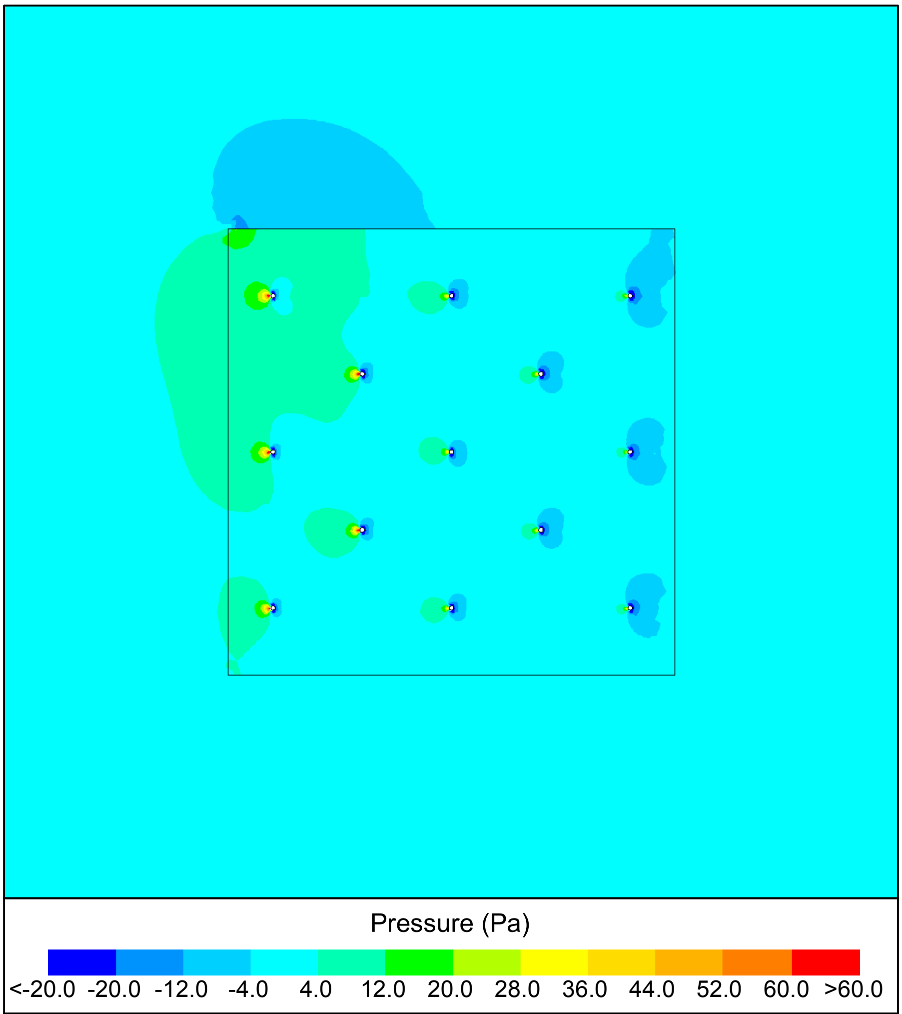

Figure 1.7.1(b) – Pressure Profile obtained for the 5 x 3 Arrangement of Pipes with a Diameter of 0.1 m. Pipes Represented Explicitly within the CFD Mesh

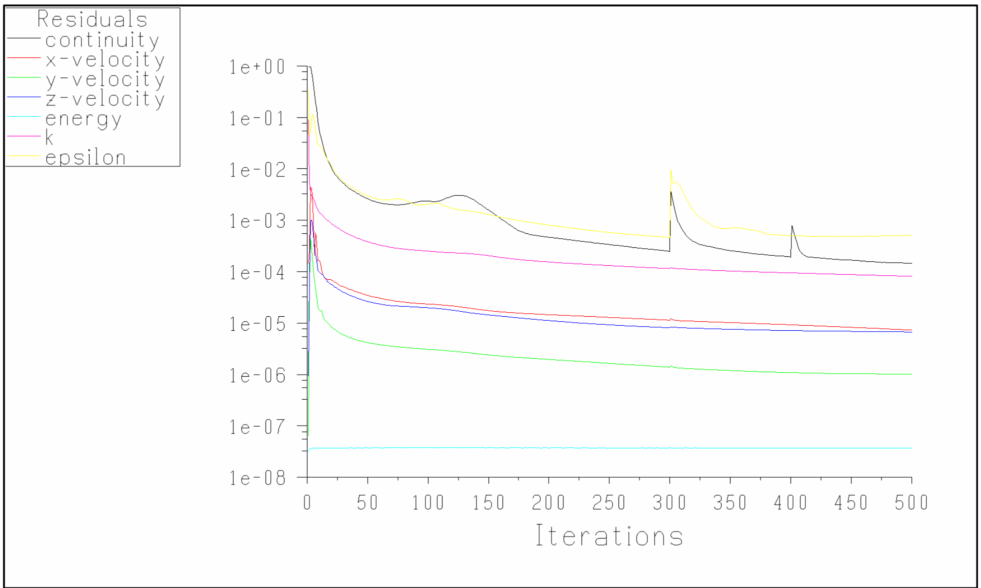

Figure 1.7.1(c) – Residual Plot Showing the Convergence History for the CFD-Predictions obtained for the 5 x 3 Arrangement of Pipes with a Diameter of 0.1 m. Pipes Represented Explicitly within the CFD Mesh

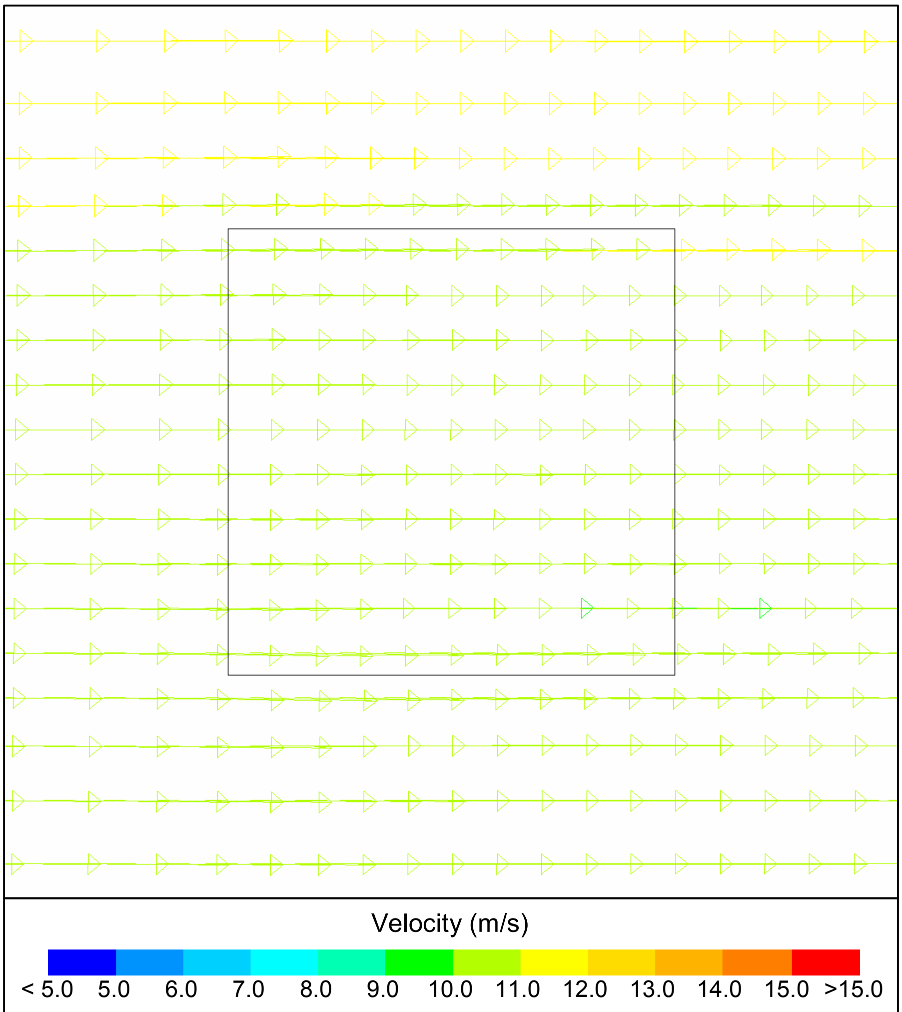

Figure 1.7.2(a) – Velocity Profile obtained for the 5 x 3 Arrangement of Pipes with a Diameter of 0.1 m. Pipes Represented using the ACE Method

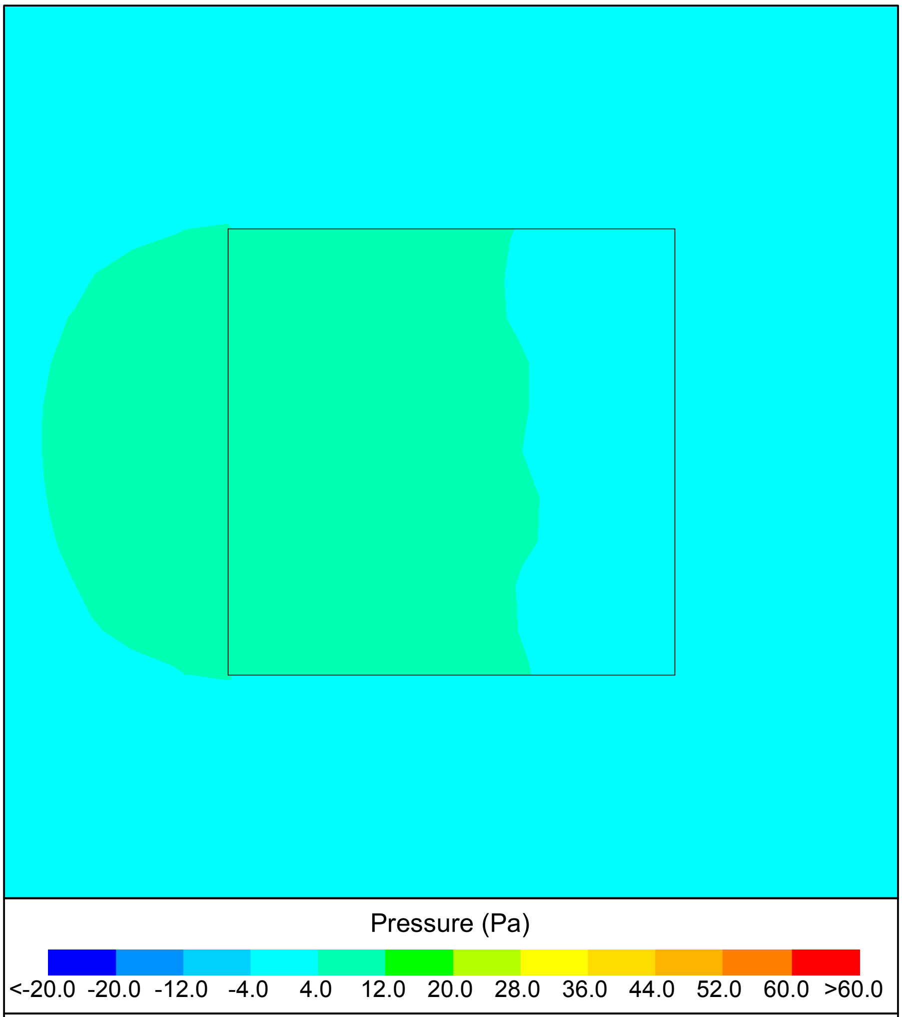

Figure 1.7.2(b) – Pressure Profile obtained for the 5 x 3 Arrangement of Pipes with a Diameter of 0.1 m. Pipes Represented using the ACE Method

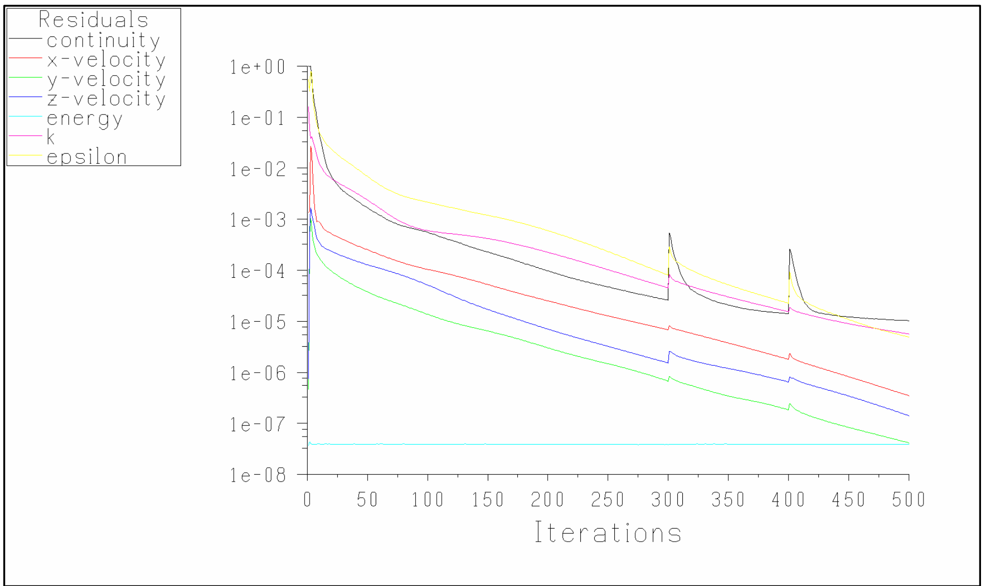

Figure 1.8.2(c) – Residual Plot Showing the Convergence History for the CFD-Predictions obtained for the 5 x 3 Arrangement of Pipes with a Diameter of 0.1 m. Pipes Represented using the ACE Method

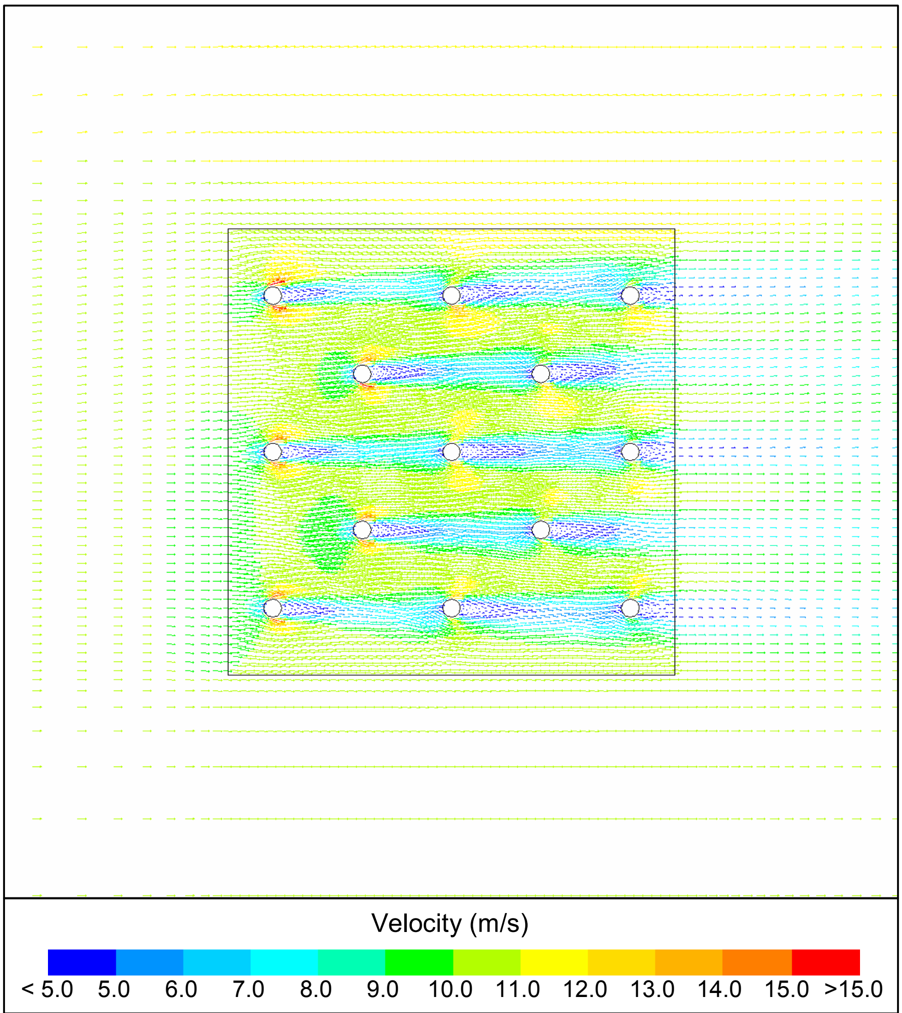

Figure 1.8.1(a) – Velocity Profile obtained for the 5 x 3 Arrangement of Pipes with a Diameter of 0.4 m and the Top and Bottom Surfaces of the Box Excluded. Pipes Represented Explicitly within the CFD Mesh

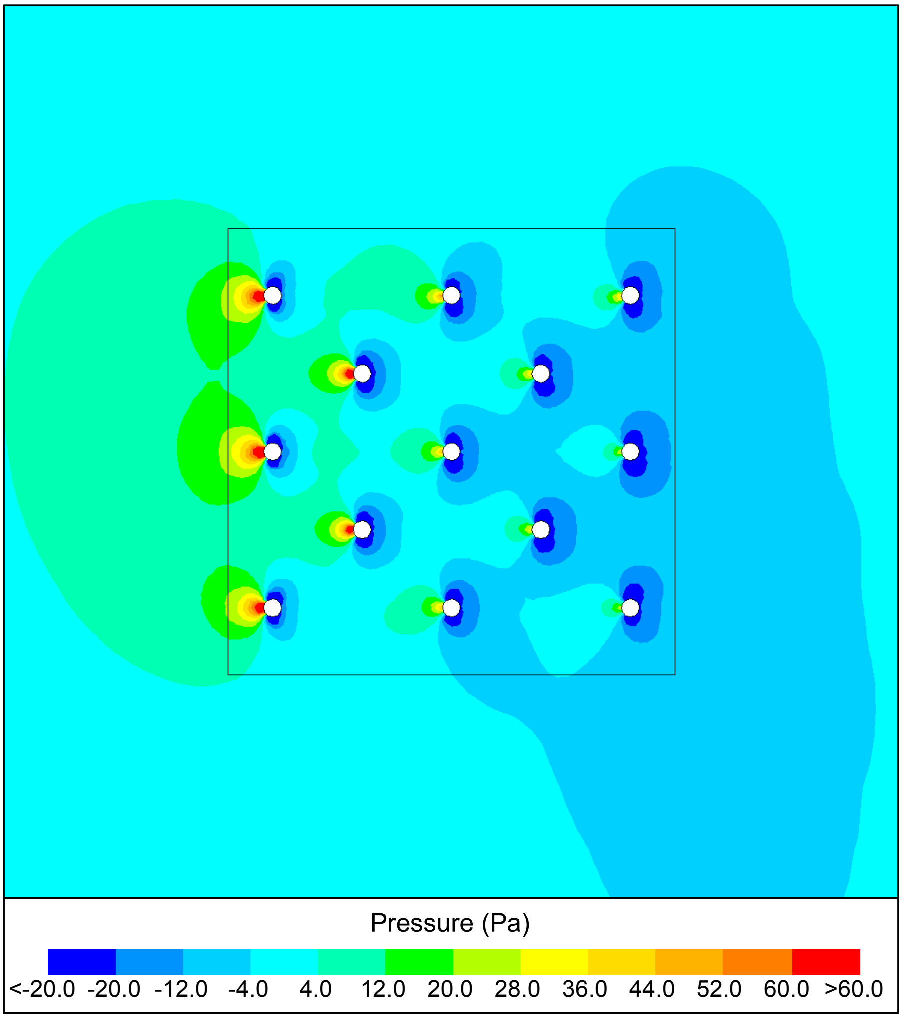

Figure 1.8.1(b) – Pressure Profile obtained for the 5 x 3 Arrangement of Pipes with a Diameter of 0.4 m and the Top and Bottom Surfaces of the Box Excluded. Pipes Represented Explicitly within the CFD Mesh

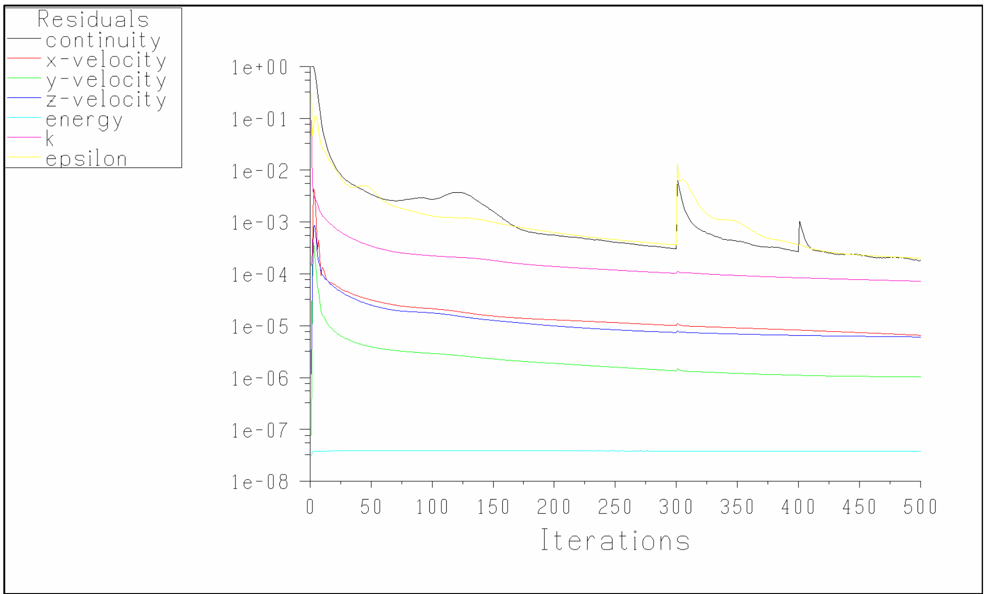

Figure 1.8.1(c) – Residual Plot Showing the Convergence History for the CFD-Predictions obtained for the 5 x 3 Arrangement of Pipes with a Diameter of 0.4 m and the Top and Bottom Surfaces of the Box Excluded. Pipes Represented Explicitly within the CFD Mesh

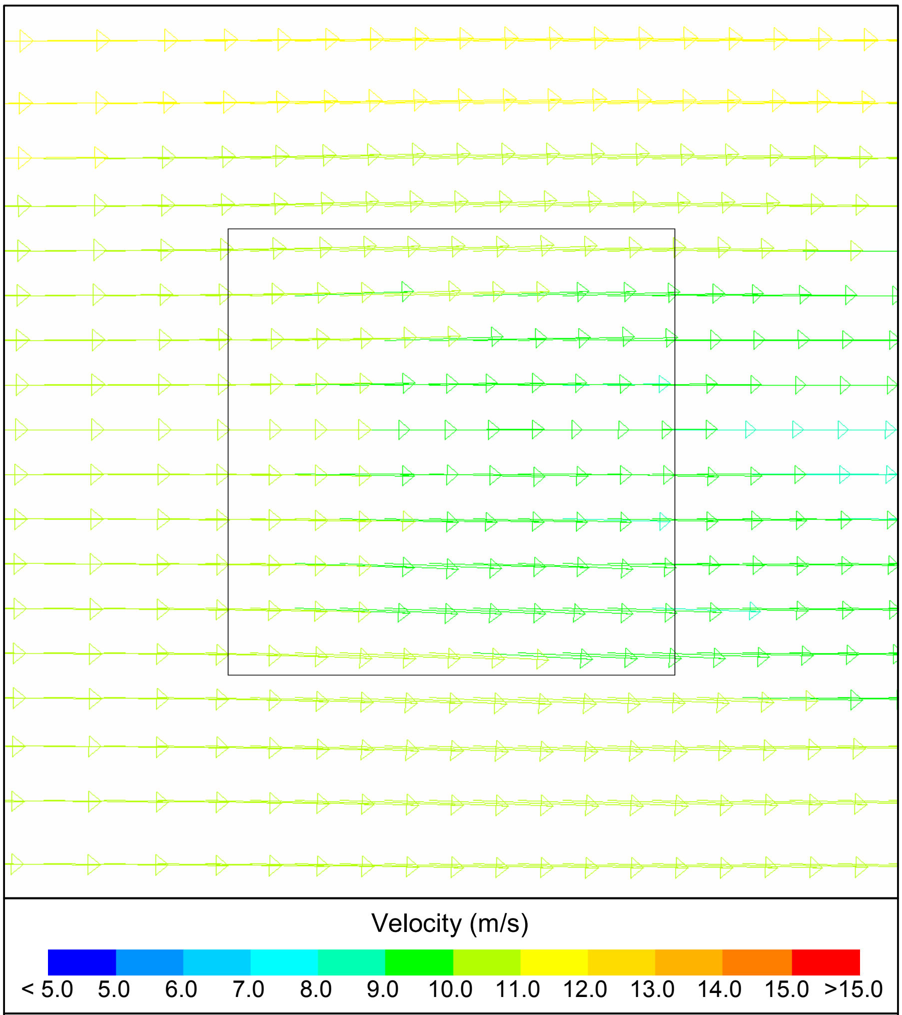

Figure 1.8.2(a) – Velocity Profile obtained for the 5 x 3 Arrangement of Pipes with a Diameter of 0.4 m and the Top and Bottom Surfaces of the Box Excluded. Pipes Represented using the ACE Method

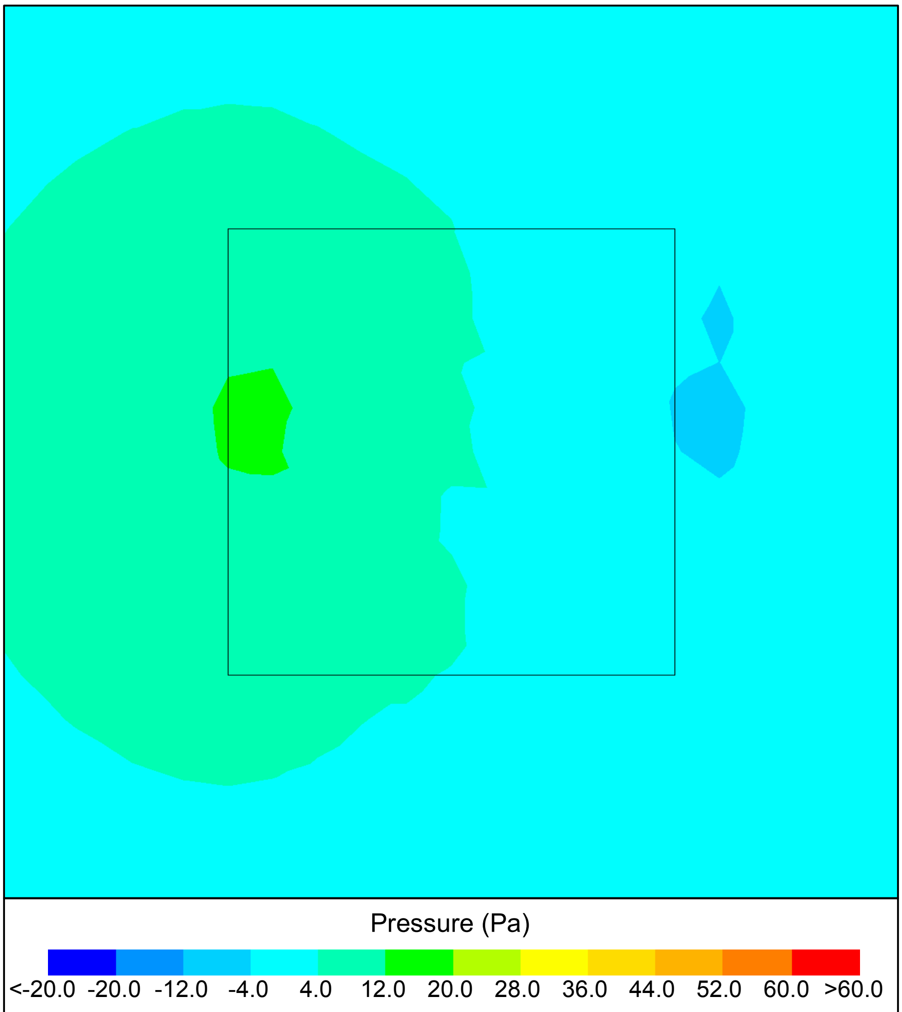

Figure 1.8.2(b) – Pressure Profile obtained for the 5 x 3 Arrangement of Pipes with a Diameter of 0.4 m and the Top and Bottom Surfaces of the Box Excluded. Pipes Represented using the ACE Method

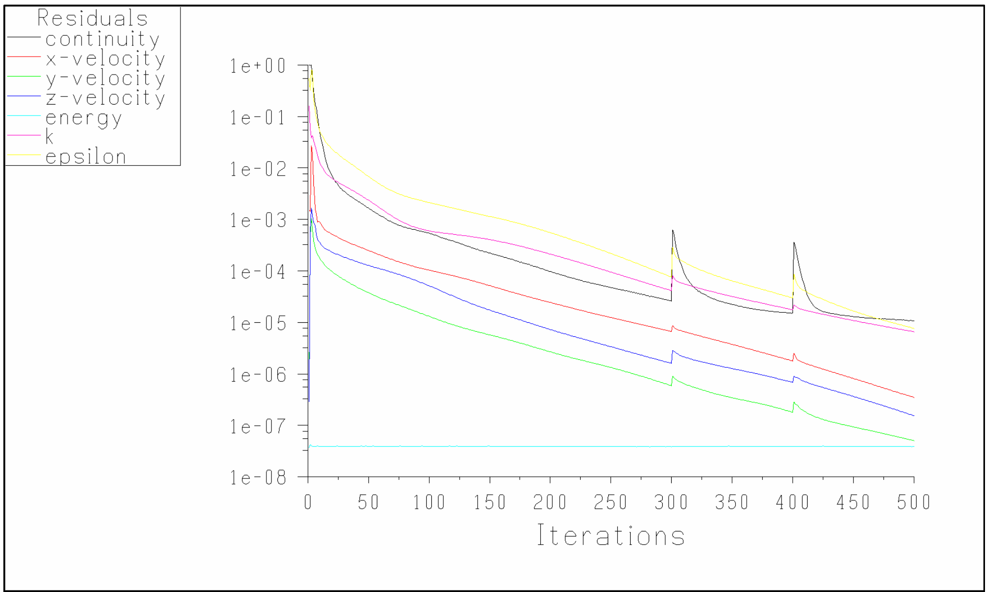

Figure 1.8.2(c) – Residual Plot Showing the Convergence History for the CFD-Predictions obtained for the 5 x 3 Arrangement of Pipes with a Diameter of 0.4 m and the Top and Bottom Surfaces of the Box Excluded. Pipes Represented using the ACE Method

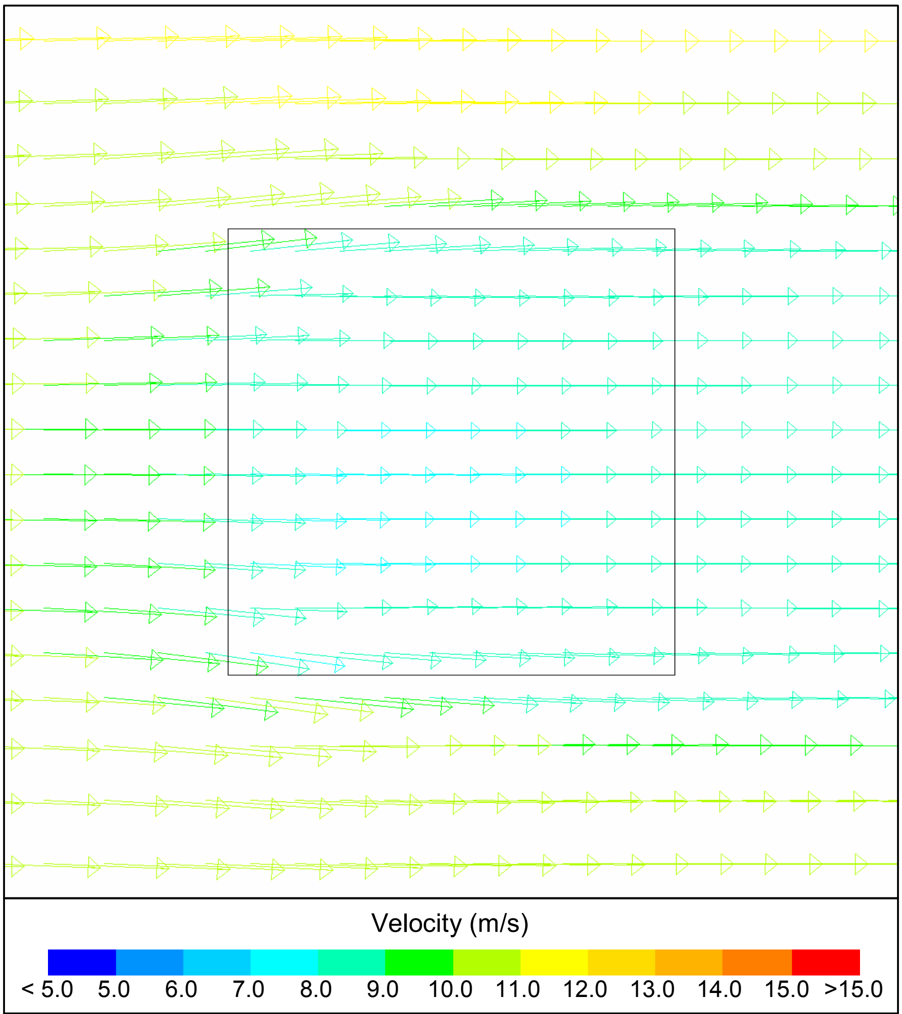

Figure 1.9.1(a) – Velocity Profile obtained for Pipes with a Diameter of 0.4 m. Pipes Represented using the VUR Method with a Pipe Spacing of 1 m

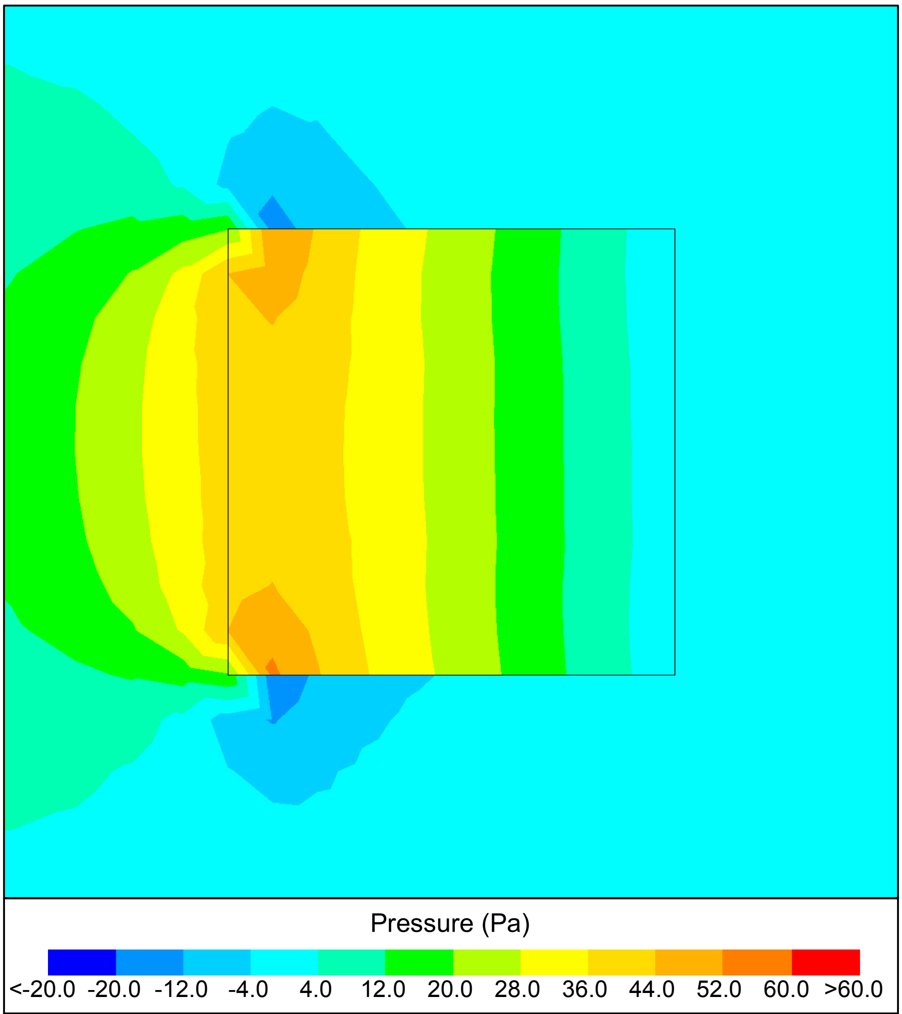

Figure 1.9.1(b) – Pressure Profile obtained for Pipes with a Diameter of 0.4 m. Pipes Represented using the VUR Method with a Pipe Spacing of 1 m

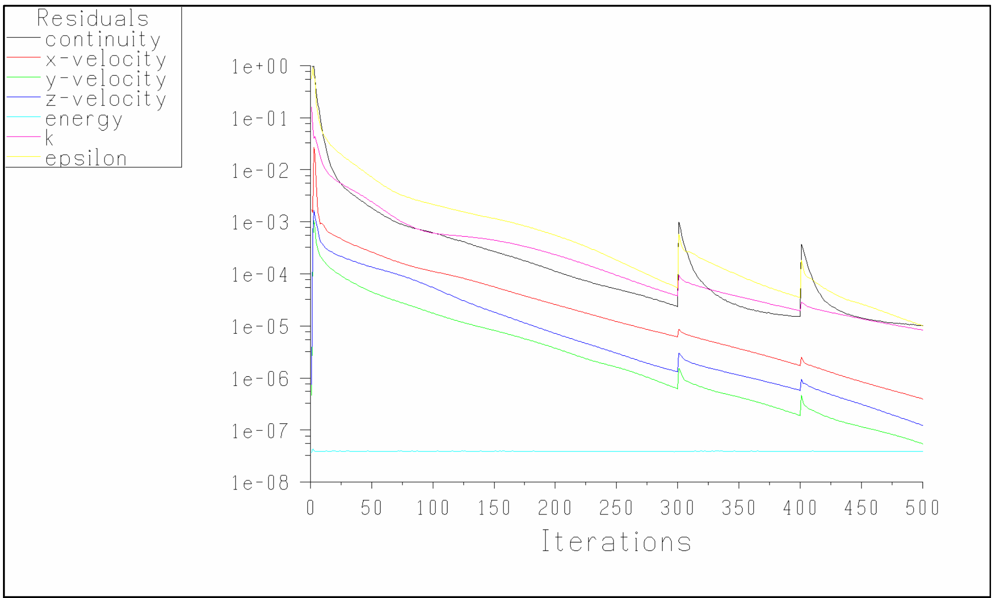

Figure 1.9.1(c) – Residual Plot Showing the Convergence History for the CFD-Predictions with a Diameter of 0.4 m. Pipes Represented using the VUR Method with a Pipe Spacing of 1 m

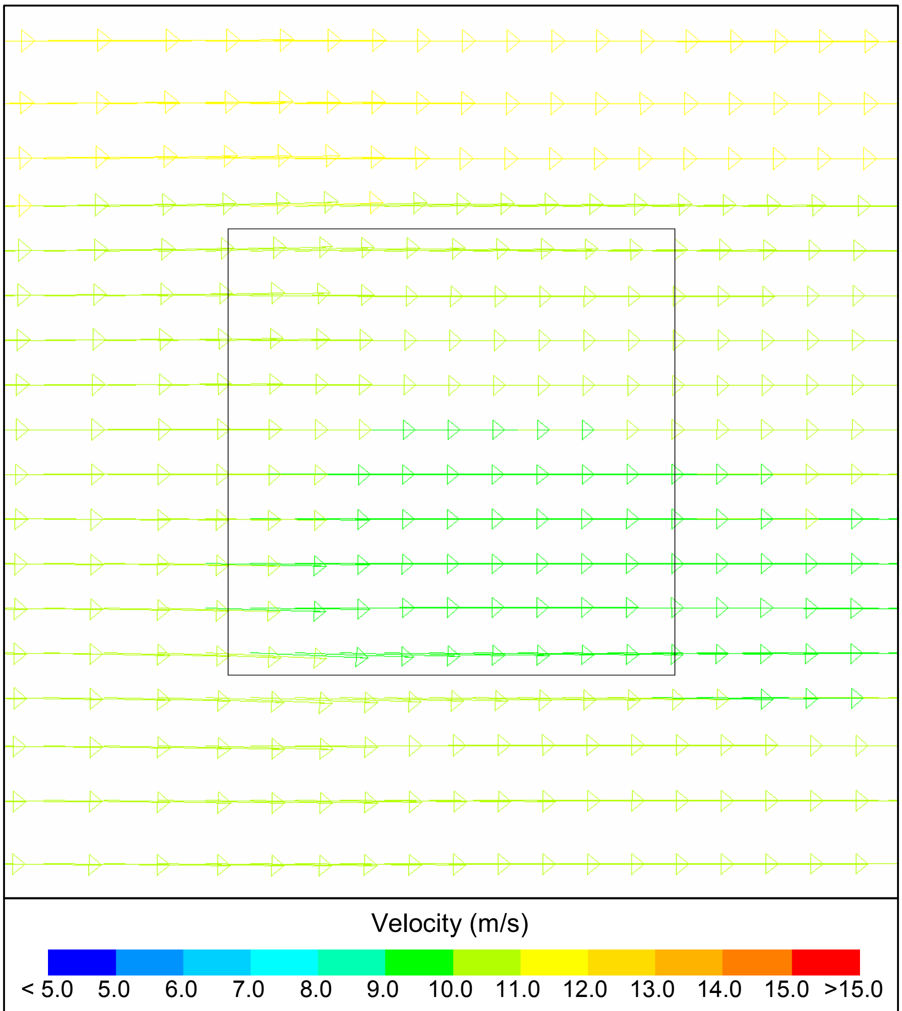

Figure 1.9.2(a) – Velocity Profile obtained for Pipes with a Diameter of 0.4 m. Pipes Represented using the VUR Method with a Pipe Spacing of 2 m

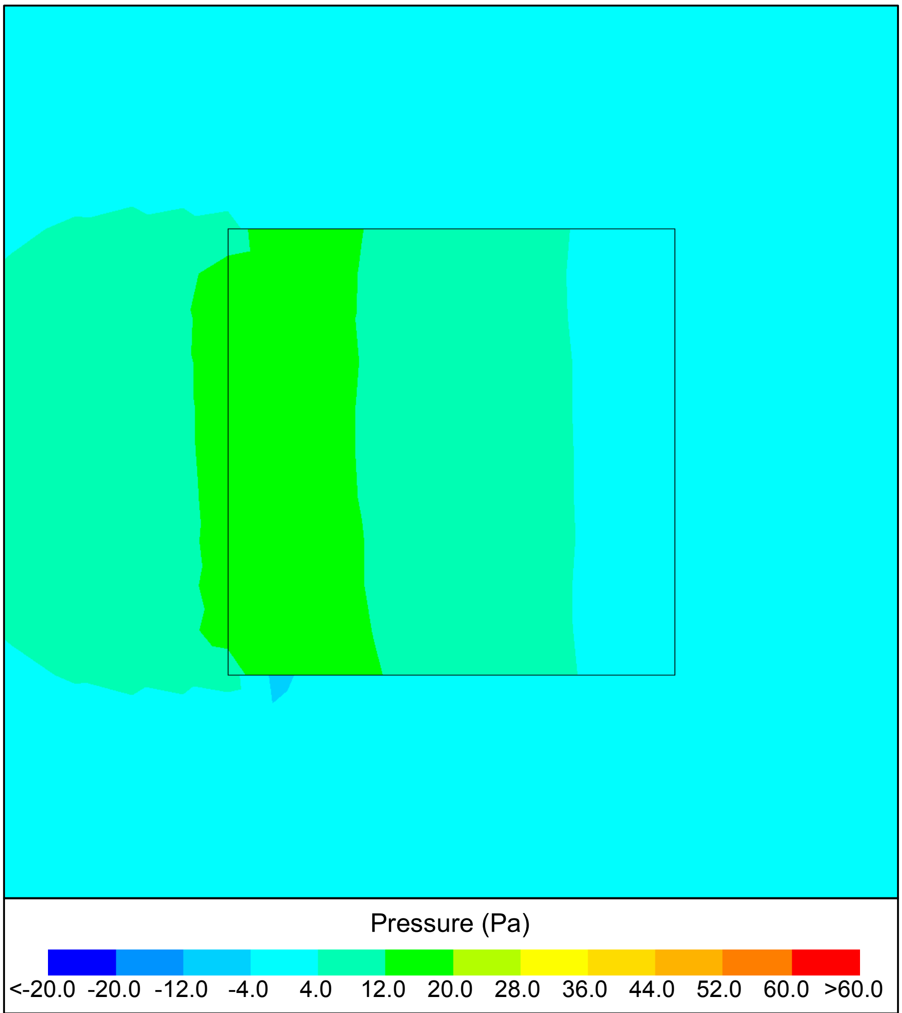

Figure 1.9.2(b) – Pressure Profile obtained for Pipes with a Diameter of 0.4 m. Pipes Represented using the VUR Method with a Pipe Spacing of 2 m

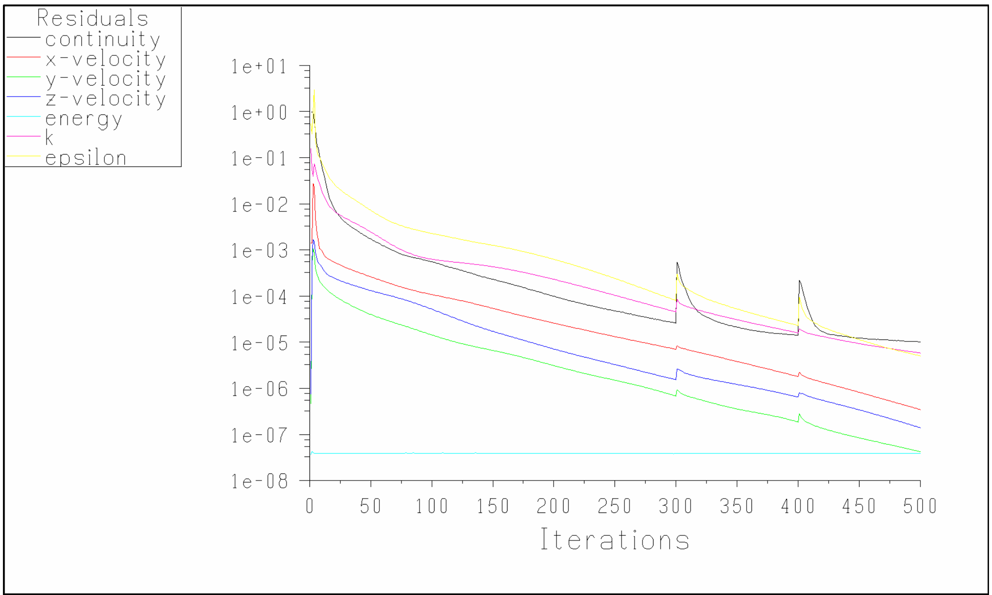

Figure 1.9.2(c) – Residual Plot Showing the Convergence History for the CFD-Predictions with a Diameter of 0.4 m. Pipes Represented using the VUR Method with a Pipe Spacing of 2 m

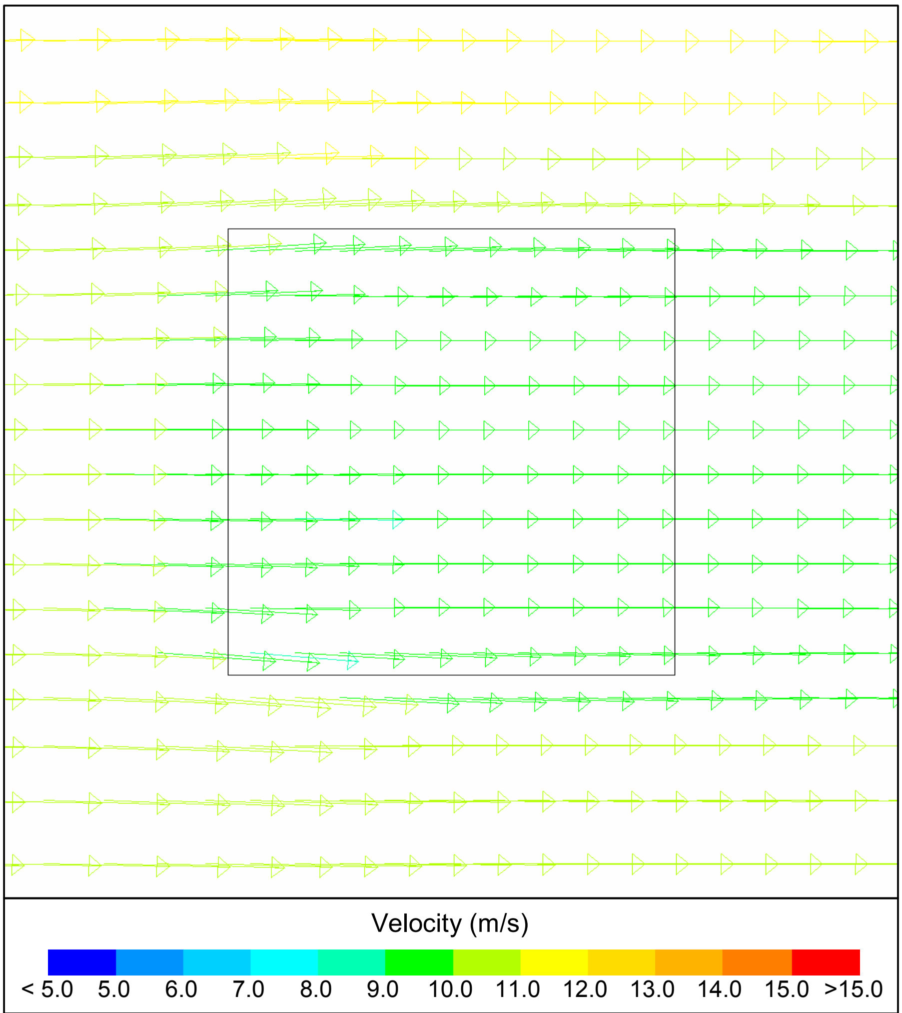

Figure 1.10.1(a) – Velocity Profile obtained for Pipes with a Diameter of 0.2 m. Pipes Represented using the VUR Method with a Pipe Spacing of 1 m

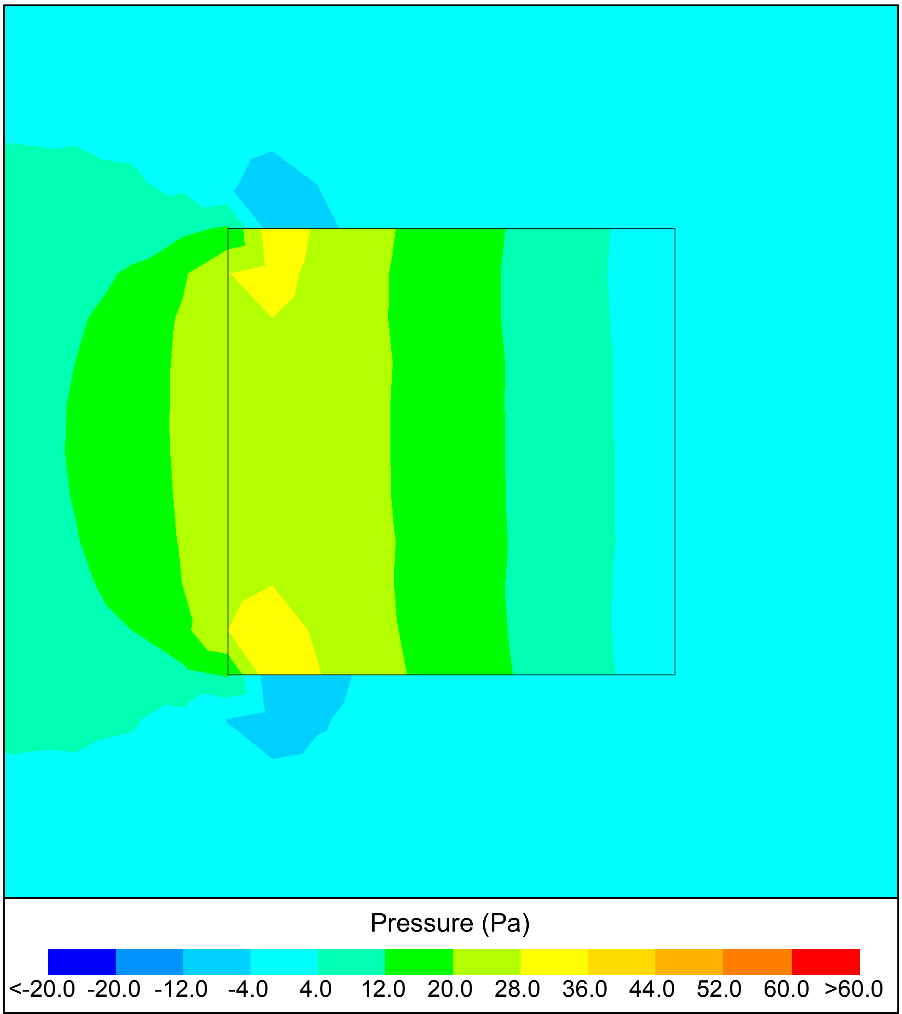

Figure 1.10.1(b) – Pressure Profile obtained for Pipes with a Diameter of 0.2 m. Pipes Represented using the VUR Method with a Pipe Spacing of 1 m

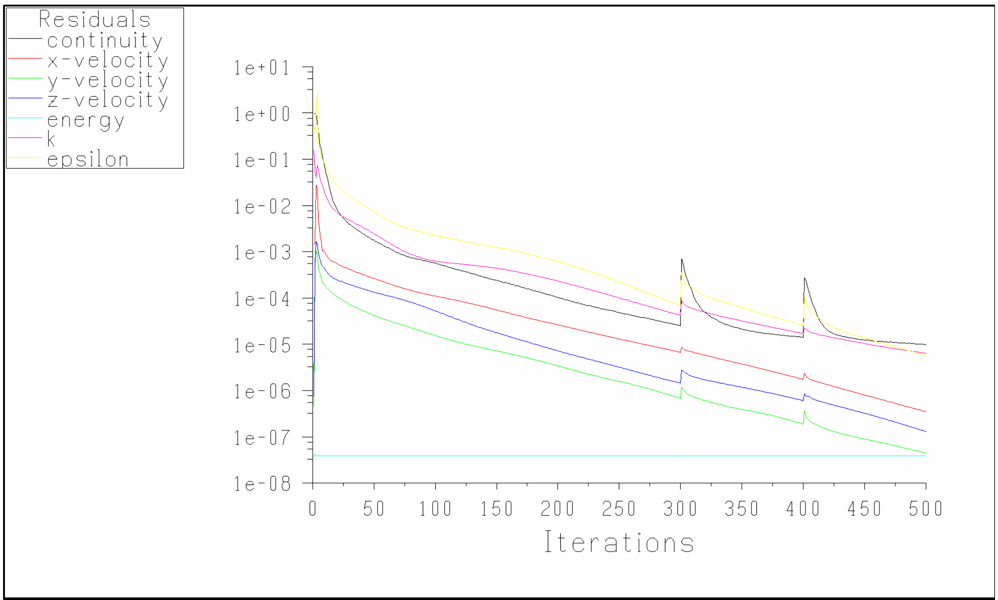

Figure 1.10.1(c) – Residual Plot Showing the Convergence History for the CFD-Predictions with a Diameter of 0.2 m. Pipes Represented using the VUR Method with a Pipe Spacing of 1 m

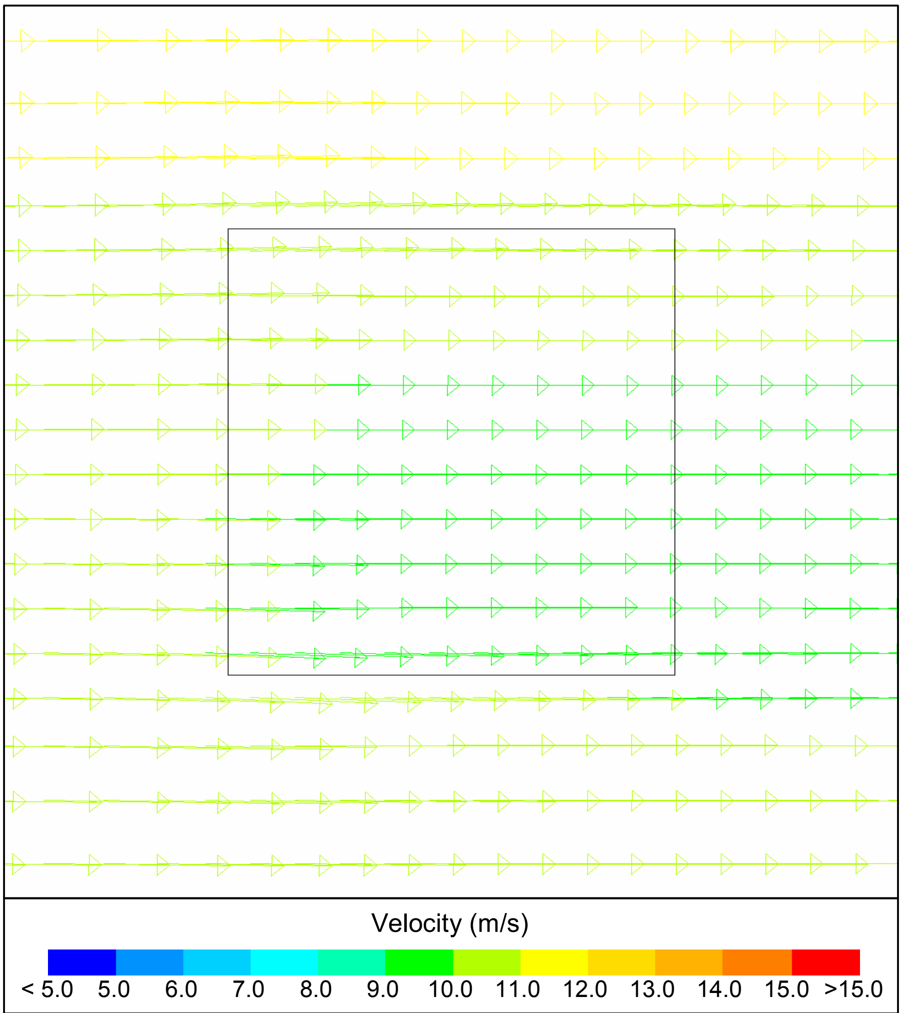

Figure 1.10.2(a) – Velocity Profile obtained for Pipes with a Diameter of 0.2 m. Pipes Represented using the VUR Method with a Pipe Spacing of 2 m

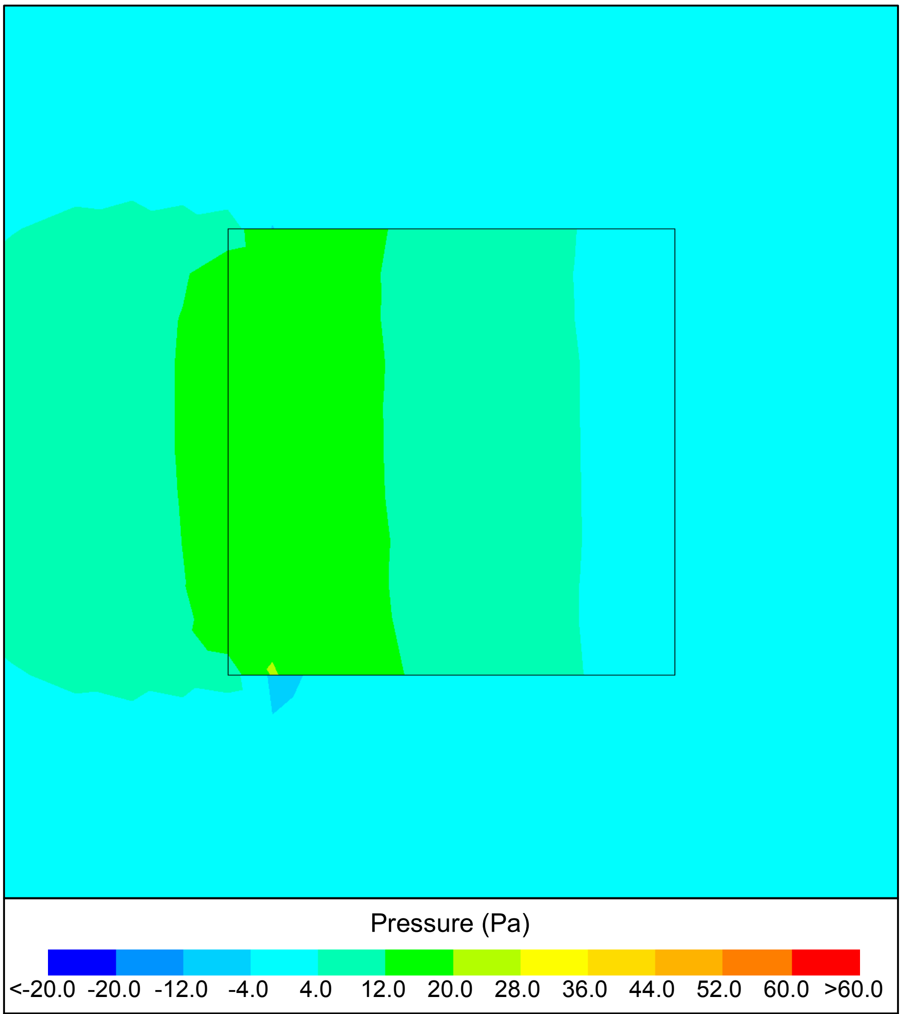

Figure 1.10.2(b) – Pressure Profile obtained for Pipes with a Diameter of 0.2 m. Pipes Represented using the VUR Method with a Pipe Spacing of 2 m

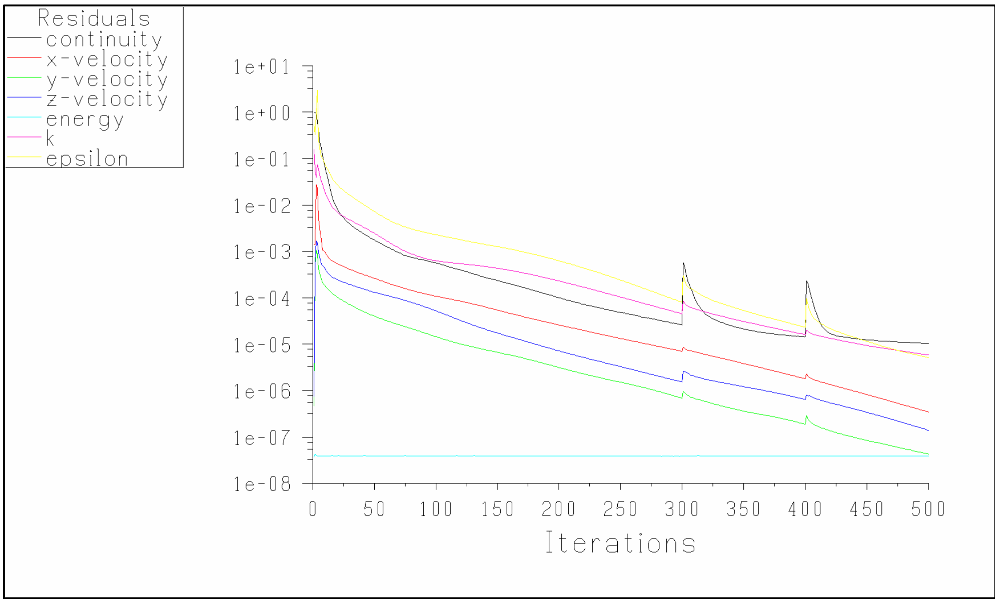

Figure 1.10.2(c) – Residual Plot Showing the Convergence History for the CFD-Predictions with a Diameter of 0.2 m. Pipes Represented using the VUR Method with a Pipe Spacing of 2 m

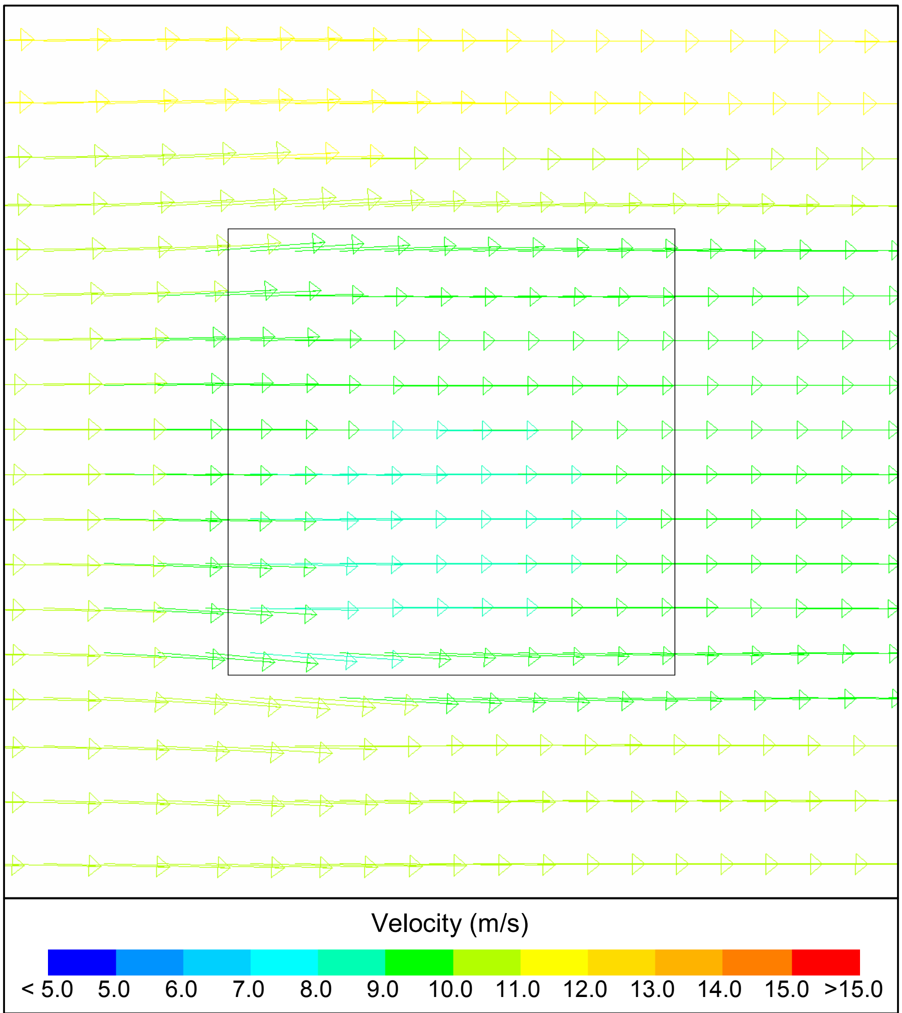

Figure 1.11.1(a) – Velocity Profile obtained for Pipes with a Diameter of 0.1 m. Pipes Represented using the VUR Method with a Pipe Spacing of 1 m

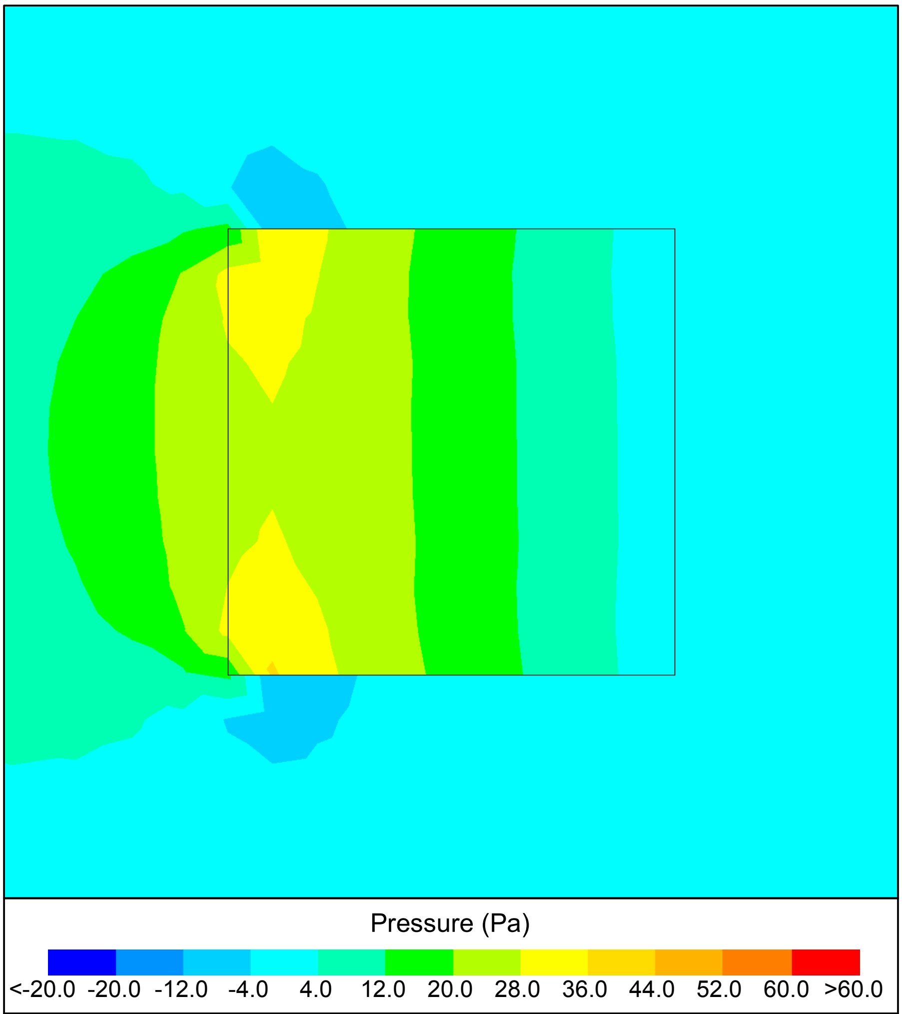

Figure 1.11.1(b) – Pressure Profile obtained for Pipes with a Diameter of 0.1 m. Pipes Represented using the VUR Method with a Pipe Spacing of 1 m

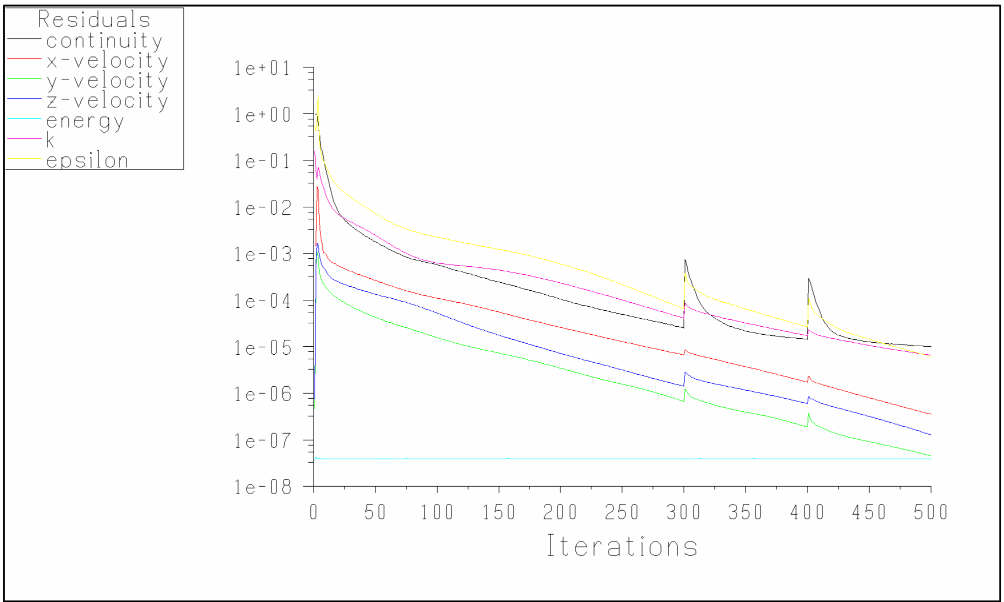

Figure 1.11.1(c) – Residual Plot Showing the Convergence History for the CFD-Predictions with a Diameter of 0.1 m. Pipes Represented using the VUR Method with a Pipe Spacing of 1 m

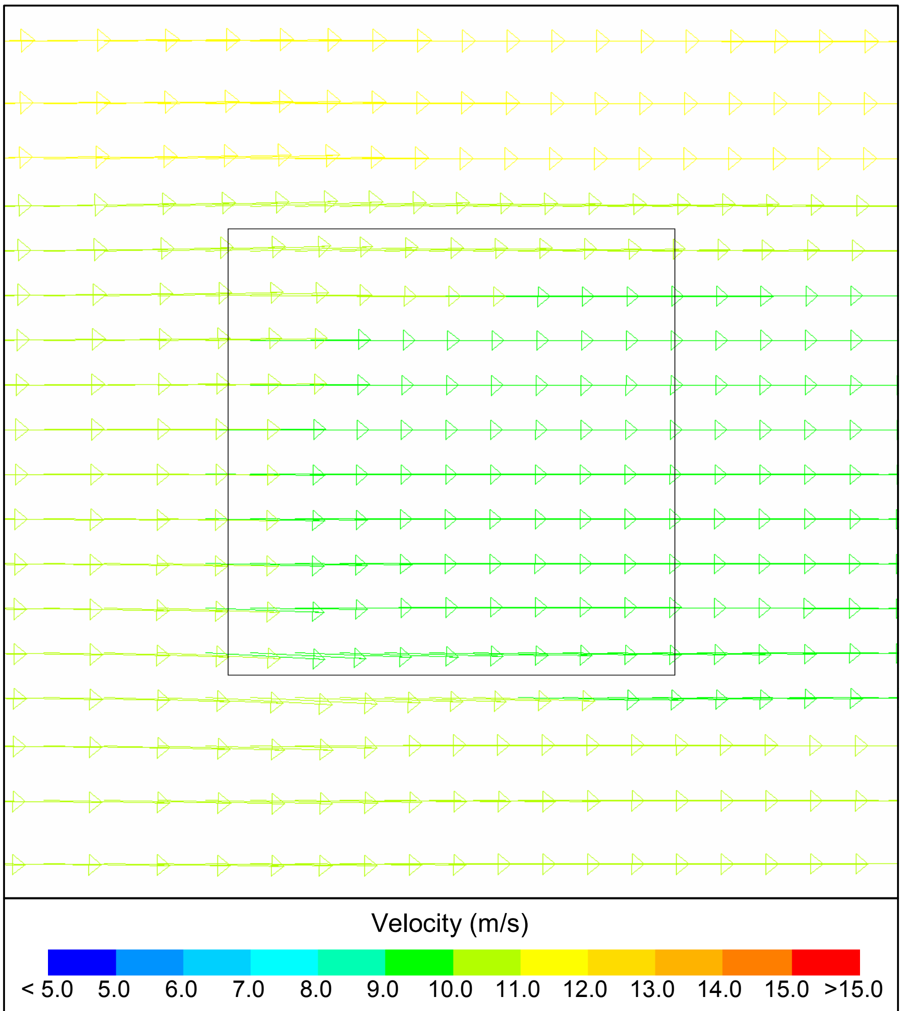

Figure 1.11.2(a) – Velocity Profile obtained for Pipes with a Diameter of 0.1 m. Pipes Represented using the VUR Method with a Pipe Spacing of 2 m

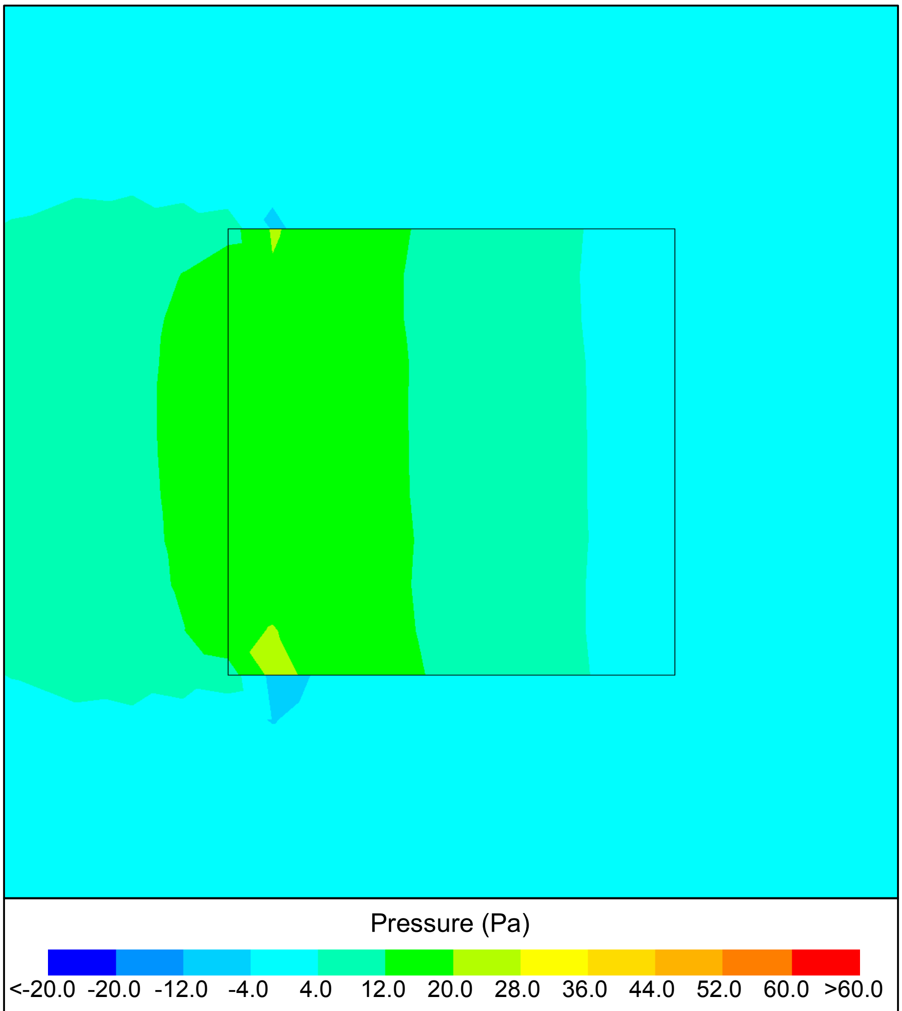

Figure 1.11.2(b) – Pressure Profile obtained for Pipes with a Diameter of 0.1 m. Pipes Represented using the VUR Method with a Pipe Spacing of 2 m

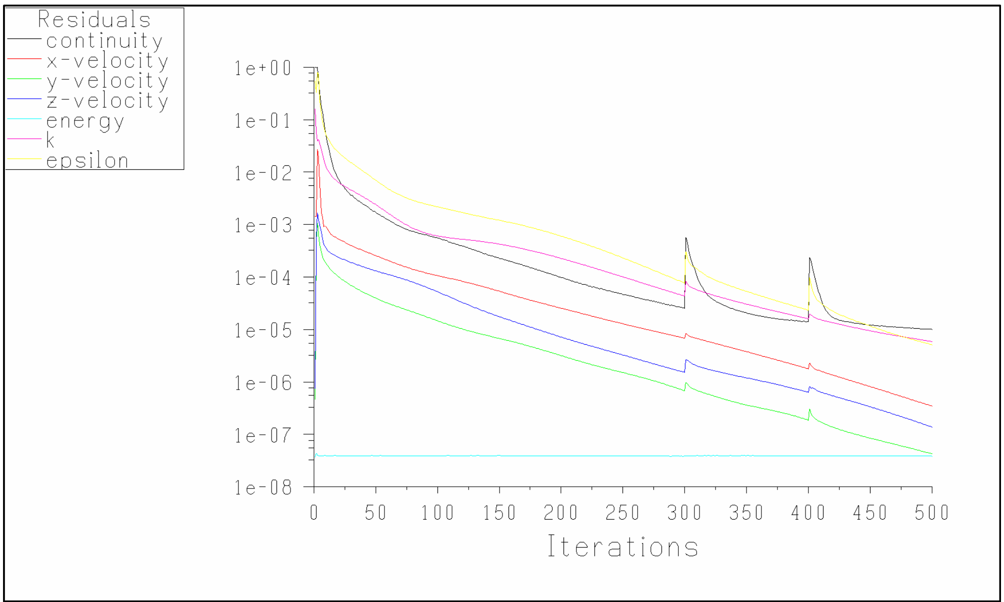

Figure 1.11.2(c) – Residual Plot Showing the Convergence History for the CFD-Predictions with a Diameter of 0.1 m. Pipes Represented using the VUR Method with a Pipe Spacing of 2 m

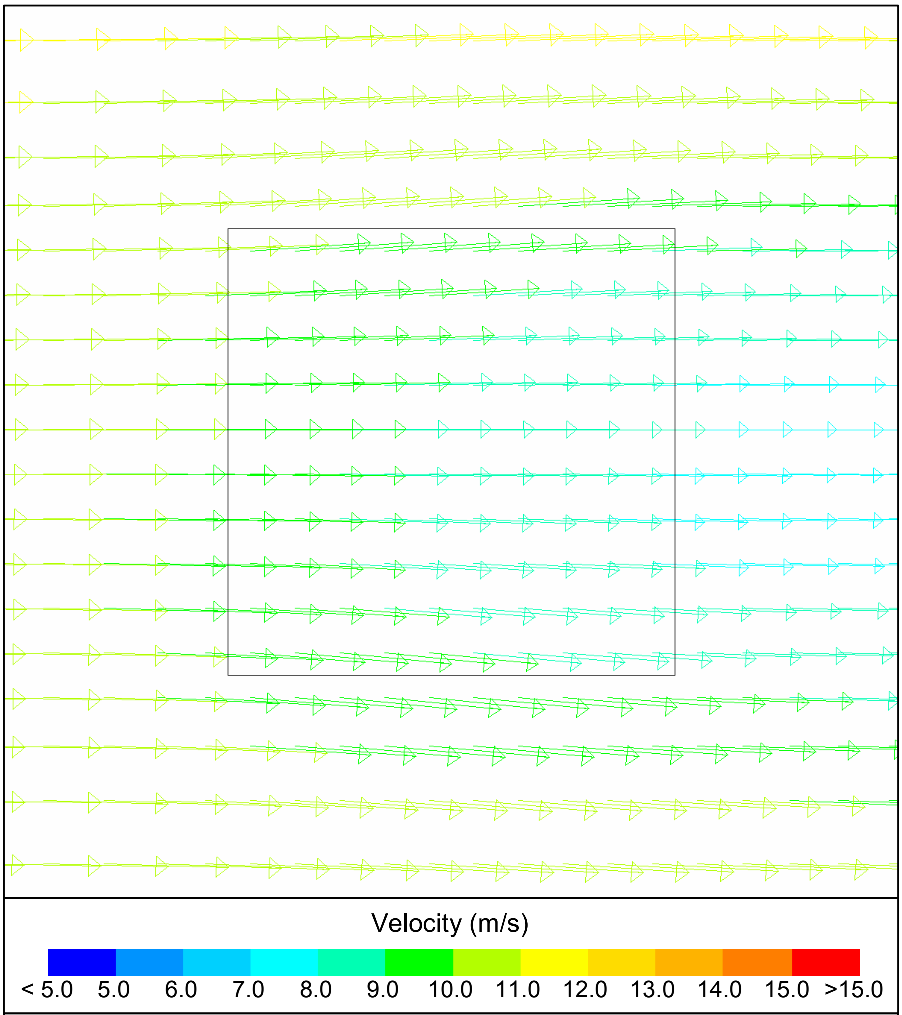

Figure 1.12.1(a) – Velocity Profile obtained for Pipes with a Diameter of 0.4 m and the Top and Bottom Surfaces of the Box Excluded. Pipes Represented using the VUR Method with a Pipe Spacing of 1 m

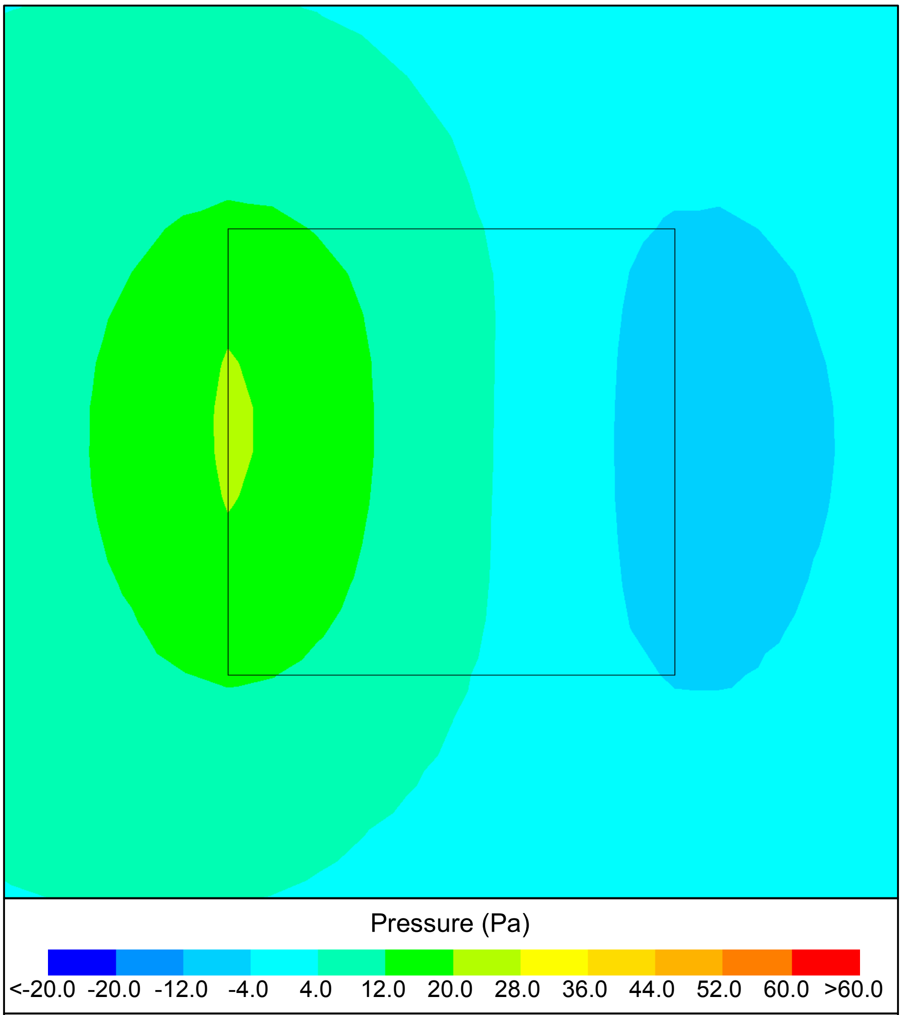

Figure 1.12.1(b) – Pressure Profile obtained for Pipes with a Diameter of 0.4 m and the Top and Bottom Surfaces of the Box Excluded. Pipes Represented using the VUR Method with a Pipe Spacing of 1 m

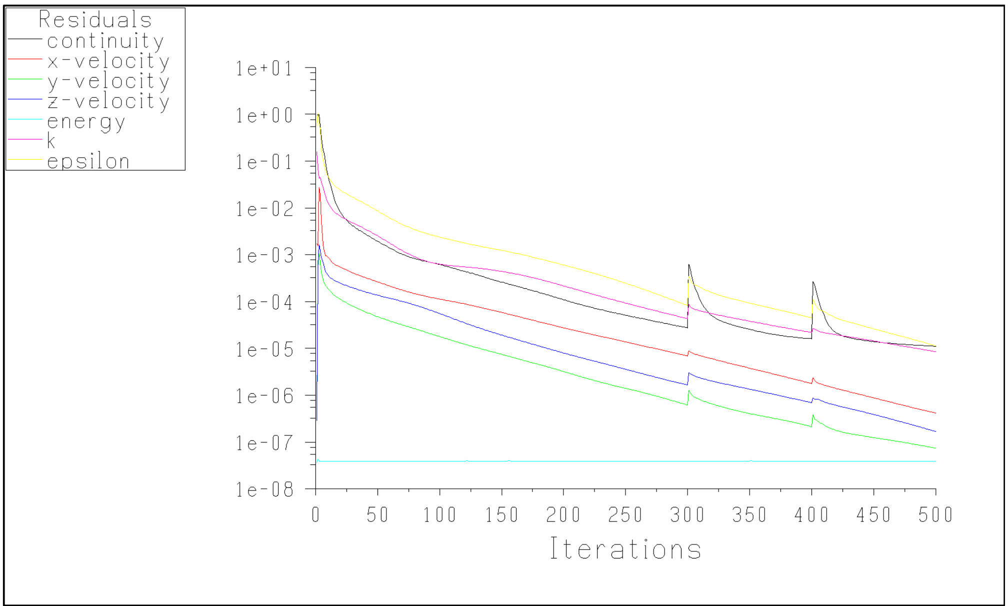

Figure 1.12.1(c) – Residual Plot Showing the Convergence History for the CFD-Predictions with a Diameter of 0.4 m and the Top and Bottom Surfaces of the Box Excluded. Pipes Represented using the VUR Method with a Pipe Spacing of 1 m

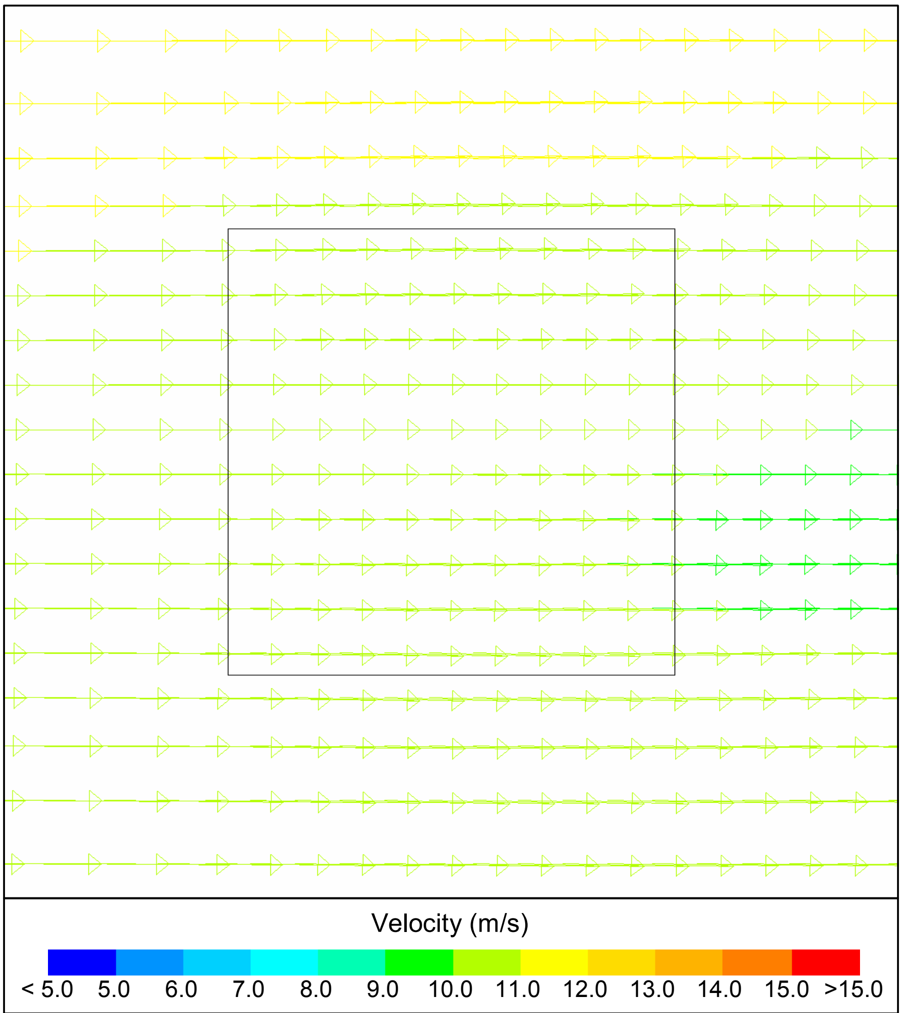

Figure 1.12.2(a) – Velocity Profile obtained for Pipes with a Diameter of 0.4 m and the Top and Bottom Surfaces of the Box Excluded. Pipes Represented using the VUR Method with a Pipe Spacing of 2 m

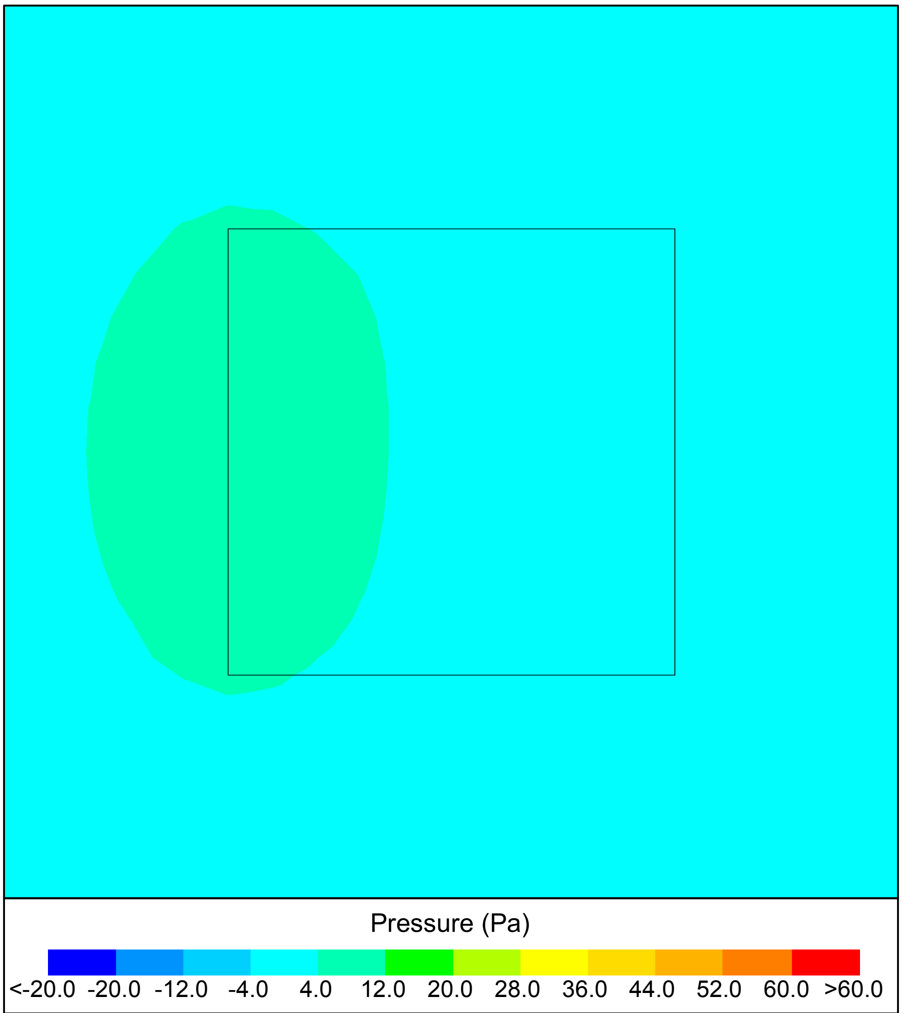

Figure 1.12.2(b) – Pressure Profile obtained for Pipes with a Diameter of 0.4 m and the Top and Bottom Surfaces of the Box Excluded. Pipes Represented using the VUR Method with a Pipe Spacing of 2 m

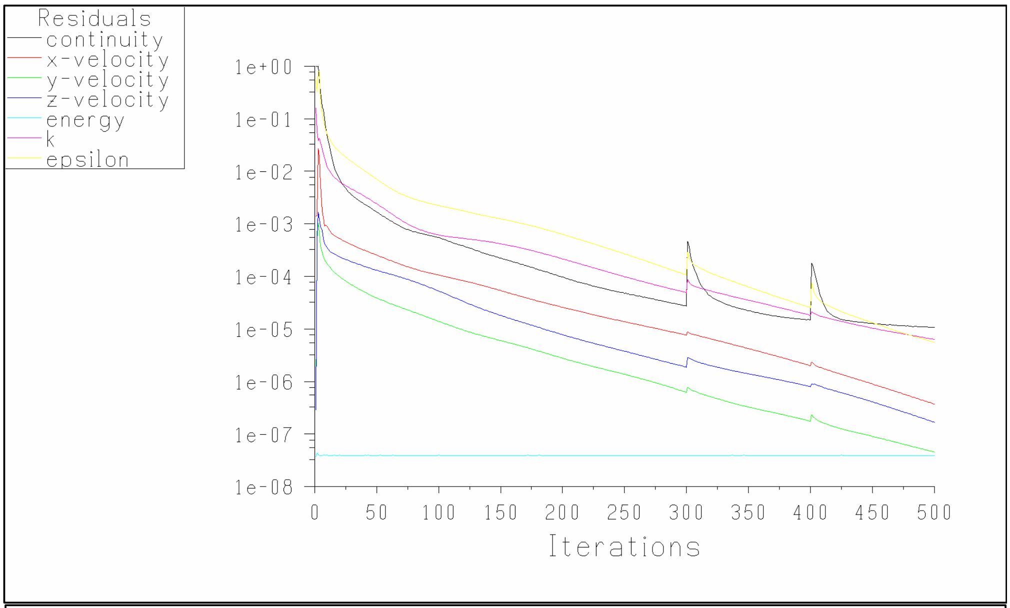

Figure 1.12.2(c) – Residual Plot Showing the Convergence History for the CFD-Predictions with a Diameter of 0.4 m and the Top and Bottom Surfaces of the Box Excluded. Pipes Represented using the VUR Method with a Pipe Spacing of 2 m

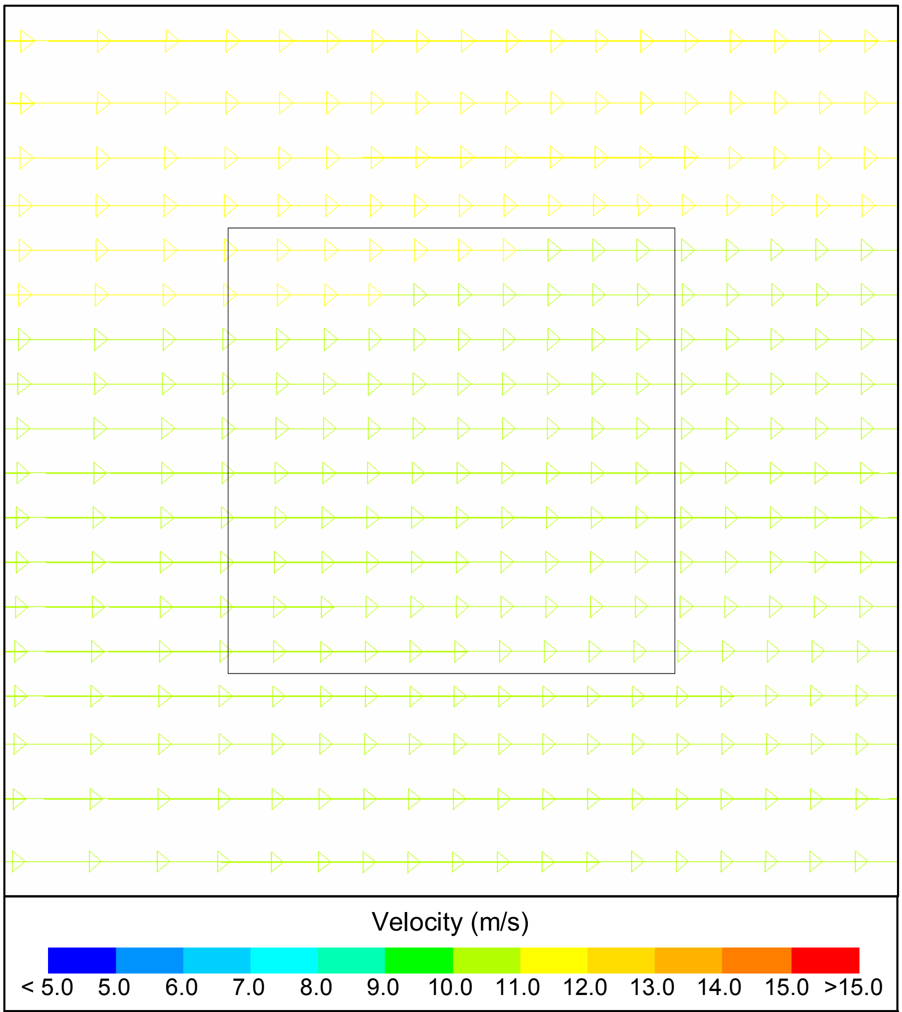

Figure 1.13.1(a) – Velocity Profile obtained for No Pipes

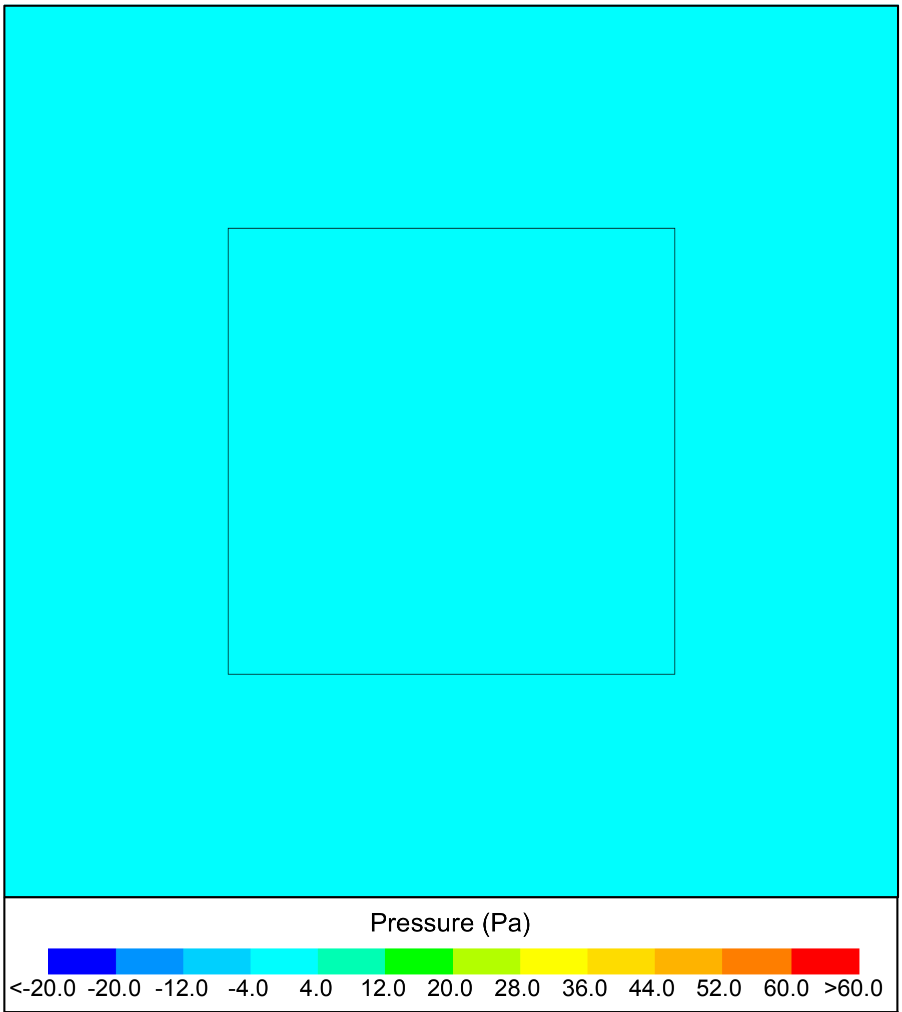

Figure 1.13.1(b) – Pressure Profile obtained for No Pipes

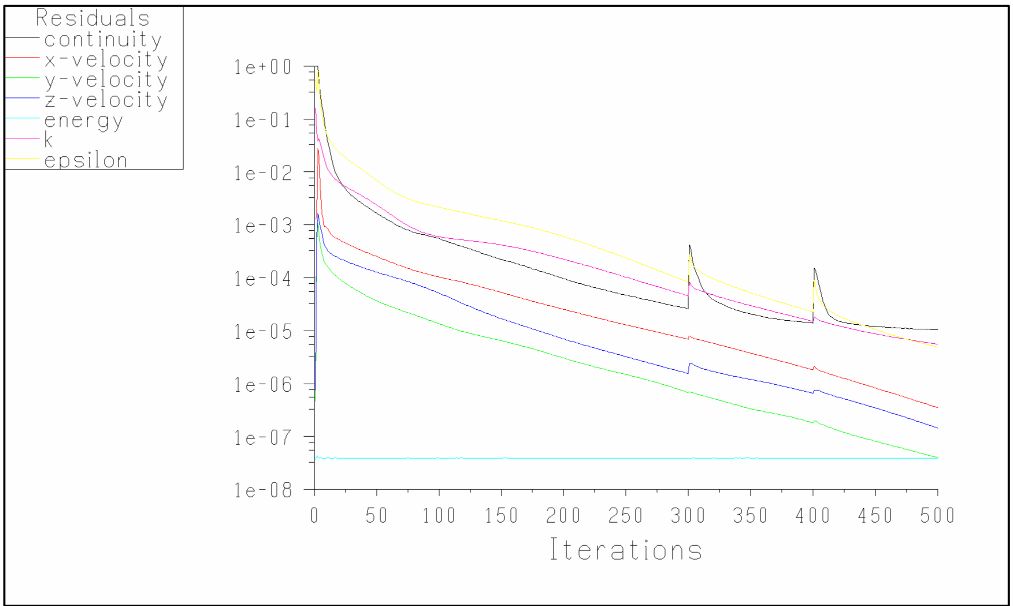

Figure 1.13.1(c) – Residual Plot Showing the Convergence History for the CFD-Predictions No Pipes

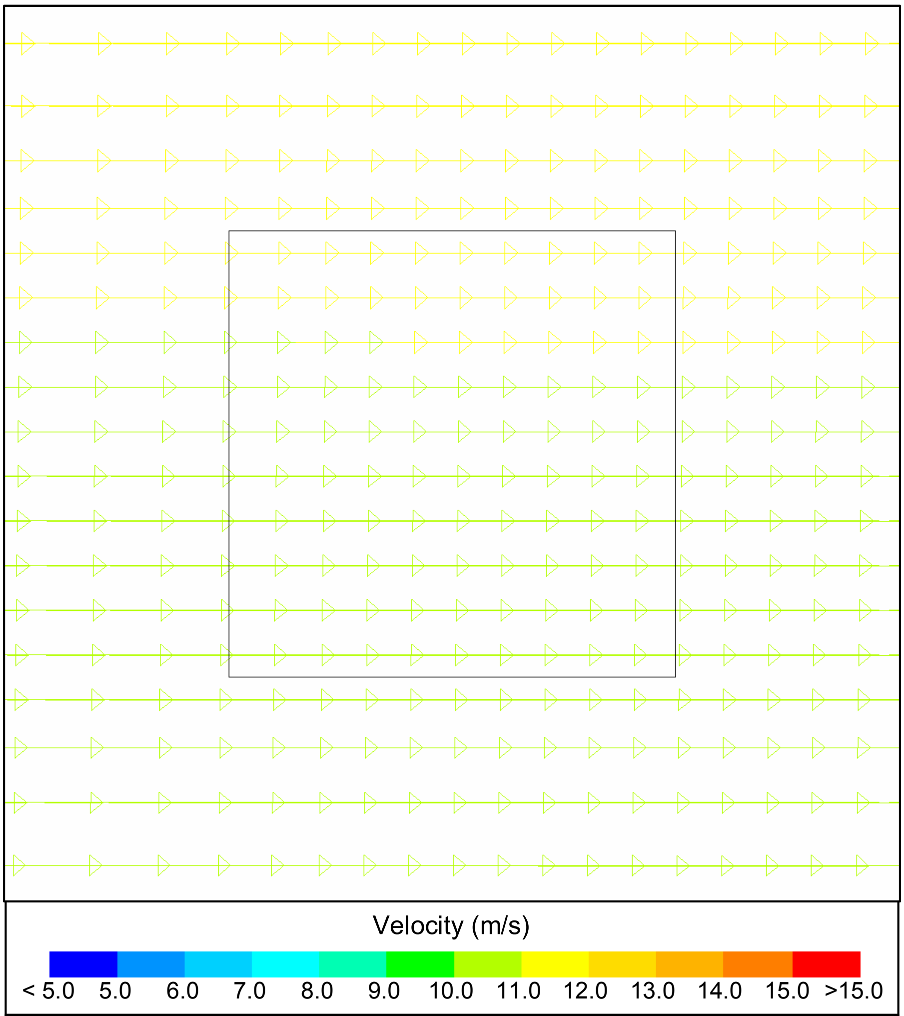

Figure 1.13.2(a) – Velocity Profile obtained for No Pipes with the Top and Bottom Surfaces of the Box Excluded

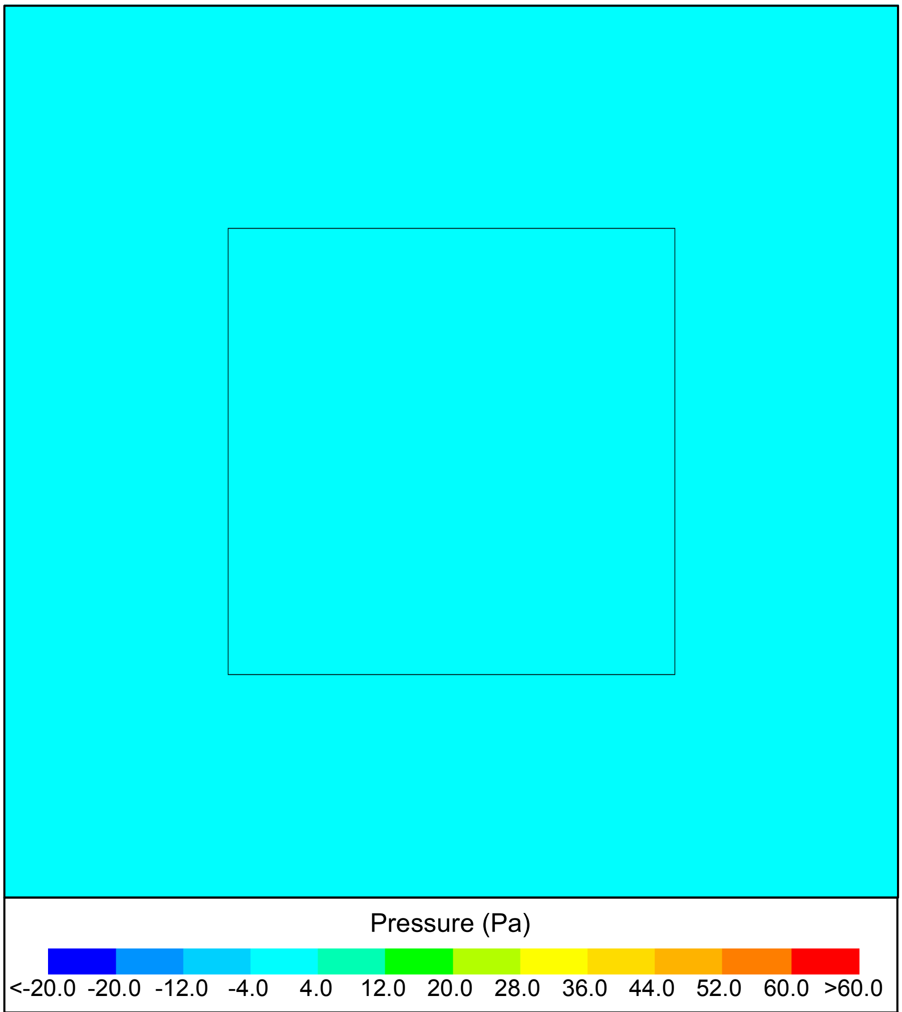

Figure 1.13.2(b) – Pressure Profile obtained for No Pipes with the Top and Bottom Surfaces of the Box Excluded

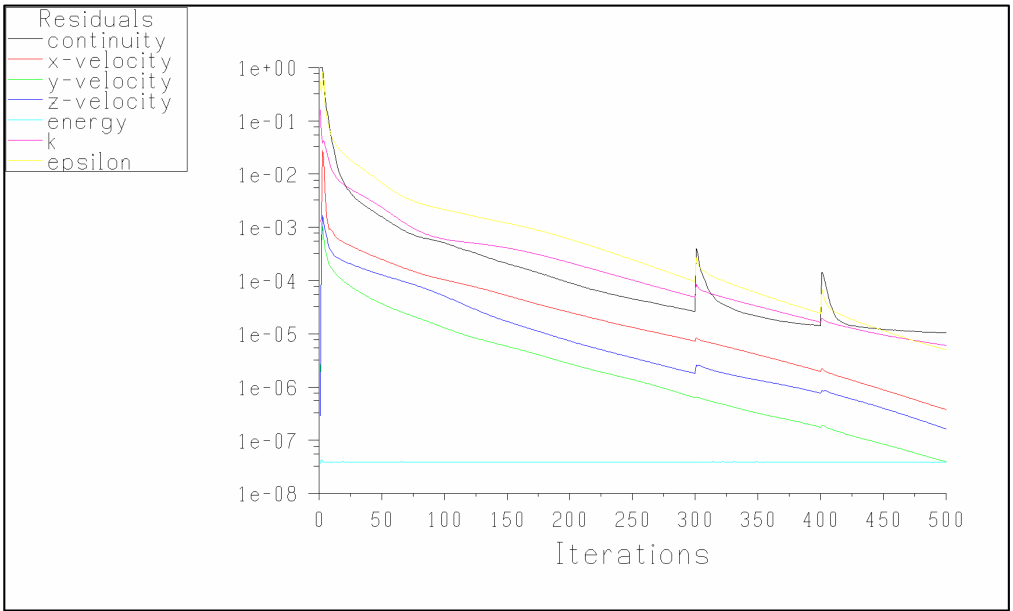

Figure 1.13.2(c) – Residual Plot Showing the Convergence History for the CFD-Predictions with No Pipes and the Top and Bottom Surfaces of the Box Excluded